

# **Dynamics of the Pebble-Bed Nuclear Reactor in the Direct Brayton Cycle**

Dynamics of the Pebble-Bed Nuclear Reactor in the Direct Brayton Cycle  
Verkerk, Ewout Casper - Petten: Nuclear Research and Consultancy Group (NRG)  
Ph.D. Thesis, Delft University of Technology.  
ISBN: 90-9014203-7  
NUGI: 837  
© E.C. Verkerk NRG 2000

All rights reserved. No part of this publication may be reproduced, stored in a retrieval system, or transmitted in any form or by any means without the prior written permission of the copyright owner.

# **Dynamics of the Pebble-Bed Nuclear Reactor in the Direct Brayton Cycle**

Proefschrift

ter verkrijging van de graad van doctor  
aan de Technische Universiteit Delft,  
op gezag van de Rector Magnificus prof. ir K.F. Wakker,  
voorzitter van het College voor Promoties,  
in het openbaar te verdedigen op maandag 6 november 2000 om 13:30 uur

door Ewout Casper VERKERK

natuurkundig ingenieur  
geboren te Heemskerk.

Dit proefschrift is goedgekeurd door de promotor:

Prof. dr ir H. van Dam

Samenstelling promotiecommissie:

Rector Magnificus, voorzitter

Prof. dr ir H. van Dam, Technische Universiteit Delft, promotor

Prof. dr ir A.H.M. Verkooijen, Technische Universiteit Delft

Prof. dr ir T.H.J.J. van der Hagen, Technische Universiteit Delft

Prof. dr G. Lohnert, Universität Stuttgart

Prof. dr ir H.E.A. van den Akker, Technische Universiteit Delft

Prof. ir O.H. Bosgra, Technische Universiteit Delft

Dr ir J.C. Kuijper, NRG Petten

This work has been performed at the Nuclear Research and Consultancy Group (NRG, Petten) with financial support from the Ministry of Economic Affairs in the framework of PINK (Programme to maintain nuclear competence).

# Contents

<b>1</b>	<b>Introduction</b>	<b>1</b>
1.1	Introduction . . . . .	1
1.2	High Temperature Gas Cooled Reactors . . . . .	1
1.3	The Energy Conversion System . . . . .	5
1.4	Objective of Thesis . . . . .	8
1.5	Outline of Thesis . . . . .	8
<b>2</b>	<b>Calculational Means</b>	<b>11</b>
2.1	Introduction . . . . .	11
2.2	Wims7 . . . . .	11
2.3	Panther . . . . .	13
2.4	Thermix-Direkt . . . . .	14
2.5	Relap5/mod3.2 . . . . .	16
2.6	Talink . . . . .	17
2.7	ACM . . . . .	18
2.8	Code configurations . . . . .	18
2.9	Summary . . . . .	21
<b>3</b>	<b>Reactor Models</b>	<b>23</b>
3.1	Introduction . . . . .	23
3.2	The Panthermix Reactor Model . . . . .	23
3.3	The Relap5 Thermal Hydraulic Reactor Model . . . . .	29
3.4	The Point Reactor Kinetics Model for Relap5 . . . . .	33
3.4.1	Definitions and Terminology . . . . .	34
3.4.2	The Point Reactor . . . . .	37
3.4.3	Calculation of Point Kinetic Parameters $\bar{\beta}_{(j)}, \Lambda, Q$ . . . . .	39
3.4.4	Determination of reactivity curves $\rho_T(T)$ . . . . .	41
3.4.5	Xenon Fission Product Poisoning . . . . .	44
3.5	The ACM Reactor Model . . . . .	47
3.6	Summary . . . . .	47
<b>4</b>	<b>Energy Conversion System Model</b>	<b>49</b>
4.1	Introduction . . . . .	49
4.2	The Brayton Cycle . . . . .	49
4.2.1	Turbine . . . . .	51
4.2.2	Radial Helium Compressor . . . . .	55
4.2.3	Recuperator . . . . .	57

4.2.4	Precooler . . . . .	58
4.2.5	Shaft and Generator . . . . .	58
4.2.6	Valves . . . . .	58
4.3	ECS Control System . . . . .	59
4.3.1	Overspeed in Shaft Rotational Velocity . . . . .	59
4.3.2	Underspeed of Shaft Rotational Velocity . . . . .	60
4.3.3	Helium Inventory Control . . . . .	61
4.3.4	Configuration of Control System . . . . .	67
4.4	Summary . . . . .	68
<b>5</b>	<b>Stand-Alone Reactor Dynamics</b>	<b>69</b>
5.1	Introduction . . . . .	69
5.2	Operational Reactor Transients . . . . .	69
5.2.1	Inlet Temperature Increase 100°C . . . . .	70
5.2.2	Inlet Temperature Decrease 100°C . . . . .	75
5.2.3	Reduction of Mass Flow to 25% . . . . .	77
5.2.4	Reactor Response Time . . . . .	79
5.3	Evaluation of the Point Reactor Kinetics Model . . . . .	80
5.3.1	Change in Shape Function . . . . .	81
5.3.2	Loss of Coolant Incident . . . . .	87
5.3.3	Loss of Flow Incident . . . . .	89
5.3.4	Analysis of Recriticality Behaviour . . . . .	91
5.4	Conclusions . . . . .	96
5.5	Recommendations . . . . .	97
<b>6</b>	<b>Total ACACIA Plant Dynamics</b>	<b>99</b>
6.1	Introduction . . . . .	99
6.2	Transient Analysis . . . . .	99
6.2.1	Load Rejection - Bypass Closed . . . . .	99
6.2.2	Load Rejection - Bypass Open . . . . .	101
6.2.3	Part-Load Operation . . . . .	103
6.3	Conclusions . . . . .	105
6.4	Recommendations . . . . .	106
<b>7</b>	<b>Safety Related Transients</b>	<b>107</b>
7.1	Introduction . . . . .	107
7.2	Temperature Distribution of Pebble . . . . .	108
7.3	Cold Helium Ingress . . . . .	111
7.4	Maximal Temperature during Loss of Cooling . . . . .	113
7.5	Maximal Temperature during Transients . . . . .	115
7.5.1	Reactor Outlet Gas Temperature . . . . .	115
7.5.2	Maximal Fuel Temperature . . . . .	120
7.6	Conclusions . . . . .	122
7.7	Recommendations . . . . .	123
<b>8</b>	<b>Conclusions &amp; Discussion</b>	<b>125</b>

8.1	Conclusions . . . . .	125
8.2	Discussion . . . . .	127
	<b>Bibliography</b>	<b>129</b>
<b>A</b>	<b>Xenon Equations</b>	<b>135</b>
<b>B</b>	<b>Recuperator Efficiency and Correction</b>	<b>137</b>
<b>C</b>	<b>Energy Balance for Filling of Tank</b>	<b>139</b>
	<b>Nomenclature</b>	<b>141</b>
	<b>Summary</b>	<b>147</b>
	<b>Samenvatting</b>	<b>151</b>
	<b>Acknowledgement</b>	<b>155</b>
	<b>Curriculum Vitae</b>	<b>157</b>





# Chapter 1

---

## Introduction

---

### 1.1 Introduction

Due to their high energy efficiency, combined heat and power plants have become increasingly popular in the Netherlands. Usually a gas, coal, or oil fired station supplies the heat, which is partly converted to electricity, partly to high-caloric heat such as industrial steam. The low-caloric waste heat can be used for district heating. The Dutch ACACIA-project (AdvanCed Atomic Cogenerator for Industrial Applications) proposes to substitute the conventional heat source with a small nuclear reactor. The High Temperature Reactor (HTR) seems a suitable candidate for a number of reasons, to be discussed later in this introduction. The second innovative proposal in the ACACIA design is the omission of the heat exchanger separating nuclear coolant circulation and secondary, conventional steam cycle. Instead, the working fluid heated in the nuclear reactor is offered directly to the energy conversion system (ECS). Helium being the working fluid, this implicates the utilisation of a gas turbine and a compressor, and therefore the so-called direct Brayton cycle has been chosen as the thermodynamic cycle for the ECS.

### 1.2 High Temperature Gas Cooled Reactors

The HTR has a tradition that stretches back to the forties [1], when the first ideas about this reactor type took shape. They led to a reactor that utilises helium as coolant, graphite as moderator, and fuel in small particles as fuel geometry. These particles are coated with graphite and loaded into graphite fuel elements.

Above all other possible advantages of the HTR stands its potential to operate as an inherently safe reactor. The concept of 'inherently safe' can be interpreted as the impossibility of the reactor to reach a state where radioactive fission products are set free above predefined levels. This implicates the usage of passive safety measures, i.e.

measures that rely on natural processes to limit core temperatures in situations where all other active control fails, and that do not require human action.

In general the following arguments are given to stress the safety and advantages of HTRs:

- The billions of coated particles in which the fuel is dispersed each form a containment for the fuel inside, and can be seen as a miniature pressure vessel that can retain fission products up to temperatures of 1600°C. Burnups of 174 MWd/t have been achieved successfully [2]. The type of coated particle considered here, the TRISO-particle [3], has a fuel kernel ( $\approx 0.5$  mm diameter) around which a buffer layer is applied of porous graphite in order to absorb fission products and to accommodate kernel swelling. A second layer of pyrolytic carbon acts as the pressure vessel, a third layer of silicon carbide functions as a barrier against metallic fission products and provides extra strength, and a fourth coating of again pyrolytic graphite forms the last barrier in the coated particle. The diameter of the coated particle is around 1 mm.
- Graphite is a material with very high thermal conductivity, comparable to metals. Combined with the fact that the coated particles easily transfer heat due to their high surface/volume ratio, the heat transport from fuel to matrix graphite passes off smoothly. High local temperature gradients are avoided in the core.
- Graphite is the moderator in the core and can at the same time be utilised as a structure material. An advantage of a solid moderator is that its moderating behaviour is fairly constant, unlike the water moderator in water-cooled reactors that can change phase.
- The helium coolant is both chemically and nuclear inert. It does not react with graphite, cannot be activated and become radioactive, and does not interfere in the neutron moderation process. Furthermore, the heat transfer and transport are uniform and well defined because helium does not experience a phase change.
- The power density in a HTR is low, some ten to twenty times lower than in a boiling or pressurised water reactor. At the same time the heat capacity of graphite is high. The combination of low power density and high heat capacity in the core becomes important in the situation where the chain reaction has stopped and all heat is produced by radioactive decay of fission products. The decay heat density for a uranium fuelled reactor lies typically in the order of 6% of its power density during operation. This percentage rapidly declines after shutdown; to 1.5% after 1 hour and 0.5% after 24 hours. If a loss of active cooling is supposed, this decay heat has to be transported by passive means (free convection, radiation, conductivity) out of the core zone towards the reactor vessel wall where it can be dissipated. A low nominal power density helps limit the amount of heat to be transported to the reactor vessel wall, and a high heat capacity helps limit the temperatures during the transfer process: firstly because decay heat deposited in the core causes a relatively modest temperature increase, and secondly because the heat storage capacity 'buys time' for the decay process intensity that reduces with time.
- The fuel in the form of coated particles leaves much room for choice: the number of coated particles per fuel element (influences power density and moderator-to-fuel ratio), the fuel in the coated particles (particles with thorium, uranium and plutonium have been fabricated), or burnable poison instead of fuel.

- The HTR produces high temperature heat for process heat applications or electricity generation at high thermal conversion efficiencies. The application of the direct Brayton cycle instead of a secondary steam cycle further enhances the high efficiency potential. If optimised for electricity generation the efficiency reaches around 44%, for cogeneration typical figures are 35% for electric efficiency and 30% for thermal efficiency when high quality industrial steam is produced. Heat applications for refinement of fossil fuels [4], hydrogen and ammonia production [5], maritime propulsion [6], etc. were/are envisaged.

Summarising, the HTR potential to fulfill the requirement for inherent safety lies primarily in the combination of a low power density and a very high temperature up to which the coated particles can retain the fission products.

From the beginning the HTR development has evolved along two main tracks, that differ in the choice how to fuel the reactor:

- The prismatic or block-type HTR. In this reactor the coated particles are loaded in cylindrical fuel compacts that are inserted in prismatic graphite fuel elements, figure 1.1. These elements contain other holes for control rods, flow of coolant gas, and rods with burnable poison. This reactor type has been propagated by the United States, United Kingdom, and more recently by Japan, France and Russia. Predecessors (with cylindrical fuel) of the prismatic type are the Peach Bottom [7, 8] and Dragon [9–11] reactors built in the sixties, and decommissioned in the seventies. The follow-up power reactor of Fort St. Vrain [12, 13] has operated from 1981 to 1990. Recently, in 1998, the Japanese test reactor HTTR [14, 15] reached first criticality. The United States, Russia, Japan and France have joined in a project for weapon-grade plutonium burning in the GT-MHR [16], based on the conceptual design of the MHTGR [17, 18].
- The pebble-bed type HTR. In this reactor the coated particles are loaded in spherical graphite elements the size of a tennis ball, figure 1.2. Such a pebble typically contains ten- to twenty thousand coated particles bedded in a graphite matrix of 5 cm diameter. This fuel zone is protected by a layer of graphite, which gives the pebble a total diameter of 6 cm. A randomly packed bed of these spheres in the core cavity of the reactor forms the core. The coolant flows through the bed, normally from top to bottom. Depending on the size of the core, control rods are inserted directly into the bed, or into the reflector encircling the bed. This reactor type has been developed and tested in Germany, first with the AVR test reactor [19, 20] and later with the THTR power reactor [21–23]. China [24–26] is currently building a test reactor, South-Africa starts the building of a series of power reactors, the PBMR [27–29], in the near future. The Netherlands performed a pre-feasibility study for nuclear cogeneration, INCOGEN [30] (INherently safe nuclear COGENeration) which, after some adaptations to the conventional part of the plant, has been renamed ACACIA [31]. Furthermore, it has been investigated whether this reactor is suitable to burn plutonium [32].

In the Dutch nuclear programme on HTRs the pebble-bed type reactor has been chosen on the following grounds:

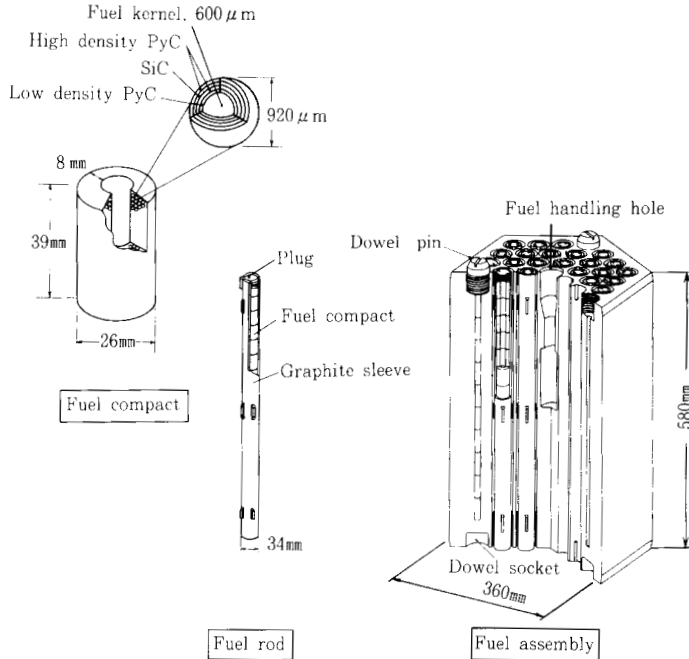


**Figure 1.1:** Hexagonal fuel element.

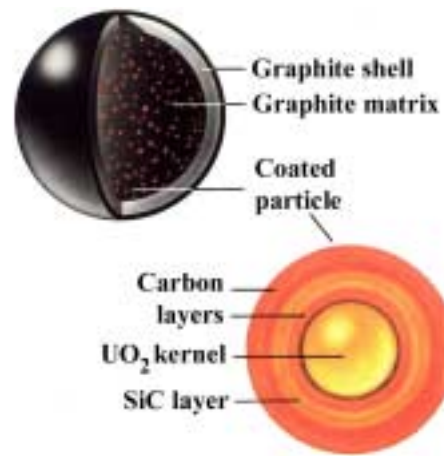


**Figure 1.2:** Spherical fuel element (diameter 6 cm).

- The overreactivity in the core is minimal. On-line fuelling is possible by adding fresh fuel pebbles on top of the bed; typically tens of pebbles per day are added. In contrast, the prismatic fuel is loaded in batches that contain fuel for about a year, and the excess reactivity at the beginning of the cycle is considerable. Neutron absorbing material is therefore added to the fuel elements that slowly disappears over the year.
- The required thermal power for the ACACIA system is modest, 40 MW<sub>th</sub>. In general, higher power densities can be reached safely with the prismatic fuel HTR than with the pebble-bed type, at the cost of high complexity in fuel management. Almost every fuel element block is loaded with coated particle compacts differing in enrichment in order to suppress peaking in the power density. Together with the fact that around 75% of the core consists of graphite (60% for a pebble-bed), which increases the heat capacity and thus limits maximal temperatures during transients, the power output can be higher for a prismatic core than for a pebble core. If simplicity in fuel management and control system is valued higher than power output, as is the case for the ACACIA, normally the pebble-bed type reactor is chosen. If nonetheless more power is necessary, more modular units of pebble-bed reactors can be installed [33, 34].
- At the time of making the decision to choose the fuel type, the German TRISO coated particle and pebble production had reached higher integrity on industrial scale than the production elsewhere. Nowadays, it is assumed that the Japanese producers equal this standard.

The fuel management in a pebble-bed type reactor knows three strategies, listed in order of decreasing complexity and power density:

1. The multipass scheme, as used in the AVR and THTR. Pebbles are added to the top of the bed, and extracted at the bottom. The burnup grade is measured, and if below a certain value the pebble is added again to the top of the bed. The result is a more or less constant pebble-bed height, with a rather flat power profile. It is

an efficient method to use fuel, but refuelling and measuring equipment is required which increases the complexity of the reactor. Furthermore, the extraction of pebbles can present problems, as has been experienced in the past [23].

2. The once-through-then-out (OTTO) scheme [35–37]. Pebbles are extracted at the bottom and discarded without measuring burnup, and new pebbles are added to the top of the bed. The pebble-bed height remains more or less constant. In this scheme the recycling and measuring equipment is not necessary, which enhances the simplicity of the reactor.
3. The peu-à-peu scheme [38–41]. The pebble-bed starts with a large cavity above it. Pebbles are added but not extracted, resulting in a steadily increasing core height. After a certain period of time the core is full, and all pebbles are discharged. This requires a complete shutdown for the reactor once every 5 to 10 years, depending on the design. In this scheme, possible problems with extraction of pebbles are avoided during operation.

The ACACIA design envisages a simple reactor design and operation, and therefore the peu-à-peu scheme has been chosen.

For the same reason, there is an inclination towards reactor operation without control rods. The control rods of the ACACIA reactor are placed in the side reflectors around the core. In principle it is possible - after the initial startup phase - to operate the reactor without control rods, as there is little overreactivity present in the core. It will be investigated in this thesis whether this is possible in terms of safety, and if so, whether it is desirable.

## 1.3 The Energy Conversion System

In the ACACIA [31, 42] design, figure 1.3, the direct<sup>1</sup>, closed<sup>2</sup> Brayton cycle [43] is used as thermodynamic cycle for the ECS. It resembles the Rankine cycle for steam cycles, but a single phase gaseous working fluid (helium) is used instead of a condensing fluid. The system consists of a single-shaft turbine-compressor with a directly coupled electricity generator. A precoolers before the compressor and a recuperator further enhance the overall efficiency. The cycle is shown in figure 1.4.

The advantageous combination of a HTR with the direct, closed Brayton Cycle as energy conversion system (ECS) had already been recognised in the forties [44]. A decade later, confidence had grown about the technical feasibility of operating such a cycle [45]. This is understandable as the jet propulsion of aeroplanes made great progression during the fifties and in fact relies on the open Brayton cycle. At the

---

<sup>1</sup>The specification 'direct' refers to the heating of the working fluid. If the heat source uses a separate cycle and a heat exchanger to transfer heat, the cycle is termed indirect. If the working fluid in the Brayton cycle is heated without intervention of a heat exchanger, the cycle is termed direct.

<sup>2</sup>The specification 'closed' refers to the use of the working fluid for the cycle. The open cycle utilises air from the environment as working fluid, which is sucked in, mixed with fuel and ignited. The hot gas is used for power generation in a gas turbine and is rejected afterwards to the environment as exhaust gas. In the closed cycle the working fluid is heated without consuming it, and after completing the thermodynamic cycle the same molecules are available for a new circulation.

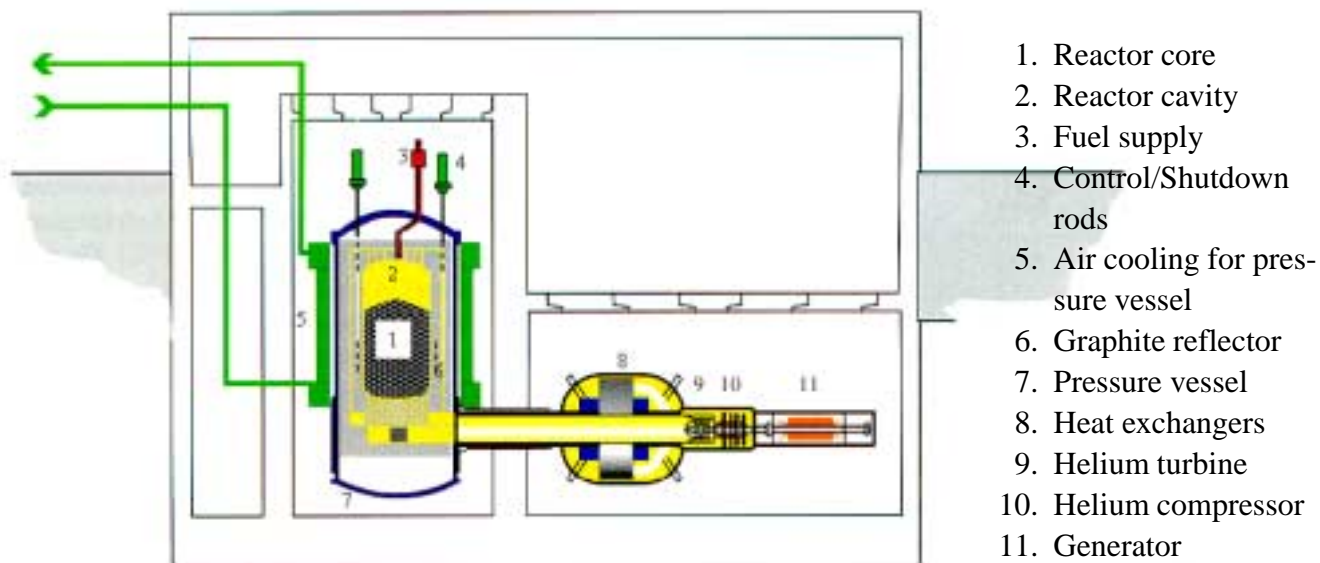


**Figure 1.3:** *The layout of the ACACIA plant.*

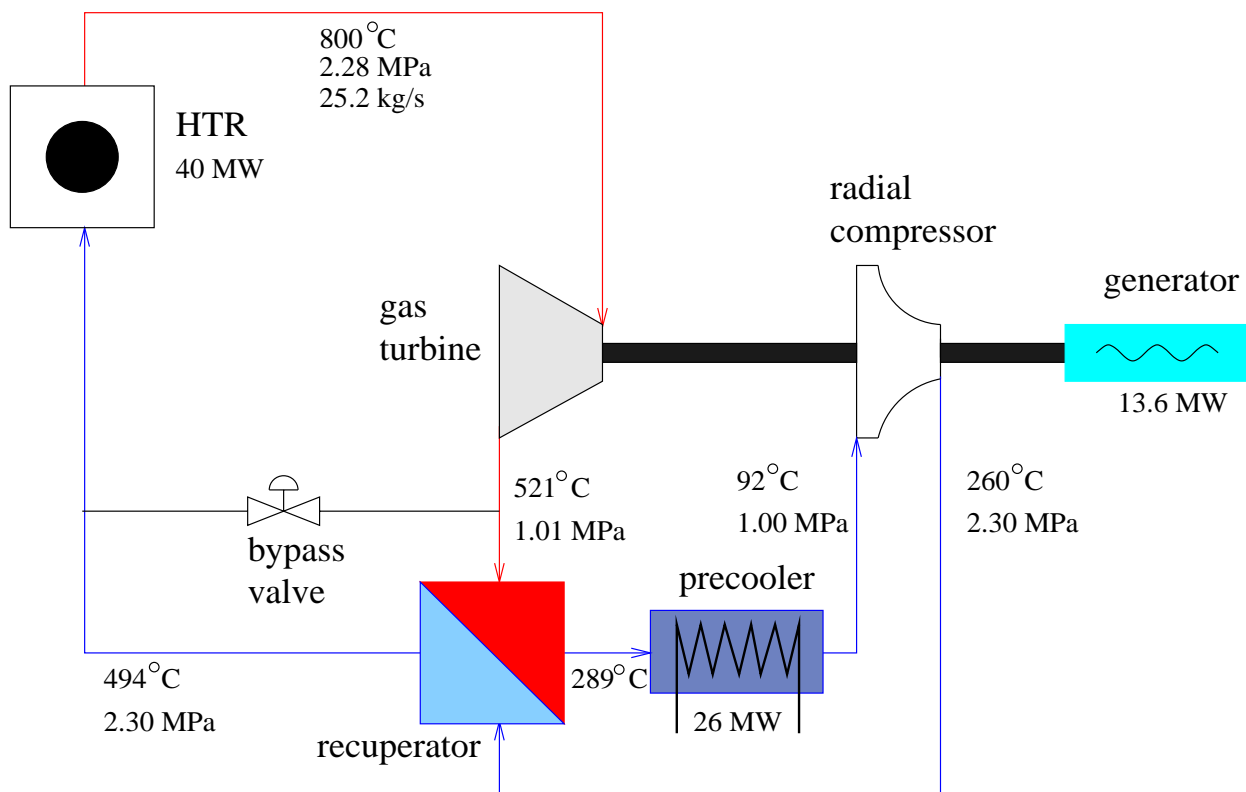


**Figure 1.4:** *The schematic Brayton cycle of the ACACIA plant.*

same time it was realised that the operation of a gas turbine was one thing, but to operate it reliably at the high temperatures proposed for the direct Brayton cycle with the HTR quite another. Together with the uncertainties at the time about the contamination of helium with fission products, it led to the development of HTRs with indirect thermodynamic cycles. Helium is heated in the primary cycle and transfers heat via a heat exchanger to the secondary cycle. For all commissioned HTRs for power production the secondary cycle has always been a steam cycle.

It took some further forty years of turbocompressor evolution before a serious direct cycle design was presented again in the nineties by General Atomics in the form of the GT-MHR [16], the redesign of MHTGR [17, 18]. Due to the lack of a launching customer this project never saw realisation up till now. The South-African energy utility ESKOM, however, decided in the mid-nineties that the growing domestic electricity demand had to be met by building HTRs, it being the most economical alternative. Expert knowledge was claimed in the field of hydrogen gas turbines, previously used for enrichment of uranium for nuclear devices. Together with the German experience of the Oberhausen gas turbine technology [46], it gave the confidence to choose for the direct Brayton cycle. The rewards are high in terms of economy when compared with the indirect steam cycle:

- the thermodynamic efficiency for the direct cycle is higher, as the highest temperature  $T_{max}$  in the direct Brayton cycle is higher than in the indirect steam cycle. Both cycles reject their waste heat at the same temperature  $T_{min}$ . The theoretical upper limit for the cycle efficiency, the Carnot efficiency  $\frac{T_{max}-T_{min}}{T_{max}}$ , is therefore higher in the direct cycle.
- the high temperature heat exchanger is no longer necessary in a direct cycle.
- the Brayton cycle requires fewer components.
- the Brayton cycle utilises relatively few and compact components.
- the risk of water ingress can be avoided in the Brayton cycle by using a helium-helium precooler.
- the ability to control the generator output power of the direct Brayton cycle by adjusting the amount of helium circulating in the system. This type of control hardly affects the working point of the cycle, as cycle temperatures and flow velocities do not change at partial power. As a result, even at low power output when only a proportionally small part of the helium inventory circulates, a high efficiency close to nominal can be attained. During these transients helium is stored in or retrieved from large storage vessels [47]. The removal or injection of helium from or to the ECS is a slow process (minutes) and will only be used for long term adjustments. For instantaneous generator power reduction a bypass valve over reactor and turbine is used.

These advantages amply compensate the drawbacks of the Brayton cycle:

- although the coated particles perfectly retain the fuel and fission products, there is a fabrication failure chance of  $2 \cdot 10^{-5}$  for a particle [3]. The released fission products are transported by the helium flow into the ECS, where they precipitate on the cooler surfaces.

- the closed, direct Brayton cycle is relatively new and cannot claim 'proven technology'.

## 1.4 Objective of Thesis

As the layout of this introduction shows, the HTR and ECS are often treated as systems that are developed separately, and integrated as far as determining each other's boundary conditions, so to speak. For steady-state modelling this approach can be justified, however, for transient analysis this can lead to inaccuracies.

It is therefore the main objective of this thesis to investigate the dynamics of the total, integrated system of HTR and ECS. This comprises the analysis of incident transients and operational transients. In this study the emphasis will lie on the reactor, in a complementary study by Kikstra the emphasis will lie on the ECS [48].

The general goal can be subdivided in several targets:

- development of a calculational system that couples the dynamic calculations for the HTR to the dynamic calculations for the ECS. Combining the two systems renders the assumptions superfluous that otherwise have to be made concerning time evolution of the boundary conditions of the two separate calculations. Until recently, long calculation times frustrated simultaneous, coupled calculations, but with faster computer hardware becoming available the combination of code packages gains in interest [49].
- construction of a detailed 3-dimensional calculational model for the HTR. The HTR model used in the INCOGEN and ACACIA study will be used as a basis, and as such the model does not have to be built from scratch.
- construction of a model for the ECS. This model has to be built from scratch. The code selected for modelling is a well proven nuclear code for steam cycle application, but with very limited experience in helium cycles. Especially the development of the gas turbine and compressor model will require much attention.
- transient analysis of the HTR, the ECS, and the total system.
- improvement of the reactor and ECS design as a result of the transient analysis.
- improvement of the calculational system. Is it possible to reduce calculation time by simplifying for instance the 3-D reactor model without compromising accuracy?

These subjects will be discussed in the following chapters.

## 1.5 Outline of Thesis

The transient analysis for the ACACIA system has been performed by two studies, one of which is presented in this thesis, and the other in the thesis of Kikstra [48]. This thesis focuses on the HTR reactor modelling, and assumes less detail for the ECS model; the other focuses on the ECS modelling and assumes an uncomplicated



reactor model. The models have been developed with entirely different codes, and can therefore be used for verifying each other.

This thesis contains the following chapters:

Chapter 2 presents the calculational means that will be utilised to construct the code system that couples the dynamic reactor calculations with the dynamic calculations for the ECS. Essentially, the codes used to build the reactor and ECS models are available, but require adaptations for the coupling. A total of four code configurations is presented, each differing in detail and calculation time.

Chapter 3 presents three reactor models that have been built to model the ACACIA reactor. The reactor dimensions and specifications can be found in this chapter. These reactor models all consist of two parts; one part for the neutronics, one part for the thermal hydraulics of the reactor. A detailed reactor model will be discussed (3-dimensional in neutronics and 2-dimensional in thermal hydraulics), a less detailed model (0-dimensional in neutronics (point reactor) and 2-dimensional in thermal hydraulics), and the simplest model (0-dimensional in neutronics (point reactor) and 1-dimensional in thermal hydraulics).

Chapter 4 presents the model for the ECS. Each component in the ECS will be discussed in detail, especially the dynamic components like the turbine and compressor. Componentwise comparison with the more detailed model [31, 48, 50] shows that a 1-dimensional description of the helium flow gives good results. The control philosophy of the ECS will be discussed, and an analytic description of the helium inventory control system with storage tanks for load following will be presented.

Chapter 5 presents dynamic calculations for the stand-alone reactor. The three reactor models discussed in chapter 3 and the reactor model from Kikstra [48] will be compared. The aim of the chapter is to decide what model should be used in which situation, and what level of detail is desirable when taking into account computing time.

Chapter 6 presents dynamic calculations for the total ACACIA plant. The results are compared to the results of Kikstra.

Chapter 7 presents a safety analysis for the reactor. Corrections to former calculations are discussed and a grid is constructed in which all possible worst-case reactor states are depicted in terms of maximal fuel temperature as a function of helium mass flow rate, inlet temperature and thermal power. A similar grid has been constructed in terms of reactor outlet gas temperature as a function of the same parameters. Both grids yield valuable information about which reactor conditions should be avoided. Changes in design turn out to be necessary, and suggestions will be given.

Chapter 8 presents the final conclusions of this thesis.

At the end of the thesis three appendices are added that give some extra information on intermediate calculation steps used for the modelling.



# Chapter 2

---

## Calculational Means

---

### 2.1 Introduction

This chapter discusses the calculational tools that have been used to model the high temperature reactor (HTR) with its energy conversion system (ECS). A number of 4 interconnected codes (computer programs) together shape the full reference model, plus an extra code to supply the required nuclear database:

- Wims7: creation of nuclear database
- Panther: calculation of the core neutronics
- Thermix-Direkt: calculation of the pebble-bed heat transfer
- Relap5/mod3.2: calculation of thermal hydraulics in ECS
- Talink: control over data transfer between Panther and Relap5

In the following subsections the codes will be discussed in more detail. The last section explains why and how these codes are interconnected. Three code configurations are used, each with a different degree of detail, accuracy, and calculation time.

A fourth code system is formed by ACM [51], an equation solver used to model both the HTR and the ECS system. The model has been developed independently at the Delft University of Technology, and serves as comparison.

### 2.2 Wims7

The first step in the reactor analysis involves the Wims7 code [52] which acts here as a lattice code generating a database of cell constants. All calculations are performed in steady state situations and therefore no kinetic parameters are involved. The nuclear database - in this case - will contain macroscopic cross sectional data for 2 energy groups for all reactor materials, depending on irradiation, temperature, and xenon density. In this case Wims7 calculated the database using the UK Nuclear Data Library (UKNDL) based 69-group '1986' cross section library [53, 54] with information about mixtures

of the resonance absorbers with various amounts of hydrogen in order to provide a table of the resonance integral versus the potential (or background) scattering cross section. The two forms of shielding by resonance absorbers, i.e. energy and spatial shielding, are treated by equivalence theory [55, 56] and the subgroup method [57]. The equivalence equations relate the heterogeneous problem under consideration to an equivalent homogeneous model with appropriate cross sections. In order to improve accuracy, Wims7 in addition contains a special module which can explicitly treat the double heterogeneity for the granular fuel. This is possible both for the resonance shielding calculations by the subgroup method [57] and the subsequent multi-group transport calculations. The fact that these fuel grains are again enclosed by a pebble is modelled by an equivalent cylinder approximation. A good agreement between equivalent cylinder and spherical unit cell has been observed [58, 59].

Part of the neutrons in a nuclear reactor do not arise directly from fission, but are emitted by some fission products, the delayed neutron precursors. As long as these neutrons make the difference between the subcritical and critical reactor state, the effects of a change in neutron population always lag behind. This gives the control system or operator of the reactor time to make adjustments. Obviously, the delayed neutrons very much influence the time behaviour of the reactor and therefore have to be taken into account for transient analysis. According to the decay time of the precursors, the delayed neutrons are divided in - normally - 6 time groups. In section 3.4 the effect of the delayed neutrons will be discussed in further detail.

Although Wims7 does not explicitly take into account the emission spectra of the delayed neutrons and assumes them to be part of the prompt spectrum, it does have the values for the delayed neutron group fractions for time group  $j$ ,  $\beta_j^q$ , hard-coded in it in order to provide transient codes such as Panther with delayed neutron data. Wims7 contains delayed data for the nuclides  $q = {}^{235}\text{U}$ ,  ${}^{238}\text{U}$ ,  ${}^{239}\text{Pu}$ ,  ${}^{240}\text{Pu}$ , and  ${}^{241}\text{Pu}$ . Table 2.1 gives the group delayed fractions that Wims7 offers to Panther. During burnup calculations, the nuclide densities vary and therefore  $\beta_j$  will vary, the overall delayed fraction based on the nuclide densities  $N^q$  and individual delayed fractions  $\beta^q$  for nuclide  $q$ . The delayed fraction Wims7 passes to Panther for each energy group  $g$  for a burnup step is given by:

$$\beta_{g,j} = \frac{\sum_q \beta_j^q \nu_g^q N^q(r) \sigma_{f,g}^q}{\sum_q \nu_g^q N^q(r) \sigma_{f,g}^q} \quad (2.1)$$

Here  $\nu_g^q$  is the number of neutrons emitted per fission by nuclide  $q$  in energy group  $g$ , and  $\sigma_{f,g}^q$  the microscopic fission cross section of nuclide  $q$  for group  $g$ . Clearly,  $\beta_j^q$  is only weighted by the group fission constants of energy group  $g$  in order to obtain energy group constants, and in advance of section 3.4.2 one notes two things: when collapsing to a few energy group structure, Wims7 refrains from weighting the  $\beta_j$  with a) the appropriate delayed neutron emission spectrum  $\chi_j(E)$  and b) the energy part of the adjoint function  $\Phi_0^\dagger(r, E)$  as in equation (3.18). As such, it neglects that delayed neutrons are more successful in inducing new fissions, because they generally appear well below the average prompt neutron energy and have a higher non-leakage prob-

ability. For some systems the increase in the effective value of  $\beta_j$  can be as large as  $\approx 20 - 30\%$ ; for a  $^{235}\text{U}$ -fueled HTR typically a few percent can be expected, [60]. The error of assuming a prompt spectrum for the delayed neutrons will then be small, knowing that the delayed fraction itself is already small,  $\approx 0.7\%$  for  $^{235}\text{U}$ . Furthermore, the neglect is conservative as the reactor behaviour now depends more on prompt neutrons.

**Table 2.1:** The group delayed neutron fractions  $\beta_j^q$  in Wims7\* for groups  $j = 1, \dots, 6$ .

$j$	decay constant [s <sup>-1</sup> ]	half life [s]	$^{235}\text{U}$	$^{238}\text{U}$	$^{239}\text{Pu}$	$^{240}\text{Pu}$	$^{241}\text{Pu}$
1	0.0127	54.67	2.506E-4	1.964E-4	8.008E-5	7.959E-5	6.476E-5
2	0.0320	21.66	1.541E-3	2.306E-3	6.825E-4	7.991E-4	1.408E-3
3	0.128	5.415	1.339E-3	1.799E-3	3.377E-4	3.852E-4	5.147E-3
4	0.304	2.280	2.588E-3	6.705E-3	8.148E-4	1.092E-3	2.232E-3
5	1.35	0.5134	8.915E-4	4.202E-3	2.437E-4	3.725E-4	1.057E-3
6	3.63	0.1909	1.643E-4	1.160E-3	5.223E-5	8.278E-5	1.738E-4
total			6.774E-3	1.637E-2	2.211E-3	2.811E-3	1.008E-2

\* In fact, in Wims7 the 3<sup>rd</sup> delayed group for  $^{241}\text{Pu}$  has been hard-coded incorrectly as 5.147E-4. The value given in this table is correct and will be tabulated in subsequent Wims versions [61].

## 2.3 Panther

The Panther code [52] calculates a steady-state or time-dependent power distribution in a reactor, taking into account the thermal hydraulic feedback of the produced heat on the cross section data. Panther solves the few energy group time dependent diffusion equations in Cartesian coordinates at position  $r = (x, y, z)$  for each neutron energy group  $g$  for  $g = 1, \dots, G$ , and delayed precursor groups  $j$  for  $j = 1, \dots, J$ :

$$\begin{aligned} \frac{1}{v_g} \frac{\partial \Phi_g}{\partial t} - \mathcal{R}_g \Phi_g + \Sigma_{r,g}(r) \Phi_g(r) &= \sum_{g'=1}^G \Sigma_{s,g'g}(r) \Phi_{g'} + \\ &+ \frac{\chi_{p,g}}{k} \sum_{g'=1}^G \left( 1 - \sum_{j=1}^J \beta_{j,g'}(r) \right) \nu(r) \Sigma_{f,g'}(r) \Phi'_g + \chi_{p,g} \sum_{j=1}^J \lambda_j C_j(r), \end{aligned} \quad (2.2)$$

with  $\mathcal{R}$  the diffusion operator operating in the radial and axial direction:

$$\mathcal{R}_g = -\nabla_R D_{R,g} \nabla_R - \frac{\partial}{\partial z} D_{z,g} \frac{\partial}{\partial z} \quad (2.3)$$

with the diffusion coefficient given by  $D = (D_R, D_z)$ . The parameter  $v_g$  is the neutron velocity,  $\Phi_g(r)$  the neutron flux,  $\Sigma_{f,g}$  the fission cross section,  $\Sigma_{r,g}$  the removal (absorption + outscattering) cross section,  $\Sigma_{s,g'g}$  the cross section for scattering from group  $g'$  to  $g$ ,  $\chi_{p,g}$  the prompt fission spectrum for group  $g$ ,  $k$  the effective multiplication factor,  $\beta_{j,g}$  the fraction of the delayed neutrons for precursor group  $j$  that are produced in energy group  $g$ ,  $\lambda_j$  the decay constant for delayed precursor group  $j$ ,  $\nu$  the number

of neutrons emitted per fission, and  $C_j$  the precursor concentration. The precursor concentrations are given by the equations:

$$\frac{\partial C_j}{\partial t} = \sum_{g=1}^G \beta_{j,g} \frac{\nu \Sigma_{f,g} \Phi_g}{k} - \lambda_j C_j(r) \quad (2.4)$$

As mentioned in the previous section, Panther accepts the delayed neutrons in this scheme as if they have a prompt fission spectrum. Any correction for the delayed spectra must be performed previously in Wims7 and enters the Panther calculations through effective values of  $\beta_{j,g}$ . Provided that this correction has been made the scheme is adequate for a few group calculation, as in that case both delayed and prompt neutrons appear in the highest energy group anyway.

Many books [55, 62, 63] treat the derivation of the diffusion equation (2.2) from the exact transport equation (to be introduced in chapter 3 as equation (3.8)), and therefore only the validity of the most important approximation will be discussed here: the flux is only linearly anisotropic. This enables one to remove the directional dependence from the flux by integration over the solid angle  $\Omega$ :

$$\int_{4\pi} d\Omega \Phi(r, E, \Omega) = \Phi(r, E) \quad (2.5)$$

This approximation is violated

- near localised sources,
- in strongly absorbing media,
- near boundaries or where large changes in material properties are to be expected within a distance of a mean free path.

The first two items give no problems in the present reactor, the third one does. In the transitions from graphite to gas in the cavity above the core the diffusion coefficient changes from centimeters to near infinite. This problem has been overcome in the model by defining an axial and radial diffusion coefficient for the gas-filled regions, specific for the dimensions of the reactor cavity above the pebble-bed [64]. Such diffusion coefficients restore the neutron current densities at a boundary between solid and gas. The reaction cross sections have been set to zero in the cavities. For the present calculations the gas diffusion coefficients have been determined for one pebble-bed height; in future calculations this value can change with cavity size but the effect will be marginal.

As the thermal hydraulic model in Panther is not capable of modelling heat transfer in a pebble-bed configuration, the code Thermix-Direkt - to be discussed in the following section - replaces the built-in model.

## 2.4 Thermix-Direkt

The Thermix-Direkt code [65, 66] calculates, in  $(r, z)$ -coordinates, the temperature distribution in the pebble-bed due to heat transport by conduction, radiation, and convection (natural and forced), given a power distribution and coolant flow conditions.

The code can perform both steady-state and transient calculations. Relations for for instance the conduction or heat transfer coefficients in the pebble-bed are partly empirical, partly exact with fitted parameters [67]. These relations have been validated by numerous experiments with the AVR test reactor which date back into the seventies [68]. In addition, tests with non-nuclear pebble-beds in the seventies [69] and eighties [70] have also been utilised in order to validate the code.

The Thermix-Direkt code replaces the internal Panther thermal hydraulics module and can be seen as a new module for Panther. It offers the temperature distribution that Panther needs for the neutronic calculation and production of the corresponding power distribution. In order to stress the integrated character of Thermix-Direkt and Panther, the combination has been named Panthermix [71, 72].

As the name suggests, Thermix-Direkt is a combination of two codes: Thermix, which solves the heat conduction equation for the solid materials, and Direkt, which solves the equations describing heat transfer by convection.

## Thermix

The Thermix code has been developed in order to describe the heat transport by conduction within a pebble-bed HTR. Although its uniqueness lies in the treatment of the pebble-bed, the reflector regions, cavities and piping can also be included in the model. For each  $(r, z)$ -mesh point an appropriate material composition can be defined, if necessary with a certain degree of porosity when part of the mesh volume has to be occupied by a fluid. The solid part of the mesh volume is homogenised with respect to conductivity, heat capacity, and heat transfer, such that only one local temperature characterises the solid temperature of a mesh volume. This approach is only valid if the heat production in a fuel pebble is low, resulting in low temperature gradients. This is the case for incidents with a scrammed reactor, but in general not for operational transients. In that case the heterogeneous solid structure model in Thermix may be used [65], or the (more straightforward) approach presented in chapter 7.

The temperature distribution of the solid structures is described by the time-dependent heat conductivity equation with temperature dependent material constants:

$$\rho_s(T)C_s(T)\frac{\partial T}{\partial t} = \nabla \cdot (\lambda_s(T)\nabla T) + q_n''' + q_c''' \quad (2.6)$$

Here  $\rho_s(T)$  is the solid structure density and  $C_s(T)$  the heat capacity at temperature  $T$ . The parameter  $\lambda_s(T)$  is the effective conductivity which consists of possible contributions in conductivity by the fluid, the solid structure and by radiation. The possible heat sources in a mesh volume are denoted by  $q_n$  and  $q_c$  for the nuclear and convective contribution, respectively. The quotes denote the volumetric value, W/m<sup>3</sup>. Panther supplies the value for  $q_n$ , Direkt the value for  $q_c$ .

## Direkt

The Direkt code has been developed in order to solve the time-dependent equations for convection and to establish the gas temperature distribution for the reactor. As such, it can be seen as the complementary calculation of Thermix, that is, it describes the fluid part of a mesh volume. The heat convection calculation allows cross element heat transfer in order to describe the circulation and eddying of the gas in the pebble-bed in transient cases with a halted mass flow rate.

The first step towards obtaining the gas temperature distribution is taken by combining the equations of continuity and motion, which yield as solution the pressure and mass flow rate distribution over the reactor at fluid temperatures of the previous iteration. The second step consists of solving the energy equation with as input the new pressure and mass flow rate distribution and the solid temperature distribution from Thermix in order to determine the new gas temperature distribution. By iteration over the two steps convergence is reached in the solutions. When the new gas temperature distribution is known, the convective source  $q_c$  needed in Thermix can be made explicit by using Newton's law of cooling:

$$q_c = \alpha A(T - T_g) \quad (2.7)$$

The parameter  $T_g$  is the gas temperature at which the heat transfer coefficient  $\alpha$  is defined,  $A$  is the surface for heat transfer. Section 3.3 treats the determination of  $\alpha$  in detail.

## 2.5 Relap5/mod3.2

The Relap5/mod3.2 code [73] has been developed for transient simulation of the light water reactor ECS during operational transients and postulated accidents. A generic modelling approach is used that permits simulating a variety of thermal hydraulic components with their control systems. The hydrodynamic model is a two-fluid model for flow of a two-phase steam-water mixture that allows noncondensable components (e.g. helium) in the steam phase and/or a soluble component in the water phase. It is possible to use Relap5 with only helium and no steam, and in that case the working fluid only exists in one phase and behaves like an ideal gas. This is quite a simplification as many empirical rheological models are no longer necessary in the ECS calculations. On the other hand, from a well known code, validated and tested with experiments [74], one enters an area in which virtually no testing and benchmarking has been done. However, reasoning that all mass and energy balances are still valid, and that the correct properties of helium are present in the code (subroutine rnoncn.f), it seems that there is no fundamental objection to using the code with helium as working fluid. Simple analytical problems such as pressurised helium flowing into or from a tank have been tested and are calculated correctly. More serious problems are to be expected with the two main dynamic components, the turbine and compressor. There is a basic gas turbine model - not validated - which has been used in developmental stages



and then only as a single stage turbine. This component will be discussed in section 4.2.1, where a model for a 4-stage turbine will be presented with improvements in the equations describing the turbine. The gas compressor altogether lacks as a component, which is understandable: water cooled systems use a pump to make up for pressure losses and the water is pressurised in the liquid phase. The solution for this problem is to construct a new compressor model, which will be described in section 4.2.2. For the dynamic reactor behaviour a space-independent point reactor kinetics model is present in Relap5. The point kinetics formulation requires core-layer averaged temperatures and reactivity feedback coefficients to determine a total reactivity for driving the kinetics calculation of total core power. Once the total core power has been determined, it is then distributed among the core layers in an invariant manner (fixed power profile). This model, together with the determination of the reactivity feedback coefficients and the power profile, is described in detail in section 3.4.

## 2.6 Talink

The Talink code [75] has been developed in order to control the data transfer required for the execution of a set of coupled transient analysis codes performing their calculations in separate operating system processes. The Talink code is regarded as being the governing component in this transfer structure with the other codes as clients. In order to provide flexible data coupling, the data values transferred by Talink are stored in its internal data base. The user can specify operations to be performed on the data before transfer. Talink writes the requested data in a temporary file which is read by the client code. In addition to the data transfer files another set of files is created and checked to identify when each data transfer operation can begin. Part of the preparatory work for this thesis has been the correct implementation of this communication software.

In the current situation Panther and Relap5 are the client codes that wish to exchange the data. In turn, Panther can pass some of the data to Thermix-Direkt. In general, Relap5 will offer the new inlet conditions for the core, based on the core outlet conditions Panther supplied to it at the start of the time interval. The Relap5 program will then temporarily be halted by Talink<sup>1</sup> until Panther and Thermix-Direkt have processed the data and come up with new core outlet conditions. At that moment the data transfer between Relap5 and Panther takes place, and a new time step starts. Notice that Talink lets the codes communicate with time intervals of typically several seconds, but that Relap5 internally has to divide such a time interval in transient time steps in the order of milliseconds in order to obtain a stable calculation of the transient behaviour.

---

<sup>1</sup>For the current calculations Relap5 has always been the first to complete the time step for data transfer. If it were the slowest, then Panther would have to wait and would temporarily be halted.

## 2.7 ACM

The ACACIA has been modelled by Kikstra with the help of the equation-solver ACM. In the ACM-code the flow path in the different components (recuperator, reactor, compressor, etc.) is axially divided in a number of so-called thermal nodes, which are small volumes, assumed to be perfectly mixed and to have a constant cross-sectional area [50]. For these thermal nodes, the mass- and energy-balances are solved. The mass flow rate between these volumes is determined by solving the momentum-balance for a flow node, which consists of the two halves of neighbouring thermal nodes. This so-called staggered grid is chosen because of its numerical stability. The model allows for negative flows, which can be necessary for incident analysis.

The mass- and momentum-balances are solved with second-order central schemes. In the momentum balance the effects of friction losses, area change, gravitational forces and forces in turbo-machinery and pumps are taken into account. The discretisation with a second order central scheme is a valid approximation as long as the velocities stay well below the velocity of sound. Choked flow therefore uses a different, specialised model.

The energy-balance is modelled with an upwind scheme. The incoming energy is only influenced by the upstream node, which leads to physically realistic behaviour under all circumstances.

The solid construction of most pieces of equipment are also discretised in flow direction only. For the reactor model however, a two-dimensional discretisation is used. The wall model is capable of combining internal heat production, convective heat transport from and to a fluid, and heat transfer by conduction to four surrounding wall elements. Closure of the set of equations describing the interaction between the one-phase and two-phase flow models and solid construction model is reached after insertion of empirical and/or component-specific relations for the source terms like e.g. energy-production in the reactor, heat input and forces in the turbo machinery, heat transfer and (two-phase) friction in the heat exchangers and a slip-velocity correlation for the two-phase flow.

The ACM model uses two-phase flow models in order to model the secondary cycle that produces steam for industrial applications. That study lies outside the scope of the current thesis, but is fully analysed in the thesis of Kikstra [48].

## 2.8 Code configurations

In the following chapters the calculations will be performed with the codes mentioned above. It is one of the goals of this thesis to establish what detail is necessary to model in order to achieve a certain accuracy. Therefore three different configurations have been built for the current study, each differing in detail. The three options are:

- Firstly there is the most detailed method of calculation, displayed in figure 2.1. This involves the full 3-D neutronic core calculations with Panther, the 2-D heat transfer calculations for the core with Thermix-Direkt, and the 1-D thermal hydraulic calculations for the ECS with Relap5. This detail comes at the cost of long calculation

times, mainly due to data transfer between the codes. The data transfer has been organised such that Relap5 supplies the core inlet helium temperature, the helium mass flow rate and core outlet helium pressure; in return it receives the pressure drop over the pebble-bed, and the heat absorbed by the helium flow, both determined by Thermix-Direkt from the Panther power distribution. The absorbed heat is 'dumped' into the helium circulation, if the mass flow rate is stable this should give the same helium temperature increase as calculated by Thermix-Direkt. The mass flow rate is slightly obstructed in the Relap5 core model in order to achieve the same pressure drop as the Thermix-Direkt model. This involves an artificial resistance in the form of a valve aperture that can be opened such that it causes the correct pressure drop.

- Secondly there are considerations - in section 3.4 - that lead to the substitution of the 3-D neutronics calculation by a 0-D point reactor kinetic model. This model can be built in Relap5. The heat transfer calculations for the core remain in Thermix-Direkt. The code configuration has been displayed in figure 2.2. Panther does not take part in the calculations any longer, but acts as an intermediary to pass data. The total thermal reactor power  $P_t$  is determined in Relap5, divided over a number of core layer in an invariant manner (determined from a steady-state Panther calculation for nominal conditions), and transported as  $P_t(z)$  through Talink and Panther to Thermix-Direkt. The surface temperature profile  $T_{surf}(r, z)$  is transported back to Relap5, where changes in temperature are processed to changes in reactivity and where a new value for the reactor thermal power is calculated. The gains in calculation time are marginal, as Panther is a fast code, and furthermore all previous connections between the codes are still in use. However, these calculations can give a decisive answer about whether it is useful to couple Thermix-Direkt directly with Relap5 or not.
- Thirdly, there is the situation where also the 2-D heat transfer model of Thermix-Direkt for the core is substituted by a 1-D (radially) model for the core structures in Relap5, figure 2.3. Dividing the core along the  $z$ -axis in segments to some extent models a second, i.e.  $z$ -dimension, but no heat transfer in that direction is possible. Each  $z$ -layer receives a fixed, pre-determined portion of the total power. In this case the whole model of the HTR with its ECS is contained by a single code, Relap5. It will be no surprise that this is the fastest way of calculation. The concessions in terms of accuracy will be discussed in section 5.3

Finally, there is the ACM model to which the calculations can be compared in order to get an idea of the correctness of the models, figure 2.4. This model, based on the ACM code, has been developed at the Delft University of Technology by Kikstra [48, 50] and contains a more detailed version of the ECS. It uses the same point reactor kinetic model with the same input as Relap5. As it is tailor-made on the direct gas cycle as ECS, and as it is using up to date programming standards, it is much faster than Relap5.

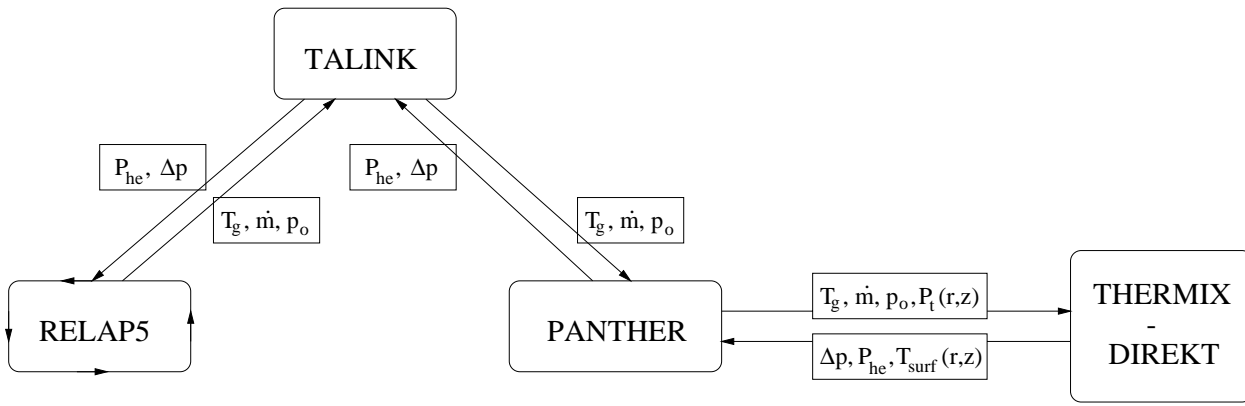


**Figure 2.1:** The most detailed calculational model for the HTR with its ECS. The core neutronics are modelled 3-D by Panther, the core heat transfer 2-D by Thermix-Direkt, and the ECS 1-D by Relap5. The parameter  $P_t$  is the total reactor thermal power,  $P_{he}$  the thermal power transferred to the helium mass flow rate,  $\Delta p$  the pressure drop over the pebble-bed core,  $T_g$  the core gas inlet temperature,  $T_{surf}(r, z)$  the temperature distribution of the solid structures in the core,  $\dot{m}$  the helium mass flow rate through the core, and  $p_o$  the core outlet pressure of the helium.

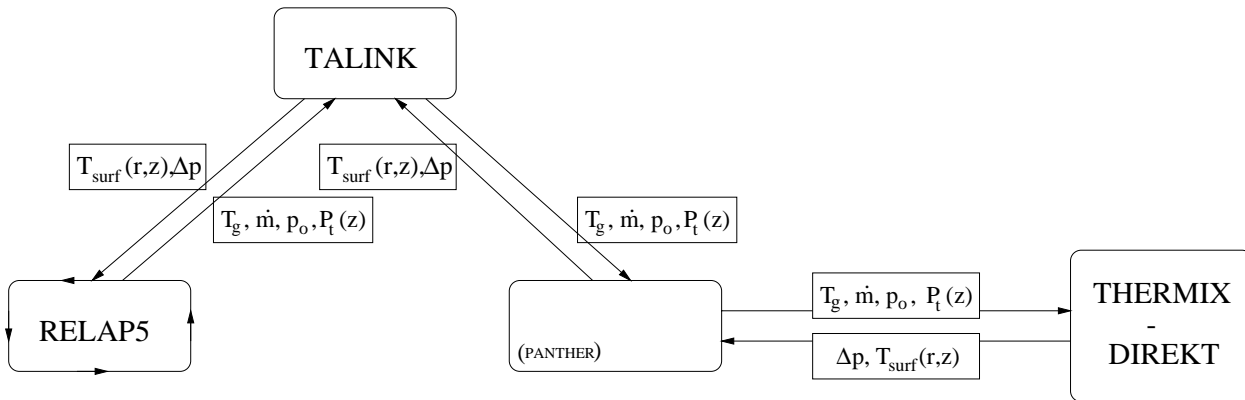


**Figure 2.2:** This model substitutes the 3-D core calculation by Panther with the 0-D point reactor kinetic model in Relap5. The parameters which are transferred between the codes have been defined in figure 2.1.



**Figure 2.3:** This model substitutes the 3-D core calculation by Panther with the 0-D point reactor kinetic model in Relap5. The 2-D core heat transfer by Thermix-Direkt makes place for a 1-D heat structure in Relap.

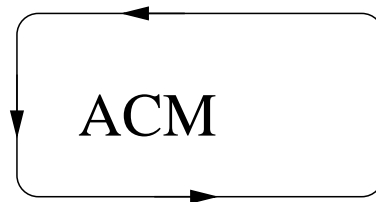


**Figure 2.4:** This model uses the same 0-D point reactor kinetic model as Relap5, but the model for the ECS has specifically been constructed for the direct gas cycle.

## 2.9 Summary

This chapter presented the calculational tools used for modelling the HTR with its energy conversion system. Three different code configurations have been constructed with these tools, each with its own merits on detail, accuracy and calculation time. A fourth, independently developed, model will be used as comparison.



# Chapter 3

---

## Reactor Models

---

### 3.1 Introduction

The HTR reactor model has been based on the conceptual design of the reactor in the Dutch INCOGEN study [30], the predecessor of the ACACIA study [31]. For both studies the reactor remained the same. It is based on the German PAP, Peu-à-Peu, reactor concept [39]. The choices that led to this design have been discussed in the introduction of this thesis, chapter 1.

In section 3.2 the Panthermix reactor model will be discussed and the steady-state reference core for nominal conditions (full power) will be defined. As Panthermix is the most adequate and detailed code system for the core calculations, its results are considered to be the reference to which the Relap5 core model is compared. In section 3.3 the difficulties of modelling the thermal hydraulic side of the core in Relap5 are presented and solved. In section 3.4 all necessary theory, steps, and data are presented in order to model the neutronic side of the reactor with the Relap5 point reactor kinetics model. Constructing a thermal hydraulic and neutronic model for the core in Relap5 makes it possible to model the total plant within one code. Together with the fact that the point reactor kinetics calculations are much faster than the 3-D Panther calculations, this also considerably increases calculation speed.

Section 3.5 briefly introduces the ACM reactor model.

### 3.2 The Panthermix Reactor Model

The ACACIA reactor design has slightly been adjusted for the present calculations. The reactor has been simplified:

- The  $^{235}\text{U}$  enrichment becomes 10 % instead of 19.75 % for new pebbles added to the small startup core. The startup core uses 10 % enrichment in order to limit the initial power density and the temperatures in case of inadvertent loss of cooling. New pebbles were envisaged to contain more fissile fuel in order to slow down the

rate at which pebbles are added to the bed and thus to extend the interval in which the reactor fills up. The reason to use a single enrichment in this study is a matter of simplicity. It avoids sudden gradients in for instance power, temperature or burnup, and facilitates interpretation of other results.

- The control rods of the reactor are not modelled. It has been assumed that they are used only in order to reach criticality with the initial core, and subsequently are made redundant. The reason, besides simplicity, is to show in the calculations that the control rods are not necessary to include in a reactor safety analysis provided that the reactor has been designed adequately. They are only there to facilitate operation of the plant. This issue will be addressed in detail in chapter 7.

Table 3.1 gives the design parameters of the reactor.

**Table 3.1:** *The design parameters for the ACACIA pebble-bed reactor. The nuclear constants are volume averaged and flux weighted for the core.*

1.	reactor thermal power	40 MW <sub>th</sub>		
2.	core diameter	2.5 m		
3.	maximum core height	4.5 m		
4.	Reactor inlet temperature	768 K		
5.	Reactor outlet temperature	1073 K		
6.	Helium mass flow rate	25.2 kg/s		
7.	Refuelling interval	4.0 y		
8.	Heavy metal load	12 g/pebble		
9.	Enrichment	10.0 <sup>w</sup> %		
10.	Design life	40 y		
11.	Fast group boundaries	10.0 MeV - 2.1 eV		
12.	Thermal group boundaries	2.1 eV - 0.0 eV		
13.	Macroscopic scatter cross section matrix $\Sigma_s$	$\begin{pmatrix} 0.0 & 0.0 \\ 0.151 & 0.0 \end{pmatrix} \text{m}^{-1}$		
		fast	thermal	
14.	Macroscopic absorption cross section $\Sigma_a$	0.0938	0.541	m <sup>-1</sup>
15.	Macroscopic removal cross section $\Sigma_r$	0.245	0.541	m <sup>-1</sup>
16.	Macroscopic fission cross section $\Sigma_f$	0.0138	0.323	m <sup>-1</sup>
17.	Macroscopic neutron yield cross section $\nu\Sigma_f$	0.0352	0.850	m <sup>-1</sup>
18.	Diffusion constant $D$	0.0190	0.0139	m
19.	Diffusion length $L, L^2 = D/\Sigma_r$	0.279	0.160	m
20.	Transport mean free path $\lambda_{tr}, \lambda_{tr} = 3D$	0.0570	0.0417	m

In figure 3.1 the reactor model used by Panther and Thermix-Direkt is shown on the left-hand side. For reasons of easy comparison later on, the Relap5 model has already been depicted on the right-hand side. The discretisation in the  $(r, z)$  geometry is given by the ticks on the axes. For a mesh point Panther calculates the power density according to the nuclear cross sections and constants, Thermix calculates the heat transfer according to the thermal hydraulic properties.

The legend of figure 3.1 mentions graphite zones with a volume percentage of less than 100%. This does not indicate porous graphite, but reflects the presence of control rod channels in the inner reflector or coolant channels in reflector number 4. The



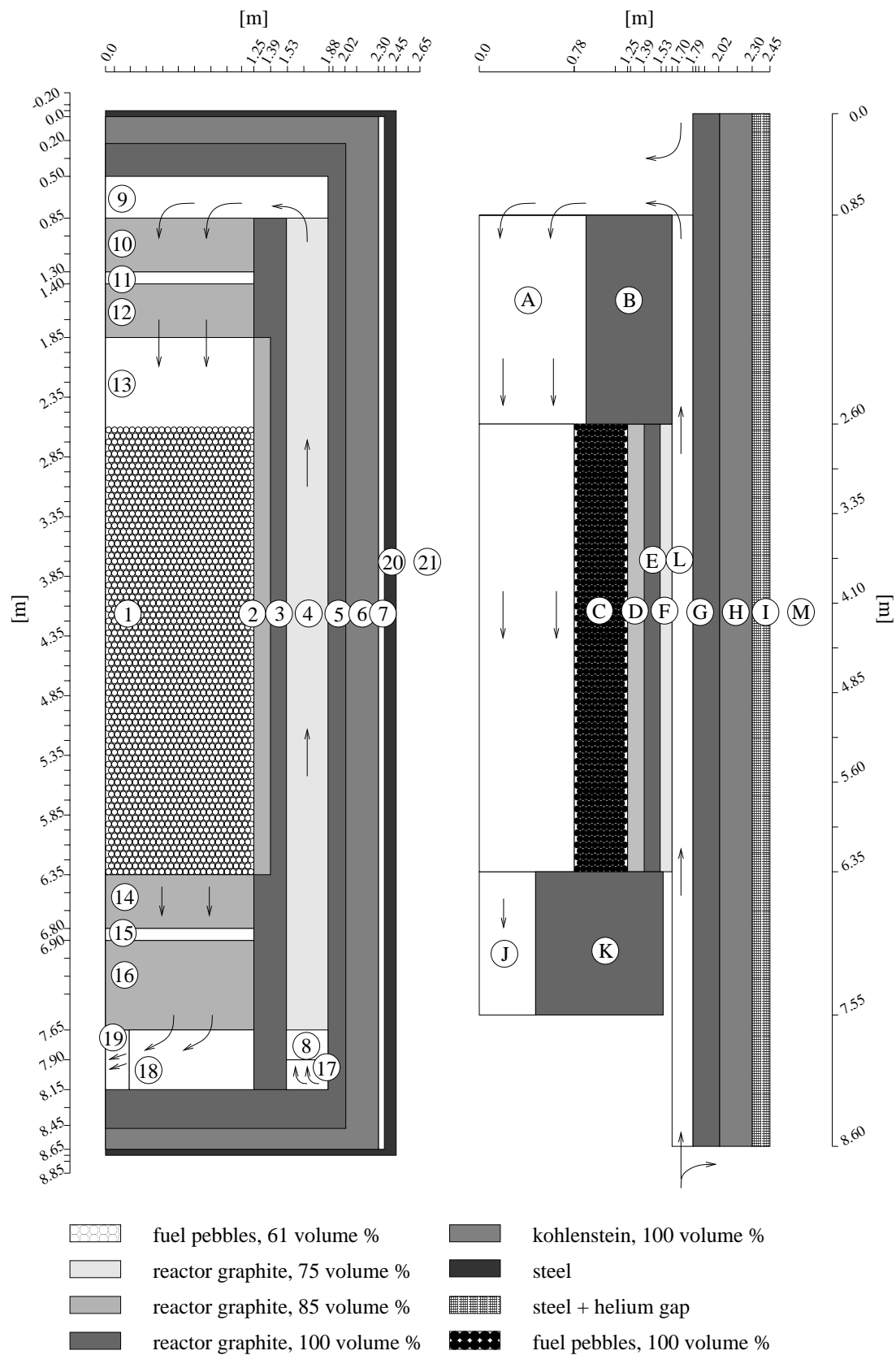


**Figure 3.1:** The thermal hydraulic reactor model for Panthermix (left hand side) and Relap5 (right hand side). For legend see overleaf.

Legend to figure 3.1:

- |   |  |
|---|--|
| 1. pebble-bed core                                  | A. coolant mixing volume   |
| 2. inner reflector                                  | B. top reflector   |
| 3. middle reflector                                 | C. effective pebble-bed core   |
| 4. reflector containing coolant channels            | D. inner reflector   |
| 5. separator reflector                              | E. middle reflector  |
| 6. outer reflector                                  | F. inner half of reflector around cooling channels                       |
| 7. gap filled with helium                           | G. outer half of reflector around cooling channels + separator reflector |
| 8. coolant distribution volume                      | H. outer reflector   |
| 9. coolant mixing volume                            | I. effective gap + steel vessel wall                                     |
| 10. upper top reflector with coolant channels       | J. coolant mixing volume   |
| 11. top reflector plenum for coolant mixing         | K. bottom reflector  |
| 12. lower top reflector with coolant channels       | L. coolant channel   |
| 13. remaining core volume to be filled with pebbles | M. air (ambient)   |
| 14. upper bottom reflector with coolant channels    |  |
| 15. bottom reflector plenum for coolant mixing      |  |
| 16. lower bottom reflector with coolant channels    |  |
| 17. coolant inlet point                             |  |
| 18. coolant mixing volume                           |  |
| 19. coolant outlet point                            |  |
| 20. steel vessel wall                               |  |
| 21. air (ambient)                                   |  |

reactor model presented here, with the core nearly full at a height of 3.75 m (30 mesh layers in the Panther model), is used to perform the calculations in order to compare the code configurations of chapter 2. The reason for this height is somewhat arbitrary, although a larger core may be advantageous as the maximum temperature and power density will be somewhat lower, and the temperature and power density gradients in the  $z$ -direction will be more gentle. Also, during operational transients the reactor will react slower due to the larger heat capacity of the core. This might somewhat facilitate the modelling of the core heat structures in Relap5, which is rather elementary and for instance cannot model heat transfer in the  $z$ -direction.

## The Reference Core

Having set the pebble-bed height at 3.75 m after a period of 1055 days burn-up, various  $(r, z)$ -distributions can be calculated for the reactor core. In figures 3.2 to 3.7 the distributions for the fast and thermal flux, the power, the gas temperature, the temperature in the solid heat structures, and the burnup are displayed for the right half of the reactor.

From looking at the neutron thermalisation process, and interpreting the flux distributions, the figures can be explained. The migration length for the neutrons is such that those neutrons born in the central core region (radius  $\lesssim 1.0$  m) are mostly thermalised by the graphite in the core. Neutrons further from the central core region are more likely to reach the side reflectors and are thermalised there virtually without losses (no parasitic absorption) compared to the thermalisation in the fuel zone. The thermal

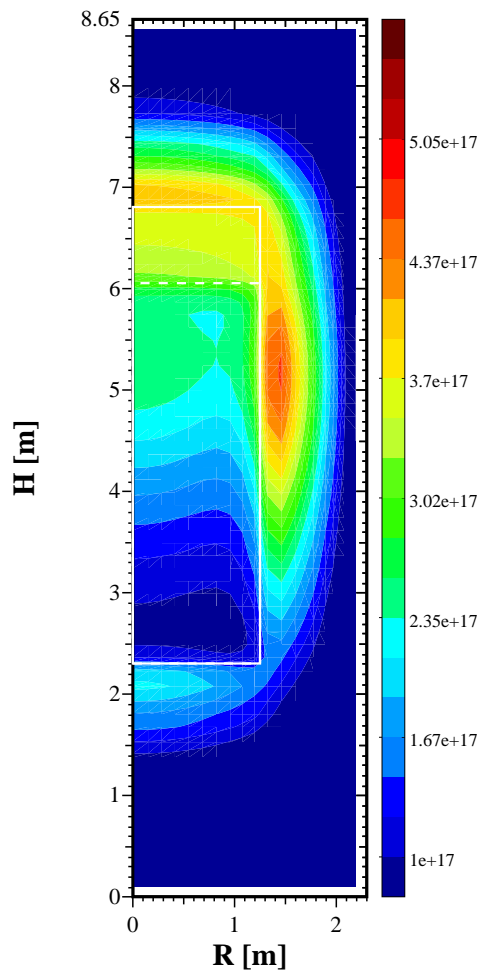


**Figure 3.2:** Thermal flux distribution [ $\text{cm}^{-2}\text{s}^{-1}$ ].

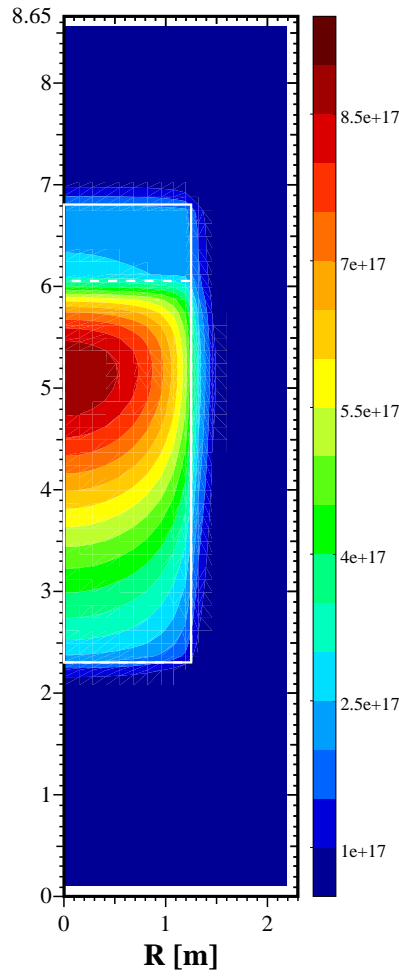


**Figure 3.3:** Fast flux distribution [ $\text{cm}^{-2}\text{s}^{-1}$ ].

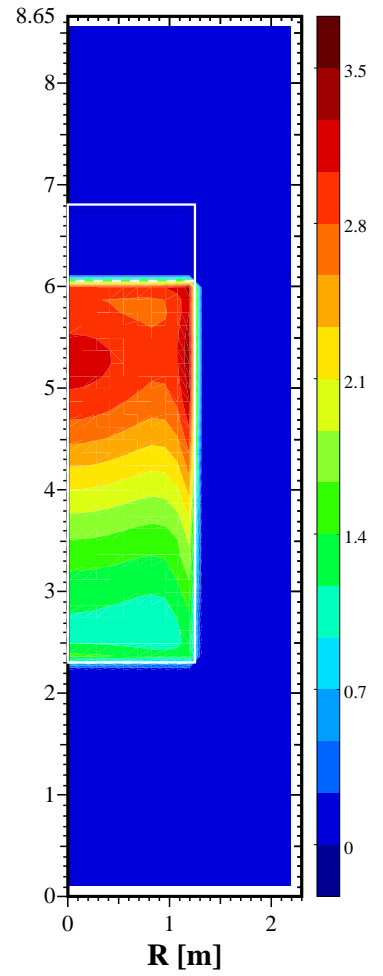


**Figure 3.4:** Power density distribution [ $\text{MW m}^{-3}$ ].

The figures characterise the steady-state situation for the ACACIA reactor. The white rectangle is the core region, which can be filled with pebbles; the dotted white line denotes the current pebble-bed height. Left, the thermal energy group flux distribution with maximal thermalisation of the neutrons in the top and side reflector. In the middle, the fast energy group flux distribution with the maximum at the region where the neutrons are produced, the active core zone. Right, the power density distribution which is limited to the pebble-bed core. Maxima are found at the positions with maximal thermal flux.

flux distribution therefore has a local maximum in the central core region, and an absolute maximum in the reflector close to the reflector-core interface. The reflector-thermalised neutrons that return into the fuel zone diffuse only a short distance back into the core before being absorbed. This is reflected by the power density distribution which is proportional to the thermal flux in the core and has the maxima in the core centre and along the side reflector. One could argue that in the fuel zone close to the side reflector, where fast fission neutrons are born, one would also expect a maximum for the fast flux. However, on average half the fast neutrons disappear into the reflector and are replaced by thermal neutrons, thus effectively halving the fast neutron density. Up to here only the side reflectors were mentioned, but the same reasoning holds for the top and bottom reflector in axial direction. The bottom reflector plays an important

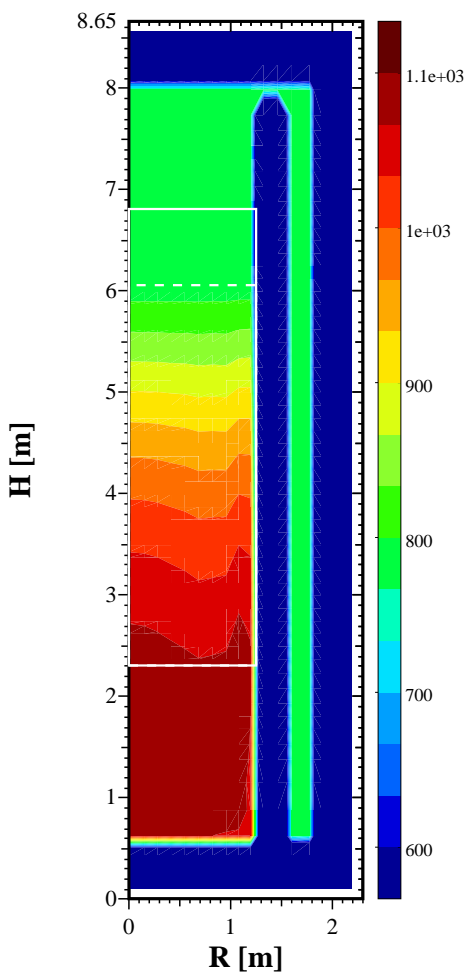


**Figure 3.5:** Helium gas temperature [K].

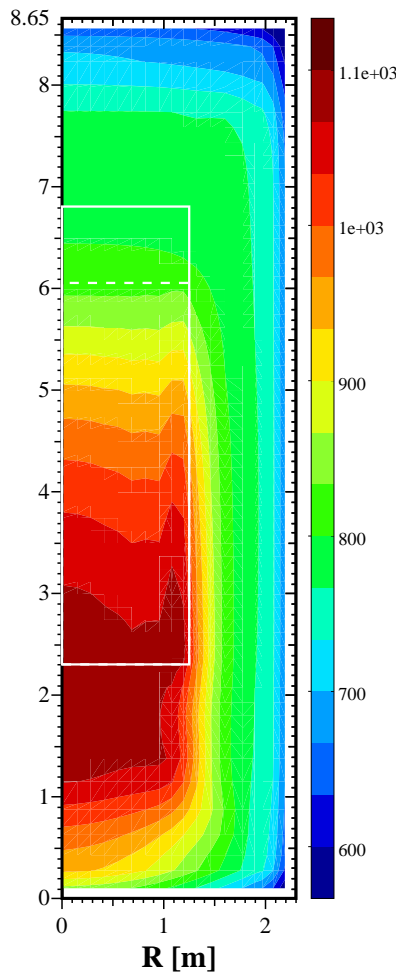


**Figure 3.6:** Temperature of solid heat structures [K].

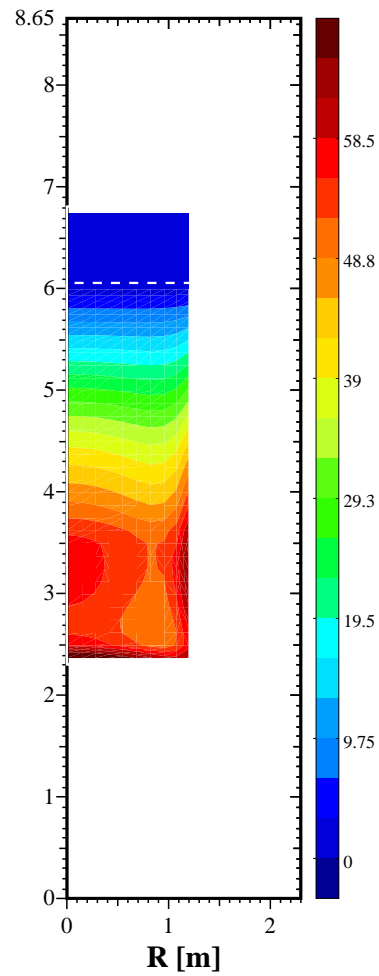


**Figure 3.7:** Burnup of fuel pebbles [MWd<sub>th</sub>/kg].

The figures characterise the steady-state situation for the ACACIA reactor. The white rectangle is the core region, which can be filled with pebbles; the dotted white line denotes the current pebble-bed height. Left, the temperature of the helium gas flowing up through the cooling channels onto the pebble-bed. In the middle, the temperature distribution for all solid heat structures. Right, the burnup for the reactor core. Outside the core there is no burnup, so no distribution is depicted.

role mainly during the early stages of the core. For the initial core the active part lies just above the bottom reflector and along the side reflector as there the thermal flux is maximal. As time advances, and fuel depletes, fresh fuel is added on top of the core. The most active part of the core then changes position and shifts from the bottom layer to the top region of the core. During the subsequent core life, the active part of the core remains in the top region of the core and slowly shifts up, keeping pace with the rate at which the fresh pebbles are added. Remnants of this shift in position of the active part of the core from bottom to top in the pebble-bed core can be seen in the burnup distribution in axial direction: near the bottom reflector the burnup is high, then decreases only to increase again to reach a maximum at a height of 3.25 m. This would typically be the centre of the active core for a pebble-bed core of 1.7 m height ( $z$ -axis 4.0 m) if it is assumed that the active core lies 0.75 m beneath the pebble-bed

surface. The fuel in the lower corners of the pebble-bed experienced a relatively low burnup considering the time the fuel spent there. The active core switched position from bottom to top of pebble-bed too quickly to affect the region, and it is too far from the side reflector to receive the high dose of thermalised neutrons.

The radial temperature distribution for the solid heat structures closely follows the radial power density distribution: regions with higher power density are hotter, i.e. the central core region and close to the reflectors. The helium gas temperature distribution is a little smoother due to gas mixing with adjacent regions. The gas heats up while flowing from top to bottom through the pebble-bed, and on exiting it streams through slits in the bottom reflector. In steady-state the bottom reflector experiences therefore a large temperature gradient. At one side flows the cold gas into the cooling channels, on the other side the hot gas is leaving the reactor.

### **3.3 The Relap5 Thermal Hydraulic Reactor Model**

As has been explained in section 2.5 the Relap5 code has as primary purpose to represent the thermal hydraulic cycle of a working fluid, in this case helium in the Brayton cycle. Heat transfer from working fluid to the enveloping structures - so-called heat structures - and the conduction towards an outer environment can be modelled, but the code has its limitations:

- heat transfer by conduction in axial direction cannot be modelled,
- heat structures cannot have mixed boundary conditions, i.e. transfer heat by conduction and convection at the same boundary,
- heat transfer relations for a pebble-bed geometry are not available.
- relations for the pressure drop over a pebble-bed are not available.

The following 4 subsections address these problems when modelling the core heat structures. In spite of the drawbacks the Relap5 core model has been constructed as part of the goal to include all calculations in Relap5. This will dramatically reduce calculation times. The neutronic reactor model for Relap5 will be discussed in section 3.4.

#### **Axial Heat Transfer**

The movement of the working fluid is for most cases in longitudinal direction and therefore the model of the energy conversion system can be 1-dimensional, along the  $z$ -axis. The heat transfer to the so-called heat structures takes place in transversal direction, and accordingly can be modelled only 1-dimensionally, now along the  $r$ -axis. Heat conduction along the  $z$ -axis is not possible in the Relap5 code, which for instance gives problems in regions that receive or transport a sizable portion of heat by conduction. The bottom reflector is such a zone, being hemmed in above by the hot core and sideways by the relatively cool zone around the coolant channels, region K in figure 3.1. The temperature of the bottom reflector is important if the temperature

reactivity coefficient is appreciable (section 3.4.4). Luckily, the active core is at a fair distance and the temperature reactivity contribution in this reflector is marginal. The problem has been solved for the bottom reflector by assuming that if there can be no heat source from axial conduction then there is no heat to be transported to the cooling channels. Thus, in order to obtain the correct temperature the bottom reflector only exchanges heat with the helium gas that flows through it. The heat transport to the coolant channels can be compensated elsewhere by tuning the heat transfer from region F to L in figure 3.1.

For the pebble-bed core itself the problems are limited, as the heat conduction in  $z$ -direction is only a fraction of the power that is generated and transferred to the helium. A choice has been made to model the core in 10 layers of 0.375 m height each.

## Mixed Boundary Conditions

Relap5 does not allow an outer surface to have mixed boundary conditions. The surface is either connected to the next mesh of that same heat structure and transports heat by conduction, or connected to a volume with the working fluid in which case the heat is transported by convection/radiation and the heat structure ends. This is a serious inadequacy, and has implications when modelling the reflector region with the coolant channels, region L in figure 3.1. This region is important and must be modelled for transient calculations. It shields the hot core, and it preheats the helium gas to some extent, thereby recovering most of the heat leaking sideways out of the core. For the steady-state, about 1.2 MW leaks out, and around 0.8 MW is transported back into the core by the helium mass flow rate. Before solving the problem with the coolant channels the relations for heat transfer by forced turbulent convection in Relap5 are discussed.

In general the following set of equations suffices to describe the heat flow  $\varphi$  from wall to fluid. Firstly, Newton's law of cooling which states that  $\varphi$  is proportional to the surface  $A$  for heat transfer and the difference between gas temperature  $T_g$  and surface temperature  $T_{surf}$  of the solid structure. The heat transfer coefficient  $\alpha$  expresses the proportion and contains everything that is not known of the heat transfer process. Secondly, from a dimensional analysis and experimental results [76], there is the equation that relates the heat transfer coefficient to the existing flow properties of the fluid:

$$\varphi = \alpha A (T_{surf} - T_g) \quad (3.1)$$

$$\begin{aligned} \text{Nu}(\alpha) &= f(\text{Re})g(\text{Pr}) \\ &= 0.021\text{Re}^{0.8}\text{Pr}^{0.4} \end{aligned} \quad (3.2)$$

$$\begin{aligned} \text{with } \text{Nu}(\alpha) &= \frac{\alpha D_h}{\lambda_f} \\ \text{Re} &= \frac{\dot{m} D_h}{\eta A_f} \\ \text{Pr} &= \frac{\eta C_p}{\lambda_f} \end{aligned}$$

where the  $f(\text{Re})$  and  $g(\text{Pr})$  denote functions of the Reynolds and Prandtl number respectively. The Nusselt number  $\text{Nu}$  gives the ratio of total heat transfer divided by conductive heat transfer, using the fluid thermal conductivity  $\lambda_f$ , the heated equivalent diameter  $D_h$ , and  $\alpha$ . The Reynolds number defines the ratio of the inertia forces divided by viscous forces, using the mass rate of flow  $\dot{m}$ , the flow area  $A_f$ , the dynamic viscosity  $\eta$ , and  $D_h$ . The Prandtl number gives the ratio between hydrodynamic and thermal boundary layer thickness, using the specific heat capacity of the fluid  $C_p$ ,  $\eta$  and  $\lambda_f$ . Equation (3.2) is valid for forced, turbulent convection, which is the state of convection for all operational transients. When entering the areas of free convection or laminar flow, the Nusselt relation must be adapted. Relap5 also contains those relations; beside that, Relap5 also differentiates between a horizontal or vertical surface for heat transfer.

In order to tackle the problem with the coolant channels, 2 heat structures have been defined, one on each side of the coolant channels, F and G in figure 3.1. In reality, 72 coolant channels exist, but in this model 1 channel has been defined that represents all the channels. Heat can then be transferred from the hotter to the colder heat structure, but solely by convection of the gas. There is no thermal contact between F and G and therefore no conduction is possible. From the Panthermix model can be learned that during the steady-state the hot side delivers 1.2 MW heat, of which 0.4 MW is mainly transported by conduction towards the outer wall of the vessel. For this Relap5 model it means that the gas has to absorb an extra amount of heat of 0.4 MW in order to supply the cooler side with the 0.4 MW which normally would be transported largely by conduction. From equation 3.1 it can be seen that in order to influence the heat transfer, one can either increase the heat transfer coefficient  $\alpha$ , or the surface  $A$ , or the temperature difference between wall and fluid. The first two options are not suitable, as increasing  $\alpha$  will also bring the fluid and wall temperature closer to each other and thereby frustrate the heat transfer, and increasing  $A$  in Relap5 automatically increases the volume of the heat structure. Increasing the fluid temperature, on the other hand, is easily achieved by halving the mass flow rate that has thermal contact with the heat structures. The other half follows a detour and is added again in region A in figure 3.1 when entering the core, in order to mix with the heated flow and again obtain the correct inlet temperature. The only drawback of this method is that the temperature distribution in the heat structures for the reflector containing the coolant channels, F and G in figure 3.1, is a little upset in the order of 10°C. This will have its effect on the reactivity, but luckily this region is relatively unimportant (section 3.4.4).

It must be stressed that it tacitly has been assumed that this way of modelling also holds for transient calculations. As all parameters of equation (3.2) still have their original dependencies on mass flux ( $\dot{m}/A_f$ ) and temperature this seems a reasonable assumption.

## Heat Transfer Relations for Pebble-Bed Geometry

In order to describe the heat transfer in the pebble-bed correctly, relations must be defined for the heat transfer by forced convection, such as equation 3.2, and for the

transport by conductance and radiation. These relations do not exist in Relap5, but are available in Thermix-Direkt.

For the conductance it is possible to give a temperature dependent table in the input. The Zehner-Schlünder equation [77, 78] could have been chosen to tabulate, a complex relation that combines the conduction through the pebbles, the conduction through the gas between the pebbles, and the conductance by radiation into one equation for 'the' conductivity of the pebble-bed. However, for the same reasons as when discussing the mixed boundary conditions, the helium flow cannot be distributed evenly over the pebble-bed core in the Relap5 model, and the core has to be modelled as a solid annulus, region C in figure 3.1. On the inside flows the helium and on the outside it is connected to the inner reflector. As a consequence the space between the point of power production and transfer to the gas is for most points in the core much larger than normal, the pebble radius (3.0 cm). In order to avoid the corresponding large temperature gradient, the heat conductivity of the graphite core annulus has been made near-infinite,  $\lambda_g = 10^8$  W/m/K. In order to avoid excessive leakage of heat towards the reflectors (realise that in the Relap5 model the core and reflector together form one heat structure and are in perfect thermal contact) a thin semi-insulating ring has been defined around the core such that only the aforementioned 1.2 MW leaks out. In this way each axial core layer has a uniform temperature, which is a realistic approximation when considering that temperature variations in the radial direction are not too large for the core (figure 3.6).

For the heat transfer by forced convection a new Nusselt relation must be defined which includes the porosity  $\varepsilon$  of the pebble-bed. An experimentally well established relation [79] is

$$\text{Nu} = 1.27 \frac{\text{Pr}^{0.33}}{\varepsilon^{1.18}} \text{Re}^{0.36} + 0.033 \frac{\text{Pr}^{0.5}}{\varepsilon^{1.07}} \text{Re}^{0.86} \quad (3.3)$$

for a pebble-bed with a height at least 4 times the pebble diameter and with a diameter at least 20 times the pebble diameter. The porosity must lie between 0.36 and 0.42, the Re number between 100 and  $10^5$ . All these conditions are fulfilled for the present core. The definition of the Nu, Re and Pr numbers from equation 3.2 remains valid if  $D_h$  is substituted by  $d_k$ , the pebble diameter, and  $A_f$  by  $A_c$ , the core cross sectional area. Equation (3.3) has been added to Relap5. The temperature dependence of  $\alpha$  that follows from equation (3.3) has been plotted in figure 3.8 and figure 3.9 for the current size of pebble-bed and for different mass flow rates of the coolant.

## Pressure Drop over Pebble-Bed

In order to model the pressure drop over the pebble-bed due to friction, the relation used by Thermix-Direkt has been modelled in the control system environment of Relap5. Every time step the pressure drop is calculated in the form of a control variable which drives the aperture of a valve placed at the exit of the core. The aperture of the valve



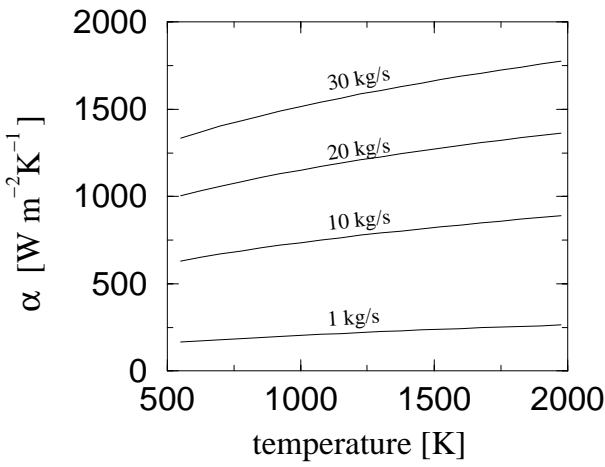


**Figure 3.8:** The heat transfer coefficient  $\alpha$  for the pebble-bed core.

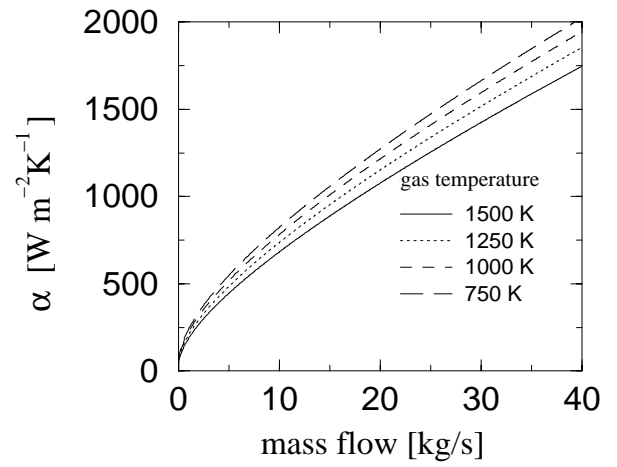


**Figure 3.9:** The heat transfer coefficient  $\alpha$  for the pebble-bed core as a function of the mass flow rate.

is such that it causes a pressure drop  $\Delta p$ , given by [79]

$$\Delta p = \psi \cdot \frac{1 - \varepsilon}{\varepsilon^3} \cdot \frac{H}{d_k} \cdot \frac{1}{2\rho_{He}} \cdot \left(\frac{\dot{m}}{A}\right)^2, \quad (3.4)$$

$$\psi = \frac{320}{\frac{Re}{1-\varepsilon}} + \frac{6}{\left(\frac{Re}{1-\varepsilon}\right)^{0.1}}, \quad (3.5)$$

$$Re = \frac{\dot{m} d_k}{\eta A_c}, \quad (3.6)$$

where only the pebble-bed height  $H$  and the helium density  $\rho_{He}$  are new variables. The equations are valid for an  $\varepsilon$  between 0.36 and 0.42, and the Re number should satisfy

$$1 \leq \frac{Re}{1 - \varepsilon} \leq 10^5 \quad (3.7)$$

This ends the description of the thermal hydraulic Relap5 model for the reactor. It must be stressed that the modelling leans heavily on equations and data from Thermix-Direkt. The final model has only been established after extensive tuning with the steady-state and transient Panthermix results found in chapter 5.

### 3.4 The Point Reactor Kinetics Model for Relap5

This section treats the method of calculation of the parameters for the point reactor kinetics model in Relap5. This model describes the time behaviour of the neutron population. Combined with the thermal hydraulic core model described above, the dynamics of the HTR reactor can be analysed. The line of approach is as follows: the point reactor kinetics model calculates the power, which now has no spatial distribution but is the integral reactor power. From the 3-D reactor model the power distribution over the core is known, so for the present case the core has been divided in 10 axial

layers and a portion of the power is allocated to each layer according to the steady-state reference conditions. During transients the power causes a temperature variation in the layers which introduces a reactivity disturbance. Together with the xenon reactivity contribution a net reactivity  $\rho$  results which is fed back into the point reactor kinetics model. The kinetic parameters of the model determine the dynamic reactor response, and the cycle starts again. It is important to notice that the axial power profile has been chosen to be fixed and has been determined once from the reference core. The same applies to the kinetic parameters.

One will notice that the point reactor kinetics model will be derived from transport theory in order to obtain a formal and consistent procedure to calculate the point kinetic parameters. It has already been discussed in section 2.3 that under certain assumptions diffusion theory can be applied and that the Panther code can be used to calculate the point kinetic parameters.

The arrangement of the remainder of the chapter is as follows: section 3.4.1 hands the equations necessary to define the point reactor in section 3.4.2. The parameters required for the point reactor kinetics model are calculated in section 3.4.3, the temperature dependent reactivity curves in 3.4.4. Finally, section 3.4.5 describes the time-dependence for the fission product poisoning by xenon.

### 3.4.1 Definitions and Terminology

In order to describe time-dependent systems accurately, it is necessary to include the delayed neutrons since their decay constants will usually determine the time behaviour of the neutron population. It is customary to divide the precursors that will yield the neutrons into six groups, each group with a different decay constant  $\lambda_j$ ,  $j = 1, \dots, 6$ . If the density of precursors in group  $j$  at position  $r$  is represented by  $C_j(r, t)$ , then the rate of emission of delayed neutrons is  $\lambda_j C_j(r, t)$  and these neutrons will have a normalised energy spectrum represented by  $\chi_j(E)$ . The normalised spectrum of the prompt neutrons will be denoted by  $\chi_p(E)$ . Define  $\nu(r, E)$  as the number of neutrons emitted per fission at position  $r$  caused by a neutron of energy  $E$ , and  $\beta_j(r)$  as the fraction of this total that originates from delayed group  $j$ . If  $\beta = \sum_j \beta_j(r)$ , then  $[1 - \beta(r)]\nu(r, E)$  is the number of prompt neutrons per fission. Introducing the precursor densities directly into the time-dependent transport equation and adjusting the fission term in order to allow for delayed neutrons [62], gives

$$\frac{1}{v} \frac{\partial \Phi}{\partial t} + \Omega \cdot \nabla \Phi + \Sigma_t \Phi = \iint \Sigma_s \Phi' dE' d\Omega' + \tilde{\chi}_p \iint (1 - \beta) \nu \Sigma_f \Phi' d\Omega' dE' + \sum_j \lambda_j C_j(r, t) \tilde{\chi}_j + Q \quad (3.8)$$

and

$$\frac{\partial C_j(r, t)}{\partial t} + \lambda_j C_j = \iint \beta_j \nu \Sigma_f \Phi(r, \Omega', E', t) d\Omega' dE' \quad (3.9)$$

where

$$\begin{aligned}
\Sigma_t &\equiv \Sigma_t(r, E, t) \\
\Sigma_s &\equiv \Sigma_s(r; \Omega', E' \rightarrow \Omega, E; t) \\
\Phi' &\equiv \Phi(r, \Omega', E', t) \\
\Sigma_f &\equiv \Sigma_f(r, E', t) \\
\nu &\equiv \nu(r, E') \\
Q &\equiv Q(r, E, \Omega, t)
\end{aligned}$$

The parameters  $\tilde{\chi}_p$  and  $\tilde{\chi}_j$  refer to energy  $E$ , where  $\tilde{\chi}$  denotes  $\chi/4\pi$ , the neutron emission per unit solid angle. The external source - if present - is represented by  $Q$ . Although equation (3.8) in principle describes the time-dependent behaviour of a system, direct solution with numerical methods requires long computing times for more complicated geometries. In order to come to a more convenient description of reactor kinetics in the next section, the adjoint transport equation is introduced:

$$\begin{aligned}
&-\frac{1}{v} \frac{\partial \Phi^\dagger}{\partial t} - \Omega \cdot \nabla \Phi^\dagger + \Sigma_t \Phi^\dagger = \\
&\iint [\Sigma_s(r; \Omega, E \rightarrow \Omega', E') + \tilde{\chi}(E') \nu(r, E) \Sigma_f(r, E)] \Phi^\dagger(r, \Omega', E') d\Omega' dE' \quad (3.10)
\end{aligned}$$

Notice that the gradient terms have opposite signs and that the incoming and outgoing parts of the scattering term are interchanged in comparison to equation (3.8). The total spectrum  $\chi(E)$  includes both prompt and delayed neutrons. The adjoint function is often regarded in terms of 'importance', i.e. suppose a neutron at position  $r$  and direction  $\Omega$  has energy  $E$  at time  $t$ ; then its importance,  $\Phi^\dagger(r, \Omega, E, t)$ , may be defined as the expected degree of contribution to the neutron population at all subsequent times by the neutron itself or by the secondary neutrons generated, as a result of scattering, fission, etc., by the neutron in question. Equation (3.10) does not, however, define the evolution of the neutron population 'at all subsequent times' (that is given by equation (3.8)), but rather defines the importances at earlier times that led to the importance at current time  $t$ . Mathematically, the reason for the difference is that the time derivatives have opposite signs in equations (3.8) and (3.10). The adjoint function has been plotted for the reference reactor from section 3.2 in figures 3.10 and 3.11 for the thermal and fast group. The calculations have been performed by Panther, i.e. diffusion theory, under the assumptions discussed in section 2.3. From the figures is indeed evident that the most important neutrons live in the active core region, as discussed in section 3.2.

For a point-reactor treatment of a time-dependent problem the angular neutron flux  $\Phi(r, \Omega, E, t)$  is first written as the product of a dimensionless amplitude factor  $P_p(t)$ , which is dependent on time only, and a shape factor (or shape function)  $\psi(r, \Omega, E, t)$ :

$$\Phi(r, \Omega, E, t) = P_p(t) \psi(r, \Omega, E, t) \quad (3.11)$$

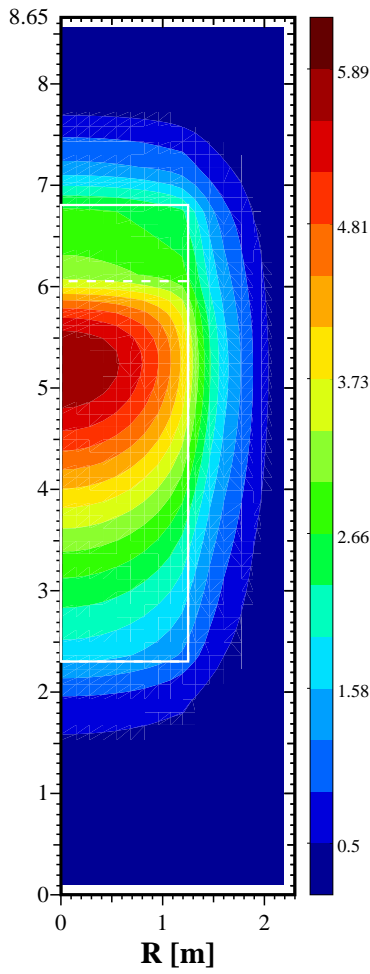


**Figure 3.10:** *Thermal adjoint function for the reference reactor. Arbitrary units.*

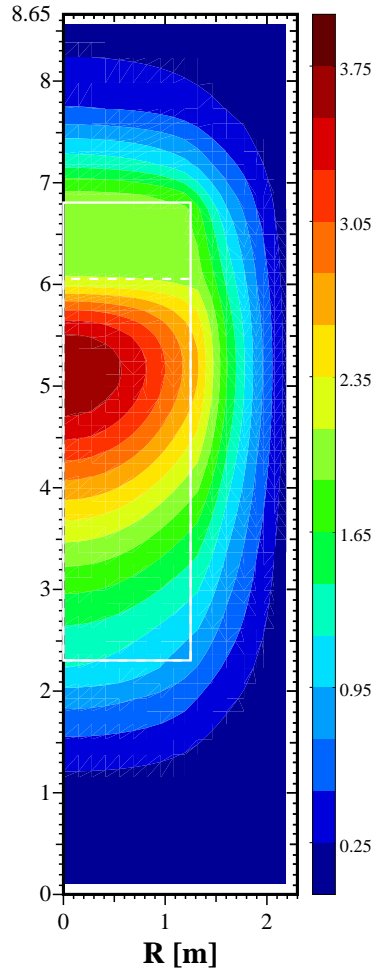


**Figure 3.11:** *Fast adjoint function for the reference reactor. Arbitrary units.*

The intent is that the amplitude factor describes most of the time dependence while the shape factor will change very little with time. The amplitude factor  $P_p(t)$  may be identified as the fission power at time  $t_0$ , if so, this fixes the normalisation of the shape function  $\psi$  at that time  $t_0$ : the fission power may be represented by

$$\begin{aligned} \text{Fission Power} &= \epsilon_f \iiint \Sigma_f(r, E) \Phi(r, \Omega, E, t) dV d\Omega dE \\ &= P_p(t) \epsilon_f \iiint \Sigma_f(r, E) \psi(r, \Omega, E, t) dV d\Omega dE \end{aligned} \quad (3.12)$$

Here  $\epsilon_f$  is the average prompt energy release per fission. Defining  $P_p(t_0)$  as the fission power at time  $t = t_0$  requires the condition

$$\epsilon_f \iiint \Sigma_f(r, E) \psi(r, \Omega, E, t_0) dV d\Omega dE = 1 \quad [\text{J} \cdot \text{s}^{-1}] \quad (3.13)$$

If the shape function indeed varies very little with time this relationship will remain fairly correct and  $P_p(t)$  can be identified as the fission power at times  $t$ , now with dimension  $\text{J} \cdot \text{s}^{-1}$ .

In order to describe the decay heat, the production of decay heat has been divided in a number of  $N = 23$  time groups [80] each with a decay constant  $\lambda_n$ :

$$\frac{\partial P_{d,n}(t)}{\partial t} = -\lambda_n P_{d,n}(t) + \gamma_n P_p(t) \quad n = 1, \dots, N \quad (3.14)$$

The parameter  $P_{d,n}$  is the decay heat production in time group  $n$ ,  $P_t$  the total power production, and  $\gamma_n$  the decay heat yield for group  $n$ . The total power is then a summation of the contributions due to fission and decay:

$$P_t(t) = P_p(t) + \sum_{n=1}^N P_{d,n}(t) \quad (3.15)$$

### 3.4.2 The Point Reactor

In order to determine the time-dependence of the system, it will be compared to some just critical time-independent reference state described by the time-independent adjoint transport equation. Using the adjoint function enables the derivation of an exact expression for the reactivity which holds for any size of perturbation. It is the same principle perturbation theory hinges on in a more general manner for any disturbance. Without producing the detailed derivation, which can be found in [62], the steps to derive the equations that describe the kinetic behaviour are basically along the lines of perturbation theory: first multiply equation (3.8) with the adjoint function of the reference state,  $\Phi_0^\dagger$ , and multiply the time-independent version of equation (3.10) with  $\Phi$ . Subtract the results and integrate over  $r$ ,  $\Omega$ ,  $E$ , and rewrite the gradient terms with the help of the divergence theorem. This will yield

$$\frac{dP_p(t)}{dt} = \frac{\rho(t) - \bar{\beta}}{\Lambda} P_p(t) + \sum_j \lambda_j c_j(t) + \frac{Q(t)}{\Lambda(t)} \quad (3.16)$$

Subsequently, multiply equation (3.9) by  $\chi_j(E)\Phi_0^\dagger$  and integrate over all variables, this gives

$$\frac{dc_j(t)}{dt} = \frac{\bar{\beta}_j}{\Lambda} P_p(t) - \lambda_j c_j(t) \quad j = 1, \dots, 6 \quad (3.17)$$

The quantities  $\bar{\beta}_j(t)$ ,  $\Lambda(t)$ ,  $c_j(t)$  are consistently defined as:

$$\bar{\beta}_j(t) \equiv \frac{1}{F} \int \cdot \int \tilde{\chi}_j(E) \beta_j \nu \Sigma_f(r, E') \psi(r, \Omega', E', t) \Phi_0^\dagger(r, \Omega, E) dV d\Omega dE d\Omega' dE' \quad (3.18)$$

$$\Lambda(t) \equiv \frac{1}{F} \iiint \frac{1}{v} \psi(r, \Omega, E, t) \Phi_0^\dagger(r, \Omega, E) dV d\Omega dE \quad (3.19)$$

$$c_j(t) \equiv \frac{1}{\Lambda F} \iiint \tilde{\chi}_j(E) C_j(r, t) \Phi_0^\dagger(r, \Omega, E) dV d\Omega dE \quad (3.20)$$

$$Q(t) \equiv \frac{1}{F} \iiint Q(r, \Omega, E, t) \Phi_0^\dagger(r, \Omega, E) dV d\Omega dE \quad (3.21)$$

with

$$F \equiv \int \cdot \int \tilde{\chi}(E) \nu \Sigma_f(r, E') \psi(r, \Omega', E', t) \Phi_0^\dagger(r, \Omega, E) dV d\Omega dE d\Omega' dE' \quad (3.22)$$

Here  $\Lambda$  is the (adjoint-weighted) neutron population divided by the (adjoint-weighted) rate of emission of fission neutrons, and named the mean neutron generation time. For neutrons of one speed in an infinite medium  $\Lambda$  becomes  $1/\nu \Sigma_f v$ , which for a critical system is equivalent to  $1/\Sigma_a v$ . The parameter  $\bar{\beta}_j$  is the effective delayed-neutron fraction from the  $j$ th group of precursors,  $\bar{\beta}$  is the sum over all  $j$  groups. Thus, the actual yield fractions have been corrected for the fact that the delayed neutrons appear at lower energies, i.e. that the delayed neutron spectrum differs significantly from the prompt neutron spectrum. Delayed neutrons do not have to slow down as much as prompt neutrons and therefore their fast nonleakage and resonance escape probabilities are higher than for the prompt neutrons. The neutron source  $Q(t)$  can represent any source present (internal or external) in the system. Assuming a constant shape function removes the time dependence from the point kinetic parameters.

At this point it is convenient to introduce the approximation which facilitates calculations with the model considerably: if the departure from criticality is small, the shape of  $\Phi(r, \Omega, E, t)$  is well approximated by that in the critical condition. In other words the shape function  $\psi(r, \Omega, E, t)$  has the same dependence on  $r, \Omega, E$  as the fundamental angular flux eigenfunction  $\Phi(r, \Omega, E)$  for the reference critical system. The shape function may then be derived from a criticality calculation. The approximation is in fact the same as the one in the perturbation formalism, that is, the perturbed flux is in first order equal to the unperturbed flux, provided that the perturbations are not too large. The exact, formal expression for the reactivity  $\rho(t)$  that can be found in [62], now reduces to

$$\rho(t) = \frac{k - 1}{k}, \quad (3.23)$$

the relation commonly used to define reactivity  $\rho$  in terms of the effective neutron multiplication factor  $k$ . Contributions to this reactivity may be temperature induced,  $\Delta\rho_T$ , xenon induced  $\Delta\rho_X$ , or control system induced  $\Delta\rho_s$ :

$$\rho(t) = \Delta\rho_T(t) + \Delta\rho_X(t) + \Delta\rho_s(t) \quad (3.24)$$

At this point the neutronic description of the total reactor has been reduced to the equations (3.14), (3.15), (3.16), and (3.17), provided that the parameters  $\Lambda, \beta_j$  can be determined as core averages, and the correct dependence of  $\rho(t)$  on the temperature and xenon can be established. The remaining sections of this chapter are devoted to these subjects. Also at this point, the link can be made towards the thermal hydraulic reactor model, that is, how the power  $P_t(t)$  is distributed over the core. It has been decided to use for all transients the fixed steady-state power distribution of the reference core along the  $z$ -axis, shown in figure 3.12. From the dissipated power in a layer a new average layer temperature is determined, and by that the link from the thermal hydraulic model back to the neutronic point reactor calculations is made, as the temperature change

induces a reactivity change.

The approximation of constant shape function is expected to hold well for the transients

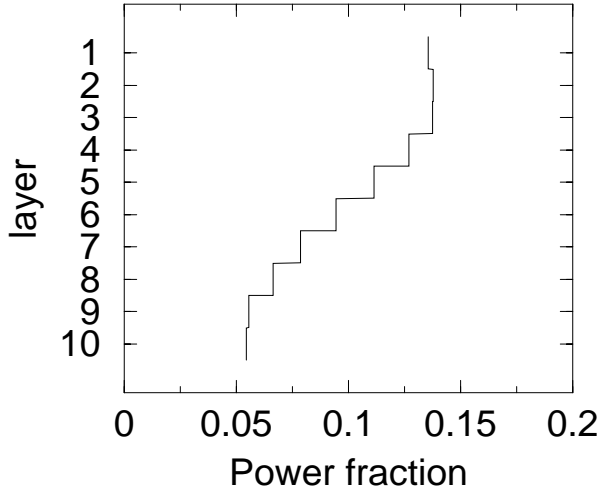


**Figure 3.12:** The axial power distribution for the core of 3.75 m height (1055 days of burnup). Along the  $x$ -axis the fraction of the total power  $P_t(t)$  is shown that is dissipated in the layer.

in the HTR; due to the long neutron migration length ( $\approx 0.3$  m) the core is expected to act as one entity. Furthermore, the present design contains no control rods, but relies solely on the fuel and moderator temperature coefficient in order to control the reactor. As such, localised disturbances in the flux are not expected. For reactor conditions which change gradually with time such as macroscopic cross sections during xenon and burnup transients, the shape factor will also change, but can be computed again from the conditions at that time.

### 3.4.3 Calculation of Point Kinetic Parameters $\bar{\beta}_{(j)}$ , $\Lambda$ , $Q$

The point kinetic parameters  $\bar{\beta}_{(j)}$ ,  $\Lambda$ ,  $c_j$  from equations (3.18) - (3.20) can be defined in the Panther calculational scheme. The adjoint function can be calculated from the same cross sectional data as for the flux. The reactivity curves  $\rho_T(T)$  will be determined in the next section.

For  $\bar{\beta}_{(j)}$  can be written in the two energy group structure of Panther (cf. equation (3.18)):

$$\begin{aligned}\bar{\beta}_j &= \frac{1}{F} \int d^3r \sum_{g=1}^2 \chi_{p,g} \Phi_{0,g}^\dagger(r) \sum_{g'=1}^2 \beta_{j,g'}(r) \nu_{g'} \Sigma_{f,g'} \psi_{g'}(r) \\ &= \frac{1}{F} \int d^3r \chi_1 \Phi_{0,1}^\dagger(r) (\beta_{j,1} \nu_1 \Sigma_{f,1} \psi_1(r) + \beta_{j,2} \nu_2 \Sigma_{f,2} \psi_2(r))\end{aligned}\quad (3.25)$$

where

$$F = \int d^3r \Phi_{0,1}^\dagger(r) (\nu_1 \Sigma_{f,1} \psi_1(r) + \nu_2 \Sigma_{f,2} \psi_2(r)) \quad (3.26)$$

Notice that the two energy group fission spectrum  $\chi = (\chi_1, \chi_2) = (1, 0)$ . The integral over space is calculated for the core volumes as only there  $\Sigma_f \neq 0$ . For the mean neutron generation time, equation (3.19) follows:

$$\Lambda = \frac{1}{F} \int d^3r \sum_{g=1}^2 \frac{1}{v_g} \psi_g(r) \Phi_{0,g}^\dagger(r) \quad (3.27)$$

and for the adjoint weighted precursor density, equation (3.20):

$$c_j = \frac{1}{\Lambda F} \int d^3r \chi_1 C_j \Phi_{0,1}^\dagger(r) \quad (3.28)$$

The time dependence has been left out of the parameters as the shape function  $\psi$  has been assumed to be constant during the transient calculations.

For long transients and slowly changing macroscopic cross sections, the  $\psi$  can be 'updated' and by that the point kinetic parameters. The reason for  $\psi$  to change is exclusively due to burnup; it is still a preposition that  $\psi$  does not change because of (xenon) transients. This so called adiabatic scheme has not been used in the present transient calculations, because the transients considered here only last up to 4 days. The change in burnup does not change the macroscopic cross sections enough to necessitate an update for the point kinetic parameters.

For the inherent neutron source  $Q(t)$  a different approach has been followed. First of all, the reason that a source will be added to the point reactor equations is to prevent the fission power to become unacceptably small ( $\ll 10^{-6} \text{W}$ ) during certain transient calculations with long subcritical periods. In real life there is always an inherent source due to spontaneous fission, its strength depending on the isotopic composition of the fuel. From adding up the point kinetic equations (3.16) and (3.17) and considering the stationary case, it follows that the source power is then:

$$P_s = \frac{Q}{-\rho} \quad (3.29)$$

For the present calculations not a constant source has been chosen to represent the spontaneous fission, but a 7<sup>th</sup> delayed neutron group with a very small yield ( $\beta_7 = 1 \cdot 10^{-9}$ ) and a small decay constant ( $\lambda_7 = 1 \cdot 10^{-5} [\text{s}^{-1}]$ ). Solving equation (3.17) for this 7<sup>th</sup> delayed group, assuming zero fission power, yields for the precursor density

$$c_7(t) = \frac{\beta_7 P_p(0)}{\Lambda \lambda_7} \exp(-\lambda_7 t) \quad (3.30)$$

where the boundary condition follows from the stationary case. From equation (3.16) it follows that during a long subcritical period - when  $P_p(t) = 0$  and  $\lambda_j c_j = 0$  for  $j = 1, \dots, 6$  - that a 7<sup>th</sup> delayed group can be incorporated as a neutron source  $Q(t) = c_7(t) \Lambda \lambda_7$ , so that  $Q(t)$  becomes (in J/s):

$$Q(t) = \beta_7 P_p(0) \exp(-\lambda_7 t) \quad . \quad (3.31)$$



The fission power  $P_p(0)$  for the current reactor during steady-state amounts to 37.39 MW.

**Table 3.2:** *The point kinetic parameter values for the reference core.*

group $j$	$\beta_j$	$\lambda_j$ [s <sup>-1</sup> ]
1	$1.806 \cdot 10^{-4}$	0.0127
2	$1.237 \cdot 10^{-3}$	0.0320
3	$1.192 \cdot 10^{-3}$	0.128
4	$1.971 \cdot 10^{-3}$	0.304
5	$6.925 \cdot 10^{-4}$	1.35
6	$1.314 \cdot 10^{-4}$	3.63
7	$1.0 \cdot 10^{-9}$	$1.0 \cdot 10^{-5}$
$\beta = 5.4045 \cdot 10^{-3}$		
$\bar{\lambda} = 0.0781$ [s <sup>-1</sup> ]		
$\Lambda = 8.703 \cdot 10^{-4}$ [s]		
$Q(t) = 3.74 \cdot 10^{-2} \exp(-\lambda_7 t)$ [W]		

The average decay constant has been defined as:

$$\bar{\lambda} = \left[ \frac{1}{\beta} \sum_j \frac{\beta_j}{\lambda_j} \right]^{-1} \quad (3.32)$$

### 3.4.4 Determination of reactivity curves $\rho_T(T)$

In order to describe the temperature dependency of the core and reflector reactivities sufficiently accurate, the reactor has been divided in 45 temperature zones. Regions are considered to be 'sufficiently' discretised with respect to temperature gradient and position. This is a subjective, initial choice. For instance, the reflectors between core and coolant channel not only have a steep temperature gradient but also an important position because it is the position of the maximum of the thermal flux. This has resulted in a discretisation of 10 axial layers over the height of the pebble-bed for the pebble-bed itself, for the inner reflector, the middle reflector, and the reflector containing the cooling channels. Added to that are the temperature regions of the top and bottom reflector, the separator reflector and the outer reflector. The last temperature region consists of the part of the inner, middle and cooling reflector that protrudes above the pebble-bed, named the sub-top reflector.

All future temperature distributions will be set alongside the nominal temperature profile, and differences in temperature for a zone will be converted to a change in reactivity by utilising the temperature versus reactivity curves presented in this section. The temperature distribution at nominal conditions has been chosen as reference from which the temperature dependent reactivity curves will be determined. This is the most logical choice based on the information available, and each effort towards adjustment would point to foreknowledge of the transients that are to be calculated. In order to calculate the reactivity change  $\Delta\rho_T$  due to a temperature change  $\Delta T$ , the initial value of the neutron multiplication factor  $k$  is determined. After changing the temperature of a region from  $T$  to  $T'$ , the new value for  $k$  is determined,  $k'$ . The change in reactivity follows from equation (3.23) as:

$$\Delta\rho_T(\Delta T) = \rho'_T(T') - \rho_T(T) = \frac{1}{k} - \frac{1}{k'}, \quad \text{while} \quad (3.33)$$

$$\Delta T = T' - T$$

The temperature step  $\Delta T$  is typically a small variation in the order of 10 K. Adding the reactivity contributions of each step and making 35 steps in the positive and 35 in the negative direction supplies one with a reactivity curve in the range of [-350 K, 350 K] around the nominal temperature of that region. It is advisable to prevent the situation that during the sampling process one region is far above its nominal temperature while the temperatures in the rest of the reactor remain unaltered. This will unrealistically distort the flux distribution, and therefore the reactivity changes  $\Delta\rho_T$  will be less accurate for normal transients. In order to circumvent this problem partially, the 10 axial core layers have been treated in conjunction with each other, just as the 10 layers of each reflector: when starting with a temperature step  $\Delta T$  in one layer, first all other layers make the same temperature step and have their  $\Delta\rho_T$  determined before the first layer makes the next  $\Delta T$  step. For each of the other zones with 10 axial layers this procedure has also been followed, however, each as a separate case. Also relating these zones to each other involves too much prior knowledge of the expected transients. Figure 3.13 illustrates the procedure.

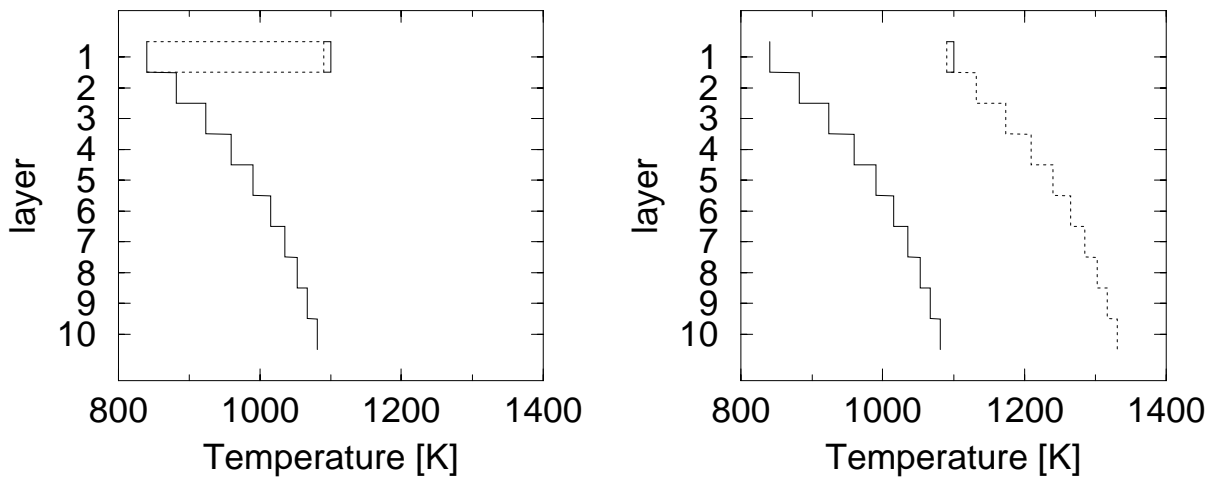


**Figure 3.13:** *The temperature distribution during determination of the reactivity curves. Left the situation that should be avoided, because the temperature distribution becomes unrealistically distorted. Right a more plausible temperature distribution for which a reactivity distribution can be determined. Shown is a basic temperature increase for all layers of 250 K, and a small extra disturbance of 10 K for layer 1.*

Figure 3.14 shows the reactivity curves for the reactor. The numbers on the left of the curves designate the associated layer, with 1 the top and 10 the bottom layer. As the curves are not perfect straight lines, they will be used in tabulated form rather than be used to determine a temperature coefficient of reactivity ( $\Delta\rho_T(\Delta T)/\Delta T$ ). Interpolation between the tabulated points will be more precise to obtain the reactivity contribution of a layer. However, it is clear that for the core such a temperature coefficient is negative for all layers and takes care of the desired negative temperature feedback, while the reflector regions all introduce a weak, positive contribution to the reactivity balance with rising temperatures. When mentioning the core temperature

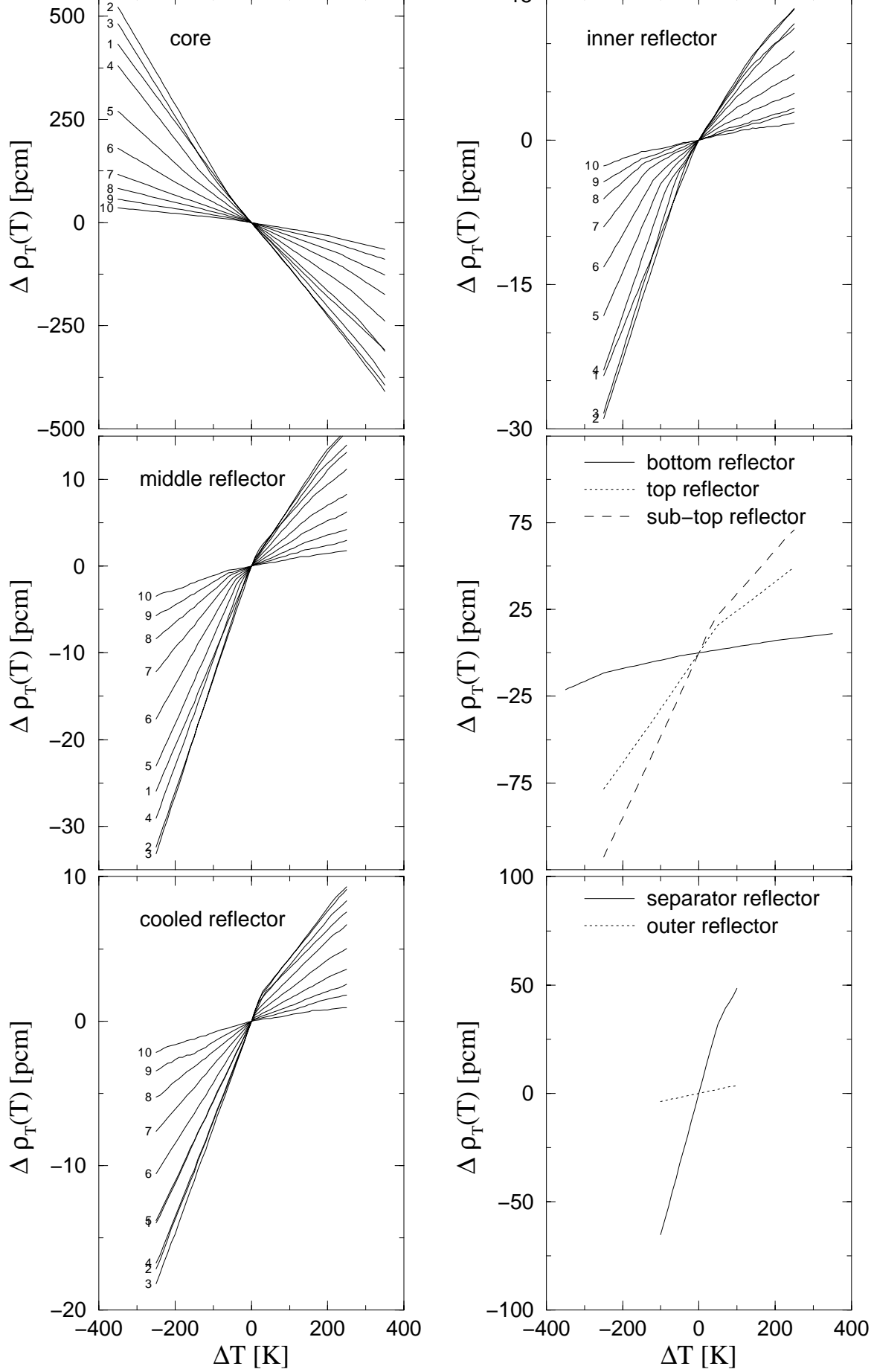


**Figure 3.14:** The reactivity curves  $\Delta \rho_T(\Delta T)$  for the reactor, with  $\Delta T$  the temperature variation around the nominal temperature for that region. The numbers left of the curves designate the associated layer, with 1 the top and 10 the bottom layer.

coefficient of reactivity, it is important to realise that it includes the fuel temperature coefficient of reactivity and the (graphite) moderator temperature coefficient of reactivity of the pebble-bed.

### 3.4.5 Xenon Fission Product Poisoning

The present calculations only consider the parasitic absorption of the most important fission product,  $^{135}\text{Xe}$ . Xenon can be produced directly, but mainly results from  $\beta$ -decay of  $^{135}\text{I}$ . The time dependent equations for the  $^{135}\text{Xe}$  concentration can then be written as a balance between production and removal for  $^{135}\text{I}$  and  $^{135}\text{Xe}$  [63]. Assuming direct decay and neglecting short-lived states of the isotopes that lead to  $^{135}\text{I}$  or to  $^{135}\text{Xe}$ , the precursor concentration  $I(r, t)$  is given by:

$$\frac{\partial I(r, t)}{\partial t} = \gamma_I(r) \Sigma_f(r) \Phi(r, t) - \lambda_I I(r, t) \quad (3.34)$$

with the assumption that the absorption cross section of  $^{135}\text{I}$  is sufficiently low and can be neglected. The concentration  $X(r, t)$  is given by the balance:

$$\frac{\partial X(r, t)}{\partial t} = \gamma_X(r) \Sigma_f(r) \Phi(r, t) + \lambda_I I(r, t) - \lambda_X X(r, t) - \sigma_a^X(r) \Phi(r, t) X(r, t) \quad (3.35)$$

In appendix A it will be derived that these equations can be space averaged and written in terms of the fission power  $P_p(t)$  consistent with the point reactor kinetic equations:

$$\frac{\partial I(t)}{\partial t} = \frac{\bar{\gamma}_I}{\epsilon_f V} P_p(t) - \lambda_I I(t) \quad (3.36)$$

$$\frac{\partial X(t)}{\partial t} = \frac{\bar{\gamma}_X}{\epsilon_f V} P_p(t) + \lambda_I I(t) - \lambda_X X(t) - \Upsilon P_p(t) X(t) \quad (3.37)$$

The parameter  $\epsilon_f$  is the energy per fission,  $V_c$  the pebble-bed core volume,  $\bar{\gamma}_I$  and  $\bar{\gamma}_X$  the space averaged iodine and xenon fission yields,  $\lambda_I$  and  $\lambda_X$  the decay constants for iodine and xenon,  $\Sigma_f$  the one group fission macroscopic cross section,  $\sigma_a^X(r)$  the microscopic absorption cross section for xenon, and  $\Upsilon$  the space averaged product of  $\sigma_a^X(r)$  with the shape function  $\psi(r)$ , weighted with  $X(r, t)$ . The Panther code indeed uses the 3-dimensional  $X, I, \gamma_X, \gamma_I, \Sigma_f, \sigma_a^X, w_f$  distributions, but for the reactor point kinetics model in Relap5 core-averaged values have been calculated.

In order to characterise the 3-D distribution  $X(r, t)$  from Panther with one integral value for the core that can be linked to the xenon concentration calculated in Relap5, the xenon worth is introduced. The xenon worth is the difference in reactivity between a core at xenon equilibrium and the same core without xenon. It is a weighted value, as xenon absent in an important region contributes more to the reactivity difference than

xenon absent in an unimportant region. The contribution to the reactivity balance (3.24) by xenon has been normalised to the reference xenon worth value  $\rho_X^0$ :

$$\Delta\rho_X = \rho_X^0 \left( \frac{X(t)}{X^0} - 1 \right) \quad (3.38)$$

On beforehand can already be noticed that this is an approximation that hinges on two assumptions:

- a constant power profile
- a constant temperature profile

The first assumption has been made throughout the reactor point kinetic model and will prove to be fairly correct. It means that the importance of xenon at a certain position in the core remains identical throughout the transients and that the average xenon density at all times can be related in the same manner to the reactivity worth by equation (3.38).

The second assumption presupposes that for a given xenon density distribution the xenon worth will be identical for all temperatures. In general this will not be true, and this can be understood by looking at the definition of the xenon worth:

$$\Delta\rho_X = \rho'_X - \rho_X = \frac{1}{k} - \frac{1}{k'} \quad (3.39)$$

where the quote denotes the situation without xenon and  $k$  the neutron multiplication factor. Looking at  $k$  as the ratio between production of fission neutrons and capture of neutrons by fuel and xenon yields

$$k = \frac{\nu \Sigma_f^F \Phi}{\Sigma_a^F + X \sigma_a^X \Phi} \quad (3.40)$$

with the superscript  $F$  denoting the fuel and  $\nu$  the number of neutrons produced by a fission. The other variables have been defined earlier in this section. Inserting equation (3.40) in equation (3.39) and writing  $\Sigma_f^F$  as  $U \sigma_f^U$  yields a result easy to analyse:

$$\Delta\rho_X = -\frac{X \sigma_a^X}{\nu U \sigma_f^U} \quad (3.41)$$

The ratio  $\sigma_a^X / \sigma_f^U$  has been plotted in figure 3.15. If the temperature of the reactor core increases, the average neutron speed will increase, and the first moment of the Maxwell spectrum will shift right towards the large peak in figure 3.15. The result is a larger xenon worth at a higher temperature for the same xenon density distribution.

Since this behaviour is only reserved for Panther that has a nuclear database at its disposal with temperature dependent cross sections, it can be expected that the point reactor model will underpredict the xenon reactivity worth when the average reactor temperature increases. The point of criticality will therefore be found at an average reactor temperature that is slightly higher and a power that is lower than for the

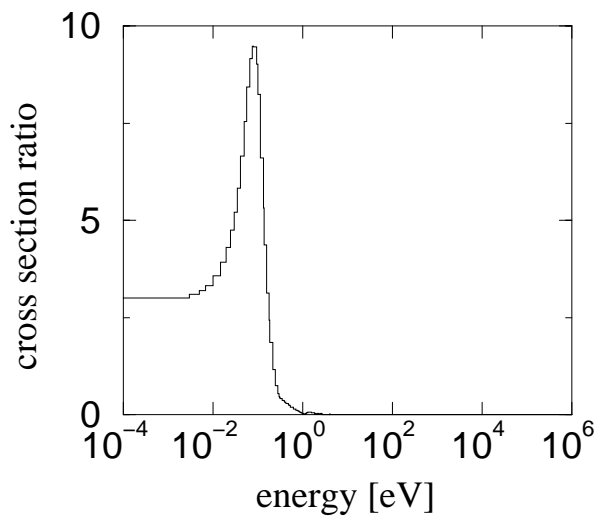


**Figure 3.15:** The ratio  $\sigma_a^X / \sigma_f^U$  as a function of energy.

Panthermix model. Reversely, an overprediction will result when the average reactor temperature decreases, with the effect that the point reactor models will operate at a slightly lower average reactor temperature and produce more power than the Panthermix model.

**N.B.:** Panther also uses equations (3.37) and (3.36) but incorrectly uses the *total* power in the balance. The xenon concentration then decreases by 1.6% for the present core (total delayed fraction of 0.0652). With a xenon worth of 0.01718 the net positive reactivity is 28 pcm and from figure 3.13 it follows that the core temperature would rise around 5°C. Although Panther is known to be in error, the same error has been introduced in the xenon calculations used for Relap5. Only then the comparison between the two reactor models will not be biased.

The values - determined for  $P_t = 40$  MW - are tabulated in table 3.3.

**Table 3.3:** Parameters for calculation of xenon poisoning.

Where necessary the values are core averaged and/or condensed from 2 energy groups to 1.

$\gamma_I$	$6.036 \cdot 10^{-2}$	
$\gamma_X$	$7.698 \cdot 10^{-3}$	
$\lambda_I$	$2.912 \cdot 10^{-5}$	$s^{-1}$
$\lambda_X$	$2.118 \cdot 10^{-5}$	$s^{-1}$
$\rho_X^0$	0.01718	
$X^0$	$1.289 \cdot 10^{20}$	$m^{-3}$
$I^0$	$1.373 \cdot 10^{20}$	$m^{-3}$
$\Upsilon$	$3.450 \cdot 10^{-13}$	$m^2$
$\Sigma_f$	$9.588 \cdot 10^{-2}$	$m^{-1}$
$\epsilon_f$	$3.28 \cdot 10^{-11}$	J

## 3.5 The ACM Reactor Model

The reactor model developed in ACM [48] is constructed along the same lines as the Relap5 model, but without its inconveniences for the thermal hydraulic description. Conduction in the  $z$ -direction is possible, mixed boundary condition do not pose a problem, and the pebble-bed core has not to be represented as a solid annulus. The same relations for conduction and convection have been used as in Thermix. The model has marginally been tuned: only the heat transfer from the pebble-bed to inner reflector by combined conduction/convection, and the steady-state heat loss of 0.4 MW have been matched to the full scope Thermix-Direkt results. The point reactor kinetics model is used to calculate the power production; the same input has been used as for Relap5.

## 3.6 Summary

In this chapter it has been described how the ACACIA reactor has been modelled. A reference reactor model has been defined with the Panther-Thermix reactor model, as this is the most adequate and detailed code system. Relap5 determines the neutronic behaviour by a point reactor kinetics model. For the thermal hydraulic modelling of the core, Relap5 has slightly been adapted in order to include pebble-bed specific relations for heat transfer. Although modelling the reactor in Relap5 is less straightforward, its advantage lies in calculational speed due to the simplifications of the neutronics model and due to the absence of coupling software between different codes.





# Chapter 4

---

## Energy Conversion System Model

---

### 4.1 Introduction

The choice for the Brayton cycle as the most advantageous energy conversion system (ECS) has been elucidated in the introduction of the thesis, section 1. The first section of this chapter, section 4.2, will discuss the various components that are part of the ECS and are modelled in Relap5. In the same way that the Panthermix model was the reference case for the reactor, now the ACM model [48] is the standard for the ECS. An important feature of the ACACIA system is its flexibility in load following at high thermodynamic efficiency. The control philosophy that leads to this flexibility will be described in section 4.3.

### 4.2 The Brayton Cycle

Before discussing the components in detail, the general working of the Brayton cycle will be explained. Figure 1.4 from the introduction has been depicted here again. The pressurised helium gas,  $p = 23$  bar, is heated in the HTR from inlet temperature  $T_{g,i} = 495^\circ\text{C}$  to outlet temperature  $T_{g,o} = 800^\circ\text{C}$ , which requires a power  $W$  of

$$W = \dot{m}C_p(T_{g,o} - T_{g,i}). \quad (4.1)$$

With a design mass flow rate  $\dot{m} = 25.2$  kg/s and the helium heat capacity  $C_p = 5195$  J kg<sup>-1</sup> K<sup>-1</sup>, the power is  $W = 40$  MW<sub>th</sub>. The helium heat capacity is considered to be independent of the temperature, which is a valid approximation within 0.15% [81] for the temperature range of the Brayton cycle. The helium flows from the core into the gas turbine that drives the shaft connected to the gas compressor and generator. The

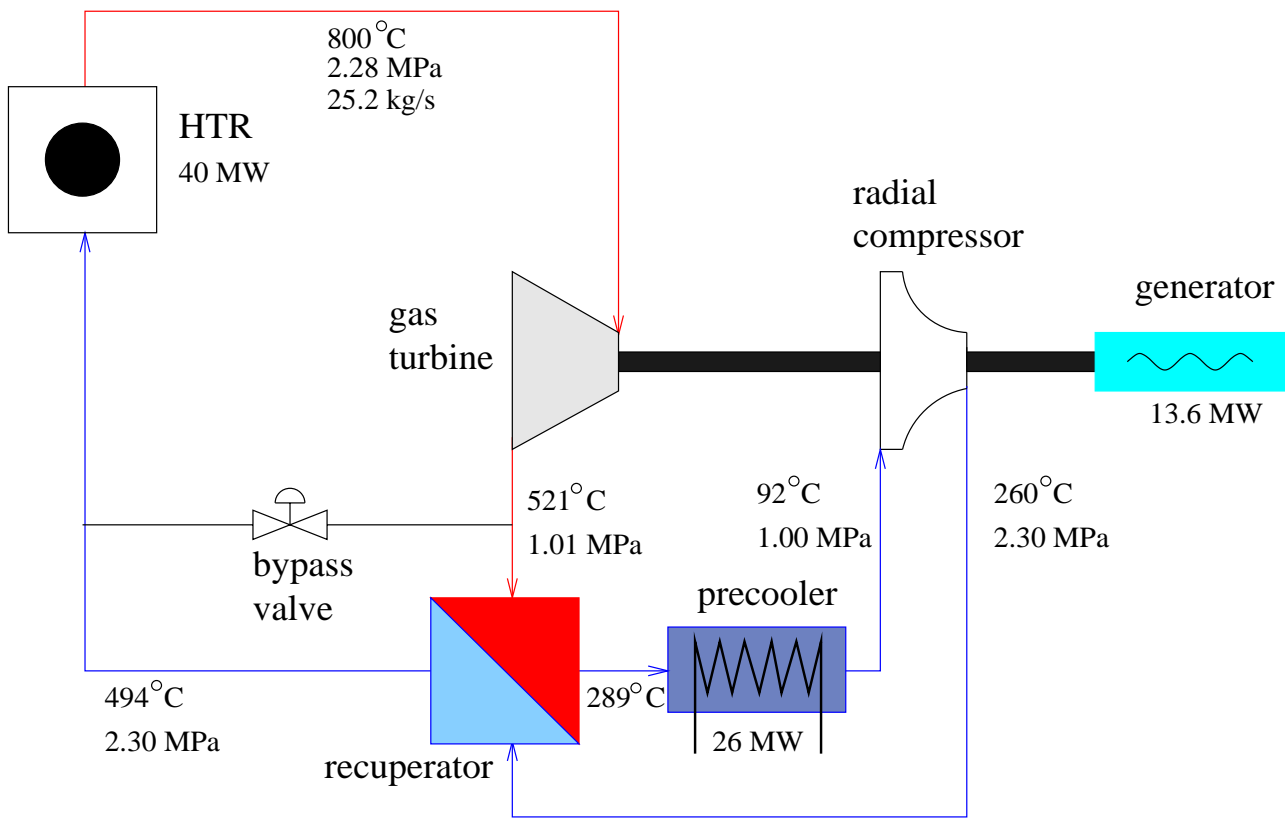


**Figure 1.4:** The Brayton cycle of the ACACIA plant.

power produced by the turbine is also given by equation (4.1) (with a minus sign in front), while the output temperature  $T_{g,o}$  due to expansion is given by

$$T_{g,o} = T_{g,i} \left( \frac{p_o}{p_i} \right)^{\eta'_t \frac{\kappa-1}{\kappa}} \quad (4.2)$$

Here  $p_i$ ,  $p_o$  are the pressure at inlet and outlet,  $\kappa$  the specific heat ratio (1.667 for helium) and  $\eta'_t$  the polytropic turbine efficiency that comprises all thermodynamic losses in the turbine system. For an ideal, isentropic system  $\eta'_t = 1.0$ , and equation (4.2) becomes the standard case for adiabatic expansion.

The pressure drop in the system will be compensated by the compressor, but first the helium flow must be cooled, as compression from a low temperature requires less energy. Noticing that the temperature of the helium flow from the compressor is below the temperature of the flow leaving the turbine clearly paves the way for a recuperator. Around 30 MW is transferred from the hotter to the colder flow. The remainder of the heat is rejected in the precooling into a secondary system where industrial steam is produced. This secondary loop has been described extensively [48] and is not the interest of the current study, although this heat production does pose conditions on the Brayton cycle. For instance, the inlet temperature of the helium flowing into the compressor has been altered from 25°C in the INCOGEN study to 92°C in the ACACIA study in order to produce steam of a decent quality. As a result the power required by the compressor increased and the generator power output dropped from 18 MW to 13.6 MW.

The required compressor power is also given by equation (4.1), if for the temperature  $T_{g,o}$  of the compressed gas is written

$$T_{g,o} = T_{g,i} \left( \frac{p_o}{p_i} \right)^{\frac{1}{\eta_c'} \frac{\kappa-1}{\kappa}} \quad (4.3)$$

which differs from equation 4.2 only in the polytropic compressor efficiency  $\eta_c'$  (design value  $\eta_c' = 0.90$ ).

### 4.2.1 Turbine

The Relap5/mod3.2 steam turbine model has been used in order to model the helium turbine. A lumped-parameter model is used wherein a sequence of stages forms the turbine. One single stage consists of a single-row fixed-blade system (nozzle) followed by a single-row rotating-blade system. The design [42] of the turbine contains 7 stages. Relap5 limits the number of items connected to a shaft component to 10 (section 4.2.5), and for that reason 4 slots have been allocated to the turbine, 5 to the compressor and 1 to the generator. In the Relap5 model one dummy stage with efficiency zero and without power production (used for governing purposes and defining inlet conditions) precedes 3 real stages. The turbine data that form the basis for the Relap5 model are given in table 4.1.

**Table 4.1:** Turbine stage data for the Relap5 model.

reaction fraction	0.94			
rotational design speed [rad/s]	1256.6			
inlet pressure [MPa]	2.282			
outlet pressure [MPa]	1.015			
stage	0	1	2	3
blade tip diameter [m]	0.722	0.722	0.730	0.739
flow area [m <sup>2</sup> ]	0.200	0.110	0.120	0.135
stator inlet temperature [K]	1069.	1065.	959.	873.
stage outlet temperature [K]	1065.	959.	873.	793.
design efficiency	0.0	0.906	0.906	0.906

Obviously, since the calculation of the expansion in the turbine is straightforward in principle (equation (4.2)), the sting must be in the determination of the efficiency relation when the turbine moves away from its design point during a transient. Complicated models, related to the geometry (blade angles and shape) and sometimes supplemented with experimental results, give an adequate description at the cost of much effort. The Relap5 turbine model is based on a more straightforward approach and utilises a single equation for a reaction stage turbine [82]. The efficiency factor is based upon momentum and energy considerations, [83]:

$$\eta_t = \eta_t^o \frac{2v_t}{v^2} \left\{ (vb - v_t) + [(vb - v_t)^2 + rv^2]^{1/2} \right\}, \quad (4.4)$$

where  $\eta_t$  = isentropic turbine efficiency, defined as the actual enthalpy change divided by the isentropic enthalpy change across the stage  
 $\eta_t^o$  = maximum turbine isentropic efficiency  
 $b = (1 - r)^{1/2}$   
 $r$  = reaction fraction  
 $v$  = the helium velocity at nozzle outlet  
 $v_t$  = tangential velocity of rotating blade tips

The maximum efficiency can be found by differentiation to occur when

$$\frac{v_t}{v} = \frac{1}{2(1 - r)^{1/2}}. \quad (4.5)$$

The reaction factor  $r$  denotes the fraction of the stage energy released (enthalpy change) in the moving blade system. By design the turbine has  $r=0.5$ , i.e. half the pressure drop takes place in the moving blade system and internal energy is transformed to kinetic energy. This is a common design value [43]. From equation (4.5) it follows that  $v_t/v = 0.71$  gives a maximum efficiency while the ACACIA turbine has been designed to run most efficient at  $v_t/v$  such that  $v = 212$  m/s for each stage. With a mean blade speed for all stages of 420 m/s the maximum efficiency should lie at around  $v_t/v = 2$ . This conflict can be solved by using efficiency relation (4.4) with  $r = 0.94$ . The more realistic behaviour now corresponds with the ACACIA design, though by definition the turbine model almost represents a reaction stage turbine for Relap5. Figure 4.1 gives the efficiency curve as a function of  $v_t/v$  for a turbine stage with  $r = 0.94$  and  $\eta_t^o = 0.906$ .

The actual turbine work,  $W_t$ , produced by the fluid mass flow rate  $\dot{m}$  on the rotating blades as its momentum is changed, is written as the efficiency factor times the idealised process, the isentropic enthalpy  $h_{isent}$  change across the stage. From the first law of thermodynamics it follows for such a process:

$$W_t = -\eta_t \dot{m} \int dh_{isent} = -\eta_t \dot{m} \int d\frac{p}{\rho_{He}}. \quad (4.6)$$

Because of easy implementation, the Relap5 model assumes  $\rho_{He}$  to be an average constant density for the stage. This assumption is unnecessary and the code has been changed to use the adiabatic density form  $p\rho_{He}^{-\kappa} = \text{constant}$ . Performing the integral of equation (4.6) over a turbine stage, with  $p_i$  the pressure at inlet, and  $p_o$  at outlet, gives

$$W_t = -\eta_t \frac{p_i}{\rho_{He,i}} \dot{m} \frac{\kappa}{\kappa - 1} \left\{ \left( \frac{p_o}{p_i} \right)^{\frac{\kappa-1}{\kappa}} - 1 \right\} \quad (4.7)$$

instead of

$$W_t = -\eta_t \frac{\dot{m}}{0.5(\rho_{He,i} + \rho_{He,o})} (p_o - p_i) \quad (4.8)$$

The remaining fraction  $(1 - \eta_t)$  of the pressure gradient will contribute to changes in the kinetic energy of the helium flow. This fraction is added to the momentum equations

in Relap5. Note that the inefficiency of the turbine should give some dissipation that is a source of internal energy. The dissipation is assumed to be a small effect and is neglected in the model. Fine tuning for the mass flow rate is possible with form loss factors which are a measure for the flow resistance.

The turbine behaviour calculated by Relap5 and by ACM has been depicted in figures 4.2 to 4.5. The mass flow rate and pressure ratio  $\pi$  (ratio  $p_i/p_o$ ) are varied by varying the downstream pressure at the turbine exit. The inlet conditions have been kept constant at design value. For a number of rotational speeds  $\omega$  the conditions have been calculated,  $\omega_{\text{scaled}} = \omega/\omega_o$  is the rotational speed scaled on the design rotational speed  $\omega_o$ . The figures show what happens with the turbine when it moves away from its design working point,  $\pi = 2.248$  and  $\dot{m} = 25.4$  kg/s:

- **Figure 4.2** shows the total turbine power as a function of the mass flow rate for the Relap5 and ACM turbine model. If the pressure ratio is small, i.e. the downstream pressure is nearly equal to the upstream pressure, the mass flow rate reduces. However, as the shaft rotational speed has been fixed, the turbine will start to function as a blower, will pump helium from inlet to outlet, and will require power instead of generating it. The validity of this region of flow is questionable for Relap5. The ACM model on the contrary is capable to describe this region and even further down to reversed mass flow rate.
- **Figure 4.3** shows the efficiency as a function of pressure ratio over the turbine. Two efficiencies are shown, the thin line denotes the theoretical stage efficiency based on the flow velocity and rotor tip speed from figure 4.1. The thick line represents the true isentropic efficiency, calculated from inlet/outlet temperatures and pressure ratio. At higher pressure ratio the true efficiency increases for  $\omega_{\text{scaled}} = 1.0$  and  $1.2$ , while it decreases for the theoretical values. This implicates that the power delivered to the shaft does not exactly match the power extracted from the helium flow (which is determined from the theoretic efficiency curve). This indicates that for the turbine model energy conservation is not guaranteed, something that can be suspected from the ad hoc addition of the turbine model to the Relap5 basic equations. It does not automatically mean that the model should not be used - after all the difference is only a few percents -, only that for turbine working points far from steady-state, the predictions become less accurate. An example will be given in chapter 6. Serious disturbance of the working point can be expected when the shaft speed changes considerably, but normally the rotational speed will not vary more than  $\pm 10\%$  around nominal value, in which region the turbine model certainly can be used. For low rotational speed the efficiency decreases: the impeller tip speed  $v_t$  reduces and from the discussion of figure 4.5 it will follow that the flow velocity  $v$  increases. In figure 4.1 it means that the efficiency of the working point shifts down on the left flank. Where the gradient is steep, the efficiency will fall rapidly with decreasing  $v_t/v$ . The opposite is true for increasing shaft speeds, where the efficiency remains fairly constant for larger  $v_t/v$ . As a result at larger shaft velocities the efficiencies will be comparable.
- **Figure 4.4** shows the true efficiencies as a function of pressure ratio over the turbine for the Relap5 and ACM model. It is clear that both turbine models yield different

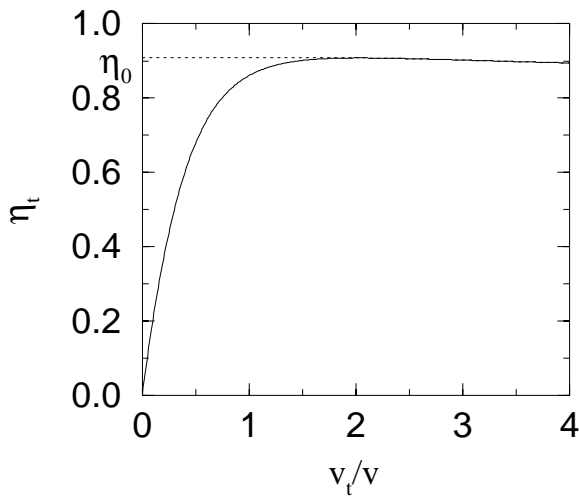


**Figure 4.1:** Analytic efficiency curve for a reaction stage turbine with reaction fraction  $r=0.94$  and efficiency  $\eta_0=0.906$ .

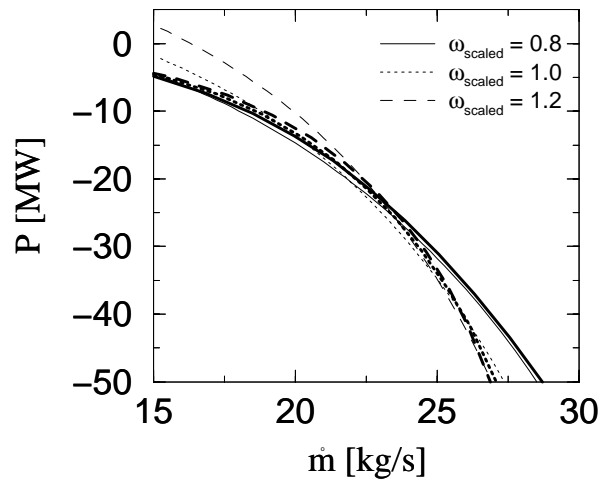


**Figure 4.2:** Total power needed to balance the turbine shaft as a function of mass flow rate. Thick line Relap5, thin line ACM.

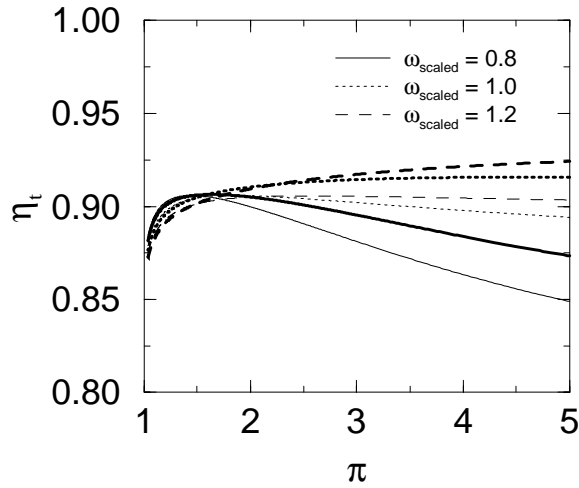


**Figure 4.3:** The isentropic turbine efficiency as a function of the pressure ratio  $\pi$ . Thick line the true efficiency, thin line theoretical  $\eta_t$  according to figure 4.1.

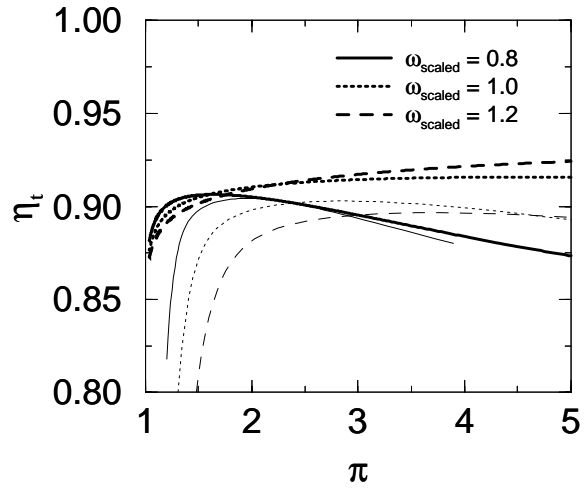


**Figure 4.4:** The isentropic turbine efficiency  $\eta_t$  as a function of the pressure ratio  $\pi$ . Thick line Relap5, thin line ACM.

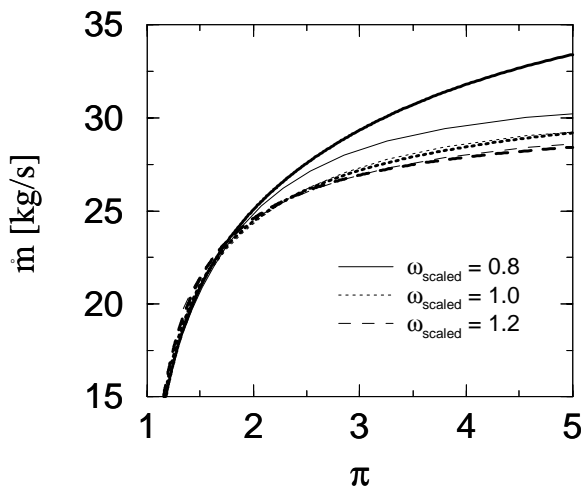


**Figure 4.5:** Turbine mass flow rate  $\dot{m}$  as a function of the pressure ratio  $\pi$ .

efficiency curves, but the shape and tendencies are comparable. Notice that it is easy to bring both curves to a closer accordance by changing the factor  $\eta_t^o$  to a lower value than the design value of 0.906.

- **Figure 4.5** shows the mass flow rate as a function of the pressure ratio over the turbine. This type of figure gives an indication of the resistance the flow experiences while flowing through the turbine. At low rotational shaft speeds when less power is extracted from the flow, it follows that the flow is larger. When the shaft stops rotating, in the Relap5 model the turbine degenerates to an ordinary nozzle and the flow will be very large, with high velocities.

As a general remark one can conclude that although the accordance between the models is not perfect, the differences are small (in the order of a few percents) and the tendencies shown are similar.

## 4.2.2 Radial Helium Compressor

For the initial modelling of the helium compressor the Relap5 water pump model was used. As a first trial it served its purpose, but now a new routine has been developed. It replaces the pump model with a compressor stage model if the fluid quality equals 1.0, i.e. the fluid is completely in the gas phase. It calculates all variables Relap5 would require from the pump model, including the compressor dissipation. The complicated configuration of a radial compressor precludes a complete first-principle model, so empirical relations are used instead for stage by stage modelling. The current compressor model contains 5 stages, the data are given in table 4.2 and based on [31, 42].

**Table 4.2:** Compressor stage data for the Relap5 model.

$\phi_{\text{design}}$	0.43					
$\lambda_{\text{design}}$	0.73					
$h_{\text{ndim,design}}$	0.677					
design efficiency (polytropic)	0.90					
inlet pressure [MPa]	1.000					
outlet pressure [MPa]	2.304					
rotational design speed [rad/s]	1256.6					
stage	1	2	3	4	5	
blade tip diameter [m]	0.83	0.80	0.78	0.75	0.74	
flow area [m <sup>2</sup> ]	0.088	0.080	0.076	0.069	0.065	
stator inlet temperature [K]	365.	397.8	430.6	463.4	496.2	
stage outlet temperature [K]	397.8	430.6	463.4	496.2	529.	
pressure ratio	1.214	1.195	1.180	1.166	1.150	

Neglecting the weak dependence on Reynolds-number and tip-speed Mach number enables a formulation with dimensionless numbers [84]. Empirical relations in the form of compressor maps are defined for the work input coefficient  $\lambda$  and dimensionless polytropic head  $h_{\text{ndim}}$ , both as a function of a flow coefficient  $\phi$ .

$$\phi = \frac{\dot{m}}{\rho_{He} A_f v_t} \quad (4.9)$$

$$\lambda = \frac{W_c}{v_t^2 \dot{m}} \quad (4.10)$$

$$h_{\text{ndim}} = \frac{gh}{v_t^2} = \frac{\Delta p / \rho_{He}}{v_t^2} \quad (4.11)$$

$$\eta_c = \frac{h_{\text{ndim}}}{\lambda} \quad (4.12)$$

with  $W_c$  the power ( $\text{J s}^{-1}$ ) required to drive the compressor,  $\dot{m}$  the mass flow rate ( $\text{kg s}^{-1}$ ),  $v_t$  the tangential velocity of the rotor blade ( $\text{m s}^{-1}$ ),  $A_f$  the flow cross sectional area ( $\text{m}^2$ ),  $g$  the gravitational acceleration ( $\text{m s}^{-2}$ ),  $h$  the head (m),  $\Delta p$  the pressure increase (Pa), and  $\eta_c$  the stage design efficiency.

The working point of a compressor stage is subsequently determined from the two compressor maps given in figures 4.6 and 4.7.

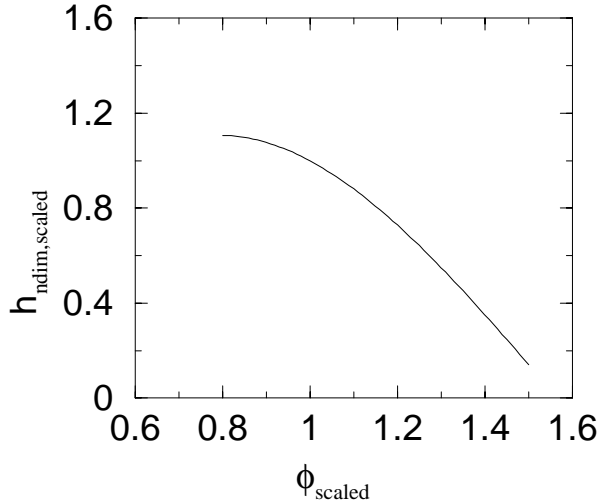


**Figure 4.6:** *Radial compressor stage map in order to determine the generated head as a function of the helium gas flow.*

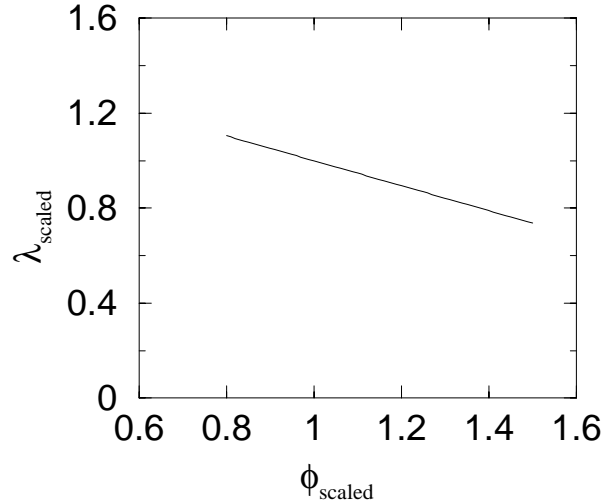


**Figure 4.7:** *Radial compressor stage map in order to determine the required torque for compression as a function of the helium gas flow.*

The data for the compressor stage maps have been obtained by scaling the stage characteristics of air-breathing compressors [84] due to lack of design- and test data for helium compressors. The dimensionless numbers  $\lambda$ ,  $h_{\text{ndim}}$  and  $\phi$  have been normalised to their design values, indicated by the subscript <sub>scaled</sub>:

$$h_{\text{ndim,scaled}} = \frac{h_{\text{ndim}}}{h_{\text{design}}} \quad \lambda_{\text{scaled}} = \frac{\lambda}{\lambda_{\text{design}}} \quad \phi_{\text{scaled}} = \frac{\phi}{\phi_{\text{design}}} \quad (4.13)$$

No attempt has been made to describe the stage characteristics during stall and surge operation for the Relap5 model, as it (presently) is beyond the scope of this study. Another reason not to include the stall and surge region for the compressor is that the turbine model for good measure should be adapted as well, which is not straightforward



at all. For the ACM compressor model - which uses the same compressor maps - this surge and stall region has been defined. In figures 4.6 and 4.7 it means that the regions for  $-0.4 \leq \phi \leq 0.8$  also have been defined [50].

### 4.2.3 Recuperator

The counterflow recuperator has been included in the ECS in order to enhance its efficiency. Instead of rejecting all the heat in the precooler before compression, the heat is used to warm the high pressure helium flow towards the reactor. The recuperator is a passive component in these calculations, for instance no effort has been made here to model an attemperation valve in order to protect the recuperator against thermal shock. Both the high and low pressure side of the recuperator have been modelled as a pipe divided in 10 volume elements. Volume element 1 of the one side has a thermal contact with element 10 of the other side, element 2 with 9, etc., in order to model the counterflow. The nodalisation with a small number of volumes reduces the driving force for heat transfer, that is, the temperature difference over the cold and hot side decreases. A correction factor  $G$ , depending on the number of nodes and mass flow rate, can be calculated to restore the true heat transfer. One value for  $G$  has been calculated for the nominal steady state and has been used throughout the transient calculations. The calculation of  $G$  can be found in appendix B. The heat transfer coefficient itself follows from the relations discussed in section 3.3 and is mainly dependent on the mass flow rate  $\dot{m}$ . It is multiplied by  $G$ .

The heat capacity of the steel that forms the recuperator, approximately 5.4 metric tons, has been included in the calculations. The slight pressure drop over the recuperator has been achieved by tuning with small form loss factors.

Table 4.3 provides an overview of the design values for the recuperator. The cold and hot side of the heat exchanger differ slightly in mass flow rate: a small leak flow exists from compressor outlet directly to turbine inlet, effectively bypassing cold recuperator side and reactor. It represents a leakage over the turbine/compressor stages and the cooling of shaft and bearings.

**Table 4.3:** *Recuperator design data.*

	cold side	hot side
mass flow rate [kg/s]	25.2	25.4
inlet temp. [°C]	260.	521.
outlet temp. [°C]	494.	288.
inlet pressure [MPa]	2.304	1.015
outlet pressure [MPa]	2.299	1.004
heat tr. coeff. [ $\text{W m}^{-2} \text{K}^{-1}$ ]	520.3	526.0
heat tr. area [ $\text{m}^2$ ]	4154.0	4154.0
correction factor	5.16	5.16

#### 4.2.4 Precooler

The precooler transfers heat from the ECS to the secondary cycle where the steam production takes place. In the current Relap5 model the secondary cycle has not been modelled, and the precooler functions as a steady heat sink that always cools the helium flow to 92°C. The heat has to be removed in order to facilitate compression and thus to obtain a higher cycle efficiency (from equations (4.1) and (4.3) can be seen that for a stand-alone compressor the work is linear with the inlet temperature). The precooler has been modelled as a pipe divided in 4 volume elements. Each element has been given a large heat transfer surface, a large heat transfer coefficient and a constant wall temperature of 92°C.

#### 4.2.5 Shaft and Generator

Attached to the shaft are the 4 turbine stages, the 5 compressor stages and the asynchronous generator. All parts exert a torque on the shaft which are related to each other by

$$\sum_i I_i \frac{d\omega}{dt} = \sum_i \tau_i - \sum_i a_i \omega + \tau_c \quad (4.14)$$

with  $\omega$  the shaft rotational speed,  $\tau_i$  the exerted torque by component  $i$ ,  $\tau_c$  an optional torque from a control system component,  $a_i$  the friction factor of component  $i$ , and  $I$  the inertia. For the total turbine, compressor and generator the inertia is 10, 10, and 30 kg m<sup>2</sup>, respectively. Mechanical losses on the shaft are estimated to be 1% of the generator torque, that makes  $a_i \approx 0.09$  for the steady state. The generator is of the asynchronous kind, which means that it does not have to run at a fixed rotational speed (for instance 50 Hz) and that a frequency converter is used to produce the grid frequency. The efficiency of the power conversion from torque to electric power by the generator is estimated to be 0.99; the efficiency of the frequency converter 0.96.

#### 4.2.6 Valves

The valves in the system have been modelled with an abrupt change of cross-sectional flow area; a smooth change is possible but requires relations between stem position and flow. This is an unnecessary detailed description compared to other components, and furthermore, the valves will be closed in most situations. Three valves have been modelled in the energy conversion system: a valve for helium entering the system, a valve for helium leaving the system and a bypass valve over reactor and turbine. During steady state conditions all valves are closed, only in the case of load following they become active. This is discussed in section 4.3.

In certain cases the pressure ratio over the valve will be larger than the critical pressure ratio, resulting in a choked flow. Choking is defined as the condition wherein the mass flow rate becomes independent of the downstream conditions (that point at which

further reduction in the downstream pressure does not change the mass flow rate), and the valve or - in terms of Relap5 - junction is passing the maximum possible mass flow rate [43]. The Relap5 choked flow model represents a first-principle approach [85, 86] to the calculation of choking for two-phase mixtures. It can also accommodate noncondensable gases, such as helium.

## 4.3 ECS Control System

The control system has been kept straightforward, and focuses only on three things:

1. protect the shaft against excessive overspeed in rotational speed,
2. protect the shaft against too much underspeed which causes the ECS to leave the stable operating region,
3. produce the power demand at high efficiency, also when operating at partial load.

These objectives will be discussed in detail in the following three sections. Contiguously section 4.3.4 will discuss the logic implementation of the control system.

### 4.3.1 Overspeed in Shaft Rotational Velocity

An overspeed in the shaft speed will develop when the generator load is decreased. A small overspeed (10%) will not damage the shaft components, however, if the overspeed is much larger the rotor components of turbine and compressor will not be able to withstand the centrifugal stresses. Large overspeed can be expected in cases of load rejection (suddenly the generator cannot deliver power to the grid), or generator trip (breakdown of generator). In both cases the generator load disappears and the excess power speeds up the shaft to over 1.5 times nominal speed as will be shown in chapter 6. The increase in shaft speed will increase the mass flow rate and pressure ratios. The increase in required compressor power will balance the power production by the turbine. As the inertia of turbine and compressor is low, the process only takes a few seconds. A fast solution is to short circuit the recuperator high- and low pressure side by opening a valve, effectively bypassing the reactor and turbine for part of the mass flow rate. The turbine power production falls with decreasing mass flow rate (figure 4.2). Opening the bypass valve decreases flow resistance, which leads to an increased mass flow rate through the compressor, so the compressor work increases. The power balance can be found at nominal shaft speed by opening the bypass valve accordingly. Fully opened, the bypass will be able to divert one third of the helium flow, which results in a reduction of generator power output to around 5% of the nominal conditions.

More positions of the valve are possible than depicted in figure 1.4, for instance one could choose to bypass only the turbine instead of both turbine and reactor, but this will upset the temperatures of the components more than is necessary: in that case the high temperature flow from the reactor is bypassed over the turbine and mixes with the turbine output flow. A flow suddenly at higher temperature enters the low pressure side of the recuperator. Such a thermal shock should be avoided at these high temperatures

as it can initiate creep, and cause a premature end of the recuperator. From studies with the ACM model [48] it turned out that the current bypass position is one of the more favourable; the difference in temperature between reactor inlet and turbine outlet flow is small (30 K), and mixing the flows gives nearly the same temperature. As explained above, the bypass valve is the fast solution for overspeed in shaft speed. The ECS will function at low efficiency, and as such it is a temporary solution. In order to restore the efficiency close to nominal operation, helium will have to be removed from the circulation. That is the subject of section 4.3.3.

### 4.3.2 Underspeed of Shaft Rotational Velocity

Not only overspeed of shaft speed should be avoided, also underspeed causes problems for the ECS. Deceleration of the shaft occurs when the generator load increases, that is, when the power demand increases. Figure 4.8 shows the generator power production as a function of the shaft rotational speed. All points on the curve represent steady-state

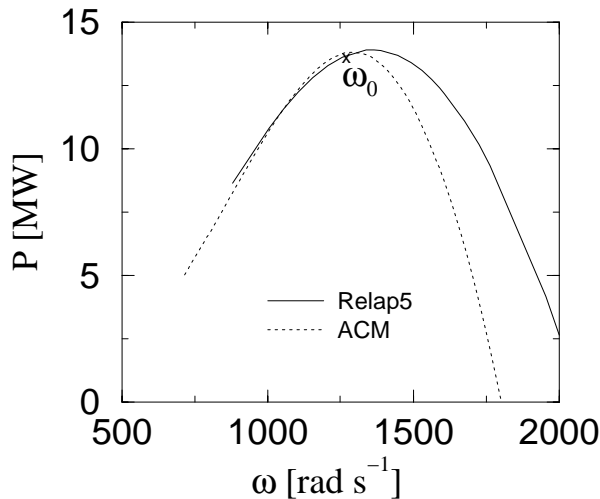


**Figure 4.8:** *The power production as a function of the shaft rotational speed*

situations with all valves closed, and without a reactor response, i.e. a fixed reactor outlet temperature of 800°C. If the ECS finds itself on the left flank of the graph, an increase in power demand (which always will decrease the shaft rotational speed) will further decelerate the shaft and the system will produce even less power. This is the instable region, and if nothing is adjusted the shaft will ultimately come to a halt. If the system finds itself on the right flank of the graph the increase in power demand will also decelerate the shaft, but increase the power production. This is the stable region. If the power demand is too large, the ECS will shoot over the top of the curve and end up in the instable region. Figure 4.8 represents nothing more than the balance of torques between turbine, compressor and generator when away from the design working point. As explained in section 4.2.1, the Relap5 efficiency relation of the turbine is different from the ACM model, and therefore the curves in figure 4.8 are not identical. Both systems find their working point slightly on the left-hand side of the top. This does not

automatically mean that the system cannot meet increasing power demand, only that there is no margin from the ECS itself, and the control system will have to intervene. As will be explained in section 4.3.3, it will be necessary to increase the helium mass flow rate. A provision has also been made to cope with large sudden power demands that exceed the rate at which power can be increased by adding helium: the control system will not allow the shaft speed to become less than 95% of the nominal value by simply refusing the excess in power demand. The system will be allowed some time (minutes) to fill with helium.

Furthermore, in real life the generator will be coupled to the grid, and if the ECS for some reason needs help not to slide down the slope towards lower shaft speed, it will supply less power to the grid. If the plant is on its own (islanding) this of course is not possible.

### **4.3.3 Helium Inventory Control**

Responding to a change in power demand, so called load following, can be achieved by opening/closing the bypass valve, as has been described in section 4.3.1. That is only a temporary solution because of poor thermal efficiency. A long term solution would be to change the helium inventory in the system. The amount of heat produced by the reactor is approximately linear with the helium mass flow rate through the core. This is a first order approximation where the effects on the gas temperature at reactor outlet from xenon decay or build-up are ignored. From section 5.2 it will follow that this assumption is reasonable for the first few hours. If for instance the power demand drops, the control system can reduce the mass flow rate and effectively reduce the cooling capacity of the flow. The reactor core will start to warm up as it can not transfer all its heat to the gas, and will lessen the power production as can be expected from a negative temperature coefficient of reactivity for the core (section 3.4.4). A new equilibrium will be found where the heat production has been reduced to match the heat transfer to the gas, and approximately the same gas temperature at reactor outlet will be maintained. The process of extracting helium from the circulation stops as soon as the shaft rotational speed reaches its design velocity, that will be the point at which the power demand can be met. At that point the gas velocities and pressure ratio in the cycle are again equal to nominal conditions (shaft rotational speed is the same) and the reactor outlet gas temperature is more or less equal to nominal conditions. Both turbine and compressor will still operate near the design conditions. Consequently, approximately the same high efficiency as under nominal conditions will be reached at partial load conditions.

Of course it is advantageous to operate at high efficiency in the Brayton cycle, but what is the energy required to remove or add helium from/to the system? This is a legitimate question: if the energy consumption is high, the time required to gain in overall efficiency is long and sometimes it may not be advantageous to change the helium inventory for a short change in power demand. Many configurations are possible and have been investigated [47], here the solution that uses the excess in turbine energy to change the helium inventory will be presented.

It is possible to design a storage system without extra inventory compressors or pumps. The system compressor in the Brayton cycle will perform the work required to store the helium in pressure tanks. Each time helium has to be removed from the ECS, part of the excess of power available in the system will be used for this purpose. At the high pressure (HP) point in the primary cycle, i.e., at compressor outlet, helium will flow out of the system into a storage tank at lower pressure. If the tank sizes and pressures have been chosen such that the end pressure of the full tank is higher than the lowest ECS pressure (LP point), then the helium can flow back into the system when necessary without the help of a pump. The LP point of the system lies between turbine outlet and compressor inlet; in order to operate the compressor at constant inlet temperature and to minimise temperature disturbances in the rest of the ECS, the tank outlet has been connected to the precooler inlet. Define for the storage system:

- $f$ , the factor by which the pressure in the primary system in/decreases due to emptying/filling the storage tanks,  $f > 1$ ,
- $d$ , the factor by which the tank pressure in/decreases when filling/emptying the tank,  $d > 1$ ,
- $g$ , the ratio of tank pressure to system pressure at which inflow from system to tank stops,  $g < 1$ ,
- $g'$ , the ratio of system pressure to tank pressure at which outflow from tank to system stops,  $g' < 1$ ,
- $K$ , the ratio of system pressure in the HP-point to the LP-point. This pressure ratio is maintained by the system compressor.

The ratio's  $g$  and  $g'$  prevent the primary system and tanks from exactly reaching an equilibrium in pressure. Minor oscillations in mass flow rate direction around equilibrium are thus avoided. Following the cycle of filling a tank from the HP-point in the primary cycle to emptying it again at the LP-point in the primary cycle gives the relation between  $f$ ,  $d$ ,  $g$ ,  $g'$ , and  $K$ :

$$d = \frac{g' \cdot g \cdot K}{f} \quad (4.15)$$

The number of stages  $n$  (= number of pressure tanks or pressure zones) required to increase the system pressure from a pressure  $p_{\min}$  (for instance at 50% power demand) to the final pressure at nominal power  $p_{\max}$  ( $p_{\min}$  and  $p_{\max}$  measured in same pressure point) is given by:

$$f^n = \left( \frac{p_{\max}}{p_{\min}} \right) \quad (4.16)$$

An important parameter is the number of storage tanks required and their respective sizes, because they tend to become large. First the simplified situation of isothermal filling and emptying of the tanks will be considered, afterwards the adiabatic case. For slow and small, partial filling/emptying of a tank the isothermal model may be used, but for a fast and substantial filling/emptying of a tank an adiabatic description must be used. The following variables are used in the descriptions:

- $p^{\text{HP}}$  = the system pressure at the high pressure point, before filling a tank
- $p^{\text{LP}}$  = the system pressure at the low pressure point, before filling a tank
- $p_1$  = the empty tank pressure, temperature in equilibrium with surroundings
- $p_2$  = the full tank pressure, immediately after ending the mass transfer
- $p_3$  = the full tank pressure, temperature in equilibrium with surroundings
- $p_4$  = the empty tank pressure, immediately after ending the mass transfer
- $T_s$  = the system temperature at high pressure point
- $T_1$  = the empty tank temperature when in thermal equilibrium with surroundings
- $T_2$  = the full tank temperature, immediately after ending the mass transfer
- $T_3$  = the full tank temperature when in thermal equilibrium with surroundings
- $T_4$  = the empty tank temperature, immediately after ending the mass transfer
- $V_s^{\text{HP}}$  = the effective ECS volume when all mass is thought to be at  $p_{\text{max}}^{\text{HP}}, T_s$
- $m_s$  = the mass in the ECS before filling a storage tank
- $V_t$  = the storage tank volume

### Isothermal tank description

The isothermal filling/emptying of a storage tank is depicted in figure 4.9. For the

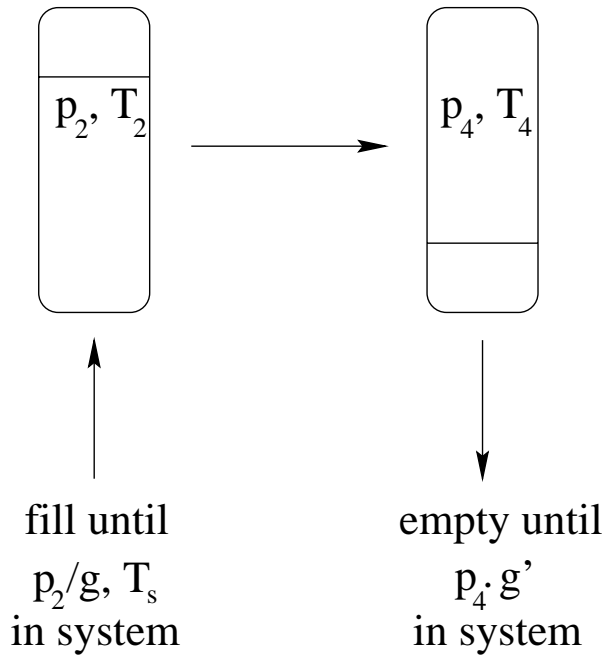


**Figure 4.9:** *The isothermal storage tank system.*

isothermal treatment,  $T_2$  and  $T_4$  are equal to the environment temperature. When a tank is filled, the pressure at the HP point drops from  $p^{\text{HP}}$  to  $p^{\text{HP}}/f$ , with  $p^{\text{HP}}$  equal to  $K \cdot g'p_4$ . The mass  $\Delta m$  flowing from ECS into vessel is then

$$\Delta m = p^{\text{HP}} \frac{\left(1 - \frac{1}{f}\right)}{RT_s} V_s^{\text{HP}} = K \cdot g'p_4 \frac{\left(1 - \frac{1}{f}\right)}{RT_s} V_s^{\text{HP}} \quad (4.17)$$

with  $R = 2077.3 \text{ J/kg/K}$  the gas constant for helium. The same mass balance can be formulated for the storage tank, with  $p_2 = d \cdot p_4$  by definition and with  $T_4 = T_2 = T_{\text{env}}$ , the ambient temperature:

$$\Delta m = \frac{V_t}{R} \left( \frac{p_2}{T_2} - \frac{p_4}{T_4} \right) = \frac{p_4 V_t}{R T_{\text{env}}} (d - 1) \quad (4.18)$$

Equating the two expressions for  $\Delta m$  and using equation (4.15) to eliminate  $d$ , yields for the storage tank size:

$$V_t = \frac{(f - 1)}{\left(g - \frac{f}{K g'}\right)} \frac{m_s R T_{\text{env}}}{p^{\text{HP}}} \quad (4.19)$$

### Adiabatic tank description

If the tank fills or empties fast ( $< 5$  minutes), the process must be treated as adiabatic compression/expansion as the heat exchange between gas and tank wall is too slow to keep the gas temperature constant in the tank. The steel tank wall will absorb or supply all heat to the gas without changing temperature more than 2 or 3°C. The process of free convection of course depends on the tank size and orientation, but normally it will take around 30 minutes to approach equilibrium with the environment within a few degrees.

The adiabatic filling/emptying of a storage tank is depicted in figure 4.10. At stage 1

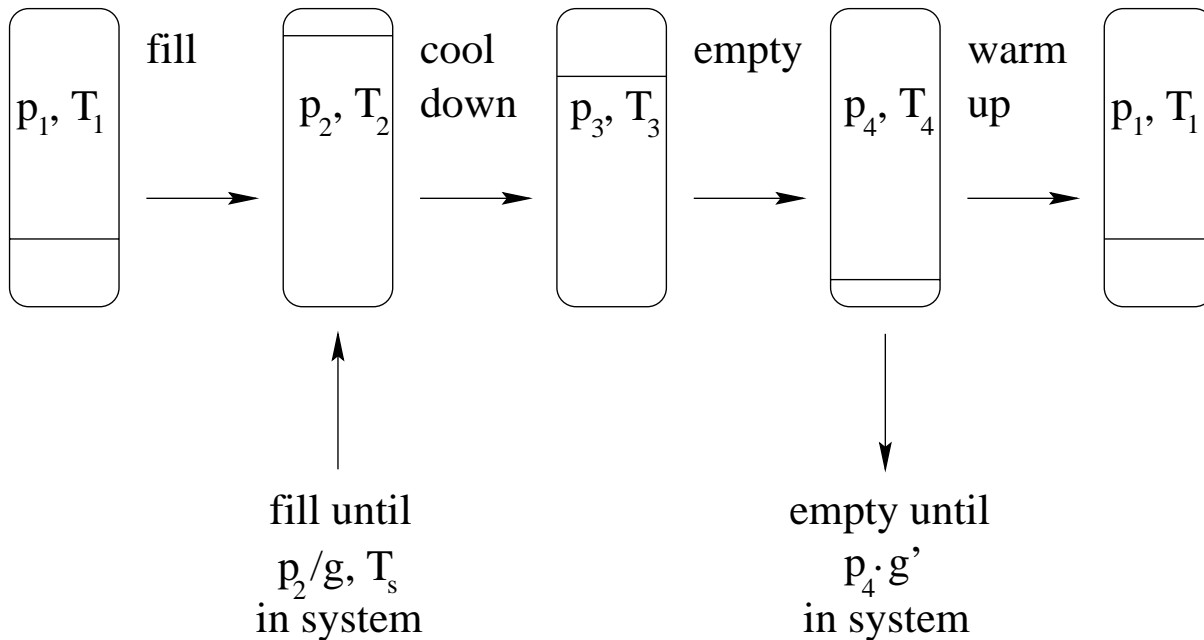


**Figure 4.10:** *The adiabatic storage tank system.*

the tank is in thermal equilibrium with the surroundings, stage 2 differs from figure 4.9 in a higher gas temperature due to adiabatic compression, stage 3 represents stage 2 in thermal equilibrium with the surroundings, and stage 4 differs from figure 4.9 in a lower gas temperature due to adiabatic expansion. Important to notice is that from the



point of view of the ECS, the tank appears to be reduced in its capacity to store/supply helium. Larger tanks will be needed than calculated for the isothermal case. In order to determine the tank size, first all 4 states of figure 4.10 must be expressed in known variables. Again two equations for the transferred mass  $\Delta m$  are formulated. The first follows straightaway from the difference in mass between stage 1 and 3:

$$\Delta m = \frac{V_t}{R} \cdot \left( \frac{p_3}{T_3} - \frac{p_1}{T_1} \right) \quad (4.20)$$

The second follows from the first law of thermodynamics (the energy balance) for the filling of a tank. This equation has been derived in appendix C:

$$\Delta m = \frac{1}{(\kappa - 1)} \cdot \frac{V_t}{C_p T_s} (p_2 - p_1) \quad (4.21)$$

Together with the following equations for the isentropically expanding helium during the emptying of the vessel:

$$T_4 = T_3 \left( \frac{p_4}{p_3} \right)^{\frac{(\kappa-1)}{\kappa}} \quad (4.22)$$

$$\frac{p_1}{T_1} = \frac{p_4}{T_4} \quad (4.23)$$

$$\Rightarrow p_1 = p_4 \frac{T_1}{T_3} \left( \frac{p_3}{p_4} \right)^{\frac{(\kappa-1)}{\kappa}} \quad (4.24)$$

$$(4.25)$$

can be written

$$\frac{1}{\kappa T_s} \left( p_2 - p_4 \frac{T_1}{T_3} \left( \frac{p_3}{p_4} \right)^{\frac{(\kappa-1)}{\kappa}} \right) - \left( \frac{p_3}{T_3} - \frac{p_4}{T_3} \left( \frac{p_3}{p_4} \right)^{\frac{(\kappa-1)}{\kappa}} \right) = 0 \quad (4.26)$$

which can be solved numerically for  $p_3$ , all other variables are known:  $T_1 = T_3 = T_{\text{env}}$ , the environment temperature,  $p_2 = p^{\text{HP}} \cdot g/f$ , and  $p_4 = p^{\text{LP}}/g'$ .

Now all tank states are known, and the tank size can be determined with equations (4.17) and (4.18), only  $T_2 \neq T_4$ :

$$V_t = \frac{(f - 1)}{\left( \frac{g}{T_2} - \frac{f}{T_4 K g'} \right)} \frac{m_s R}{p^{\text{HP}}} \quad (4.27)$$

From equations (4.19) and (4.27) it follows that minimising  $f$  results in a smaller tank volume, but from equation (4.16) it follows that the number of tanks  $n$  will increase. Multiplying  $n$  with  $V_t$  and taking the limit of  $f \rightarrow 1$  will give the theoretical minimal total storage volume required:

$$\lim_{f \downarrow 1} n V_t = \lim_{f \downarrow 1} \frac{\ln \left( \frac{p_{\text{max}}}{p_{\text{min}}} \right)}{\ln f} \cdot \frac{f - 1}{\left( \frac{g}{T_2} - \frac{f}{T_4 K g'} \right)} \frac{T_{\text{env}} V_s^{\text{HP}}}{T_s} = \frac{\ln \left( \frac{p_{\text{max}}}{p_{\text{min}}} \right)}{\left( \frac{g}{T_2} - \frac{1}{T_4 K g'} \right)} \cdot \frac{m_s R T_{\text{env}}}{p^{\text{HP}}} \quad (4.28)$$

In real life this limit will not be feasible as  $f = 1.000015$  means for the current design installing 0.15 million tanks the size of a Coca Cola can. However, it shows that reducing  $f$  results in a smaller total tank volume. The following observations can be made:

- The tank volume has a linear dependency on the mass  $m_s$ . If the inventory mass doubles because of design adjustments, the size of the storage tanks will double.
- The tank volume depends on  $T_s$  in the adiabatic description. This is not straightforward to see in equation (4.27), but from equation (4.21) one concludes that decreasing  $T_s$  increases the helium mass  $\Delta m$  stored in a volume  $V_t$ , ergo, less tank volume is necessary. Reducing the temperature of the gas that flows into the tank,  $T_s$ , by a heat exchanger will reduce the tank size. Notice that this result does not result from the isothermal description, there the temperature of the incoming helium and helium residing in the tank is always in equilibrium with the environment.
- The tank volume has a linear dependency on  $T_{\text{env}}$ . Therefore the tanks should be stored in a cool, ventilated space.
- The tank size will decrease if the compression ratio  $K$  in the main system increases. For the isothermal case this becomes clear when  $p^{\text{HP}} \propto K$  is substituted in equations (4.19). For the adiabatic case it is also true, but difficult to derive from equation (4.27) as  $p_3$  cannot be expressed explicitly which is needed to substitute  $T_2$ .
- If the fractions  $f$  and  $d$  remain the same for each of the  $n$  tanks, then the  $\Delta m$  transferred from the ECS to the last tank will be less by a factor  $f^{n-1}$  compared to the first tank. This follows from equation (4.18) when realising that  $p_4$  drops by a factor  $1/f$  each time a tank is filled. If  $f^n$  is large, that is, for instance 90% of the helium has to be stored in the tanks, then the last number of tanks will hardly contribute to the helium storage capacity while occupying the same space as the first tanks. As a practical rule, it is wise to use a compressor for the regime from 50% to 10% inventory reduction.

## Choice of configuration for ACACIA storage system

The choice in optimising between the number of vessels (total volume) and increasing complexity (number of components) is rather complex and depends on many choices in design. However, in most cases there will be an upper limit on the available space for the storage tanks. From figure 4.11 it can be estimated for the adiabatic case what degree of inventory reduction will be available. Say for instance the total volume available is  $120 \text{ m}^3$ , then for 3,4,6, or 12 tanks ( $40,30,20,10 \text{ m}^3$ ) the inventory reductions are depicted, roughly around 50% for all of them. Further constraints might be that at least 50% reduction must be reached with the tank system; this eliminates a 3 tank system (over  $120 \text{ m}^3$  storage space needed). The difference in storage capacity between 6 or 12 tanks is negligible, while the production costs in general will not, so the choice remains between 4 or 6 tanks. Additional information about room dimensions (ceiling height and floor surface) may be used to settle the issue; otherwise a 4 tank system has a slight advantage by being more simple. From figure 4.11 it becomes clear that

further inventory reduction to 90% would require 9 additional tanks of 30 m<sup>3</sup>.

For the ACACIA system there has tentatively been decided on a 4 tank system of 30 m<sup>3</sup> each for inventory reduction in the range 100% to 50%, and an additional positive displacement compressor (also called reciprocal or piston compressor) will be used for the range below 50%. Table 4.4 gives the values used for the calculation.

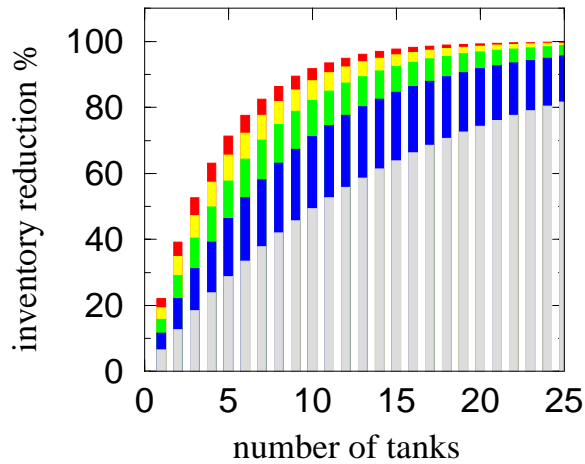


**Figure 4.11:** For 5 tank sizes the inventory reduction for the adiabatic case has been plotted as a function of the number of full tanks. From top to bottom: 50 m<sup>3</sup> (red), 40 m<sup>3</sup> (yellow), 30 m<sup>3</sup> (green), 20 m<sup>3</sup> (blue) and 10 m<sup>3</sup> (grey).

**Table 4.4:** Inventory Storage System design data. The pressures  $p^{\text{HP}}$ ,  $p^{\text{LP}}$  and mass  $m_s$  are given for a 100% ECS inventory. Four tanks store 50% inventory.

$T_1, T_3, T_{\text{env}}$ [K]	300.0
$T_s$ [K]	300.0
$p^{\text{HP}}$ [MPa]	2.30
$p^{\text{LP}}$ [MPa]	1.00
$m_s$ [kg]	126.0
$K$	2.3
$g$	0.99
$g'$	0.99
$f^n$ [%]	50.0
$V_t$ [m <sup>3</sup> ]	30.2

#### 4.3.4 Configuration of Control System

The previous three sections showed that both sudden variations in generator load and load following at high efficiency will induce variations in shaft speed. In that case all three objectives of the control system mentioned at the beginning of section 4.3 can be

related to one signal: the deviation of the shaft rotational speed from its nominal value. It has been chosen that this signal controls the three valves, a bypass valve for fast response to overspeed, and two valves for changing the helium inventory of the ECS. In the Relap5 model one of these valves is connected to a helium mass sink, the other to a helium mass source. If the shaft rotates too fast, the signal becomes positive and opens the bypass valve proportional to the magnitude of the signal; at the same time this is an indication that too much power is produced and helium can be extracted from the system. The same signal is therefore used for opening the valve to the helium mass sink. If the shaft rotates too slow the bypass signal becomes negative and the bypass valve closes or remains closed. The negative signal also indicates that an extra load has been placed on the shaft and that more helium should be added to the inventory. The bypass signal now opens the valve connected to the helium mass source. In order to prevent a valve system that continually opens and closes valves due to small variations in shaft speed, a low threshold value has been placed on the bypass signal activating the valves. The bypass valve remains slightly open during steady state and accommodates small variations in the shaft speed.

## 4.4 Summary

This chapter describes the ECS and the modelling of the Brayton cycle for the energy conversion system with the Relap5 code. The models of the various components have been compared to the more detailed reference ACM model. Differences are found in

- the behaviour of the turbine models. Relap5 uses a single, simple equation for the turbine efficiency which is only valid for normal forward flow conditions, and which might be too simple. In the ACM code the turbine model is based on a mean diameter flow path analysis which also is valid during very low and reversed flows.
- the behaviour of the recuperator models. Both ACM and Relap5 use a correction factor for the heat transfer. The factor increases the heat transfer which had been decreased due to the nodalisation of the component. In ACM this correction factor is continuously updated according to flow conditions, while Relap5 uses a fixed factor for steady-state design.
- The valve model in Relap5 - contrary to ACM - does not use relations between stem position and flow. An abrupt change of the cross-sectional flow area obstructs/regulates the mass flow rate.

All the differences are considered to be small and explicable, and both models predict the same trends. Therefore, the ECS model of Relap5 has been accepted.

This chapter also presents the design for the control system in Relap5. It has been kept very straightforward, and only focuses on keeping the shaft rotational speeds within bounds. Furthermore, the control system optimises the efficiency of the power production by matching the mass flow rate to the power demand. The operation of this helium inventory system has been described and suggestions for its design have been made.

# Chapter 5

---

## Stand-Alone Reactor Dynamics

---

### 5.1 Introduction

In this chapter the dynamic behaviour of the pebble-bed reactor will be discussed for operational transients in order to demonstrate the validity of the point reactor kinetic model. The four reactor models, viz. Panthermix, Relap5 point kinetics with its thermal hydraulics, Relap5 point kinetics with the thermal hydraulics of Thermix-Direkt, and ACM point kinetics with its thermal hydraulics, will be compared. The Panthermix calculations serve as reference because it is the most detailed model.

Three representative operational transients will be considered in section 5.2. In section 5.3 the assumptions and approximations made for the point reactor kinetic model will be (re)evaluated with the help of the operational transients. Two loss of cooling incidents will be calculated in order to test the limits of the point reactor kinetic model. A theoretical model [87, 88] will be used to describe the recriticality behaviour of the loss of cooling incidents.

### 5.2 Operational Reactor Transients

Three operational transients will be discussed that are considered to be representative for a broad range of possible operational reactor transients:

- From nominal conditions the inlet gas temperature increases abruptly with 100°C,
- From nominal conditions the inlet gas temperature decreases abruptly with 100°C,
- From nominal conditions the mass flow rate decreases abruptly to 25%.

In the cases presented, the transient ends when a new steady-state situation is reached, that is, when xenon also reaches a new equilibrium after a few days. The choice of

the transients mentioned above has been made by looking at the power  $P_{he}$  transferred from pebble-bed to gas, given earlier by equation (3.1):

$$P_{he} = \alpha A (T_{surf} - T_g) \quad (5.1)$$

with  $T_{surf}$  as the pebble-bed surface temperature,  $T_g$  the gas temperature,  $A$  the heat exchanging surface, and  $\alpha$  the heat transfer coefficient. The coupling between the neutronics and thermal hydraulics of the core can be influenced by varying either  $T_g$  or  $\alpha$  (or both), which explains the choice of transients to analyse. From figure 3.8 it follows that  $\alpha$  depends mostly on the mass flow rate  $\dot{m}$ , and that it is only weakly temperature dependent.

During the transient the temperatures  $T_{surf}$  in the core will change as result of altered heat transfer conditions. Due to conduction the fuel temperature  $T$  changes, which influences the reactivity and subsequently the power production. Before and after the initial stage of the transient (duration approximately 5 minutes) the reactivity  $\rho$  equals zero as both situations represent a situation with long (infinite) reactor periods:

$$\Delta\rho = \rho - \rho' = \alpha_T (T - T') = 0 \quad (5.2)$$

or, when looking at individual axial layers of the reactor:

$$\sum_i \Delta\rho_i = \sum_i \alpha_{T,i} (T_i - T'_i) = 0, \quad i = 1, 2..10 \quad (5.3)$$

with  $\alpha_T$  the temperature coefficient of reactivity, not to be confused with  $\alpha$  from equation (5.1). A subscript  $i$  denotes the  $i^{th}$  layer, and the quote denotes the new situation before xenon starts to decay or buildup.

The reactor acts like a thermostat: it tries to keep the average fuel temperature - weighted with  $\alpha_{T,i}$  - constant. Only when the xenon concentration starts to change and effectively the reactivity starts to change, this balance is disturbed and the average core temperature will start to change.

The next three sections will present the transients and the calculational results of the 4 reactor models will be compared.

## 5.2.1 Inlet Temperature Increase 100°C

### Calculational Results

Increasing the reactor inlet gas temperature will heat up the reactor, which will reduce its reactivity and decrease the thermal power. Figure 5.1 shows the normalised power, outlet temperature and xenon worth for the 4 calculational models. The concept of 'xenon worth' has been defined in section 3.4.5 as the difference in reactivity between a core with and a core without xenon. For interpretation of the figures presented in this chapter, it is useful to realise that the xenon worth is in good approximation proportional to the xenon concentration, but with a minus sign in front of it.

The results are shown on two time scales, left the long term, right the short term.

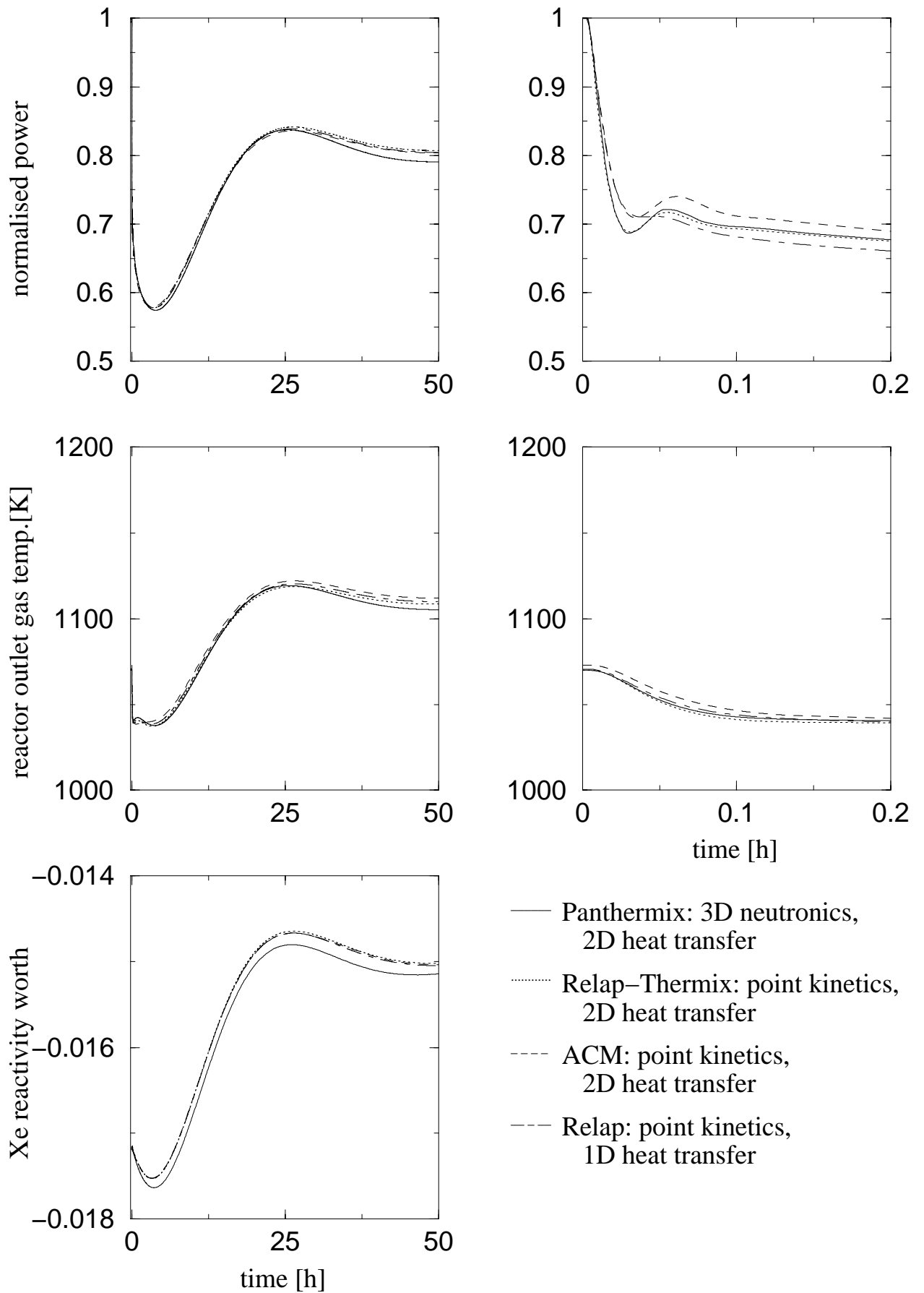


**Figure 5.1:** The gas inlet temperature for the reactor was increased instantaneously with 100 K at the start of the transient. The calculations were performed for a stand-alone reactor, i.e. fixed inlet mass flow rate, pressure, and temperature.

The reactor behaviour on the long term time scale is governed by the xenon decay or buildup. The short term time scale shows the first 12 minutes of the transient and is indicative of the correctness of the thermal hydraulic part of the reactor model. It shows the details of the transition to the new inlet conditions.

**The long term figures** demonstrate clearly that the point reactor kinetic models are in good agreement for the normalised power. The initial powers have been normalised to 40.41, 39.89 and 39.68 MW for the ACM, Relap5 and Relap5-ThermixDirekt models, respectively. As the mass flow rate is constant, it can be expected that the reactor outlet gas temperature will be the highest for ACM and the lowest for the Relap5-ThermixDirekt model when comparing point kinetics. In the same manner a high reactor power yields a higher xenon equilibrium concentration that results in a more negative xenon reactivity worth, so the ACM model has a more negative xenon worth than the Relap5 model which in turn is more negative than the Relap5-ThermixDirekt model (though barely discernible in figure 5.1).

The progress of the xenon worth can be explained from the reduction in power: when the power decreases, the xenon concentration will initially increase because the balance between production and removal (equation (3.35)) is disturbed. The maximum in xenon concentration can be expected for this reactor core (height 3.75 m) after about 4 hours (shown as a minimum in the xenon worth in figure 5.1), and from that point on xenon will decay to its end value.

The small differences between the point reactor model and the Panthermix model can be explained from the burnup and the more detailed xenon calculations. The point reactor models do not include burnup calculations and therefore the power will remain higher than for the Panthermix model. By looking at the first 5 to 10 hours of the xenon reactivity worth (there the burnup is still low) one may conclude that the point reactor models underestimate the xenon reactivity worth for transients where the reactor power is less than nominal. This has been predicted in section 3.4.5: the most important core region for the xenon worth, the top, has increased in temperature. This leads to an increase in the xenon absorption cross section, which has not been modelled for the point reactor. Furthermore, replacing the xenon point model in the point reactor model by a 10-layer model would also reduce the difference in xenon worth, but this attempt has not been pursued further.

**The short term figures** demonstrate the differences between the thermal hydraulic reactor models. Comparison between the Panthermix and Relap5-ThermixDirekt model learns that the reactor point kinetics model almost exactly reproduces the Panthermix results. As they use the same thermal hydraulic reactor model (Thermix-Direkt), it can be concluded that the point reactor kinetics model adequately represents the 3-D Panther model. Having said so, the remaining differences with the ACM and Relap5 model can be attributed exclusively to their thermal hydraulic reactor model.

## Analysis of Temperature- and Power Density Profile

After the initial disturbance the reactor reaches a new situation with  $\rho' = 0$ . Looking at the core as one entity, the *average* core temperature - weighted with  $\alpha_T$  - has not in-



creased as follows from equation (5.2). Looking closer at the reactor core, and dividing the core in axial layers, will show a tilt in the temperature profile. The top layers will increase in temperature because suddenly the temperature of the pebble-bed is lower than the helium gas entering the core. Consequently, no heat can be transferred from pebble-bed to gas and the 'trapped' power will heat up the layer until its temperature becomes again higher than that of the gas and heat can be transferred. The higher layer temperature comes at the cost of a lower nuclear power production due to the feedback by the negative temperature coefficient of reactivity. The negative reactivity has to be balanced elsewhere in the core in order to maintain overall criticality, and the bottom layers indeed decrease in temperature. As a result, the power density profile will also tilt a little: relatively less power will be generated in regions with a temperature increase, and relatively more in regions with a temperature decrease. Since the bottom layers produce little power (the most active part of the core can be found near the top of the pebble-bed), the helium is almost in thermal equilibrium with the bottom layer, i.e.  $T_{surf} \approx T_g$  in equation (5.1). Therefore, if the bottom layer temperature decreases, so does the helium outlet temperature. This behaviour can be seen in the short term plots of figure 5.1. A more phenomenological description would read that as a result of the decreased power output in the top layers, the gas will pick up less heat on its way down to the outlet and arrives cooler in the bottom region.

The situation described above exists during the first, say, 10 hours of the transient, when the xenon dynamics is not very pronounced. From that time on, xenon will start to decay to its end value and the power will rise. The  $\Delta\rho$  in equation (5.2) is then no longer zero, and the core temperature will also rise. Since the xenon reactivity is approximately proportional to the power, the reactivity increase in the top layers is considerable. Due to the local high temperature coefficient of reactivity, the temperature increase is still modest (approximately 20 K). The same holds for the bottom layers, there the reactivity increase is much lower but the temperature coefficient is also much lower, resulting in, in principle, approximately the same temperature rise. In principle, because for these layers the helium temperature will have risen due to the increase in power in the previous layers. The bottom layers will further increase in temperature and the tilt in temperature- and power density profile, observed during the first 10 hours, will thereby end.

The deformation of the power density profile will only be possible in the Panthermix calculations; for the point reactor models the power distribution has been fixed. The temperature profile is free to change shape in all models. Figure 5.2 and 5.3 show the temperature- and power density profiles after 50 h for the +100°C transient, and - in advance - for the other two transients which will be discussed in sections 5.2.2 and 5.2.3. The solid lines represent the Panthermix reference case, the dotted lines the Relap5-Thermix-Direkt model. From the other two point reactor models only the Relap5 results are plotted - dashed line - in order to retain readability. The ACM profiles are almost identical.

Figure 5.2 shows that the temperature profiles with the Thermix-Direkt thermal hydraulic model agree very well with the Panthermix profiles, the small differences result from the point reactor kinetics approximation. The stepwise temperature curves for the Relap5 thermal hydraulic model reflect its nodalisation of the core in 10 instead of

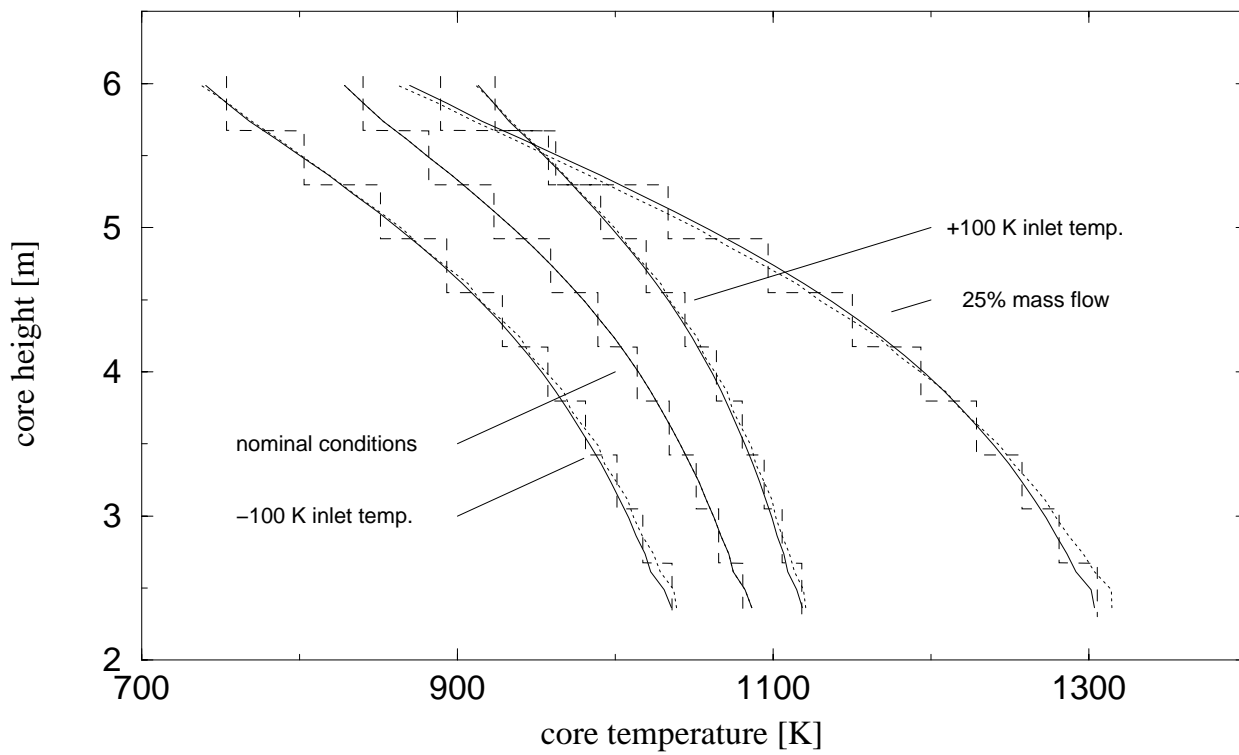


**Figure 5.2:** The core temperature at the END of the transients, averaged in radial direction, along the  $z$ -axis of the core. The solid lines are the Panthermix results, the dotted lines the Relap5-Thermix-Direkt results, and the dashed lines the Relap5 results.

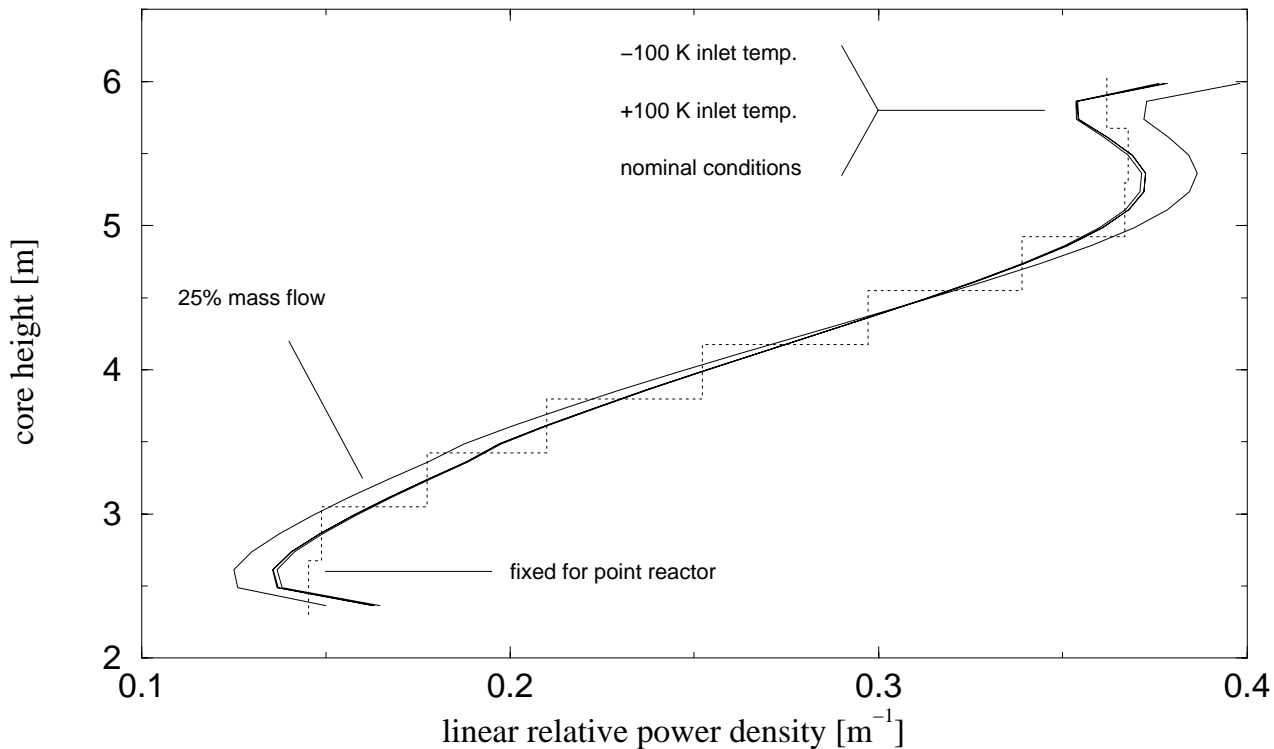


**Figure 5.3:** The linear relative power density at the END of the transients along the  $z$ -axis of the core. In radial direction the power production has been summed. The curve is relative to the total power produced in the core. The solid lines are Panthermix results; The only solid line not coinciding with the nominal curve stems from the mass flow rate reduction transient. The dotted line is the fixed power profile used in the three point reactor models.

30 layers. In fact the Thermix-Direkt temperature curves are stepwise too, but with smaller steps, and in order to facilitate comparison a smooth line has been drawn. Figure 5.3 shows that the power density profile after 50 hours is identical for the transients with a changing inlet temperature. It will be explained in section 5.2.3 why the power density profile of the mass flow rate reduction transient has changed shape. Summarising this section with respect to the temperature- and power density profiles, it can be concluded that:

- if the inlet temperature increases, a large deformation in profile will exist during the first 10 hours of the transient when the xenon concentration is still close to the pre-transient value. More precisely, the maximal deformation exists at the xenon peak in buildup after 4 hours since the start of the transient. At the end of the transient, when a steady state is reached, the power density profile will again resemble the original and the temperature profile has almost regained its nominal orientation, only at a higher average temperature.

## 5.2.2 Inlet Temperature Decrease 100°C

### Calculational Results

Decreasing the inlet temperature will cool the reactor, which will increase its reactivity and increase the thermal power. Figure 5.4 shows the normalised power, outlet temperature and xenon worth for the 4 calculational models.

**The long term figures** again show good agreement between the point reactor kinetic models. The differences in the reactor outlet gas temperatures between the point reactor models can be explained along the same lines as for figure 5.1, that is, a matter of slightly different nominal reactor powers at the same mass flow rate. The deviations - though small - of the point reactor model from the Panthermix model can be explained from the burnup and the more detailed xenon calculations. The point reactor models do not include burnup calculations and therefore the power will remain higher than for the Panthermix model. The burnup for this transient is even higher than nominal, because the power during the transient is higher than nominal. This explains why the difference in normalised power between the point reactor model and the 3-dimensional model is larger in this transient than in the transient from section 5.2.1. The point kinetic models overpredict the xenon worth at lower temperatures as foreseen in section 3.4.5 due to not being sensitive to the change of the average reactor temperature which influences the ratio  $\sigma_a^X / \sigma_f^U$ .

**The short term figures** again show that the thermal hydraulic model of Relap5 has most problems with reproducing the oscillation in power. The Relap5 model with Thermix-Direkt as thermal hydraulic model neatly coincides with the Panthermix calculations.

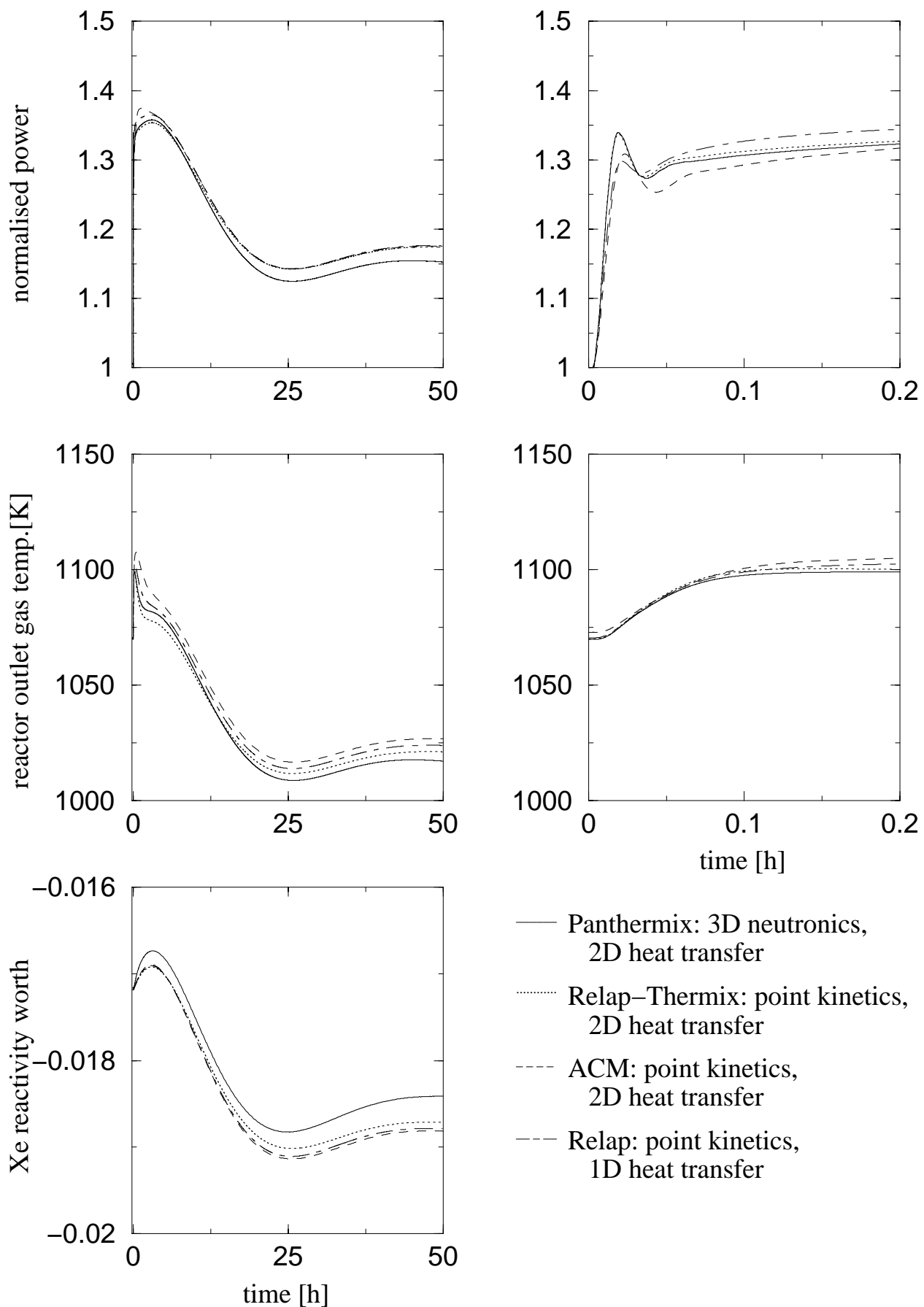


**Figure 5.4:** The gas inlet temperature for the reactor was decreased instantaneously with 100 K at the start of the transient. The calculations were performed for a stand-alone reactor, i.e. fixed inlet mass flow rate, pressure, and temperature.

## Analysis of Temperature- and Power Density Profile

For this transient in fact the opposite behaviour can be expected as for the transient with increasing inlet temperature. That is, the colder helium flowing into the core will force the top layers of the core to decrease in temperature. In order to maintain an overall zero reactivity, the bottom core layers increase in temperature. The tilt in the temperature- and power density profile is now opposite to the one observed in the previous section. This results in an increasing helium outlet temperature as can be seen in the short term plot of figure 5.4. In the long term, the xenon concentration will increase in each layer, and the power production will decrease. The power density profile close to nominal will again be adopted. The temperature- and power density profile at the end of this transient are shown in figures 5.2 and 5.3, respectively.

With respect to the temperature- and power density profiles, it can be said that:

- if the inlet temperature decreases, the opposite behaviour will be displayed as for the transient with inlet temperature increase. The maximal deformation in profiles will exist when the xenon concentration reaches its minimum (a maximum in the xenon worth) after some 3 hours, a little earlier than the previous transient. At the end of the transient the original power density profile will be restored and the temperature profile resembles the original but now at lower temperature.

### 5.2.3 Reduction of Mass Flow to 25%

#### Calculational Results

Reducing the helium mass flow rate means reducing the cooling capacity of the helium flow. The reactor will warm up and decrease the thermal power due to the negative temperature coefficient of reactivity. Figure 5.5 shows the set of figures similar to figures 5.1 and 5.4.

**The long term figures** show the usual good agreement between the point reactor models. For this transient the burnup is low as the reactor power is low during the transient. Again the point reactor models underpredict the xenon reactivity worth. For all models the low xenon reactivity worth after 50 hours represents a high positive reactivity which can only be balanced by increasing the reactor temperature. Therefore the reactor outlet gas temperature rises considerably higher than in the previous transients. **The short term figures** show that this transient is fiercer than the previous ones; the power reduction is twice as high and consequently the oscillations have a larger amplitude and last longer. As the power reduces to approximately 25%, like the mass flow rate, the reactor outlet gas temperature remains more or less the same.

## Analysis of Temperature- and Power Density Profile

This transient reduces  $\alpha$  of equation (5.1) by reducing the mass flow rate. This type of transient will be encountered most as it is used in cases of load-following (chapter 4). By reducing the heat transfer coefficient  $\alpha$ , the pebble-bed is hindered

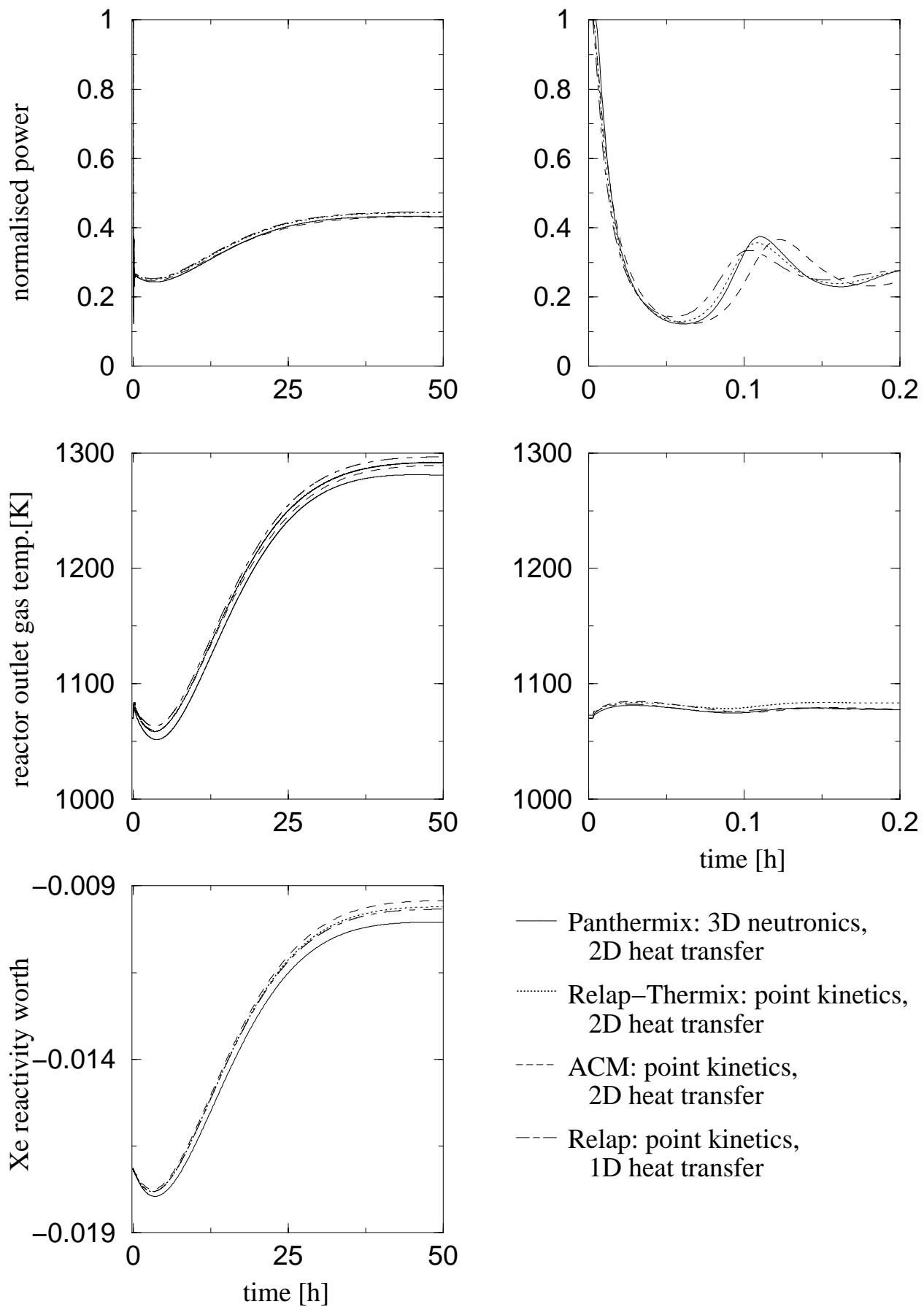


**Figure 5.5:** The helium mass flow rate through the reactor was decreased instantaneously to 25% nominal value at the start of the transient. The calculations were performed for a stand-alone reactor, i.e. fixed inlet mass flow rate, pressure, and temperature.

in its heat transfer and consequently the pebble-bed will increase in temperature. As the temperature feedback to the power production is fast, the power production will decrease immediately. This will prevent the reactor to heat up significantly. The power production decrease will stop at the point that it matches the reduced capacity of the helium flow to transport heat. For this transient that will be the point of 25% nominal power production. Unlike the previous transient, this time the disturbance in heat transfer takes place homogeneously through the core and therefore the temperature distribution for pebble-bed and helium remains nearly unchanged. Looking closer reveals a slight adjustment of the power density profile due to the fact that the heat transfer coefficient has not reduced to 25% but to 40%. A relatively good heat transfer can take place compared to the nominal situation and for the top layers the temperature lowers by 5-10 K, thereby slightly increasing the power production and the fluid temperature. In order to balance in reactivity, the bottom layer will increase in temperature and slightly reduce the power production. The result will be a somewhat (5-10 K) higher gas outlet temperature. This is shown in the short term plot of figure 5.5.

As soon as the xenon decay becomes important, say after 10 hours, the power and temperature distribution will start to deform. Each layer will experience a positive reactivity contribution and the fuel temperature in the layer will rise due to the power increase. With constant gas inlet temperature this means a higher driving force ( $T_{surf} - T_g$ ) for heat transfer of which the top layers will profit by increasing their power production further. For the bottom layers the increase in power means that each previous layer has extra increased the gas temperature, thus compelling the layers to further increase in temperature and to decrease power production.

The temperature- and power density profile at the end of this transient are shown in figures 5.2 and 5.3, respectively.

From the discussion above it can be concluded for the power density and temperature profile that:

- if the mass flow rate in- or decreases the profiles initially will change little. Only after about 10 hours, when the xenon decay or buildup starts to go to its final value, the profiles start to change. At the end of the transient, at the new steady state situation the profiles will be deformed maximally.

## 5.2.4 Reactor Response Time

Having seen the progress in time in the short term plots of figures 5.1, 5.4, and 5.5, as an afterthought a remark must be made concerning the response time of the reactor to changing inlet conditions.

### Response time related to conduction

In the current Thermix-Direkt model the pebble surface temperature is the parameter at which the cross sectional data are tabulated, and therefore the reactivity change due

to temperature change will be faster than in reality, when the heat first has to travel through half a centimeter of graphite before reaching the outer boundaries of the fuel zone. In real life the fact that the outside temperature changed will be perceptible in the fuel zone after a few seconds, but then it takes around a minute to establish the new temperature distribution over the pebble. In contrast, in the Thermix-Direkt calculations the temperature distribution over a mesh volume (containing a number of pebbles) is flat. Given a change of heat flow for such a mesh volume, the time it takes to change the temperature is only governed by the specific heat capacity of that mesh volume, and not by the heat conductivity for the mesh volume. Of course, when exchanging heat with other mesh volumes the heat conductivity is used in order to determine the heat flow. Summarising, one can expect that in reality the reactor response to changing operating conditions will be delayed in the order of one minute.

### Response time related to heat capacity

It is instructive to estimate the reactor response time to changing inlet conditions governed by the heat capacity during the initial transient stages. In that case only the pebble-bed has to be considered, assuming that the temperature changes in the reflector will be much slower. The heat capacity has been tabulated in table 5.1 for the reference core (nearly full) and a fresh core. With a nominal reactor power of 40 MW, it will be

**Table 5.1:** *The heat capacity for the fresh and reference pebble-bed.*

	fresh pebble-bed (height 1.26 m)	reference pebble-bed (height 3.75 m)
heat cap. [MJ/K]	13	38

clear that changing the temperature of the core only requires a fractional in- or decrease of the power production for a short period of time. Especially for the load-following transients, with small temperature changes, the calculational models will react on a time scale set by the neutronic properties of the core, not so much by the thermal hydraulic properties. Again, in real life the delay will be in the order of a minute as changes in heat transfer need some time to penetrate a pebble by conduction.

## 5.3 Evaluation of the Point Reactor Kinetics Model

During the discussion and derivation of the reactor kinetics equations in section 3.4 it has been assumed that the shape function  $\psi$  is constant during the transient calculations and its period of burnup. Having calculated some stand-alone reactor transients, the assumption can now be evaluated.

From the previous section it can be learned that the shape function in general will not be constant. For instance, at the end of the mass reduction transient the axial power density profile changed shape, which indicates a flux redistribution. As an example



the shape function at the end of the transient with mass flow rate reduction of 25% will be discussed in more detail in the next section, that is, also in radial direction. As a logical extension the most severe cases of mass flow rate reduction, the so-called loss of cooling incidents will be calculated with the point reactor kinetic model in sections 5.3.2 and 5.3.3.

### 5.3.1 Change in Shape Function

In order to evaluate the shape function of the mass flow rate reduction transient, first the normalisation as in equation (3.13) for the initial state has been performed. For all subsequent times this normalisation procedure must hold, so if at the end of the transient the macroscopic fission cross section has changed from place to place, so has the flux shape function. It is this difference that has been plotted for both energy groups in the following figures, i.e.

$$\Delta\psi(r, E) = \frac{\psi_e(r, E) - \psi_i(r, E)}{\psi_i(r, E)} \quad (5.4)$$

where subscripts  $i$  and  $e$  denote the initial and end situation, respectively.

The change in the shape function at the end of the transient originates from two contributions: changes due to burnup effects and changes due to the transient conditions. As the changes due to the transient always will be mixed with the burnup changes, it is instructive first to isolate and estimate the importance of the burnup effects. In figure 5.6 the results of burnup at nominal conditions for the duration of the transient are shown. Due to burnup the power level declines and the helium gas is leaving the reactor at a lower temperature. However, compared to the changes due to the transient as was shown in figure 5.5, the reactor conditions have hardly changed.

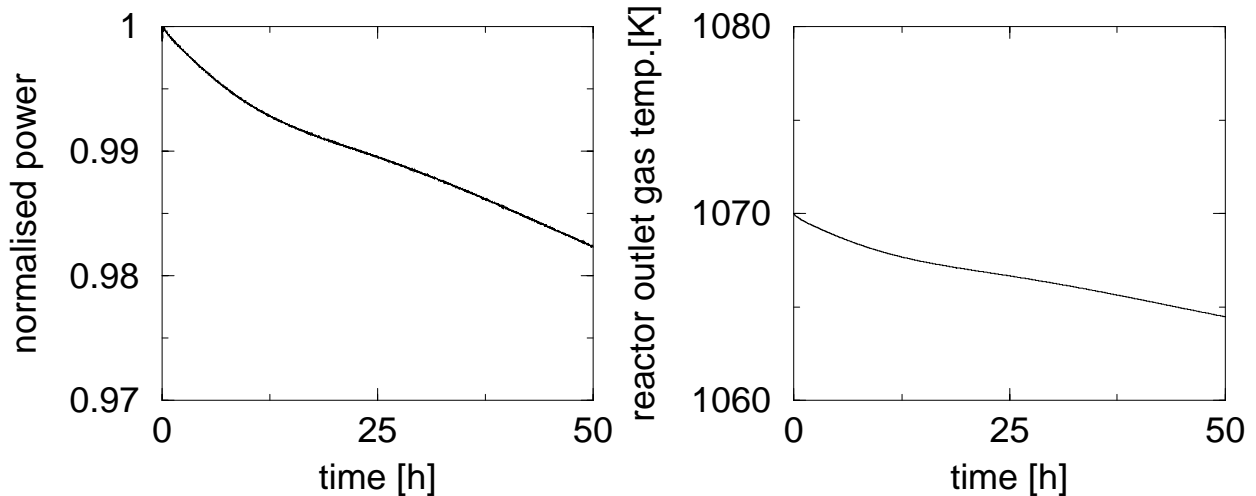


**Figure 5.6:** The results of 50 hours burnup for the reactor thermal power and outlet gas temperature. The inlet conditions for mass flow rate, temperature and pressure are kept constant.

For the shape functions this is confirmed by the two pairs of figures 5.7 and 5.8. They show in  $r$ -direction the difference in shape function according to equation (5.4) for a core layer at height 5.5m, one of the most reactive layers. Figure 5.7 shows the difference in shape function solely due to 2 days burnup at fixed core height. It will be an overprediction for the current transient, as the power (burnup) during the mass flow rate reduction will be less by around 60%. The change in shape is small compared to figure 5.8, that shows the difference in shape function at the end of the mass flow rate reduction transient and includes the changes in shape function due to burnup.

Three things can be noticed in figure 5.8:

- The  $\Delta\psi$  for this layer is positive for the transient,
- The  $\Delta\psi$  changes more for the thermal group,
- The  $\Delta\psi$  has an extra protrusion in the core region for the thermal energy group.

The explanation of the first observation can be inferred from figures 5.9 and 5.10 that show the temperature and shape difference for the mass flow rate reduction transient between initial and end conditions for the total reactor. Figure 5.9 indicates that the temperature rise at the bottom part of the reactor is about 5 times higher than at the top part. As a result the flux has tilted and rose in the colder part of the reactor and lowered in the hotter parts: the power density profile changes. This effect would have been even more outspoken and localised would the core region not have a relatively strong neutronic coupling due to the long neutron migration length (0.3 m, from table 3.1) The explanation of the second observation relates to the first, in that the top reflector now increases its contribution of thermalised neutrons due to the higher flux it receives. This causes the 'epicenter' of the thermal flux to shift upward a little more than the fast flux, which shifts upward mainly due to the new temperature distribution. As for the third observation, this can be explained from the positive reflector temperature coefficient. Due to the overall temperature increase of the side reflector more thermalised neutrons escape from that reflector back into the core. Therefore in the core region, close to the side reflector, the maximum  $\Delta\psi$  can be found.

The same line of reasoning for the three observations holds for the burnup as is shown in figure 5.7, only there the bottom part becomes colder and the flux tilts the opposite way, the top reflector reduces its contribution of thermalised neutrons, and the side reflector absorbs more thermal neutrons. It clearly is safe to conclude that changes in shape function due to burnup are small and that validity of the point kinetic reactor model will solely depend on the transient behaviour.

At this point it is instructive to relate the geometric size of the reactor to the neutron physics. According to [89] one has to consider the average range of the prompt neutron fission chain compared to the reactor size. Large changes in the shape function can occur if the size of the reactor is much larger than the average range of the prompt chain; a reactivity change in one part of the core will not be felt in another part of the core [90,91]. In such cases the point kinetics equations are known to be in error, sometimes quite seriously and especially when applied to above prompt critical reactivity excursions [92]. The prompt criticality scenario for an HTR can be ruled out (lack of sufficient surplus of positive reactivity in core). Therefore the focus lies on estimating the range of the prompt fission chain. The average square distance covered

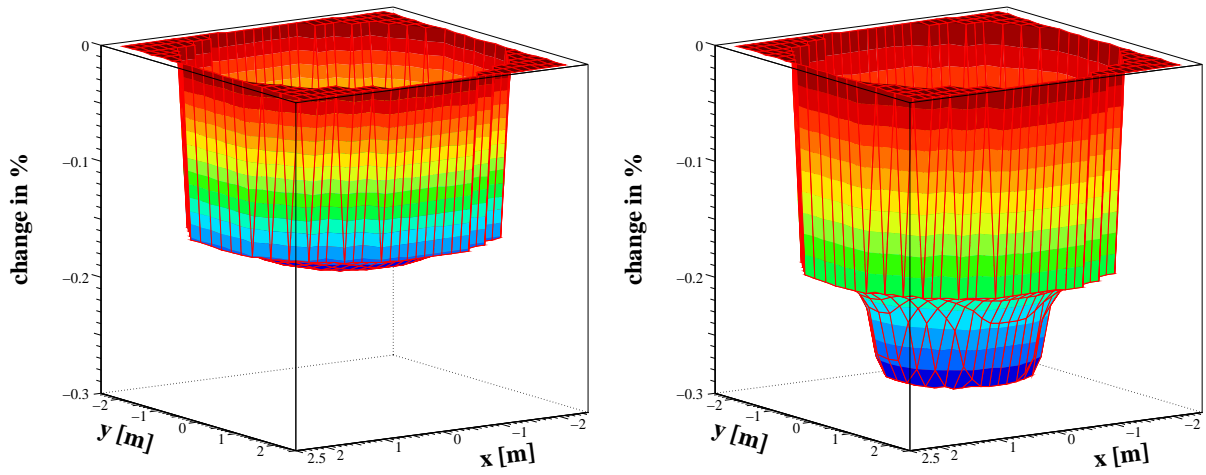


**Figure 5.7:** The difference in shape function after 2 days of burnup at nominal conditions for a reactor layer at 5.5 m height. Left the difference in shape function for the fast group, right for the thermal group. Along the  $z$ -axis the difference is presented in %.

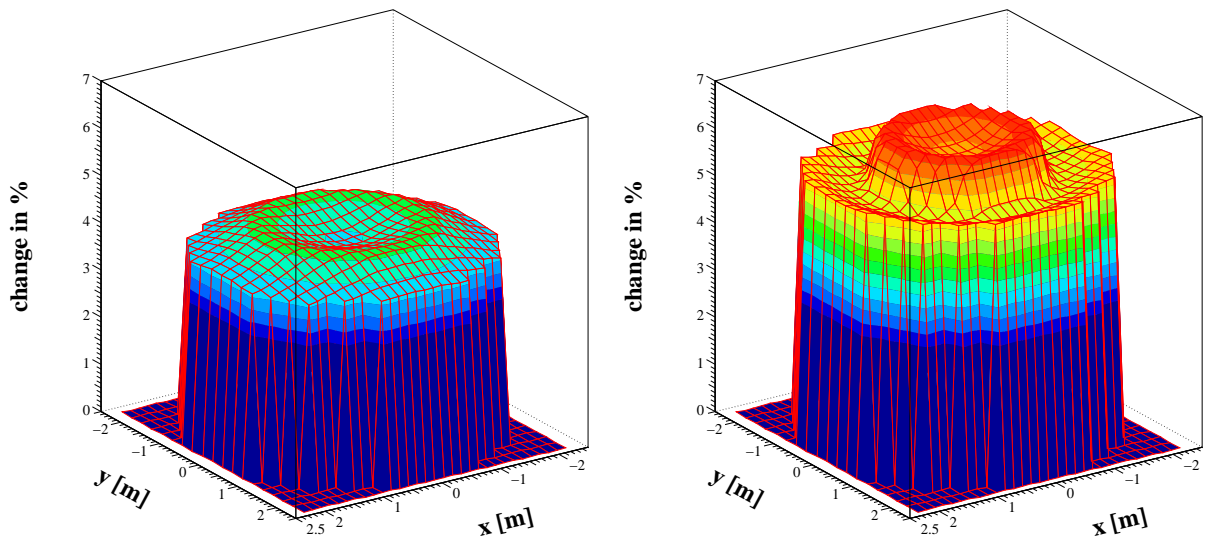


**Figure 5.8:** For the reactor layer at 5.5 m height the difference in shape function has been plotted at the end of the transient with mass flow rate reduction to 25%. Left the difference in shape function for the fast group, right for the thermal group. Along the  $z$ -axis the difference is presented in %.

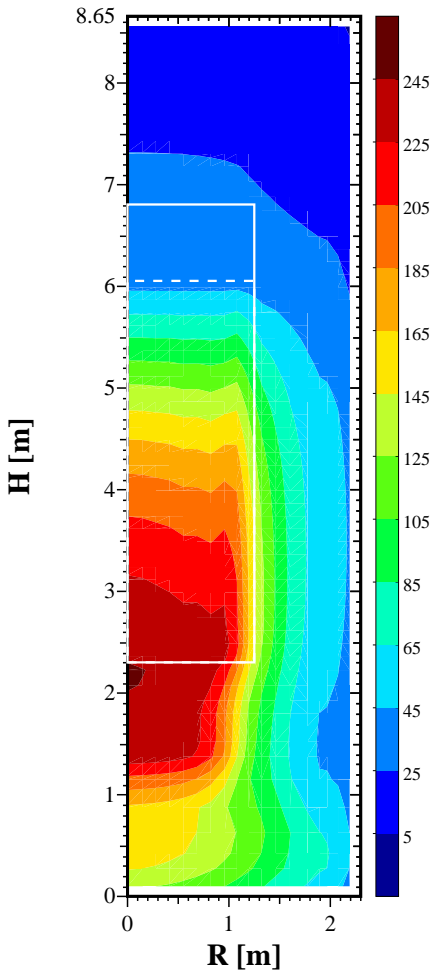


**Figure 5.9:** The initial temperature subtracted from the final state for the entire reactor for the transient with mass flow rate reduction to 25% nominal flow. The colour bar alongside the plot has units Kelvin. The white drawn line denotes the core region, the dashed line the pebble-bed height.

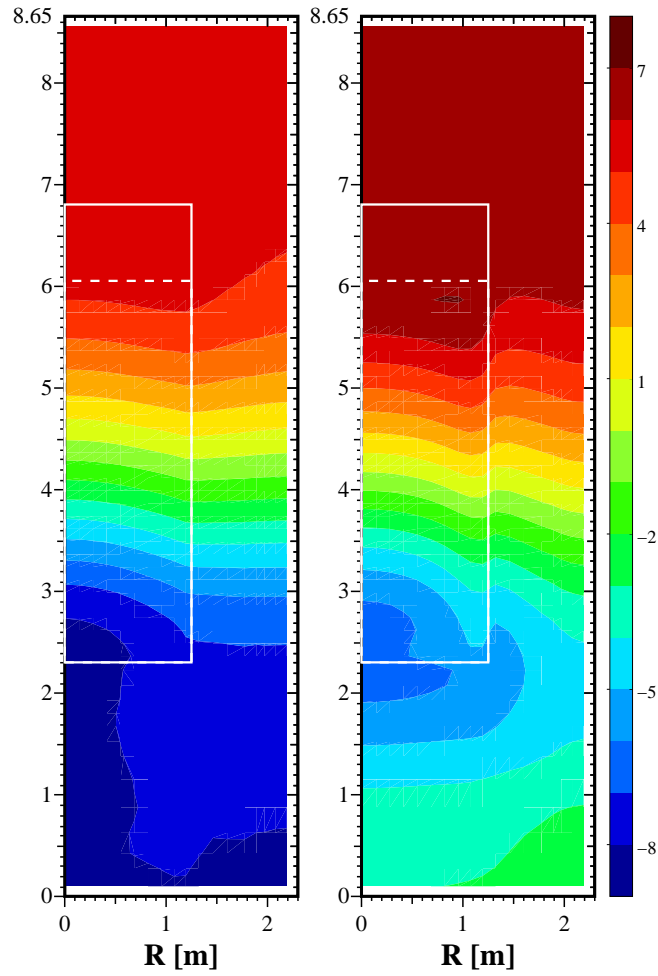


**Figure 5.10:**  $\Delta\psi$  for the entire reactor for the transient with mass flow rate reduction to 25% nominal flow. Left the fast group, right the thermal group. The colour bar alongside the plot is in %. The white drawn line denotes the core region, the dashed line the pebble-bed height.

by a neutron - as the crow flies - is  $6M^2$ , with  $M$  the migration length. The average number of neutrons participating in a prompt fission chain (below prompt criticality) is  $1/(\beta - \rho)$ . Multiplying this number with the  $6M^2$  and taking the square root, yields the average chain length  $\langle \ell^2 \rangle^{1/2}$ :

$$\langle \ell^2 \rangle^{1/2} = \sqrt{\frac{6}{\beta - \rho}} \cdot M \quad (5.5)$$

With  $M^2 = L_1^2 + L_2^2$ ,  $L_{1,2}$  the diffusion lengths for energy group 1 and 2 from table 3.1, it follows that for the reactivities during the first minutes of the transients discussed ( $\rho < 30$  pcm,  $\beta = 0.0054$ ), the fission chain range is in the order of 10 meter. This is more than twice as large as the core size, and therefore reactivity changes in one part of the core certainly are felt in all other parts of the core. The core is tightly coupled, and only limited variations in the shape function can be expected.

As was shown, the main driver for changes in the shape function is the core temperature resulting from changes in gas inlet temperature or mass flow reduction. The mass flow rate reduction transient has been pursued further, and the steady state end situations for mass flow rate reductions to 1% have been calculated with the Panthermix model and the Relap5-Thermix-Direkt model. Recollect that differences in results can be attributed exclusively to the neutronic calculations, as the thermal hydraulic reactor model is identical. For steady state calculations the Panthermix results - like the point reactor kinetics model - are not affected by burnup, and the two models can be compared directly. Figure 5.11 gives the normalised total power production. Figure 5.12 gives the normalised gain in gas temperature, that is, the gas outlet minus gas inlet temperature for the reactor. The values have been normalised to the 3-D Panthermix results. The axial temperature- and power density profiles are shown in figures 5.13 and 5.14.

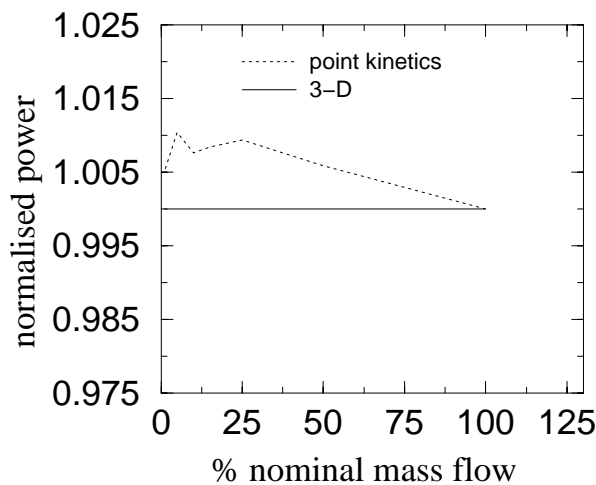


**Figure 5.11:** The difference in reactor power between 3-D and point kinetics calculations for various mass flow rates. The point kinetics values have been normalised to the 3-D results.

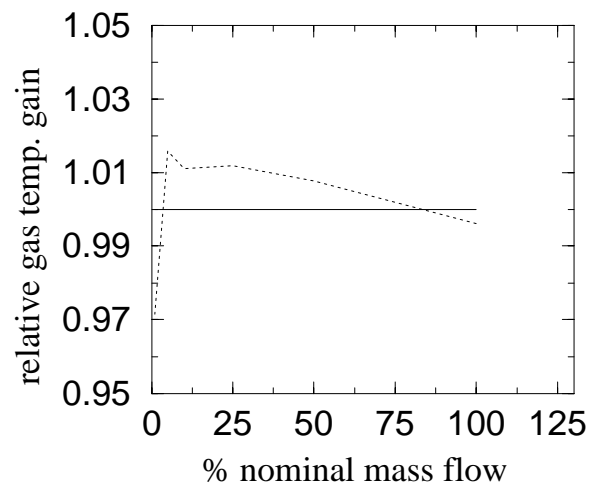


**Figure 5.12:** The difference in outlet gas temperature gain  $T_{g,o} - T_{g,i}$  between 3-D and point kinetics calculations for various mass flow rates. The point kinetics values have been normalised to the 3-D results.

Due to the fixed power density profile, the temperature profile tends to deviate from the Panthermix results, but the differences along the profile are never higher than  $\pm 25$  K for the most severe transient, the reduction to 1% of the mass flow rate. More important is that for both models the total power and the gain in gas temperature are equal within 2%. This means that for studying operational transients that give interaction between ECS and reactor, the point reactor model is accurate within 2%.

The steady state of the 1% mass flow rate transient has a temperature profile different from the rest. Due to the low power production, 1.8 MW, a relatively large amount of heat is transported to the side reflectors. Especially at the height of the bottom layer the temperature gradient over the side reflector is high: at one side the hottest part of the core, at the other side the cold helium flow through the coolant channels. As a result the bottom layers have a lower temperature. From the power density profiles this is implied by the higher relative power production in the bottom layer for the 1% transient that lies between the 10% and 5% transient.

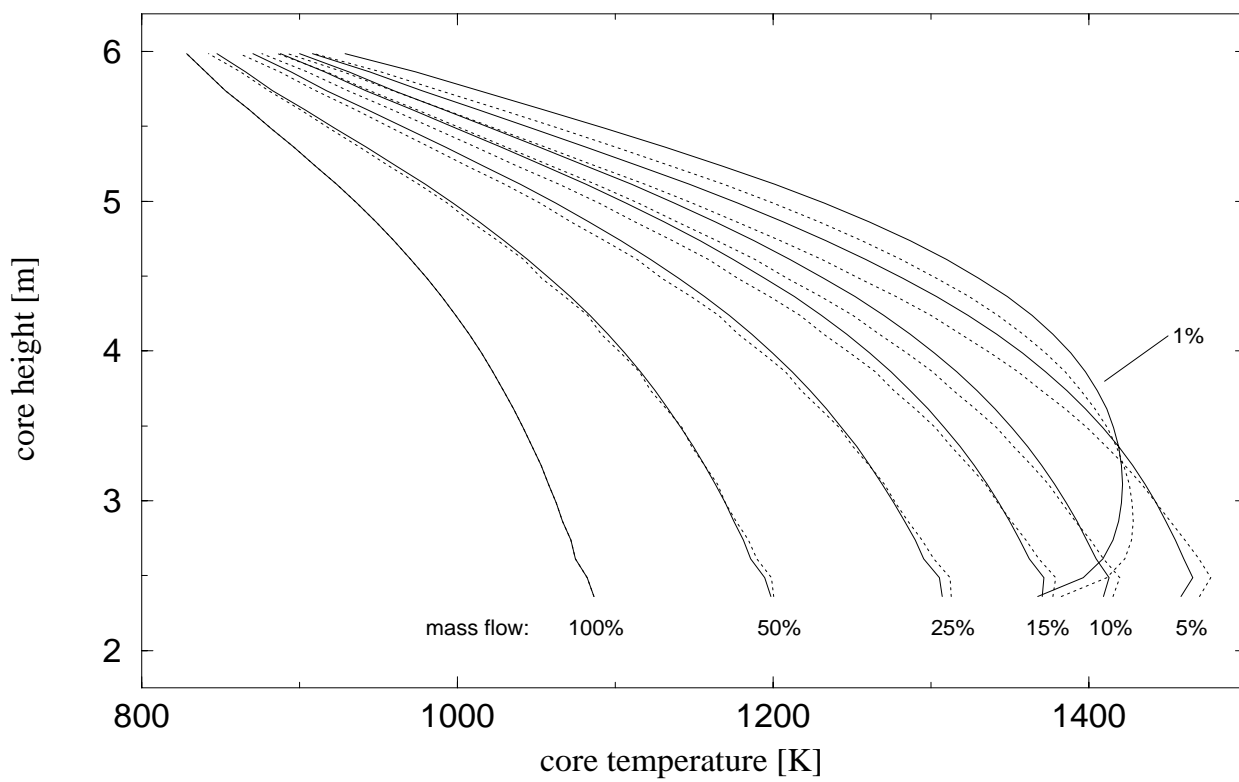


**Figure 5.13:** The core temperature at the end of transient, averaged in radial direction, along the  $z$ -axis of the core. The solid lines are the Panthermix results, the dotted lines the Relap5-Thermix-Direkt results, and the dashed lines the Relap5 results.

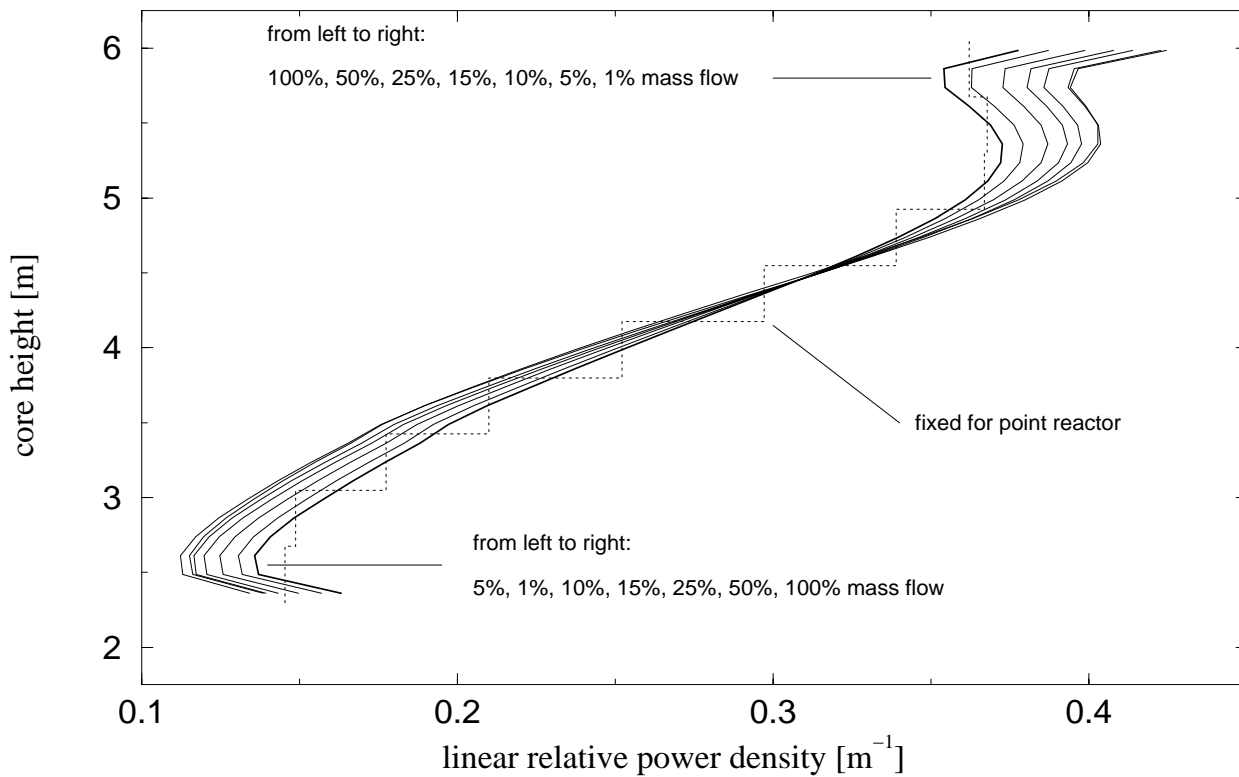


**Figure 5.14:** The linear relative power density at the end of transient along the  $z$ -axis of the core. In radial direction the power production has been summed. The curve is relative to the total power produced in the core. The solid lines are Panthermix results; the dotted line is the fixed power profile used in the three point reactor models

Realising that a mass flow rate reduction to 1% is only a small step away from loss of cooling incidents, and taking into account the good results by the point kinetic model, it might well be possible to use the point reactor model in order to calculate these incidents. The next section will treat these incidents and their calculations in detail.

### 5.3.2 Loss of Coolant Incident

Besides a halted mass flow rate, the loss of coolant incident (LOCI) also presupposes a depressurisation to 1 bar. Such a scheme could occur as result of a rupture (guillotine break) of the manifold connecting the ECS to the reactor. Helium will flow out of the containment into the reactor building until the pressures are stabilised at 1 bar. The eventuality of air entering the core and the oxidisation of graphite will not be discussed here.

For a loss of cooling incident the prompt fission power will rapidly decrease and after a few minutes become negligible compared to the decay power. Passive cooling processes have to transport the decay heat from core to pressure vessel steel wall where it can be transferred to the environment by free convection. It is a slow process, and it takes days before an equilibrium is reached. Notice that no human intervention is needed to control the incident and to limit the consequences. For the nearly full reference core, the fuel temperatures will be well below the 1600°C limit. The considerations when and for which core configurations a loss of cooling incident can result in higher fuel temperatures will be deferred to chapter 7.

For the reference core the incident has been calculated with the 3-D Panthermix model, the Relap5 point reactor model connected to Thermix-Direkt, and the Relap5 point reactor model with Relap5 thermal hydraulic reactor model. Figure 5.15 shows the total (fission + decay) reactor power, the maximum fuel temperature, the reactivity, the xenon worth, and the heat leakage to the environment for the LOCI. As mentioned earlier, the Thermix-Direkt code works with the pebble surface temperature rather than the fuel temperature. In the case of the LOCI or LOFI this temperature is virtually identical because the power production in the fuel zone is low and it cannot form a large temperature gradient over the pebble.

From the figure it follows that the reactor reaches (re)criticality after 22.5 hours. Prior to that point, the reactor power consisted of decay heat with only a tiny fraction of spontaneous or prompt fission. Two effects bring the reactor back to criticality: firstly the gradual decrease in decay power results in a cooler reactor thereby increasing reactivity and secondly, the xenon concentration decreases which also introduces a positive reactivity. Both models with Thermix-Direkt as thermal hydraulic core description give good agreement, though the one with the Relap5 point kinetic calculations predicts recriticality after 22 hours. This is consistent with the earlier observation in sections 3.4.5 and 5.2.2 and the xenon worth graph in figure 5.15, that is, the xenon worth is underestimated in the point reactor kinetic model for a reactor core at higher average temperature than nominal. The point kinetic model calculates a slightly lower xenon worth, resulting in a slightly higher positive reactivity and thus a shorter time

# Loss Of Coolant Incident

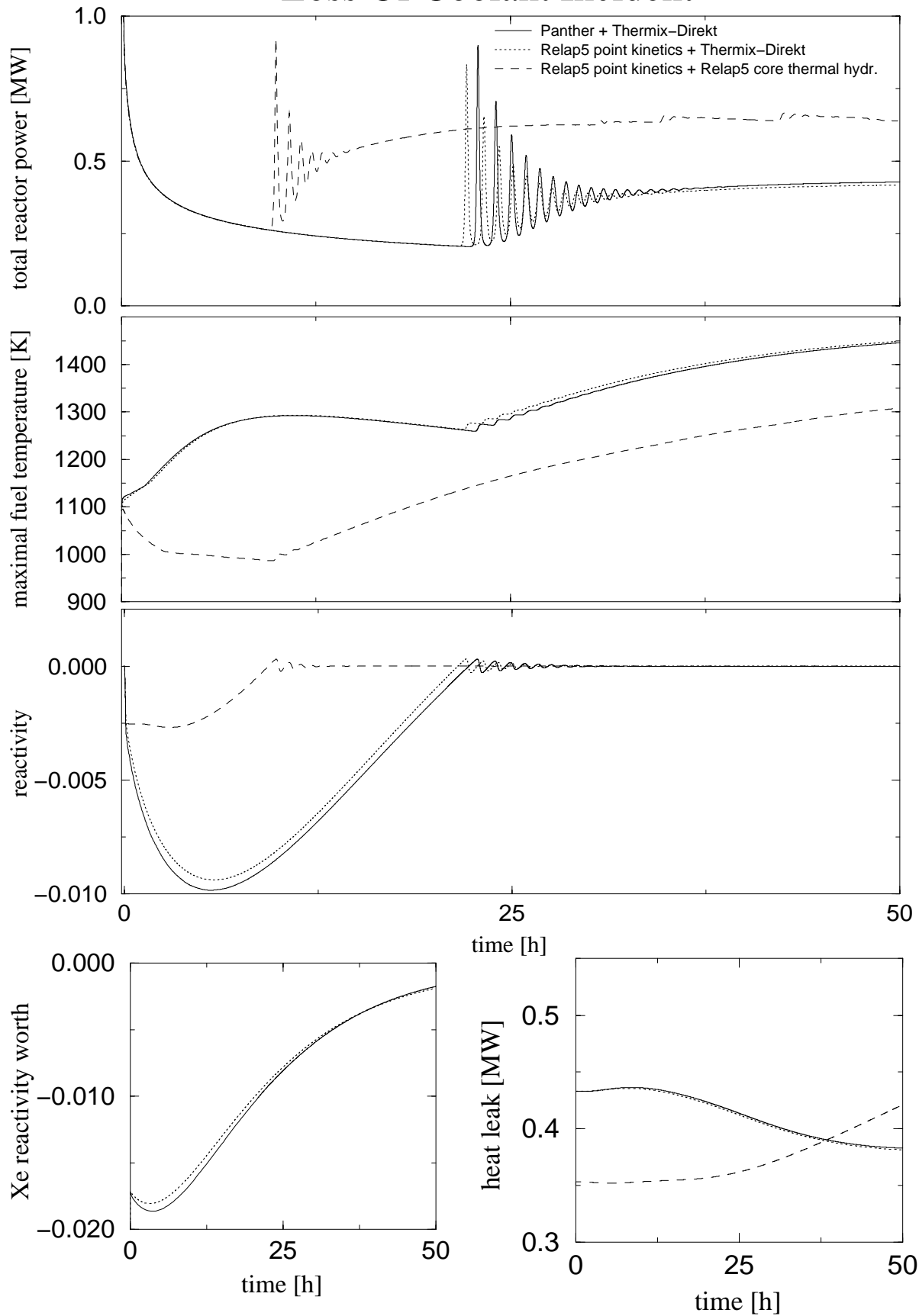


**Figure 5.15:** The calculational results for a LOCI for the reference core (nearly full with pebbles).



interval before recriticality.

The Relap5 thermal hydraulic description of the core clearly fails to describe the incident properly. Although the neutronic recriticality behaviour with the characteristic wiggles is present, the time of recriticality is too early. This can be attributed exclusively to the problematic modelling of the heat flow leaking out of the core as has been described in section 3.3. During normal operational transients this leakage is small compared to the power production and as such it does not play an important role. However, for the loss of cooling incidents it is the only way of transferring heat to the environment. Remember that the Relap5 model uses a near-infinite conduction in the pebble-bed in order to distribute the heat production evenly. This was done on the assumption that the temperature gradient in radial direction is small. When the heat removal depends entirely on radiation, conduction and free convection, and no longer on forced convection, this assumption is false and a temperature difference between pebble-bed center and edge will exist of typically over 300 K. In the Thermix-Direkt model the heat remains 'trapped' in the pebble-bed, while in the Relap5 model it rapidly flows out at the edges. In the figure for the maximum fuel temperature the Relap5 value is not a mesh point as for Thermix-Direkt, but the average for a whole layer.

At first sight it might be surprising, that the subsequent heat leakage to the environment is lower for the Relap5 model, but this can be explained from the way the cooling channels are modelled. This involved a helium-filled annulus around the reflectors within a radius of 1.7 m, which now (without forced convection) forms a large heat resistance.

Up to the point of recriticality all models predict a higher heat removal than production rate, which lowers the core temperature.

### **5.3.3 Loss of Flow Incident**

The loss of flow incident (LOFI) presupposes a halted mass flow rate while all helium in the primary cycle is still present and at equal pressure in both reactor and ECS. The Relap5 model predicts an averaged pressure of approximately 1.6 MPa. A LOFI will occur when the rotational speed of the shaft becomes zero. A possible reason might be that the power demand was too high which decelerated the shaft. Without intervention the shaft would come to a halt, as has been explained in section 4.3.2. Another possible reason is a turbine trip which constitutes a loss of driving power for the compressor and generator, causing a rapid deceleration of the shaft.

For the LOFI a similar set of figures as for the LOCI has been produced in figure 5.16. The main difference between the LOCI and LOFI is the enhanced effect of free convection in the pebble-bed plus cavity in the case of the LOFI. This results in a better heat transfer from pebble-bed to - at first - side reflectors and - later - environment. A lower pebble-bed temperature is the result and, as the xenon worth will be nearly identical, an earlier point of recriticality. The somewhat erratic behaviour of the total reactor power after recriticality can also be attributed to the better free convection; with the core being just critical, the prompt power is sensitive to small, localised changes in temperature caused by free convection.

# Loss Of Flow Incident

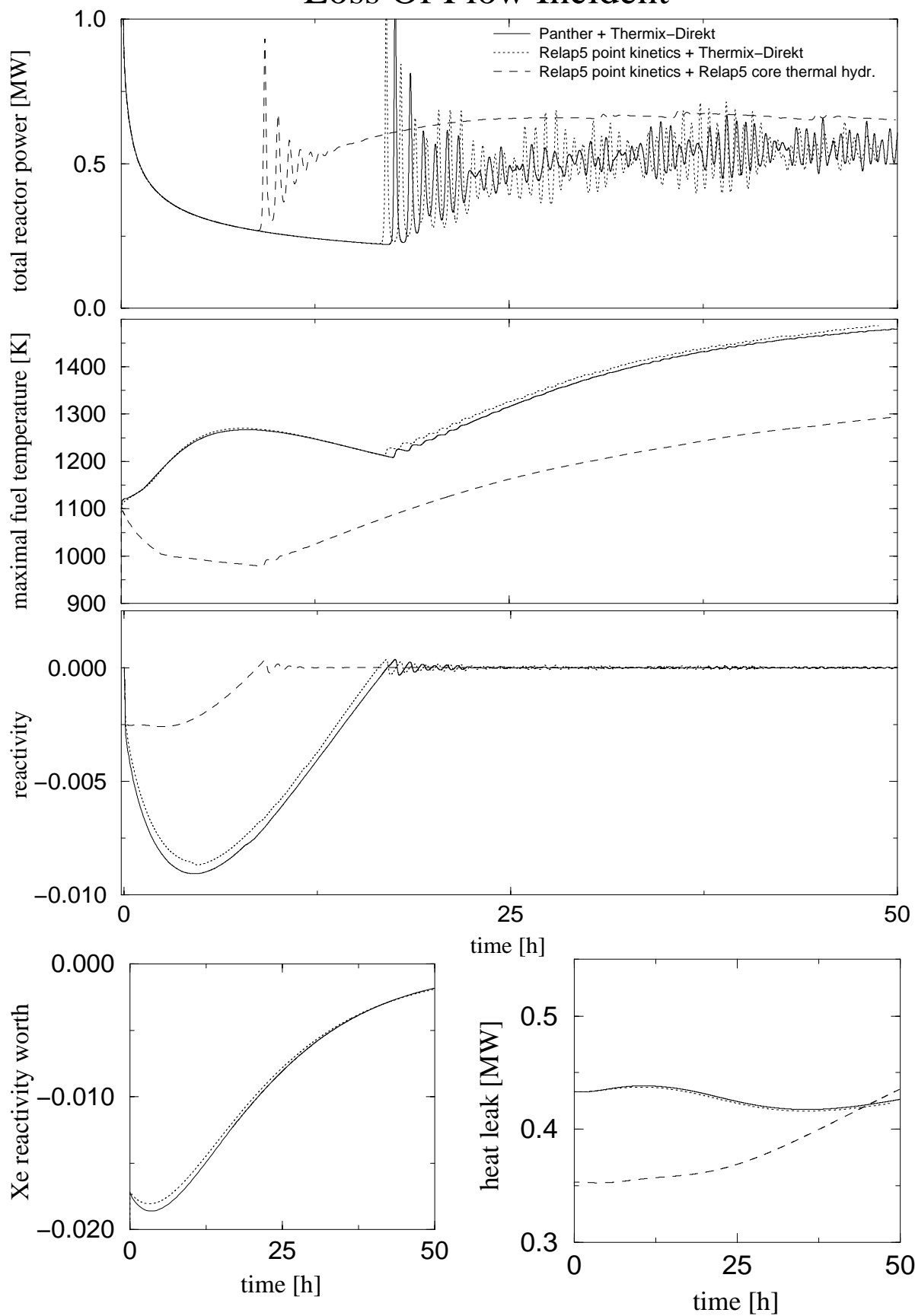


**Figure 5.16:** The calculational results for a LOFI for the reference core (nearly full with pebbles).

With respect to the calculational models the same observation can be made as for the LOCI. The point reactor kinetic model is suitable to describe the neutronic side of the incident, but it is more important to provide a good thermal hydraulic description of the core in the form of the Thermix-Direkt model. One can verify that the Relap5 thermal hydraulic model hardly makes a difference between a LOCI and a LOFI which is understandable as the model does not support convection *through* the pebble-bed, but alongside it. The heat transport through the helium in the cooling channels towards the outer reflector and finally to the environment has improved when compared to the LOCI, which shows in the graph for the heat leak.

### 5.3.4 Analysis of Recriticality Behaviour

The publications of Van Dam [87, 88] treat the reactor dynamics during inherent shut-down and recriticality after a loss of cooling incident. In this section the predictions made by the expressions derived in publication [87] will be compared with the results from the previous two sections. The model used in order to describe the reactor dynamics consists of the point kinetic equations for the prompt power (equations (3.16), (3.17)), a kinetic equation for fission product decay heat, the xenon equations from section 3.4.5, an expression for the reactivity due to temperature and xenon feedback,

$$\rho = \alpha_T(T - T_0) - \xi(X - X_0) \quad , \quad (5.6)$$

and an equation for heat transfer via Newton's law of cooling:

$$C \frac{dT}{dt} = P_p(t) + P_d(t) - \alpha AT(t) \quad , \quad (5.7)$$

with in equation (5.6)  $\xi$  defined as the  $^{135}\text{Xe}$  coefficient of reactivity,  $X_0$  the nominal xenon concentration,  $X$  the actual xenon density,  $T$  the (uniform) reactor temperature, and  $T_0$  the (uniform) nominal reactor temperature. In equation (5.7)  $C$  is the heat capacity of the reactor,  $P_d$  the heat produced by fission product decay,  $\alpha$  the heat transfer coefficient, and  $A$  the surface for heat transfer. In principle it is possible to determine the time of recriticality with the equations (5.6), (5.7) and the xenon equations, but an analytic expression will seldom result due to the function  $P_d(t)$  which in general consists of a superposition of exponentials with a broad range of decay constants. Given that recriticality occurs, the prompt power at time of recriticality, the maximum fission power in the first power surge, and the oscillation period of the power surges can be predicted.

#### Prompt power at first recriticality

The xenon decay and cooling down of the reactor together occasion the recriticality. From figures 5.15 and 5.16 it follows that the approach to recriticality can be approximated by a linear reactivity ramp. For such a slow approach the prompt power at

recriticality,  $P_{crit}$ , can be formulated for a one-group delayed neutron approach and prompt-jump approximation as (equation (18) in [87]):

$$P_{crit} = Q \sqrt{\pi \bar{\lambda} / (2 \gamma \beta)} \quad . \quad (5.8)$$

The inherent source strength  $Q$ , the one-group decay constant  $\bar{\lambda}$ , the effective delayed neutron fraction  $\beta$  can be found in table 3.2 and are for convenience repeated in table 5.2 at the end of this section. The reactivity ramp rate  $\gamma$  has been determined for the LOCI and LOFI from figures 5.15, 5.16. From the Panthermix calculations it follows that for the LOCI at the time of recriticality ( $t_{crit} = 79936$  s)  $P_{crit} = 195$  W, and for the LOFI ( $t_{crit} = 61250$  s)  $P_{crit} = 210$  W. From equation (5.8) it follows that  $P_{crit} = 192$  W, 197 W, respectively.

### Maximum fission power for the first power surge

For the maximum power  $P_{max}$  during the first power surge, Van Dam derives (equation (25) in [87]):

$$P_{max} = \frac{1}{P_{crit}^{0.064}} \left( \frac{6 \gamma C}{\alpha_T} \right)^{1.064} \quad . \quad (5.9)$$

It presupposes that the 'prompt' heat generated during the power surge does not flow out of the core region, and consequently terminates the surge by the temperature reactivity feedback. This adiabatic model assumes a uniform reactor temperature. It does not preclude a constant heat leakage out of the core from the decay power; that positive reactivity effect is incorporated in the reactivity ramp rate  $\gamma$ . For the neutron kinetics an effective-lifetime model has been used which is appropriate as from neutronics point of view the power surge is slow.

If now the values of the core during the LOCI are substituted, that is  $P_{crit} = 194$  W,  $\gamma = 0.0176$  pcm/s,  $C = 38$  MJ/K at an average temperature of 1200 K,  $\alpha_T = 6.54$  pcm/K, it follows that  $P_{max} = 1.03$  MW. This is too high a value compared to the Panther result of 0.67 MW, presumably due to the assumption of the uniform temperature distribution. Therefore, as a refinement to [87], an effective heat capacity  $C_{eff}$  will be defined here which corrects for the fact that not the same amount of heat is deposited at each point in the pebble-bed. Again the 10-layer core will be used with known axial power distribution and reactivity curves.

First a new, effective uniform temperature increase  $\Delta T$  during the power surge can be identified from

$$\rho_T = \sum_i \alpha_{T,i} \Delta T_i = \Delta T \sum_i \alpha_{T,i} \quad (5.10)$$

with  $\alpha_{T,i}$  the temperature coefficient of reactivity for layer  $i$ , and  $\Delta T_i$  the individual temperature rise for each layer due to the prompt power during the surge. In general, the temperature rise in the most reactive layer will be higher than the core average  $\Delta T$ ,

and the temperature rise in the least reactive layer will be lower. Adjusting the heat capacity for each layer,  $C_i \longrightarrow C_{eff,i}$ , remedies this variation:

$$C_{eff,i} = C_i \frac{\Delta T_i}{\Delta T} \quad (5.11)$$

At the same time  $\Delta T_i$  is given by:

$$C_i \Delta T_i = f_i P_p dt \quad (5.12)$$

where  $f_i$  denotes the fraction of the prompt power deposited in layer  $i$ , and  $dt$  the time interval of observation. Combination of the three equations (5.10), (5.11), and (5.12) yields

$$C_{eff,i} = \frac{f_i \sum \alpha_{T,i}}{\sum \alpha_{T,i} f_i} \cdot C_i \quad (5.13)$$

This reduces the total heat capacity to 85% of its original value, i.e. the correction factor is 0.85, as follows from table 5.2 where the correction for each layer has been tabulated. For  $P_{max}$  now follows 0.86 MW, still some 25% too high. One could apply the same strategy to the radial distribution, but in that direction the variations in power density and temperature coefficients of reactivity are smaller. It has been calculated that the correction factor to multiply  $C$  with is 0.99, hardly worth the effort. It is not clear what causes the remaining discrepancy in  $P_{max}$ . In [87] the same discrepancy is attributed to the fact that the power is already decreasing at the second recriticality for the exact point kinetics model and the buildup of power is interrupted, while for the effective lifetime model maximum power occurs exactly at second recriticality and the power can fully develop itself. However, for the Panther calculations the maximum power occurs only 25 seconds before second recriticality and as such more or less corresponds with the effective lifetime model.

Including even more detail, such as heat leakage of prompt power, and the resulting positive reactivity of the surrounding reflectors are considered to be minor effects and not easy to include in the model. Incidentally, these effects would result in a slightly higher prediction for  $P_{max}$ .

At this point, all data necessary to make the predictions have been derived from the core at nominal conditions, except for the time of recriticality and the reactivity ramp rate. The ramp rate could have been guessed from the nominal conditions, as the xenon part of the ramp rate is straightforward to calculate from the xenon equations, but the temperature induced reactivity rate is more difficult to determine. For the Panther calculations for the reference core, the temperature induced part of the reactivity ramp rate is roughly 25%.

For completeness, figures 5.17 - 5.19 show the temperature and prompt power distribution at  $P_{max}$  and the difference in core temperature before (at time of recriticality) the surge and at its maximum.

The last remark of this paragraph concerns the importance of the inherent neutron

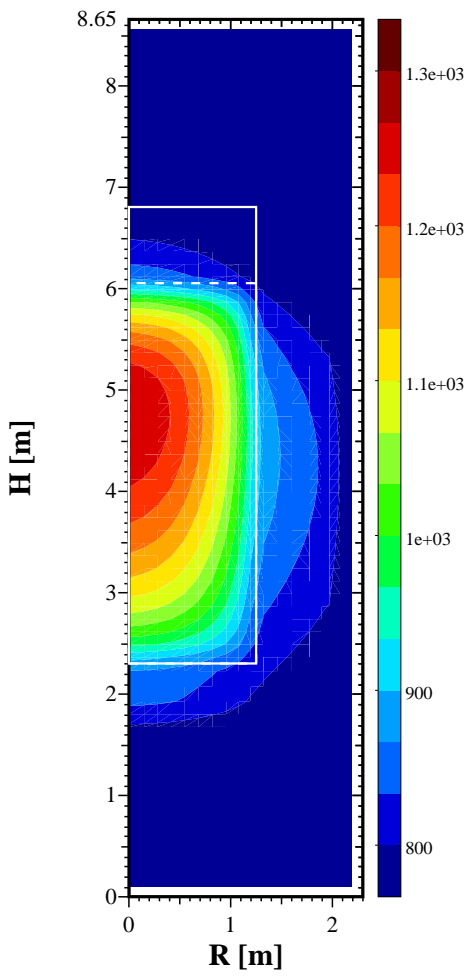


**Figure 5.17:** *Temperature of solid structures in core at maximum of first power surge [K].*

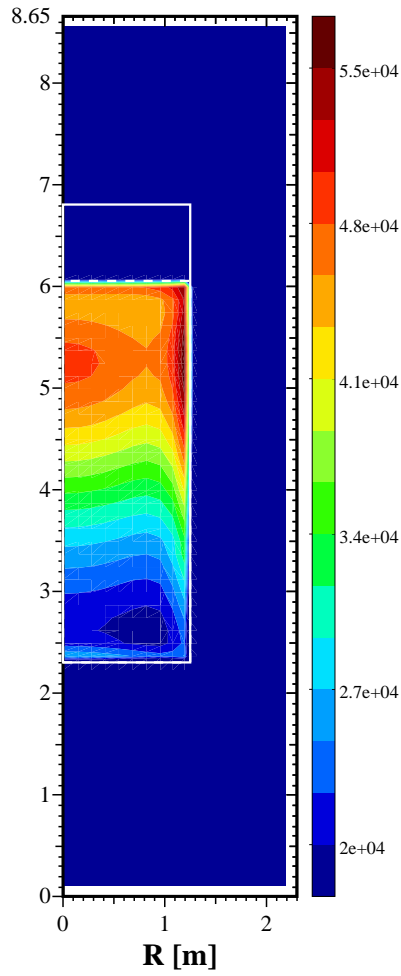


**Figure 5.18:** *Prompt power at maximum of first power surge [ $W m^{-3}$ ].*

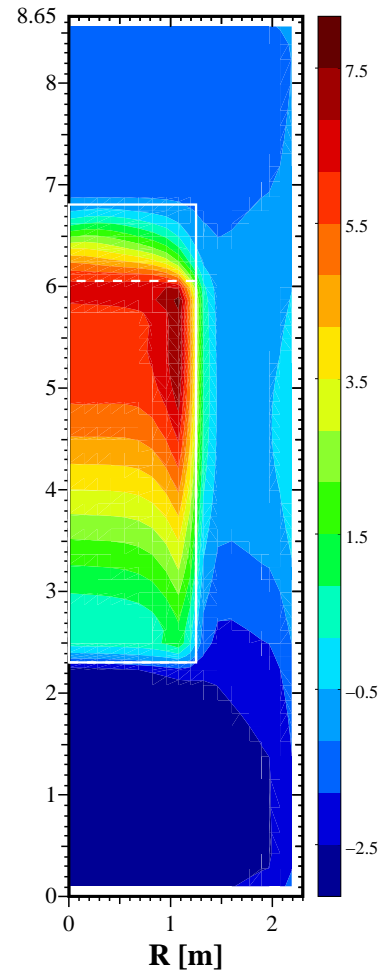


**Figure 5.19:** *Temperature increase at maximum of first power surge [K].*

source  $Q$ . Inserting equation (5.8) in (5.9) yields (equation (28) in [87])

$$P_{max} \propto \frac{\gamma^{1.096}}{Q^{0.064}} \quad . \quad (5.14)$$

The maximum power in the surge is only very weakly dependent on the inherent neutron source, which is a convenient result as it relieves one of precisely knowing the source strength. It can be explained by looking at the time it takes for the prompt power to build up from the inherent source strength to a value at which the heat production starts to feed back to the power production. If the source is extremely small <sup>1</sup> ( $\approx 10^{-300}$ , which would be the case if the 7<sup>th</sup> delayed neutron group had not been added) at the time of first recriticality, it would take several extra hours (!) before a noticeable prompt power level would be reached. In the mean time a high positive reactivity would have been formed by further xenon decay and cooling down of the core. On the other hand, if a source strength of 0.1 Watt is compared to one of 1 Watt, then it takes

<sup>1</sup>This is only possible in a calculation; in real life the inherent source is always present in the form of spontaneous fissions and ( $\alpha$ ,n)-reactions on oxygen. For the present calculations the source strength during nominal conditions is 37.4 mW (section 3.4.3).

**Table 5.2:** Results of analysis of recriticality behaviour for LOCI and LOFI [87] with the reference core.

$\beta = \sum \beta_i$		0.0054		
$\bar{\lambda} = \frac{1}{\beta} \sum_i \beta_i / \lambda_i \text{ [s}^{-1}\text{]}$		0.0781		
$\alpha \text{ [pcm/K]}$		6.54		
	layer $i$	$\alpha_i \text{ [pcm/K]}$	$f_i$	$\sum_i \left( \frac{f_i \alpha}{\sum_i \alpha_i f_i} \right)$
top layer	1	−1.02	0.136	1.15
	2	−1.16	0.138	1.17
	3	−1.09	0.137	1.17
	4	−0.94	0.127	1.08
	5	−0.74	0.111	0.94
	6	−0.55	0.095	0.80
	7	−0.40	0.079	0.67
	8	−0.29	0.067	0.56
	9	−0.21	0.056	0.47
bottom layer	10	−0.14	0.054	0.46
total correction factor $\sum_i \left( \frac{f_i \alpha}{10 \sum_i \alpha_i f_i} \right)$				0.85
$C_{eff} \text{ [MJ/K]} \text{ (pebble-bed)}$				32
$Q = 3.74 \cdot 10^{-2} \exp(-10^{-5}t) \text{ [W]}$				
scenario	LOCI		LOFI	
	Panther	theory	Panther	theory
$t_{crit} \text{ [s]}$	79936	—	61250	—
$\gamma \text{ [pcm/s]}$	$1.76 \cdot 10^{-2}$	—	$2.41 \cdot 10^{-2}$	—
$P_{crit} \text{ [W]}$	195	192	210	197
$P_{max} \text{ [MW]}$	0.67	0.86	0.94	1.19
$P_0 \text{ [MW]}$	0.26	—	0.33	—
$T_{osc} \text{ [h]}$	0.72	0.63	0.56	0.56

about 25 minutes for the weaker source to reach the level of 1 Watt. During the 25 minutes, the buildup of reactivity is  $\approx 25$  pcm extra, not too high and easily cancelled by temperature increase later on during the surge. According to equation (5.14) the power maximum for the surge will be a factor of 1.16 higher.

### Oscillation period (without decay heat)

In the case where the kinetics of the decay heat is neglected, an analytical stability analysis is possible for the reactor system. With a slightly adapted form of the prompt-jump approximation with one delayed neutron group and by the subsequent analysis of the reactivity transfer function, Van Dam derives for the oscillation period of the power surges (equation (36) in [87]):

$$T_{osc} \approx 2\pi \sqrt{\frac{C\beta}{\bar{\lambda}\alpha P_0}} \quad . \quad (5.15)$$

Here  $P_0$  is the equilibrium power of the passively cooled condition when the oscillations have damped. As the equation is the result of a *linearised* transfer function, the oscillation period for the Panthermix results should be measured in the region with small oscillation amplitude, that is, as far in time as possible towards the stable end situation. In that case satisfactory results are obtained and theory corresponds within 15% with the calculations. Table 5.2 shows the results.

## 5.4 Conclusions

In this chapter operational transients have been analysed for the stand-alone reactor. From the reactor point of view the driving force for all transients can be reduced to either a change in inlet temperature, a mass flow rate variation, or both. Two inlet temperature change transients and a number of mass flow rate reduction transients have been calculated with the four models:

- The Panthermix model has been used as reference as it produces the most detailed core analysis. It has been used to analyse variations in the axial power density profile, and - more general - the shape function. It has been found that in axial direction the power density profile can change up to 20% during the transients, and that in radial direction only small variations exist in the order of a few percent. The latter result justifies the approach of dividing the core only in axial direction when using a point kinetic model, the former result challenges the assumption of a fixed power density profile that is used in the point kinetic model for the thermal hydraulic calculations.
- The Relap5 point kinetic reactor model with the Thermix-Direkt model is the model to give a decisive answer on the question when the point kinetic model can be used. The thermal hydraulic module for the pebble-bed is identical to the module in Panthermix, and therefore all differences found between Panthermix and Relap5 + Thermix-Direkt will result from the point reactor model. For all operational transients, and even the loss of cooling incidents, the results of the two models are in good agreement. The origin of the small differences is clear: firstly the fixed power density profile in the point reactor model that yields a slightly different temperature profile over the core, and secondly the xenon reactivity worth that is used in the point reactor model to characterise the xenon reactivity. For the point reactor model the xenon worth is proportional to the concentration, and the ratio has been determined once from the nominal situation. This approach ignores the fact that there is also a temperature dependence in the relation between xenon concentration and reactivity. Most important is that for both models the difference in *total* power and thus the gain in gas temperature never exceeds 2%. This means that for studying operational transients that give interaction between ECS and reactor, the point reactor model is accurate within 2%.
- The Relap5 total reactor model shows that for the operational transients with sufficient power production (that means house load, 5%, and more) the model is in fairly good agreement with the Panthermix results. As such, it is a very convenient tool to perform quick and accurate tests for transient behaviour, and it is worth the effort



to create the point kinetic model. The thermal hydraulic core model has been tuned to Thermix-Direkt and contains some tricks that break down for low power output when the radial heat leakage also becomes important.

- The ACM total reactor model calculates the transients with approximately the same accuracy as the Relap5 total reactor model, but it, for its part, is faster than Relap5. Furthermore, the thermal hydraulic modelling for the core does not require extensive tuning or tricking, and is easier to build.

As a general, concluding remark, one can confidently postulate that the analysis of operational transients does not require a more-dimensional transient reactor code. The point reactor kinetic model is very accurate, and can derive the necessary parameters and reactivity curves from a steady-state model. This result is specific for this small pebble-bed HTR, as the core is small in terms of the average fission chain length and therefore tightly coupled.

## 5.5 Recommendations

Presently, much computing time is lost in the coupling software between the connected codes. Would that be streamlined and only form a marginal part of the calculations, then one could advise:

- use Panthermix for transient calculations where detailed information is necessary regarding the reactor core, for instance locations of maximum power density and fuel temperature during incidents where the ECS continues to interact with the reactor.
- use (Relap5) point kinetics with Thermix-Direkt if accurate information is required during operational transients with respect to interaction between reactor and ECS, and at the same time a fair degree of detail is desired for the reactor.
- use Relap5 or ACM for analysis of transient behaviour, where a detailed temperature and power distribution in the core is not important.

The streamlining of the code systems could consist of:

- the Panthermix-Relap5 connection Talink presently creates and deletes files to signal to both codes whether they are allowed to read or write. Problems exist that the deletion of such files is sometimes executed faster than the read action, which results in both codes waiting indefinitely for each other. Therefore, a connection with sockets would be faster, relieve the network, and would be more reliable.
- the Relap5 point kinetic model connected with Thermix-Direkt currently also uses Talink and Panther (as a dummy) to swap data. Its complexity would reduce, and velocity increase, if a (not necessarily Relap5) point kinetic model would be connected or even included as a subroutine in Thermix-Direkt. Such a scheme is mentioned to exist [65], but not yet available here.



# Chapter 6

---

## Total ACACIA Plant Dynamics

---

### 6.1 Introduction

In the previous two chapters the dynamic behaviour has been analysed for the reactor and the components of the ECS. In this chapter the ECS components will be connected and coupled to the reactor model. With this model of the entire ACACIA system three representative transients will be calculated. The first two transients will be utilised to demonstrate the dynamics of the ECS; they comprise two load rejection transients that force the ECS to react on a time scale that is too short ( $< 1$  minute) for the reactor outlet temperature to change significantly. The third transient consists of a long term load following transient (100 hours) in order to show the interaction between ECS and reactor.

In order to assess the validity of the calculations for the ECS with Relap5, the results will be compared to the calculations performed with the ACM code. It must be emphasised that no fit parameters have been tuned to improve the agreement between the two models.

### 6.2 Transient Analysis

#### 6.2.1 Load Rejection - Bypass Closed

The first transient simulates a load rejection without opening the bypass valve over reactor and turbine. In such a scenario the produced power suddenly can no longer be transferred to the electricity grid. The excess in power will directly speed up the shaft, and only at much higher speed and mass flow rate the required compressor power balances the power produced by the turbine. The generator no longer constitutes a load and has been decoupled from the grid. It must be noted that in reality this transient will not last for a long time before turbine or compressor blades will be torn loose by the high centrifugal force. However, it is of theoretic interest as it presents the highest

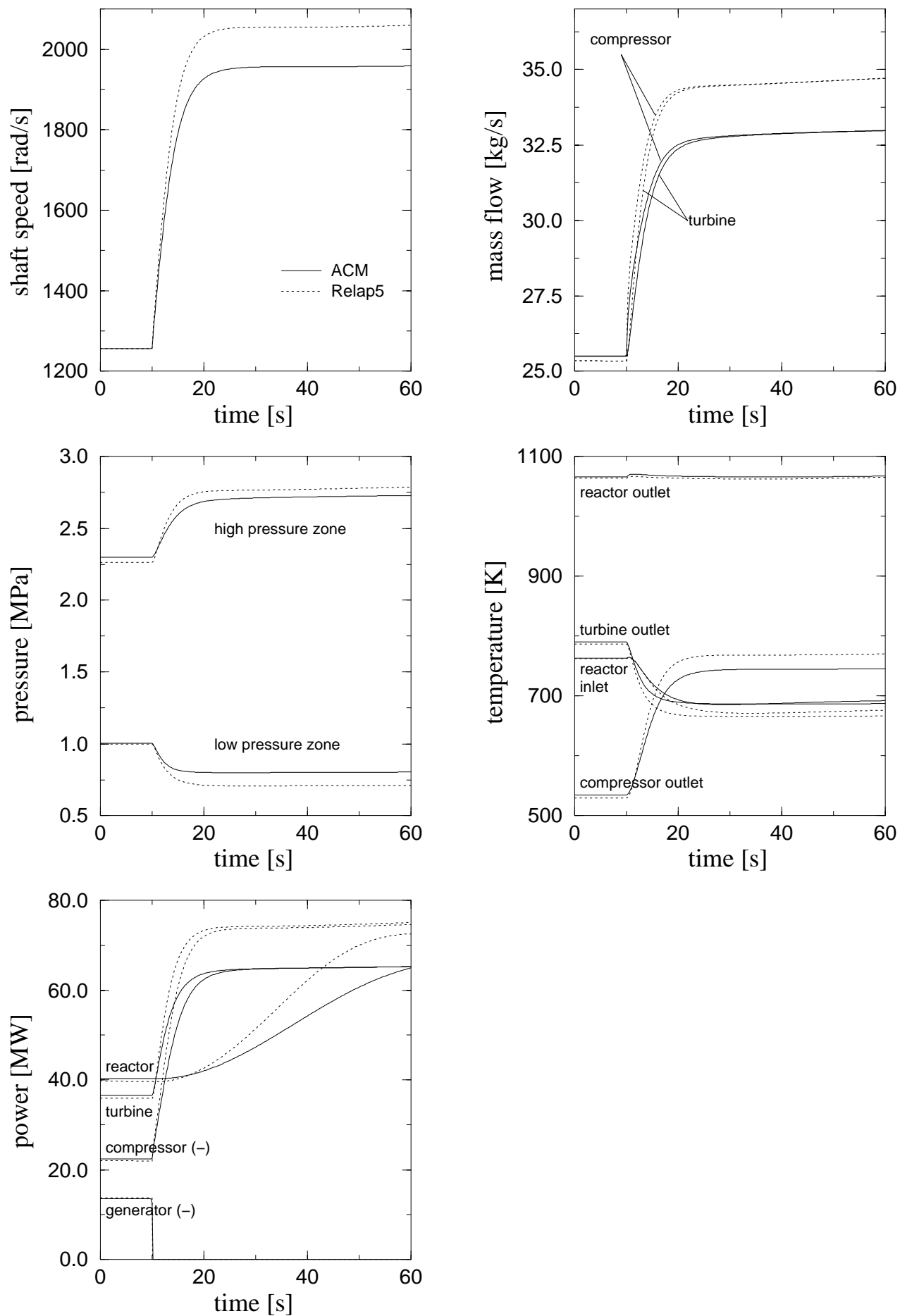


**Figure 6.1:** Calculational results for load rejection transient with bypass valve closed. The Relap5 and ACM models have been compared.

possible shaft speed for the ECS.

In the calculations the transient has been initiated by a step-wise reduction of the generator load to zero. The response of the system mainly depends on the inertia of the shaft components. As the inertia is small compared to the forces that drive the rotation of the axis, the shaft will reach its new steady rotational speed within seconds. On such a short time scale the reactor outlet temperature hardly changes, and the reactor model used is not very important. Had it not been for the already implemented point kinetics model, one could even consider to use a fixed reactor outlet temperature independent of mass flow rate. The transient has been calculated with the Relap5 model (ECS + reactor) and compared to the ACM results. In order to obtain the same boundary conditions the compressor inlet temperature has been kept constant at 365 K, i.e. the cooling capacity of the precooler has been made very large.

Figure 6.1 shows the calculational results. In spite of the differences between the models, the results are satisfactory as both models predict the same trends in dynamic behaviour. The differences can be attributed to the turbine models used in Relap5 and ACM. As has been discussed in section 4.2.1, the efficiency curve of the Relap5 turbine has been determined on completely different principles than that of the ACM turbine. Figures 4.4 and 6.1 demonstrate that for high rotational velocity (leading to a higher pressure ratio) the Relap5 turbine model uses a higher efficiency value. In comparison with ACM more power is produced, which results in higher shaft speed, mass flow rate and pressure ratio. A higher turbine efficiency also means a lower turbine outlet temperature.

The reactor outlet temperature remains constant during the time interval, as explained in chapter 5 for transients with changing mass flow rates. Soon the reactor outlet temperature will start to rise, because the reactor inlet temperature has decreased some 100 K; the time scale being determined by the thermal inertia of the core (see chapter 5).

## **6.2.2 Load Rejection - Bypass Open**

The second transient shows a load rejection with prevention of the high rotational velocity of the shaft. High mechanical stresses in the turbine and compressor blades will be avoided, just as the thermal stresses in particular for the recuperator. As discussed in chapter 4.3 a bypass valve will be utilised in order to - partially - bypass the power generating component on the shaft, the turbine. In order to prevent a temperature shock due to mixing helium flows at different temperatures, the valve has been placed between reactor inlet and turbine outlet. In that configuration the turbine plus reactor will be bypassed.

Just as in the previous transient of section 6.2.1 the precooler cools to a constant temperature of 365 K, and the generator load is rejected instantaneously. The bypass valve will be forced to open instantaneously by a constant signal that overrides the control system. The value of the signal has been chosen such that the nominal rotational velocity of the shaft results after some initial readjustment of mass flow rates through the system. From figure 6.2 it follows that the shaft first goes into overspeed before

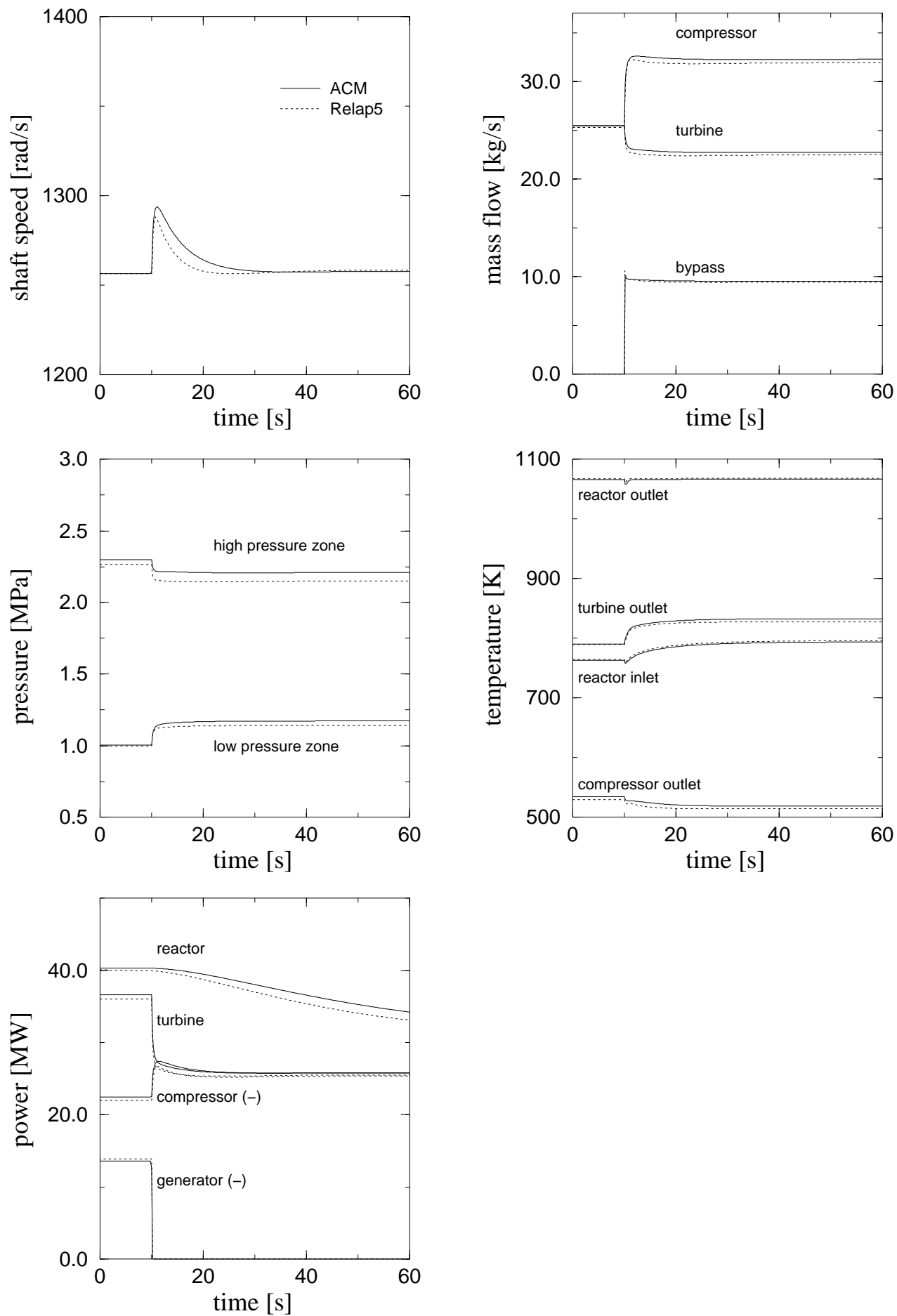


**Figure 6.2:** *Calculational results for load rejection transient with bypass valve open. The Relap5 and ACM models have been compared.*

the nominal rotational velocity is reached. This can be explained from the time it takes to reach the new pressure ratio and the time it takes to redistribute the mass over the high and low pressure zones. The mass flow rate figure nicely shows that opening the bypass valve in fact reduces the flow resistance, and that therefore the velocity of flow increases. For instance, the mass flow rate through the turbine only slightly reduces in spite of opening the bypass, and the mass flow rate through the compressor increases significantly. The changes in flow velocity of the helium gas reduce the efficiency of the turbine and compressor, i.e. the turbine produces less power and the compressor requires more. This can be seen in the figure for the power produced or consumed by the components. A decrease in turbine efficiency together with a decreased pressure ratio causes a higher turbine outlet temperature that feeds back through the recuperator to a higher reactor inlet temperature. A decrease in compressor efficiency produces a higher compressor outlet temperature, but a decreased pressure ratio causes a lower outlet temperature. From figure 6.2.2 it can be seen that the combined effects produce an approximately 15 K lower compressor outlet temperature.

The reactor power starts to decrease due to the higher reactor inlet temperature and the lower mass flow rate; for the time being, however, the reactor outlet temperature remains constant.

### 6.2.3 Part-Load Operation

The ACACIA has been designed with the ability of load following at high efficiency. The control of the helium inventory system that makes this possible has been described in section 4.3.3. In this section a transient will be discussed in which the helium inventory is reduced to 50% at which state the system operates for two days. Subsequently the helium inventory returns to 100%, and the system again will be monitored for two days. Strictly speaking this is not a load following transient, because in this case the inventory determines the load, rather than that the load determines the inventory. However, when comparing two models it is more straightforward to extract or inject helium during a short period of time, than to utilise a control system that continuously has to adjust the helium inventory according to a preset load. For the same reason - omission of a control system - the comparison is facilitated by keeping the shaft rotational velocity fixed at the nominal value. This corresponds to a very fast control loop in the asynchronous generator system.

During this long term transient the reactor behaviour becomes important because of the xenon transient. Both the point kinetics model in Relap5 and the more-dimensional model in Panthermix have been utilised to calculate the transient. The effects due to burnup being the only difference between the two models, for reasons of clarity only the point kinetics version with the Relap5 model has been compared to the ACM model in figure 6.3.

The transient starts with opening a valve connecting the helium storage tanks. The pressure difference has been made large such that the flow out of the system through the valve will be choked. Therefore the mass flow rate through the valve reduces linearly with the system pressure as depicted in figure 6.3. When filling the system from the

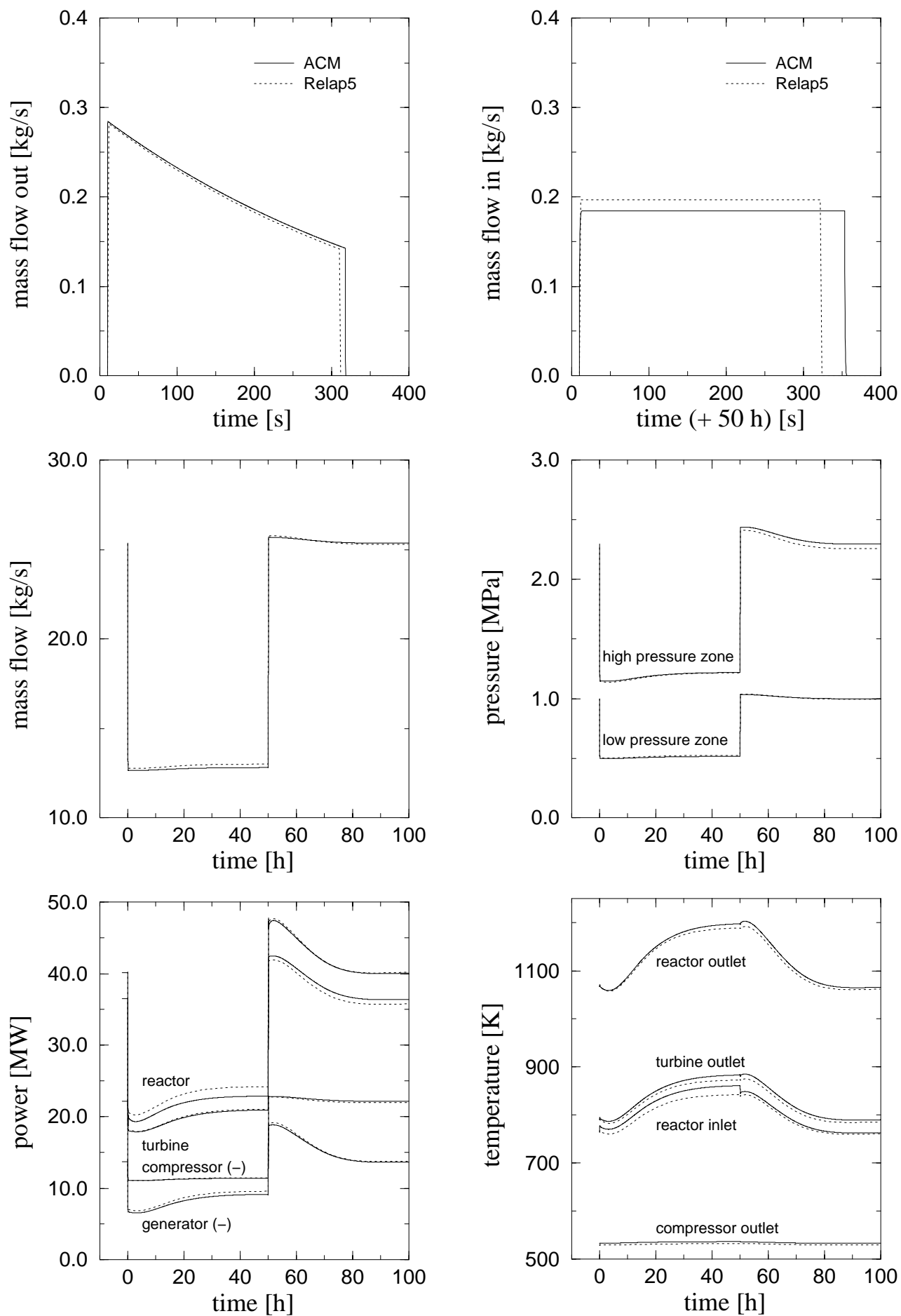


**Figure 6.3:** Comparison between Relap5 and ACM models for a long term transient with inventory changes from 100% to 50% back to 100%.



storage tanks, it has been assumed that helium is drawn from an infinite reservoir at constant pressure. Again the flow is choked, but now stays constant. During this transient the turbine and compressor working points remain close to the steady-state situation, and can therefore not be responsible for significant differences between the models. What emerges during this transient is that the recuperator models are not identical, indicated by the different behaviour of the reactor inlet temperature. When the mass flow rate reduces, the efficiency of the recuperator increases as is the case in the ACM model. Heat is transferred better from the hot (turbine outlet) side to the cold (compressor outlet) side, resulting in a higher reactor inlet temperature. The Relap5 recuperator model, however, has not been discretised as fine as the ACM model and the correction factor for this discretisation error is not adjusted for different flow conditions (see section 4.2.3 and appendix B). The lower reactor inlet temperature in the Relap5 model results in a slightly higher reactor power and electricity production.

The xenon transient shows clearly in the power plot of figure 6.3; after the fast power reduction to approximately 50% a further (small) reduction in power follows within a time span of 3 hours, followed by a gradual increase in power until 50 hours later. The small power reduction originates from buildup of xenon, which stands for buildup of negative reactivity. Its subsequent decay causes the gradual increase in power until the xenon concentration is again in balance with the fission power density. From 50 hours onwards, the power rises again due to restoration of the nominal helium inventory, but the xenon concentration is too low for the intended power level of 40 MW and an overshoot in power occurs (some 20%). Initially the xenon concentration will reduce even further due to 'burning away' xenon with the higher neutron flux, which causes the maximum in power around 52-53 hours. After this maximum the xenon concentration builds up, which decreases reactivity, and finally reaches equilibrium with the fission power density. The nominal situation has returned with a power production of 40 MW.

## 6.3 Conclusions

In this chapter three transients have been discussed which are representative for the comparison between the Relap5 and ACM ACACIA model. Both ACM and Relap5 utilised the point reactor kinetics model with equal kinetic parameters. In chapter 5 it has already been shown that the reactor models are in very good agreement, so that differences in the transients can be attributed entirely to the ECS model. Two load rejection transients, one with and one without control of the shaft rotational velocity, have been discussed, and one load following type of transient.

The load rejection transient without control of the shaft rotational velocity produced a high overspeed of the shaft, resulting in a large pressure ratio over turbine and compressor. This strongly influences the efficiencies of the turbine and compressor. It has been shown that the differences between the turbine models of ACM and Relap5 are responsible for the differences in the transients. Nevertheless, both models show the same trends, and in that sense the agreement is satisfactory.

The load rejection transient with control of the shaft rotational velocity also disturbs the working point of compressor and turbine, but less vehemently; the change in pressure

ratio is smaller. A bypass valve over turbine and reactor is utilised to prevent shaft overspeed. The ACM and Relap5 model show a good agreement for this transient. In the load following type of transient the inventory is reduced to 50% in a few minutes, and after 50 hours the inventory is restored to 100% (also in a few minutes). The ensuing xenon transients after the inventory changes have been monitored. This transient barely affects the working points of turbine and compressor, and revealed a more subtle difference between the recuperator models of ACM and Relap5. Both recuperator models have been corrected for the discretisation error as discussed in appendix B, but the Relap5 model utilises the (fixed) correction factor of the steady-state flow conditions for all transient calculations. The correction factor used in the ACM recuperator model is continually updated according to the flow conditions. During transients this can result in (small) differences between the two models in reactor inlet helium temperature. Otherwise the calculations are in good agreement. Summarising, the ECS models of ACM and Relap5 are in good agreement, and can further be improved by tuning or redesigning the Relap5 turbine model.

## 6.4 Recommendations

Further improvements can be made in the Relap5 ECS model by:

- Improving the Relap5 turbine model. This model is considered to be inferior to the ACM turbine model, and a new turbine subroutine could be written, just as has been done for the compressor. Furthermore, and more important, the implementation of the turbine model in the Relap5 basic equations should be reconsidered. As discussed in chapter 4 it is questionable whether the turbine model obeys the law of conservation of energy, i.e. whether the power extracted from the helium and transferred to the shaft exactly corresponds to the power that should be extracted according to the efficiency formula. As remarked in section 4.2.1 the accordance is correct within a few percent, which is not a problem for these investigations, but which may be a cause for concern for licensing authorities.
- Improving the Relap5 recuperator model. A finer discretisation comes at the cost of longer calculation times, as in Relap5 the calculation time is roughly proportional to the number of mesh points. The correction factor for the discretisation error cannot be made dependent on the flow conditions in a straightforward manner, but its importance decreases with finer discretisation.

# Chapter 7

---

## Safety Related Transients

---

### 7.1 Introduction

One of the most urgent questions concerning the HTR has hitherto not been answered: what are the transients that may threaten the nuclear safety of the reactor system and its energy conversion system? In order to narrow down the field of search for transients, a distinction is made between the effects of possible transients on the reactor and on the energy conversion system. It is generally accepted that damage to the energy conversion system is only important in terms of safety if it directly threatens the nuclear safety of the reactor. For instance, according to the Safety Report of the German HTR-Modul [93], it was possible to licence the plant even for incidents that would release the total helium inventory - including its radioactive contamination - to the surroundings. So if anything ruptures in the energy conversion system it may well mean the (economic) end of the power plant, but it is not always a nuclear safety related issue.

In fact, one is looking for transients that will cause release of fission products, or to put it more directly: what transients will cause the temperature in the coated particles to exceed  $1600^{\circ}\text{C}$ ?<sup>1</sup> For the currently deployed 'TRISO' coated fuel kernels this limit is a well established value [94–96] as a conservative design criterion for passively safe reactors<sup>2</sup>. In general, two conditions determine the fuel temperature in the pebble:

- the surface temperature of the pebble,
- the power generated by a pebble.

The first condition is determined by the temperature of the helium, and therefore the hottest surface temperatures are to be found at the bottom of the core for all transients

---

<sup>1</sup>The  $1600^{\circ}\text{C}$  upper limit is not absolute: coated particles can withstand higher temperatures such as  $1800^{\circ}\text{C}$  for a short duration (hours), but if they are heated far above  $1600^{\circ}\text{C}$  for extended periods the particles start to release fission products.

<sup>2</sup>There is in fact another reason that a pebble may fail. If the power generation in a pebble exceeds 4.5 kW, the fuel integrity is no longer guaranteed. For the current reactor this situation can only arise if too many pebbles are added to the bed; otherwise the maximum value for the power per pebble during the most unfavourable transients lies around 3.2 kW per pebble with a total power over 70 MW.

with a sustained helium flow. The second condition is also determined by the position of the pebble in the core, for instance close to reflectors local maxima exist in the thermalised neutron flux and power density. It will be clear that the combination of the two conditions will yield the highest internal temperature for a pebble. This situation can be found at the bottom of a fresh core where the thermal flux is at its maximum. The effect is enhanced by the anyhow higher power density due to the smaller volume of the fresh core.

Before starting with the safety transient analysis, first the temperature assessment for a pebble has to be refined. Up to now all calculations in this thesis have been performed with a uniform temperature distribution over the pebble which is equal to the pebble surface temperature. It will be shown that this leads to a serious underestimation of the fuel temperature inside the pebble. Instead of repeating all previous calculations, one should realise that up to now the calculations only have been used in order to compare models, and not to perform safety studies. Therefore, the consequences are limited. The opposite is true for the design and safety studies performed in the past for the ACACIA model [30, 97], they are no longer valid and have to be replaced by the new and more complete method of analysis presented in this chapter. Section 7.2 will discuss the corrections that are necessary in the temperature assessment of the fuel in the Panthermix calculational scheme. In section 7.3 an example will be given to show the importance of the correction. The LOCI and LOFI for a fresh core will be calculated in section 7.4. Section 7.5 will treat the problems that may arise for load following transients due to the xenon dynamics. It will be proven that the current design can fail under certain circumstances, and that the design requires changes in order to rectify this.

For all transients the Panthermix code will be used in order to assess the core behaviour.

## **7.2 Temperature Distribution of Pebble**

Before starting with the safety transient analysis, first the temperature assessment for a pebble has to be refined. For reactor operations at a significant level of power, the assumption of a uniform temperature equal to the surface temperature will in general not be valid for a pebble. The central (fuel) region of the pebble will experience a higher temperature than the surface. The two most important consequences will be that *a)* the maximum fuel temperature will be underestimated and *b)* the temperature at which the nuclear cross sections are tabulated is in fact the wrong, viz. surface, temperature. Both errors can be rectified quite easily in the Panthermix calculations. Recall that Thermix-Direkt passes at each time step a new temperature distribution to Panther, and it is simple to add an extra temperature calculation. The correction can be inferred from the power distribution that Panther calculates and from solving the stationary heat equations for the fuel zone in the pebble and the pebble shell. This analytic exercise is straightforward and has been performed before [32, 79], therefore only the results will be presented here.

## Maximal Pebble Temperature

Solving the Fourier law for a stationary situation in sphere-coordinates yields for the temperature in the fuel zone,  $T_{FZ}$ , and the temperature in the outer shell,  $T_{Sh}$ , as a function of the radius  $r$ :

$$T_{FZ} = T_{surf} + \frac{P_{peb}}{4\pi\lambda_g} \left\{ -\frac{1}{R_o} + \frac{3}{2R_i} - \frac{r^2}{2R_i^3} \right\} \quad 0 \leq r \leq R_i \quad (7.1)$$

$$T_{Sh} = T_{surf} + \frac{P_{peb}}{4\pi\lambda_g} \left\{ -\frac{1}{R_o} + \frac{1}{r} \right\} \quad R_i \leq r \leq R_o \quad (7.2)$$

Here  $T_{surf}$  is the pebble surface temperature,  $P_{peb}$  the power homogeneously generated in the fuel zone of a pebble,  $\lambda_g$  the conductivity of graphite,  $R_i$  the radius of the fuel zone (2.5 cm), and  $R_o$  the outer radius of the pebble (3.0 cm). The maximal temperature difference over the pebble follows from these equations and reads:

$$\Delta T = \Delta T_{FZ} + \Delta T_{Sh} = \frac{P_{peb}}{4\pi\lambda_g} \left\{ -\frac{1}{R_o} + \frac{3}{2R_i} \right\} \quad (7.3)$$

## Conductivity of Graphite

A large difference in conductivity exists between irradiated and unirradiated graphite. Figures 7.1 and 7.2 serve as an example of the dependency of conduction on the irradiation. In the Panthermix code system it is not possible to define the conduction as a function of the irradiation dose, and therefore the calculation for a scenario will be performed with both the irradiated value and the unirradiated value for conduction.

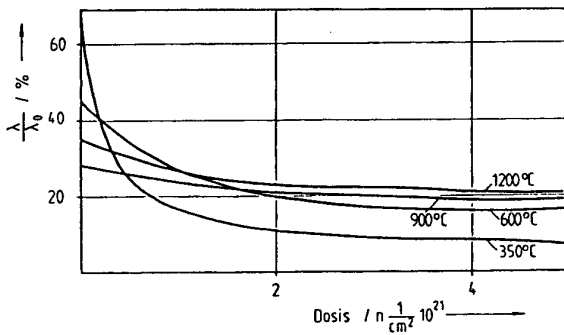


**Figure 7.1:** Example of reduction of graphite conductivity due to irradiation by fast neutrons ( $>100$  keV) [79].

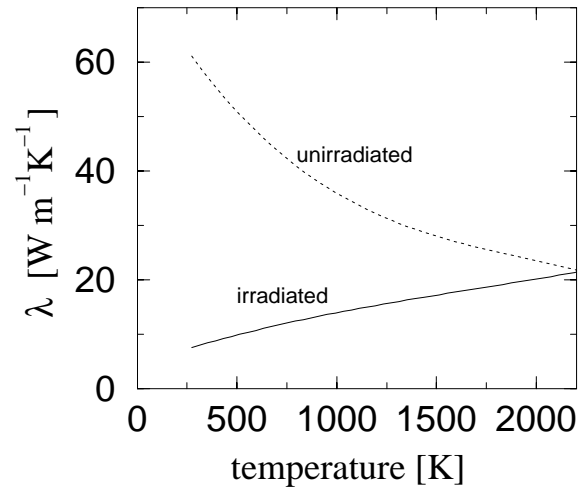


**Figure 7.2:** Conductivity of pebble graphite (A3-4) for the irradiated and unirradiated case in Thermix.

The conductivity of graphite as a function of its temperature has been taken from the Thermix-Direkt code [98]; for unirradiated pebble matrix graphite  $\lambda_{unirr}$  reads

$$\lambda_{unirr}(T) = 61.1502 - 5.0309 \cdot 10^{-2} \cdot T + 0.2516 \cdot 10^{-4} \cdot T^2 - 5.0 \cdot 10^{-9} \cdot T^3 \quad (7.4)$$

and for irradiated pebble matrix graphite  $\lambda_{irr}$  reads

$$\lambda_{irr}(T) = 7.6098 + 1.0917 \cdot 10^{-2} \cdot T - 0.0348 \cdot 10^{-4} \cdot T^2 + 8.0 \cdot 10^{-10} \cdot T^3 \quad (7.5)$$

The units of  $\lambda_{(un)irr}$  are W/m/K, the temperature is the  $T_{Peb}^{ave}$  inserted in Celsius. The two conductivities are depicted in figure 7.2.

## Temperature for Nuclear Cross Sectional Data

In the present case no thermal distinction has been made in the nuclear cross sectional data between the shell and fuel zone and therefore the volume weighting for the average temperature of the pebble has been performed over the entire pebble, yielding:

$$T_{Peb}^{ave} = \frac{R_i^3 T_{FZ}^{ave} + (R_o^3 - R_i^3) T_{Sh}^{ave}}{R_o^3}, \quad (7.6)$$

with the average fuel and shell temperature given by:

$$T_{FZ}^{ave} = \frac{\int_0^{R_i} T_{FZ}(r) 4\pi r^2 dr}{\int_0^{R_i} 4\pi r^2 dr} = T_{surf} + \frac{P_{peb}}{4\pi \lambda_g} \left\{ -\frac{1}{R_o} + \frac{6}{5R_i} \right\} \quad (7.7)$$

$$T_{Sh}^{ave} = \frac{\int_{R_i}^{R_o} T_{Sh}(r) 4\pi r^2 dr}{\int_{R_i}^{R_o} 4\pi r^2 dr} = T_{surf} + \frac{P_{peb}}{4\pi \lambda_g} \left\{ -\frac{1}{R_o} + \frac{3}{2} \frac{R_o^2 - R_i^2}{R_o^3 - R_i^3} \right\} \quad (7.8)$$

One should realise that the volume averaged temperature does not exactly represent the correct temperature value in order to determine the cross sections. In general the temperature dependence of the fuel will be  $\sqrt{T}$  (resonance absorption) and that of the moderator  $1/\sqrt{T}$  (scattering), and  $T_{FZ}$ ,  $T_{Sh}$  should be inserted in that form in the equations (7.7) and (7.8). However, it can be shown that the difference between the original average and thus determined effective temperature is small [32], typically in the order of 1%.

The temperature correction of equation (7.6) will result in a higher fuel temperature which means a decrease in reactivity, and therefore new fuel has to be added to the previously critical core. Table 7.1 gives the maximal fuel temperature values for the different core configurations at nominal power production, 40 MW. As shown, the fuel temperature in the core with irradiated graphite is higher than in the core with unirradiated graphite. Therefore the pebble-bed is higher for the irradiated case. In general the following results can be expected:

- the most conservative estimate of the maximal pebble temperature will follow from the calculations with the  $\lambda_{irr}$  value. In this case the  $T_{Peb}^{ave}$  is higher than in the unirradiated case, and the  $\Delta T$  from surface to center of pebble will be much higher due to the lower conductivity.
- as it is not entirely certain for the present calculations at what point of time the unirradiated conduction has to be replaced by the irradiated value, it is conservative to calculate a fresh core with the conductivity for irradiated graphite. At the same time it is not conservative to use the conduction for unirradiated graphite, although

**Table 7.1:** *The results of the corrections on the pebble temperature profile compared to the uncorrected situation. The maximum fuel temperature values in a fresh core of 5 days old are given.*

	uncorrected		corrected	
scenario	$\lambda_{irr}$	$\lambda_{unirr}$	$\lambda_{irr}$	$\lambda_{unirr}$
$T^*$ (average pebble) [K]	1206	1206	1289	1249
$T^{**}$ (pebble surface) [K]	1206	1206	1203	1204
$T^{***}$ (pebble center) [K]	1460	1328	1440	1327
pebble-bed height [m]	1.266	1.266	1.297	1.279

\*  $= T_{Peb}^{ave}$ , used for cross sectional data

\*\* used for heat transfer to helium

\*\*\* used as maximal temperature during transients

it may be more realistic for a fresh core. From looking at figure 7.1 (from [79]) and other similar data [99] it follows that (with a fast neutron flux ( $>100$  keV) of  $10^{14} \text{ cm}^{-2} \text{ s}^{-1}$ ) roughly after 2 weeks the graphite irradiation dose is such that all calculations should be performed with a conductivity value for irradiated graphite.

- for high temperatures the irradiated and unirradiated value for the graphite conduction converge towards the same value (figure 7.2). This behaviour has been reported earlier [68] and has been attributed to the process of annealing that repairs to a high extent the lattice defects due to radiation. However, the conclusion must not be drawn that utilising the irradiated or unirradiated value for graphite conduction for a LOCI or LOFI will yield the same result. Realise that the pebble-bed height from which the transient starts will differ for the irradiated and unirradiated case. The irradiated pebble-bed will be higher and will contain more fuel. This extra reactivity has to be balanced by a higher fuel temperature in the irradiated case (from table 7.1 follows that it compensates 40 K during steady state).

## 7.3 Cold Helium Ingress

As a first example of the importance of using a correct temperature distribution in a pebble, the ingress of cold helium into the core will be considered. This situation could arise if one of the partitions between in- and outflow at the cold recuperator side ruptures; the small pressure difference ( $\approx 0.2$  bar) will feed the relatively cold helium from the compressor outlet directly into the core. This transient is a consequence of working with the *direct* Brayton cycle. In the indirect cycle with a heat exchanger separating reactor and energy conversion system, the large drop in temperature is not possible: firstly, the temperature of the helium flowing into the reactor is lower in general ( $250^\circ\text{C}$  versus  $495^\circ\text{C}$ ) [79], and secondly, it would require an increased cooling capacity in the secondary cycle. The latter would only be feasible if the mass flow rate increases or the heat exchanger inlet temperature decreases in the secondary cycle. An increase in mass flow rate would require extra power for the pump in the

secondary cycle, which is not installed. A decrease of inlet temperature is possible in the secondary (steam) cycle if the feedwater preheating stage malfunctions. Such a scenario has been considered before [100] and it has been concluded that the decrease in temperature would be small and slow.

For the ACACIA design the worst case scenario will be considered where the ECS has been used in the mode for maximal electric power production. The precooler functions as a heat sink at 300 K. In fact, this case represents the design of the ACACIA predecessor, INCOGEN. For these calculations it is not necessary to involve the ECS in the calculations, as there is no recuperative coupling from the reactor outlet temperature to the reactor inlet temperature for the helium. In other words, the gas inlet temperature is fixed for this transient. A compressor inlet temperature of 300 K yields a compressor outlet temperature of 468 K, and the mass flow remains at 25.2 kg/s. This temperature has been taken as reactor inlet temperature on the assumption that all helium bypasses the cold recuperator side<sup>3</sup>. The cold helium ingress transient has been calculated for the fresh core for the scenarios:

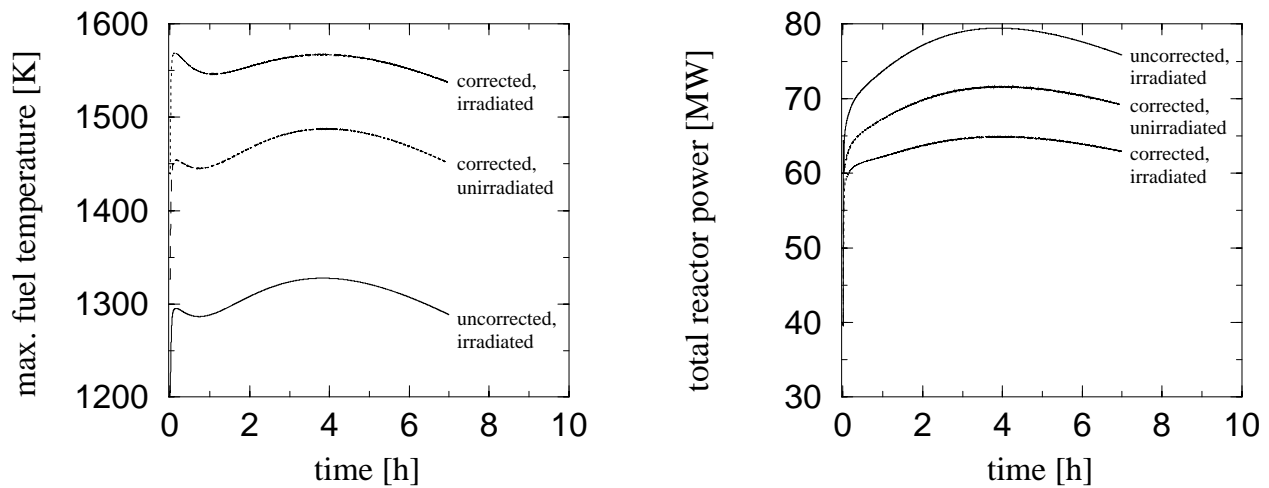
- uncorrected, which utilises the surface temperature for the nuclear cross sections, and the irradiated graphite conductivity. This corresponds to the situation of all previous safety calculations, [30, 97].
- corrected, which utilises the average pebble temperature (equation (7.6)) for the nuclear cross sections, and the irradiated graphite conductivity.
- corrected, which utilises the average pebble temperature (equation (7.6)) for the nuclear cross sections, and the unirradiated graphite conductivity.

Figure 7.3 shows the results; it is clear that completely different values are calculated for the three scenarios. The uncorrected case produces the highest power, because the pebble fuel (=surface) temperature is lower. Especially for this transient, where the cold helium helps to lower the pebble surface temperature, the discrepancy with the corrected cases is large. Looking at the corrected cases, the irradiated case produces a higher fuel temperature at lower power than the unirradiated case due to the lower graphite conductivity. From this transient it can be concluded that it is essential to utilise the correct fuel temperature. Furthermore, it is important to realise that the difference between irradiated and unirradiated graphite can be large. In case of doubt which conductivity to utilise, the irradiated conductivity should be chosen as it provides a conservative scenario.

---

<sup>3</sup>One could be tempted to look for the worst combination of mass flow rate and gas inlet temperature as inlet conditions by varying the shaft rotational speed. Indeed, it can be shown that a lower than nominal shaft speed will result in slightly higher maximal pebble center temperatures. The compressor efficiency increases for lower rotational speeds, yielding a lower compressor outlet temperature (= reactor inlet temperature and leading to a power increase) that apparently is of more importance than the reduction of mass flow rate (proportional to the rotational speed and leading to a power decrease). However, as has been shown in section 4.3, the region of lower than nominal speed does not represent a stable state and therefore either the control system will be designed such as to bring the working point rapidly back to normal, or the shaft will soon come to a halt.





**Figure 7.3:** The total reactor power and maximum fuel temperature during the cold helium ingress incident. The uncorrected case refers to temperature assessment with the pebble surface temperature.

## 7.4 Maximal Temperature during Loss of Cooling

The Loss Of Coolant Incident (LOCI) and Loss Of Flow Incident (LOFI) have been presented for the nearly full core near end of life in chapter 5. At that time the objective was the testing of the point kinetic models, now the objective is to determine the maximal fuel temperature during the loss of cooling incidents. For these transients the active cooling is absent, and the transport of heat out of the core relies entirely on passive mechanisms: conduction, radiation and free convection. As discussed in the introduction, the fresh core will give the highest decay heat density and consequently the highest fuel temperatures.

In this section it will again be shown that it is important to take into account the correct temperature distribution of a pebble. Determining the cross sectional data with the averaged pebble temperature (equation(7.6)) will give a higher initial pebble-bed at identical nominal conditions. This extra positive reactivity is necessary in order to compensate the negative reactivity of the higher pebble temperature. This effect is strongest for the irradiated pebble-bed as has been shown in table 7.1. The fuel temperature development in time will therefore take place at higher temperatures than predicted in the previous analysis of the LOFI and LOCI in the INCOGEN and ACACIA studies [30, 97]. Figure 7.4 depicts the results of the calculation with the corrected fuel temperatures. The LOFI and LOCI calculations are shown for the unirradiated and irradiated case.

The point of recriticality depends on two factors:

- the volume of the irradiated pebble-bed is a little larger while producing the same power. The thermal flux, and consequently the xenon concentration, will be a little lower. Purely on grounds of xenon concentration, recriticality would occur earlier in the irradiated pebble-bed.
- an increase in temperature will enhance the reactivity worth of the xenon concentration, as discussed in section 3.4.5

These two factors counteract as the more compact (unirradiated) pebble-bed is cooler, and the bigger (irradiated) pebble-bed is hotter. On beforehand it is not certain which process is more important, but it turns out that for both the LOFI and the LOCI

# Loss Of Cooling Incidents

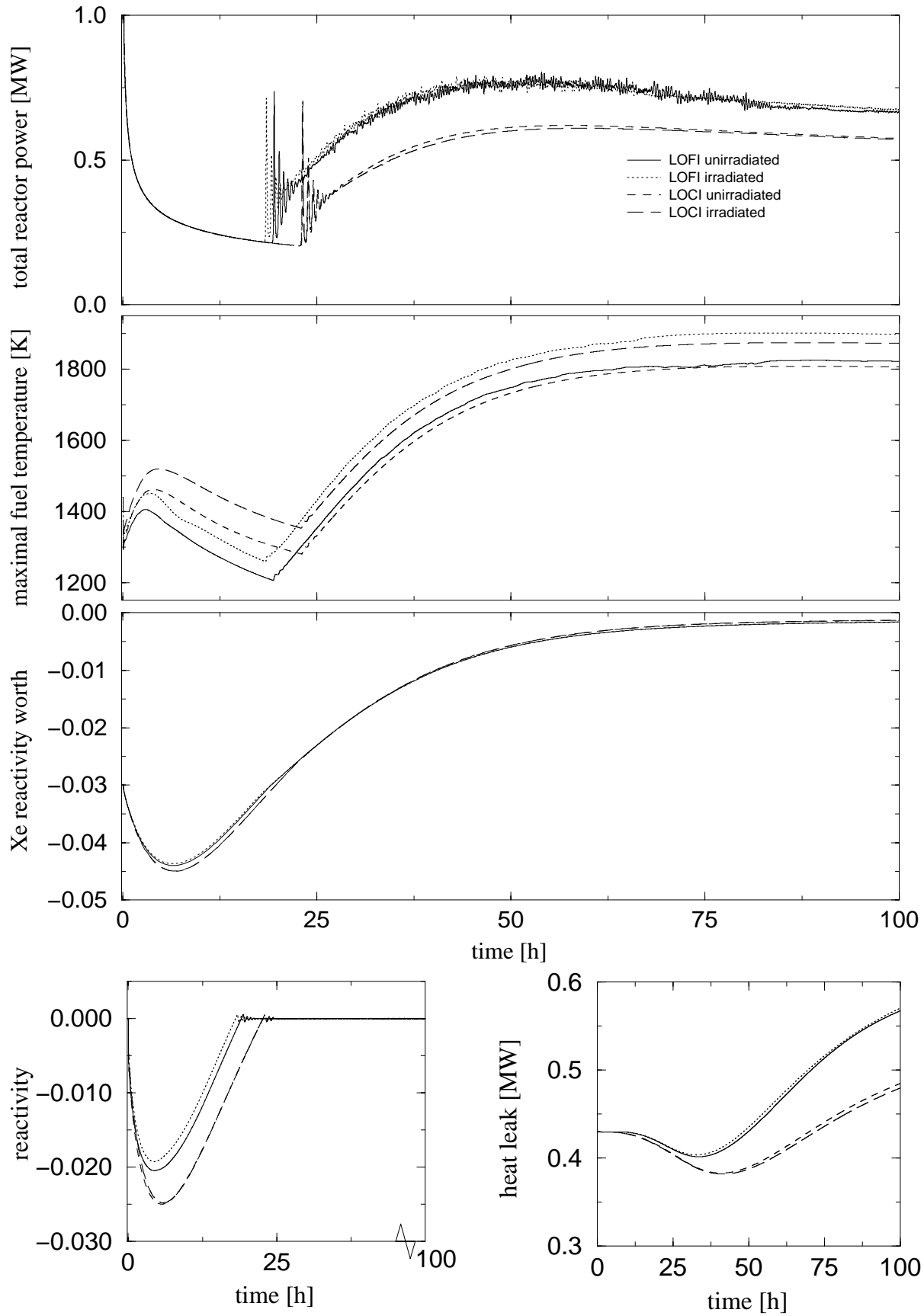


**Figure 7.4:** The calculations for a LOCI and a LOFI are depicted for the fresh core (5 days burnup) for a conductivity of irradiated and unirradiated graphite.

recriticality occurs earlier for the irradiated case. For the LOCI the difference is small (a few minutes) and not discernible in figure 7.4. The fuel temperature steadily increases after recriticality as the fission power slowly returns while xenon further decays. At the point in time that the xenon decay is maximal and in equilibrium with the prompt power, the fuel temperature will reach its maximum. Due to burnup, slowly the power will decrease and with it the temperature eventually will drop.

Figure 7.4 shows that the maximal fuel temperatures will exceed the 1600°C (or 1873 K) temperature limit for the irradiated LOFI scenario and reach 1900 K. The irradiated LOCI scenario reaches exactly 1873 K. The maximal fuel temperature for the unirradiated scenarios remains under the 1600°C the limit. These results are in sharp contrast with the earlier results that predicted a fair temperature margin of some 100 K during these transients.

The same conclusion can be reached as in the previous section: it is essential to utilise the correct fuel temperature, and utilising the irradiated graphite conductivity represents a conservative version of the transient.

## **7.5 Maximal Temperature during Transients**

Up to this point the nuclear safety of the ACACIA has been tested for some specific, well established [65, 79], incident situations. The question remains whether the reactor remains under the 1600°C limit during all operational transients. At the same time, one would like to know what the reactor outlet temperature is during operational transients in order to prevent damage to the gas turbine due to too high temperatures. It might turn out, for instance, that control rods are indispensable in order to limit temperatures, and have to be included in the design as active components.

These questions can be answered by systematically calculating the steady final states for a large number of load following transients. In the case of a load reduction, the final states of the transient will represent the worst-case situation in terms of fuel and outlet temperature. High fuel temperatures must then compensate the decrease of the negative xenon reactivity. The section will be split into two parts, the first part will focus on the gas outlet temperature during the transients and how to control it, the second part will focus on the maximal fuel temperature during the transients.

### **7.5.1 Reactor Outlet Gas Temperature**

#### **Control philosophy of gas outlet temperature**

Before presenting the actual calculational results, a discussion will be started whether it is possible to control the reactor outlet gas temperature by changing the reactor gas inlet conditions, i.e. mass flow rate and/or temperature. Consider the case that the load on the reactor has to be reduced to a certain *fixed* power level for a prolonged period of time (days). At the start of the load reduction the helium inventory will be reduced accordingly. From that point on a choice has to be made: are the future power

variations due to the xenon dynamics to be compensated by changing the reactor inlet temperature, or by changing the mass flow rate, or both? And what is the effect on the reactor outlet temperature?

- **Changing the mass flow rate.** Initially the xenon concentration will build up and the mass flow rate has to be increased in order to maintain the required power level. After some time (typically hours) the xenon concentration will start to decay towards its end value. The power will increase which can be countered by reducing the mass flow rate. For the reactor outlet temperature this will mean a temperature rise, as less gas will transport the same amount of heat. The temperature rise is considerable as can be deduced from figure 5.5. There the power at end of transient is 43% of the nominal value at a 25% of the nominal mass flow rate. Suppose that the desired constant power level would have been 43% during the entire interval of time, then initially the mass flow rate would also have been reduced to 43%. Apparently, at the end of the transient the mass flow rate has shrunk to 25%, while transporting the same heat flow. That means that the gas temperature difference over in- and outlet has nearly doubled, and rose from (nominal) 300 K to 516 K. The outlet gas temperature rose from 1070 K to 1286 K, which coincides nicely with the value in the temperature plot of figure 5.5.
- **Changing the gas inlet temperature.** In order to keep pace with the xenon decay after the initial buildup, the gas inlet temperature can be increased continually in order to try to limit the gas outlet temperature. This will keep the produced power and thus the heat added to the gas, constant. However, due to the constant temperature difference between gas in- and outlet, the outlet gas temperature will still rise because of the increasing gas inlet temperature. From figure 5.1 it follows that in order to achieve a power reduction to 80%, an inlet temperature increase of 100 K is necessary. The outlet temperature rises approximately 40 K. One can also see from figure 5.1 that the temporary effect of an increase in the gas inlet temperature can result in a temporary lower gas outlet temperature. This is not always the case, for instance for the fresh core the short term reaction to an increase in inlet temperature is an *increase* in outlet temperature. This behaviour depends on the pebble-bed height and the associated power profile, and will be explained shortly hereafter.
- **Changing both gas inlet temperature and mass flow rate.** It will now be of no surprise that the combined efforts of reducing the mass flow rate and increasing the gas inlet temperature can also not prevent an increase in the gas outlet temperature in the long run.

One can intuitively predict the results for the three control scenarios discussed above, by realising that the xenon decay must and can only be balanced by increasing the reactor temperature. That will always result in a higher gas outlet temperature.

As mentioned above, for the fresh pebble-bed core the increase of inlet temperature will result in an increase in the gas outlet temperature. This is contrary to the results for the high pebble-bed core from chapter 5, and can be explained from the different power profile. In order to clarify this, the axial power profile, the axial pebble surface temperature profile, and the axial gas temperature profile have been plotted for the fresh core in figures 7.5 and 7.6. The solid line refers to nominal conditions, the dotted

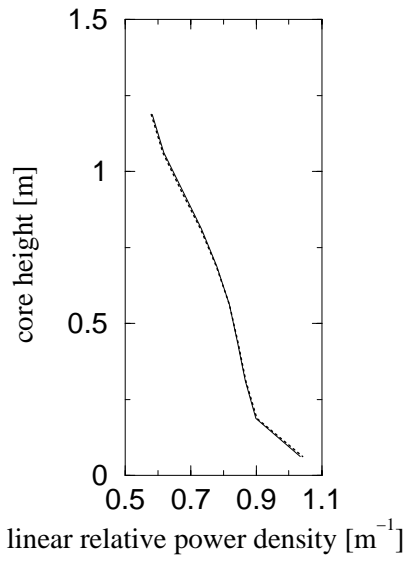


**Figure 7.5:** The linear relative power density at nominal (solid line) conditions and 10 minutes after the increase in gas inlet temperature with 100 K (dotted line).

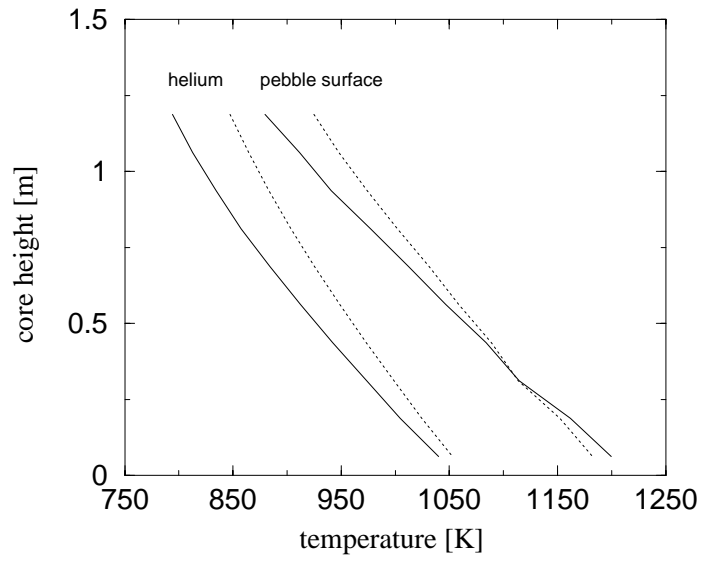


**Figure 7.6:** The temperature of the helium gas (left two lines) and of the pebble surface (right two lines). The nominal situation has been depicted (solid lines) and the situation 10 minutes after the increase in gas inlet temperature with 100 K (dotted lines).

line to the situation 10 minutes later after an increase of the gas inlet temperature with 100 K (resulting in power decrease to 80%). The maximal power density for this core will be found in the bottom layer, as already discussed in the introduction of this chapter. Moreover, the power profile hardly changes, certainly if one realises that at this point in time the power profile will deviate significantly from the nominal profile (explained in chapter 5). Evidently, this small core is tightly coupled. The increase in gas inlet temperature will increase the pebble temperature in the top layers, and in order to maintain an overall zero reactivity the bottom layers have to lower their temperature. As can be seen, due to the high temperature coefficient of reactivity in the bottom layer of the reflector, the decrease in temperature only has to be in the order of 30 K. Still, the outlet gas temperature becomes higher than before, and this can be explained from equation 5.1, which has been repeated here:

$$P_{\text{he}} = \alpha A (T_{\text{surf}} - T_g)$$

with  $T_{\text{surf}}$  as the pebble-bed surface temperature,  $T_g$  the gas temperature,  $A$  the heat transfer area, and  $\alpha$  the heat transfer coefficient. This steady-state equation can safely be used, as after 10 minutes the reactor core has already adapted to the new heat production/removal balance. Knowing that  $\alpha$  is hardly temperature dependent, and that the power has dropped to 80%, requires a decrease to 80% of  $(T_{\text{surf}} - T_g)$ . The decrease of  $T_{\text{surf}}$  only accounted for a decrease to 90%, so  $T_g$  still has to rise. Physically speaking, a higher transfer of heat to the helium gas results in a higher temperature difference between helium and pebble-bed with a large driving force for heat transfer. A reduced heat production will allow the helium temperature to come closer to the pebble-bed surface temperature. This phenomenon hardly mattered for the large core of chapter 5,

because the bottom layer produced little power and was nearly in thermal equilibrium with the helium flow.

## Calculation of gas outlet temperature

In order to show the maximal gas outlet temperature as a function of inlet gas temperature and mass flow rate, a number of load following transients have systematically been calculated for the fresh core. The calculations reflect the steady-state of the load following transient, that is, the stable end situation with the xenon concentration in equilibrium with the power density. In cases of load reduction, these states represent the worst-case scenario in terms of temperature and contain the maximal attainable fuel and outlet gas temperature.

For a fixed mass flow rate the gas inlet temperature has been varied (250, 500, 750 and 1000°C), yielding a power, a gas outlet temperature, and a maximal fuel temperature in the center of the hottest pebble. This has been repeated for a number of mass flow rates. The helium pressures have been scaled with the mass flow rate, with a minimum of 1.0 bar. The calculations have been performed with a conductivity for irradiated and unirradiated graphite, thus providing a conservative and a non-conservative (optimistic) limit, respectively. Figure 7.7 shows the gas outlet temperature at a certain mass flow rate as a function of the gas inlet temperature. The 'iso-power' lines show the corresponding power. Such a grid completely characterises the thermal steady-state of the reactor for any given combination of inlet conditions. The earlier prediction that a change of gas inlet temperature will hardly influence the gas outlet temperature in the stable end situation, is confirmed by the nearly horizontal iso-power lines: if a constant power is required, one can change the gas inlet temperature, but at the same time a change in mass flow rate is necessary and the gas outlet temperature more or less remains the same. If a maximum temperature of 1300 K can be allowed for short periods of time as turbine inlet temperature, it turns out that in theory with this reactor load following down to 20 MW (i.e. 50%) can be performed by adequate reduction of helium inventory and adjustment of gas inlet temperature. Utilising the bypass valve can reduce this further at the cost of loss in efficiency: from chapter 6.2.3 it follows that during a complete loss of load the core will still experience nearly a nominal cooling. A nominal gas outlet temperature will then result.

In practise, load following may be required at high efficiency over a larger range, and - more important - the higher turbine inlet temperature may not be desirable especially if frequent load reduction exercises are expected. Therefore, it seems strongly advisable to abandon the ACACIA principle of reactor operation without control rods. These control rods are present anyhow in order to assist reactor startup and shutdown so they might as well be used to compensate the lack of negative reactivity due to xenon decay at the end of the load reduction transient.

The last remark about the interpretation of figure 7.7 concerns the 2.0 MW iso-power line and the 0.25 kg/s iso-massflow line. These lines seem to be misplaced, but they reflect the fact that a maximum in the outlet temperature is reached around 0.5 kg/s. For lower mass flow rates the outlet temperature 'maps back' to lower temperature

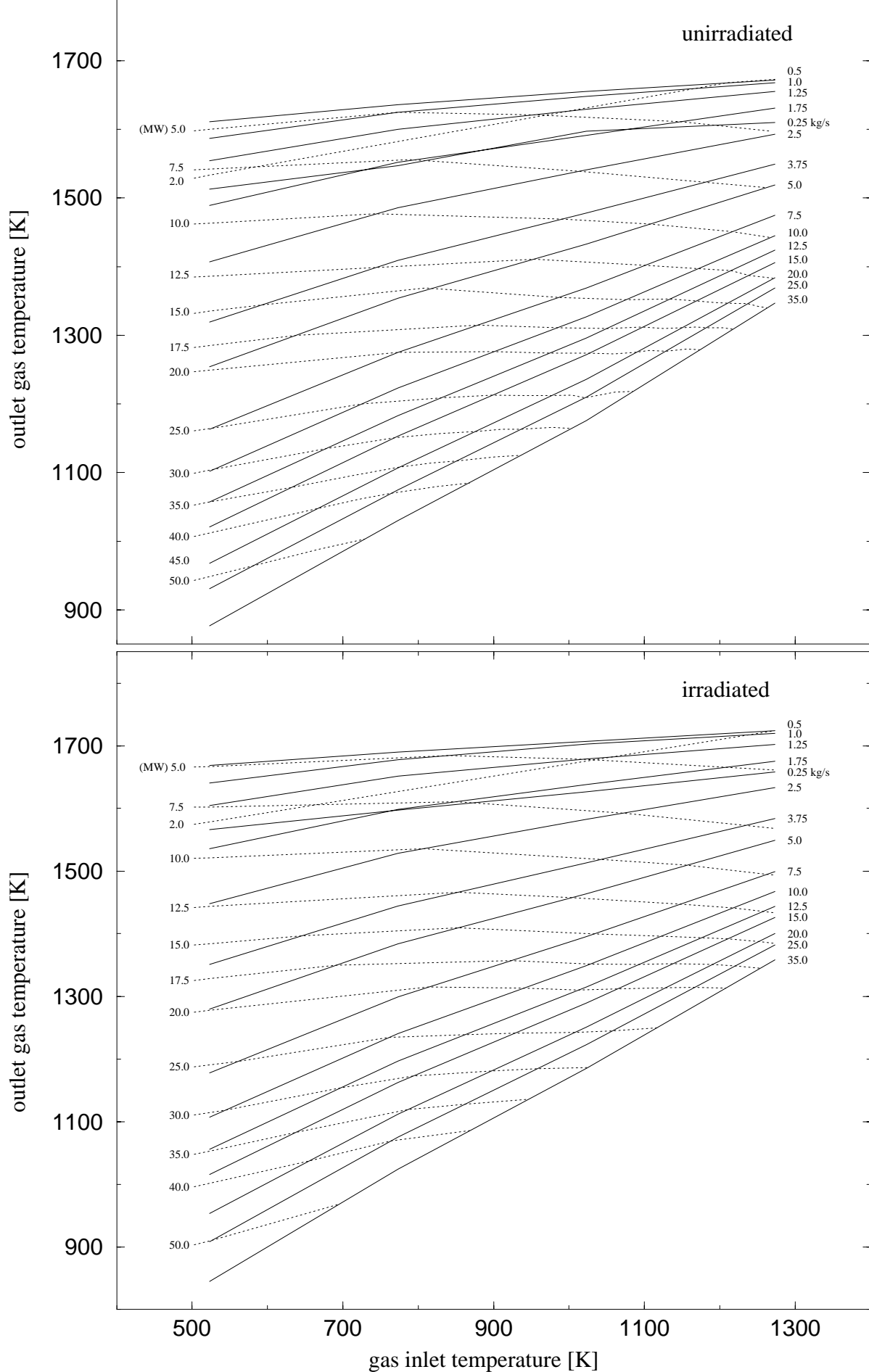


**Figure 7.7:** The reactor outlet temperature of the gas at certain mass flow rate as a function of the gas inlet temperature. The corresponding iso-power lines for these working points have also been drawn. The irradiated and unirradiated case have been depicted. The calculations reflect the stable END situation of load following transients at xenon equilibrium.

values. This behaviour can be attributed to the fact that a relatively increasing portion of heat is transported out of the core by conduction and radiation, while at the same time the heat transfer coefficient further reduces as a function of mass flow rate. The latter can be seen in figures 3.8 and 3.9.

## **7.5.2 Maximal Fuel Temperature**

### **Load following transients**

Figure 7.8 has been derived from the same calculations as for figure 7.7, but has the maximal fuel temperature as y-axis. For the startup core this maximum is normally located at the center of the bottom layer. Figure 7.8 shows that also a maximum exists in the fuel temperature which is mainly dependent on the mass flow rate. Around 0.25 kg/s the maximal fuel temperature is reached, after which the temperature drops eventually below the 1600°C (1873 K) temperature limit for very small mass flow rates (0.001 kg/s). It can be explained by looking at the temperature distribution in the core; for 0.25 kg/s the profile still resembles something like shown in figure 7.6, but for the lower mass flow rate the distribution becomes like shown in figure 5.17. In the former situation, the heat is still collected and transported towards the bottom of the core, which results in a high pebble surface temperature. In the latter case, however, there is no accumulation of heat at a certain point due to forced convection, and the heat leaks directly away into the side reflectors.

Two important conclusions can be drawn from figure 7.8: firstly, the LOCI and LOFI do not represent a situation where the maximal fuel temperature is reached, and secondly, according to this ACACIA design the reactor must be prevented from operating in the region below mass flow rates of 1.0 kg/s as the 1600°C will then be exceeded. The latter conclusion can be relaxed if one starts operating the reactor with control rods, but in that case the predicate and concept of 'inherently safe' must be abandoned. The fact that the maximal fuel temperature is not reached during a LOFI or LOCI, but during low mass flow rate transients, is not specific for this design. A calculation with the plutonium burning HTR as described in [32] revealed the same behaviour. That reactor not only utilises a different fuel, but also has different dimensions.

### **Subsequent return to nominal mass flow rate**

Even more severe restrictions must be placed on the range of load following transients if the return to nominal mass flow rate is considered.

If for some reason the nominal mass flow rate is restored, 25 kg/s, then the power will rise above nominal because of the relatively low xenon concentration. Especially for the load following cases that remained at low power for a few days, the power rise will be high, around twice the normal value, for a long (day) period of time. The situation that suddenly the nominal mass flow rate returns can arise due to a human error in the



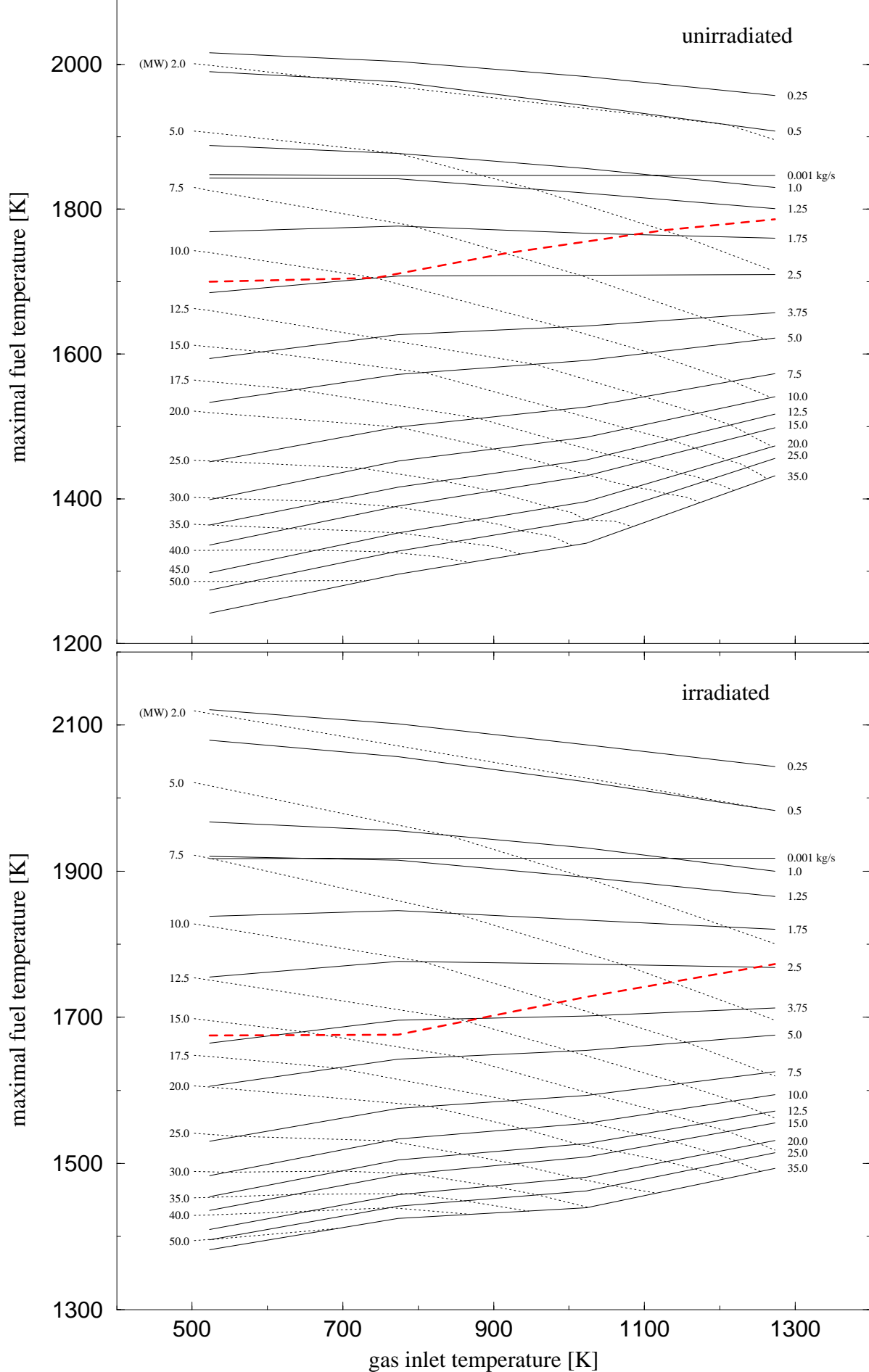


**Figure 7.8:** The maximal fuel temperature at certain mass flow rate as a function of the gas inlet temperature. The corresponding iso-power lines for these working points have also been drawn. The irradiated and unirradiated case have been depicted. The calculations reflect the stable END situation of load following transients at xenon equilibrium. The dashed red line has been explained in the text.

control room, or for instance a failure of the valve connecting the helium storage tank to the primary cycle.

The calculation of the maximal fuel temperature during the transient where the mass flow rate returns to nominal has been performed for the stand-alone reactor. This has been done in order to reduce calculation time, but in fact this type of transients demonstrates the value of a coupled reactor and energy conversion system if exact values are required. In the present study the aim is not to present exact values, but more to show that the maximal allowable fuel temperature can be exceeded. Ignoring the feedback of the energy conversion system will result in an underestimation of the fuel temperatures during the transient due to the drop in the gas outlet temperature (figure 7.6). This is the result of the relative increase in mass flow rate being relatively higher than the increase in power, and per kilogram helium less heat is absorbed (more specifically: the heat transfer coefficient does not increase proportionally to the mass flow rate, see figure 3.9). The energy conversion system reacts by offering a lower reactor inlet temperature due to the recuperative coupling of reactor in- and outlet mass flow rate. This will increase the reactor power and increase the maximal pebble center temperature. Therefore, if it is required to use the correct inlet temperature the energy conversion system should be involved in the calculations.

The return to nominal cooling will for some steady final states result in fuel temperatures over  $1600^{\circ}\text{C}$ . In figure 7.8 the red line denotes this boundary. If a return to nominal mass flow rate is made from the region above the line, then the fuel temperature exceeds  $1600^{\circ}\text{C}$  in the subsequent transient.

The conclusion can be again that for a certain part of the operational region of the ACACIA control rods are needed to support load following transients. A better solution might be to reconsider the design and to re-develop a reactor with less high power densities at places where the surface temperature is already high. This will limit the xenon reactivity worth. Burnable poison could be considered in such places or simply enlargement of the pebble-bed. If with such measures it can be guaranteed that the maximal permissible temperature is never exceeded, then the reactor can again be called inherently safe.

## 7.6 Conclusions

This chapter treated safety related transients. It has been shown that previous ACACIA safety analyses are in error due to an erroneous assessment of the fuel temperature in the pebble. As an example a transient with cold helium ingress in the core has been discussed that clearly shows the importance of determining the correct fuel temperature. In conjunction with this discussion the importance of graphite conductivity has been demonstrated; the conductivity of irradiated graphite is lower and yields higher fuel temperatures than the conductivity of unirradiated graphite. For a fresh core it remains uncertain at which point the switch has to be made from unirradiated to irradiated fuel. Immediately after startup the conductivity quickly deteriorates and after two weeks the value for irradiated graphite should be used. To be on the safe side during this period, one should use the irradiated value.

A LOFI and LOCI transient have been calculated for the fresh core (5 days old), and when utilising the conductivity for the irradiated graphite (conservative), the LOCI yields a maximal temperature of 1600°C and the LOFI 1627°C. This is in sharp contrast with the fair margin of around 100°C predicted by earlier calculations, and is the result of the fuel temperature correction.

In order to investigate the maximal temperature for fuel and outlet gas during operational transients, the steady final states of load following transients have been calculated for a comprehensive grid of inlet conditions. These final states represent the worst-case state in terms of maximal temperature as the fuel temperature will be maximal in order to compensate the reduction of the negative xenon reactivity by decay. Three conclusions can be drawn from these calculations:

1. the gas outlet temperature of the reactor (= turbine inlet temperature) exceeds 900°C for load reduction transients below 50%. Control rods are necessary to bring down the temperature.
2. the fuel temperature can exceed 1600°C for load reduction transients below 20%-10% of nominal power.
3. the maximum gas outlet and fuel temperatures are not reached during a LOFI or LOCI with a halted mass flow rate, but for situations with a small mass flow rate, 1-0.5%. *As such, a LOFI or LOCI does not represent the worst-case scenario in terms of maximal fuel temperature.*

As a continuation of the load following transient, the return to a nominal cooling of 25 kg/s has been calculated. Especially for the load reduction transients to low load (< 40%) this can result in fuel temperatures above 1600°C. The xenon concentration is low and the fuel temperature has to rise in order to balance the sudden increase in reactivity due to increased cooling.

Summarising, the current ACACIA design requires adaptations in order to be called 'inherently safe'. The retention of fission products is not guaranteed during all possible transients. The following section with recommendations gives some possible solutions in order to improve the design.

## 7.7 Recommendations

In order to improve the calculations and design of the ACACIA reactor the following recommendations are given:

- Instead of correcting the fuel temperature of the pebble within Panther, one could also consider to tabulate the nuclear cross sectional data against the pebble surface temperature (currently) and the power density (improvement). However, that is no real calculational advantage over the current situation, so for the time being it is advised to keep the temperature correction in Panther.
- In order to reduce the maximal fuel temperature, especially during transients, a decrease in power density is necessary. This can be achieved in a general way by enlargement of the core volume while keeping the same power production. One could think about mixing fuel pebbles with 'dummy' pebbles consisting solely of

graphite. However, knowing that the maximal power density occurs in the bottom layer of a fresh core, more specific measures can be taken. For instance, the lower part of the reactor core can be filled with lower enriched fuel pebbles (currently 10% enrichment), or mixed with pure graphite pebbles. Another possible action is to add burnable poison to the pebbles in the bottom layer, or to add burnable poison to the bottom reflector. The advantage of burnable poison over lower enrichment is that its effect is maximal during the beginning of the pebble-bed life and diminishes towards the end of life. This is desirable because at the end of life the bottom layers of the pebble-bed become depleted of fuel.

- If load following transients are expected to occur often, the usage of control rods is advised. The reactor has first to be redesigned along the lines of the previous recommendation such that control rods are not necessary for the nuclear safety (retention of fission products) of the reactor. The next step is then to add control rods in order to temper the gas outlet temperature of the reactor in order to protect the gas turbine. The best situation would be never to exceed the nominal value of the reactor gas outlet temperature, which would give the turbine its (longest) design lifetime. If for some reason control rods are not desirable, the problem can to some extent be circumvented by designing a helium storage system that can only store 40% of the helium inventory. In that case - if the inlet gas temperature of the reactor remains more or less constant - the temperature will be 100 K higher than nominal. The remaining load following range from 60%-5% can be covered by utilising the bypass valve.

# Chapter 8

---

## Conclusions & Discussion

---

This thesis presents a transient analysis of the pebble-bed High Temperature Reactor (HTR) coupled to its Energy Conversion System (ECS) for the Dutch ACACIA-project (AdvanCed Atomic Cogenerator for Industrial Applications). In order to perform the analysis, a code system has been developed that couples a HTR core code to a thermal hydraulic code for the ECS. This coupling has been developed in order to come to a more detailed and realistic simulation of the entire system. It renders the assumptions superfluous that otherwise have to be made concerning the time evolvement of the boundary conditions of the two separate systems.

The transient analysis for the ACACIA system has been performed by two studies, of which one is presented in this thesis, and the other in the thesis of Kikstra [48]. This thesis focuses on the HTR reactor modelling, and assumes less detail for the ECS model; the other focuses on the ECS modelling and assumes an uncomplicated reactor model. The models have been developed with entirely different codes, and can therefore be used for verifying each other.

### 8.1 Conclusions

#### Reactor model

A reactor model in general consists of two sides: one for the neutronics, one for the thermal hydraulics of the core. For the neutronics part of the core a 3-dimensional model in Panther and a point kinetic model in Relap5 have been built, for the thermal hydraulics part of the core a 2-dimensional model in Thermix-Direkt and a 1-dimensional model in Relap5. Combinations of these different parts made it possible to assess what detail is required for the reactor calculations, and what gain in calculation time can be achieved.

It has been proved that the neutronics calculations can greatly be reduced in complexity - without compromising accuracy - by using the point kinetic reactor model. This is the result of the long fission chain range in a graphite moderated reactor. In the case of the

ACACIA reactor the fission chain length is twice as long as the physical dimensions of the ACACIA core. Reactivity changes in one part of the core certainly are felt in all other parts. Although the point reactor model still needs a more-dimensional, detailed code to derive its parameters from, it is important to notice that this not necessarily has to be a code such as Panther with capability to calculate transients. A steady-state code would also meet the requirements, and is in general less complex.

It turns out that it is more important to provide a detailed thermal hydraulic description of the pebble-bed, such as is available in Thermix-Direkt. In order to describe for instance conduction properly during transients, a 2-dimensional code is a requirement. The fact that the 1-dimensional model still gave reasonable results, is because it had been tuned in steady-state to the 2-dimensional model.

## **Energy Conversion System model**

The modelling of the ECS has been performed with the Relap5 code that has been developed and validated for steam-cycle applications. The Brayton cycle, however, requires an extra component in the form of a gas compressor. A new subroutine has been written that replaces the pump model of the steam cycle with a gas compressor. This model functions satisfactorily. The available steam turbine model has been utilised for the gas turbine model, but it is advised to replace it in the future with a better model; it is suitable for conceptual studies, but a licensing authority would probably advise against it. With the help of the detailed model of Kikstra [48] the characteristics of the gas turbine have nevertheless satisfactorily been modelled. All other components also have been compared to the detailed model of Kikstra; the (small) differences all could be explained and were considered to be acceptable for a conceptual study.

The control system for the ECS has been kept straightforward, and focuses on keeping the shaft rotational speeds within bounds. Furthermore, the control system optimises the efficiency of the power production by matching the helium inventory in the cycle to the power demand. If less power is needed, helium is extracted from the cycle and temporarily stored in tanks. An analytic model has been derived for this helium storage tank system in order to determine the optimum in number of tanks and their sizes.

## **Transient analysis**

For the total ACACIA model the representative transients have been shown. The results have been compared to the total ACACIA model of Kikstra, and it has been concluded that the agreement is good. The agreement tends to become less for far off-design conditions, where the Relap5 gas turbine model becomes less accurate.

Stand-alone reactor calculations have been performed in order to consider the inherent safety aspect of the ACACIA reactor in more detail. This implies reactor operation without control rods. It has been shown that previous ACACIA safety analyses are in error due to an erroneous assessment of the fuel temperature in the pebble. Corrections are discussed and implemented, and a grid has been constructed in which all possible

worst-case reactor states are depicted in terms of maximal fuel temperature as a function of helium mass flow rate, inlet temperature and thermal power. A similar grid has been constructed in terms of reactor outlet gas temperature as a function of the same parameters. It turned out that for the present design the fuel temperatures can exceed the 1600°C by more than 200°C at low mass flow rates. With the reactor operating at partial load, the xenon concentration reduces in time which means that - if no control rods are used - the reduction in negative reactivity has to be compensated by rising fuel temperatures. Furthermore, the reactor outlet gas temperature can reach such high temperatures that the gas turbine lifetime shortens dramatically.

Most strikingly probably is the conclusion that the highest fuel temperatures are not experienced during a total loss of active coolant flow, but for transients with a small (1%) sustained mass flow rate. In that case the produced heat is still collected and transported towards the bottom of the core, which results in a high pebble surface temperature. In contrast, during loss of flow, there is no accumulation of heat at a certain point due to forced convection, and heat leaks away into the reflectors evenly distributed.

## **8.2 Discussion**

### **Adaptations in ACACIA design**

The safety study in chapter 7 of this thesis clearly demonstrated that the current design of the ACACIA reactor can lead to temperatures over 1600°C. This situation arises due to the unadvantageous combination of a maximal helium temperature and a maximal power density in the bottom layer of the startup core. The maximal helium temperature is a matter of course at that spot, but the power density distribution can be influenced in order not to coincide. For a peu-à-peu filling scheme, the bottom reflector zone can for instance contain burnable poison, or the first few layers contain pebbles with less fuel. Mixing fuel pebbles with pure graphite pebbles in order to 'dilute' the fuel in the bottom region may also help. These topics promise interesting research for the future.

### **Control rods**

The original idea of not using control rods during operation is not feasible. During partial load operation of the reactor the fuel and outlet gas temperature rise can be large due to the reduction in xenon concentration. Control rods can compensate the according reduction in negative reactivity, and limit these temperatures. At all times, however, the control rods will only serve to protect the ECS system against too high temperatures, not to guarantee nuclear safety. The nuclear inherent safety must be ascertained by the reactor design.

## **Helium inventory control system**

The helium inventory control system regulates the amount of helium circulating in the energy conversion system. In theory, all helium could be stored in storage tanks without utilising active components such as auxiliary pumps. In practice, however, this would require large volumes as storage space. Moreover, only a few tanks (for the reduction of 100% to 50% inventory) would store a substantial amount of helium, while the remaining would successively contain less helium in the same volume. Therefore, it seems advisable to provide helium storage tanks to passively store helium down to 50% inventory, and install pumps for further active storage in the same tanks.

## **Turbine model**

The turbine model in Relap5 needs to be reconsidered. In the first place the model is too straightforward in trying to describe the two dimensional flow processes in a one dimensional fashion. A new, more detailed expression for the efficiency must be used. In the second place the way of implementation of the turbine model into the basic equations of Relap5 is unclear. The calculated efficiency is utilised to determine the torque transferred to the shaft, and the pressure drop over the turbine. The helium outlet temperature, however, does not exactly match the theoretical value. The differences are small, typically less than 10 degrees on a total of 300 degrees, and the model is certainly suited for conceptual studies.

## **Code system**

All communication between the different codes currently utilises the configuration of the most detailed model for the ACACIA, viz. Panthermix-Talink-Relap5. Firstly, the coupling of Panther(mix)-Talink can be improved by communicating on socket level, instead of constantly checking for certain files that indicate completion of a time step. Secondly, it has been proved in this thesis that instead of Panthermix/Relap5 also a code system of point kinetics with Thermix and Relap5 would suffice to calculate transients. In that case, the Talink connection can be replaced by a direct link between Thermix and Relap5, using the point kinetic model in Relap5 for the neutronics, Thermix for the core thermal hydraulics and Relap5 for the thermal hydraulics of the energy conversion system.



# Bibliography

- [1] F. Daniels. Suggestions for a High Temperature Pebble Pile. Technical Report MUC-FD-8, Oak Ridge National Lab., 1944.
- [2] H. Nabielek, *et al.* *Fuel for Pebble-Bed HTRs*. *Nucl. Eng. & Design*, 78:155–166, 1984.
- [3] H. Nabielek, *et al.* *Development of Advanced HTR Fuel Elements*. *Nucl. Eng. & Design*, 121:199–211, 1990.
- [4] H. Barnert *et al.* *The HTR and Nuclear Process Heat Applications*. *Nucl. Eng. & Design*, 78:91–98, 1984.
- [5] W. Jäger *et al.* *Nuclear Process Heat Applications for the Modular HTR*. *Nucl. Eng. & Design*, 78:137–145, 1984.
- [6] MGCR Staff. Evaluation of Coolants and Moderators for the Maritime Gas-Cooled Reactor. Technical Report GA-570, GA&EB, General Dynamics, 1958.
- [7] P. Fortescue, *et al.* *HTGR - Underlying Principles and Design*. *Nucleonics*, 18(1):86, 1960.
- [8] J.L. Everett III and E.J. Kohler. *Peach Bottom Unit No.1: A High Performance Helium Cooled Nuclear Power Plant*. *Annals of Nuclear Energy*, 5:321–335, 1978.
- [9] *DRAGON, details of the 10 MW HTGR*. *Nuclear Power*, April:102–103, 1959.
- [10] H.W. Schmidt. *Der 10-MW-Hochtemperaturreaktor Dragon*. *Die Atomwirtschaft*, Mai:211–215, 1959.
- [11] C.A. Rennie. *Achievements of the Dragon Project*. *Annals of Nuclear Energy*, 5:305–320, 1978.
- [12] H.G. Olson, H.L. Brey *et al.* *The Fort St. Vrain High Temperature Gas-Cooled Reactor I-VII, IX-XIII*. *Nucl. Eng. & Design*, pages 53:117–140, 61:295–329, 72:111–152, 76:71–77, 1979, 1980, 1982, respectively.
- [13] H.L. Brey. *Fort St. Vrain Operation and Future*. *Energy*, 16(1/2):47–58, 1991.
- [14] S. Saito, *et al.* *Present Status of the High Temperature Engineering Test Reactor (HTTR)*. *Nucl. Eng. & Design*, 132:85–93, 1991.
- [15] K. Yamashita *et al.* *Nuclear Design of the High-Temperature Engineering Test Reactor (HTTR)*. *Nucl. Sc. and Eng.*, 122:212–228, 1996.
- [16] A.I. Kiryushin *et al.* *Project of the GT-MHR High-Temperature Helium Reactor with Gas Turbine*. *Nucl. Eng. & Design*, 173:119–129, 1997.
- [17] F.A. Silady and A.C. Millunzi. *Safety Aspects of the Modular High Temperature Gas-Cooled Reactor*. *Nuclear Safety*, 31(2):215–225, April-June 1990.
- [18] P.G. Kroeger. *Safety Evaluations of Accident Scenarios in High Temperature Gas-Cooled Reactors*. *Nucl. Eng. & Design*, 122:443–452, 1990.

- [19] E. Ziermann. *The AVR Nuclear Power Facility - Progress Report*. Nucl. Eng. & Design, 78:99–108, 1984.
- [20] K. Krüger, G. Ivens and N. Kirch. *Operational Experience and Safety Experiments with the AVR Power Station*. Nucl. Eng. & Design, 109:233–238, 1988.
- [21] H. Harder *et al.* *Das 300-MW-Thorium-Hochtemperaturkernkraftwerk (THTR)*. Die Atomwirtschaft, Mai:238–245, 1971.
- [22] E. Baust. *Inbetriebnahme des THTR-300*. Die Atomwirtschaft, Aug/Sept:422–427, 1985.
- [23] R. Baumer and I. Kalinowski. *THTR Commissioning and Operating Experience*. Energy, 16(1/2):59–70, 1991.
- [24] X. Yuanhui and S. Yuliang. *Nuclear Heats up in China*. Nuclear Engineering International, November:45–46, 1995.
- [25] *Various Contributions*. In *IAEA TCM on Safety Related Design and Economic Aspects of High Temperature Gas-cooled Reactors*, number IAEA-TECDOC-?, (not published yet), Beijing, China, 2-4 Nov 1998.
- [26] Yuanhui Xu and Yuliang Sun. *Der gasgekühlte 10-MW-Hochtemperaturreaktor in Peking*. VGB KraftwerksTechnik, November:19–23, 1999.
- [27] D.R. Nicholls. *The Pebble-Bed Modular Reactor*. Nuclear Engineer, 38(4):105–107, 1997.
- [28] D.R. Nicholls. *Eskom Sees a Nuclear Future in the Pebble-Bed*. Nuclear Engineering International, December:12–16, 1998.
- [29] *Eskom Takes a Cool Look at High Temperature Reactors*. Modern Power Systems, October:35–37, 1998.
- [30] A.I. van Heek (editor). *INherently safe nuclear COGENeration (INCOGEN) Pre-Feasibility Study*. Technical report, Netherlands Energy Research Foundation (ECN), Petten, The Netherlands, 1997.
- [31] J.F. Kikstra. *Conceptual Design for the Energy Conversion System of the ACA-CIA Nuclear Cogeneration Plant*. Technical Report ECN-I-98-042, Netherlands Energy Research Foundation (ECN), Petten, The Netherlands, 1998.
- [32] E.E. Bende. *Plutonium Burning in a Pebble-Bed Type High Temperature Nuclear Reactor*. Delft University of Technology, Delft (NL), 1999. Ph.D. thesis commissioned by NRG, Petten (NL).
- [33] H. Reutler and G.H. Lohnert. *Advantages of Going Modular in HTRs*. Nucl. Eng. & Design, 78:129–136, 1984.
- [34] G.H. Lohnert. *Technical Design Features and Essential Safety-Related Properties of the HTR-Module*. Nucl. Eng. & Design, 121:259–275, 1990.
- [35] E. Teuchert, *et al.* *Basisstudie zum Kugelhaufenreaktor in OTTO-Beschickung*. Technical Report JÜL-858-RG, FZ Jülich, Jülich (D), 1972.
- [36] U. Hansen, R. Schulten, E. Teuchert. *Physical Properties of the 'Once Through Then Out' Pebble-Bed Reactor*. Nucl. Sc. and Eng., (47):132–139, 1972.
- [37] V. Maly, R. Schulten, E. Teuchert. *500 MWth-Kugelhaufenreaktor für Prozesswärme in Einwegbeschickung*. Atomwirtschaft, April:216–220, 1972.

- [38] E.Teuchert *et al.* *Simplification of the Pebble-bed High Temperature Reactor.* In *International Specialists' Meeting on Potential of Small Nuclear Reactors for Future Clean and Safe Energy Sources*, Tokyo, Oct 23-25 1991.
- [39] E.Teuchert *et al.* *Features of passive control of a small pebble bed HTR for gas turbine cycle.* In *8<sup>th</sup> Proc. Thermal Hydraulics Division of the ANS*, Nov 1992.
- [40] E.Teuchert *et al.* *Strikte Ausnutzung der Eigenschaften des Kugelhaufen-Hochtemperaturreaktors.* In *Monographien des Forschungszentrums Jülich "Fortschritte in der Energietechnik"*, herausgegeben von K. Kugeler, H. Neis, G. Ballensiefen, Band 8, 1993.
- [41] E.Teuchert *et al.* *Features of Safety and Simplicity of Advanced Pebble-bed HTRs.* In *Proceedings of IAEA TCM on Development Status of Modular High Temperature Reactors and their Future Role*, ECN Petten, Nov 28-30 1994.
- [42] X.L. Yan, L.M. Lidsky. *Conceptual Design of the HTR Gas Turbine Cogeneration Plant.* Technical Report LPI-HTR-11019501, LPI, Cambridge USA, 1996.
- [43] G. van Wylen, R. Sonntag and C. Borgnakke. *Fundamentals of Classical Thermodynamics.* John Wiley & Sons, New York, 1994.
- [44] E.S.C. Smith *et al.* *Applied Atomic Power*, 1947.
- [45] F. Daniels. *Small Gas-Cycle Reactor Offers Economic Promise.* *Nucleonics*, 14(3):34–41, 1956.
- [46] K. Bammert. *Dynamic Behavior and Control of Single-Shaft Closed-Cycle Gas Turbines.* *ASME paper*, (71-GT-16), 1971. also in *Journal of Engineering for Power*, Vol. 93, pp447-453, October 1971.
- [47] E.C. Verkerk. *Helium Storage and Control System for the PBMR.* In *IAEA TCM on HTGR Technology Development*, number IAEA-TECDOC-988, pages 195–203, Johannesburg, Nov 1996.
- [48] J.F. Kikstra. *Modelling, Design and Control of a Cogenerating Nuclear Gas Turbine Plant.* Delft University of Technology, Delft (NL), 2001 (*to be published*). Ph.D. thesis commissioned by NRG, Petten (NL).
- [49] Various contributors. *Advances in Coupled Thermal-Hydraulic and Neutronic Codes.* In *Transactions of the ANS*, volume 80, pages 239–251, 1999.
- [50] J.F. Kikstra and A.H.M. Verkooijen. *Dynamic Modeling of A Closed Cycle Gas Turbine CHP Plant With A Nuclear Heat Source.* *ASME paper*, (99-GT-5), 1999.
- [51] *Aspen Custom Modeler.* Cambridge MA, USA, 1999.
- [52] P.K. Hutt *et al.* *The UK core performance code package.* *Nucl. Energy*, 30(5):291–298, 1991.
- [53] J.S. Story *et al.* *Evaluation, Storage and Processing of Nuclear Data for Reactor Calculations.* In *3<sup>rd</sup> Geneva Conference on Peaceful Uses of Atomic Energy*, page 168, 1964.
- [54] M.J. Marshall, C.J. Taubman. *The '1986' Wims Nuclear Data Library.* Technical Report AEEW-R2133, AEA, Winfrith (UK), 1986.
- [55] R.J.J. Stamm'ler and M.J. Abbate. *Methods of Steady-State Reactor Physics in Nuclear Design.* Academic Press, 1983.

- [56] M.J. Roth. The Wims-E Module WHEAD. Technical Report AEEW-R921, AEA, Winfrith (UK), 1980.
- [57] E.C. Verkerk. *Resonance treatment with the Subgroup Method in Wims7*. Technical Report ECN-I-98-061, Netherlands Energy Research Foundation (ECN), Petten, The Netherlands, 1998.
- [58] A. Hogenbirk *et al.* HTR-PROTEUS Benchmark Calculations. Part 1: Unit cell results LEUPRO-1 and LEUPRO-2. Technical Report ECN-C-95-087, Netherlands Energy Research Foundation (ECN), Petten, The Netherlands, 1995.
- [59] H.Th.Klippel (editor). Reactor Physics Calculations of HTR-Type Configurations. In *ECN workshop on the role of modular HTRs in the Netherlands*, number ECN-R-95-027, Petten, The Netherlands, Nov 1994.
- [60] G.R. Keepin. *Physics of Nuclear Kinetics*. Addison-Wesley Publishing Company, Inc, 1965.
- [61] J. Martindill, L. Hutton (AEA Technology). *Private communications*. March, 1999.
- [62] G.I. Bell and S. Glasstone. *Nuclear Reactor Theory*. Van Nostrand Reinhold Company, New York, 1970.
- [63] J.J. Duderstadt and L.J. Hamilton. *Nuclear Reactor Analysis*. John Wiley & Sons, 1976.
- [64] H. Gerwin and W. Scherer. *Treatment of the Upper Cavity in a Pebble-Bed High Temperature Gas-Cooled Reactor by Diffusion Theory*. *Nucl. Sc. and Eng.*, 97:9–19, 1987.
- [65] J. Banaschek. *Berechnungsmethoden und Analysen zum Dynamischen Verhalten von Kraftwerksanlagen mit Hochtemperaturreaktor*. Forschungszentrum Jülich, JÜL-1841, Jülich (D), 1983. Ph.D. thesis.
- [66] S. Struth. *Thermix-Direkt: Ein Rechenprogramm zur instationären, zweidimensionalen Simulation thermohydraulischer Transienten*. FZ Jülich (D), 1995. manual.
- [67] K. Holzkamp. *Thermohydraulische Untersuchungen zum Primärkreis des HTR's für die Nachwärmeabfuhr mit Naturumlauf am Beispiel des HTR-500*. Forschungszentrum Jülich, JÜL-2187, Jülich (D), 1988. Ph.D. thesis.
- [68] K. Petersen. *Zur Sicherheitskonzeption des Hochtemperaturreaktors mit natürlicher Wärmeableitung aus dem Kern im Störfall*. Forschungszentrum Jülich, JÜL-1872, Jülich (D), 1983. Ph.D. thesis.
- [69] K. Verfondern. Experimentelle Überprüfung des Thermohydraulikprogramms THERMIX und rechnerische Analyse der transienten Temperatur- und Strömungsfelder im Core-Bereich des THTR-Reaktors nach Ausfall der Nachwärme Abfuhr. Technical Report FFA-IRE-IB-13/78, Diplom-Arbeit, FZ Jülich, Jülich (D), 1978.
- [70] M. Schürerkrämer. *Theoretische und experimentelle Untersuchungen der Naturkonvektion im Kern des Kugelhaufen-Hochtemperaturreaktors*. Forschungszentrum Jülich, JÜL-1912, Jülich (D), April 1984. Ph.D. thesis.
- [71] J.Oppe, J.B.M. de Haas and J.C. Kuijper. Panthermix (Panther-Thermix) User Manual. Technical Report ECN-I-98-019, Netherlands Energy Research Foundation (ECN), Petten, The Netherlands, 1998.

- [72] J.Oppe, J.B.M. de Haas and J.C. Kuijper. Panthermix. A Panther-Thermix interaction. Technical Report ECN-I-96-022, Netherlands Energy Research Foundation (ECN), Petten, The Netherlands, 1996.
- [73] The Relap5 Code Development Team. Relap5mod3 Code Manual, Vol I, II, III and IV. Technical Report NUREG/CR-5535, INEL-95/0174, INEL, Idaho, 1995. Also available on [www.nrc.gov/RES/RELAP5/index.html](http://www.nrc.gov/RES/RELAP5/index.html).
- [74] C.D. Fletcher, R.R. Schultz. Relap5mod3 Code Manual, Vol V: User's Guidelines. Technical Report NUREG/CR-5535, INEL-95/0174, INEL, Idaho, 1995. Also available on [www.nrc.gov/RES/RELAP5/index.html](http://www.nrc.gov/RES/RELAP5/index.html).
- [75] R.Page and J.R. Jones. *Development of an Integrated Thermal-Hydraulics Capability Incorporating Relap5 and Panther Neutronics Code*. In *OECD/CSNI Workshop on Transient Thermal-Hydraulic and Neutronic Codes Requirements*, number NUREG/CP-0159, pages 389–394. The American Nuclear Society Inc., La Grange Park, Illinois 60526, USA., Oct 1998.
- [76] F. Kreith and M.S. Bohn. *Principles of Heat Transfer*. Harper and Row, 4<sup>th</sup> edition, 1986.
- [77] P. Zehner und E.U. Schlünder. *Einfluss der Wärmestrahlung und des Druckes auf den Wärmetransport in nicht durchströmten Schüttungen*. *Chemie-Ing.-Techn.*, 44(23):1303–1308, 1972.
- [78] H. Barthels, M. Schürenkrämer. Die effektive Wärmeleitfähigkeit in Kugelschüttungen unter besonderer Berücksichtigung des Hochtemperatur-Reaktors. Technical Report JÜL-1893, FZ Jülich, Jülich (D), 1984.
- [79] K.Kugeler and R.Schulten. *Hochtemperaturreaktortechnik*. Springer-Verlag, 1989.
- [80] Berechnung der Nachzerfallsleistung der Kernbrennstoffe von Hochtemperaturreaktoren mit Kugelförmigen Brennelementen. Technical Report DIN 25485, May 1990.
- [81] W.C. Reynolds. *Thermodynamic Properties in SI*. Stanford University, 1979.
- [82] The Relap5 Code Development Team. Relap5mod3 Code Manual, Vol I. Technical Report NUREG/CR-5535, INEL-95/0174, INEL, Idaho, 1995. Also available on [www.nrc.gov/RES/RELAP5/index.html](http://www.nrc.gov/RES/RELAP5/index.html).
- [83] J.K. Salisbury. *Steam Turbines and Their Cycles*. Kreiger, New York, 1995.
- [84] M.V Casey and F. Marty. *Centrifugal Compressors - Performance at Design and Off-Design*. In *The Proceedings of the Institute of Refrigeration*, volume 82, pages 71–82, Surrey (UK), 1986.
- [85] V.H. Ransom and J.A. Trapp. *The Relap5 choked Flow Model and Application to a Large Scale Flow Test*. In *Proceedings of the ANS/ASME/NRC International Topical Meeting on Nuclear Reactor Thermal-Hydraulics*, pages 799–819, Saratoga Springs, New York, October 5-8 1980.
- [86] J.A. Trapp and V.H. Ransom. *A Choked-Flow Calculation Criterion for Nonhomogeneous, Nonequilibrium Two-Phase Flows*. *International Journal of Multiphase Flow*, 8(6):669–681, 1982.
- [87] H. van Dam. *Role of Neutron Sources, Xenon, and Decay Heat Dynamics in Autonomous Reactor Shutdown and Recriticality*. *Nucl. Sc. and Eng.*, 129:273–282, 1998.

- [88] H. van Dam. *Dynamics of Passive Reactor Shutdown*. *Progress in Nuclear Energy*, 30(3):255–264, 1996.
- [89] J. Keijzer. *Investigations of Spatial Effects in Nuclear Reactor Kinetics*. Delft University of Technology, IRI, Delft (NL), 1996. Ph.D. thesis.
- [90] D. Randall and D.S. St. John. *Xenon Spatial Oscillations*. *Nucleonics*, 16(3):82–86, 1958. also in *Nucl. Sci. and Eng.*, 14, pp204–206, 1962.
- [91] A.F. Henry. *Oscillations in the Power Distribution within a Reactor*. *Nucl. Sc. and Eng.*, 2:469–480, 1957.
- [92] J.B. Yasinsky and A.F. Henry. *Some Numerical Experiments Concerning Space-Time Reactor Kinetics Behavior*. *Nucl. Sc. and Eng.*, 22:171–181, 1965.
- [93] Siemens-Interatom. *Hochtemperaturreaktor-Modul-Kraftwerksanlage, Sicherheitsbericht*. (Confidential), 1988.
- [94] G.H. Lohnert, et al. *The Fuel Element of the HTR-Module, a Prerequisite of an Inherently Safe Reactor*. *Nucl. Eng. & Design*, 109:257–263, 1988.
- [95] T.D. Gulden and H. Nickel. *Coated Particle Fuel*. *Nuclear Technology*, 35:206–213, 1977. The total September issue is devoted to coated particle fuels.
- [96] K. Verfunderen, W. Schenk and H. Nabielek. *Passive Safety Characteristics of Fuel for a Modular High-Temperature Reactor and Fuel Performance Modeling under Accident Conditions*. *Nuclear Technology*, 91:235–246, 1990.
- [97] J.C. Kuijper et al. *Reactor Physics Calculations on the Dutch Small HTR Concept*. In *IAEA TCM on HTGR Technology Development*, number IAEA-TECDOC-988, Johannesburg, Nov 1996. (Also published as Technical Report ECN-RX-97-020, ECN, the Netherlands).
- [98] R.E. Schulze, H.A. Schulze, W. Rind. *Graphitic Matrix Materials for Spherical HTR Fuel Elements*. Technical Report JÜL-Spez.-167, FZ Jülich, Jülich, (D), 1982.
- [99] Ja. Iyoku et al. *Radiation Behaviour of Graphite for HTGR*. In *IAEA Specialist Meeting on Graphit Moderator Lifecycle Behaviour*, number IAEA-TECDOC-901, pages 251–262, Bath (UK), September 1997.
- [100] H.-D. Heckhoff. *Untersuchung von Betriebsstörungen ohne Reaktorschnellabschaltung (ATWS) beim Hochtemperaturreaktor*. Forschungszentrum Jülich, JÜL-1743, Jülich (D), 1981. Ph.D. thesis.
- [101] W.M. Kays and A.L. London. *Compact Heat Exchangers*. USA, 1985.

# Appendix A

---

## Xenon Equations

---

The xenon equations were defined in section 3.4.5 as:

$$\begin{aligned}\frac{\partial I(r, t)}{\partial t} &= \gamma_I(r) \Sigma_f(r) \Phi(r, t) - \lambda_I I(r, t) \\ \frac{\partial X(r, t)}{\partial t} &= \gamma_X(r) \Sigma_f(r) \Phi(r, t) + \lambda_I I(r, t) - \lambda_X X(r, t) - \\ &\quad \sigma_a^X(r) \Phi(r, t) X(r, t)\end{aligned}\tag{A.1}$$

In the point reactor kinetic model the mono-energetic flux has been defined in section 3.4.2 as:

$$\Phi(r, t) = P_p(t) \psi(r, t) \equiv P_p(t) \psi(r)\tag{A.2}$$

Inserting this in the equations (A.1) gives:

$$\begin{aligned}\frac{\partial I(r, t)}{\partial t} &= \gamma_I(r) \Sigma_f(r) P_p(t) \psi(r) - \lambda_I I(r, t) \\ \frac{\partial X(r, t)}{\partial t} &= \gamma_X(r) \Sigma_f(r) P_p(t) \psi(r) + \lambda_I I(r, t) - \lambda_X X(r, t) - \\ &\quad \sigma_a^X(r) P_p(t) \psi(r) X(r, t)\end{aligned}\tag{A.3}$$

Integrating equations (A.3) over the core volume  $V_c$  and dividing by  $V_c$  in order to obtain a space average for the core gives:

$$\begin{aligned}\frac{1}{V_c} \int dV_c \frac{\partial I(r, t)}{\partial t} &= \bar{\gamma}_I \frac{P_p(t)}{\epsilon_f V_c} \int dV_c \epsilon_f(r) \Sigma_f(r) \psi(r) - \frac{\lambda_I}{V_c} \int dV_c I(r, t) \\ \frac{1}{V_c} \int dV_c \frac{\partial X(r, t)}{\partial t} &= \bar{\gamma}_X \frac{P_p(t)}{\epsilon_f V_c} \int dV_c \epsilon_f(r) \Sigma_f(r) \psi(r) + \frac{\lambda_I}{V_c} \int dV_c I(r, t) - \\ &\quad \frac{\lambda_X}{V_c} \int dV_c X(r, t) - \Upsilon P_p(t) \frac{1}{V_c} \int dV_c X(r, t),\end{aligned}\tag{A.4}$$

Define the volume averages as:

$$\begin{aligned}
I(t) &= \frac{1}{V_c} \int dV_c I(r, t) \\
X(t) &= \frac{1}{V_c} \int dV_c X(r, t) \\
\bar{\gamma}_I &= \frac{\int dV_c \gamma_I(r) \Sigma_f(r) \psi(r)}{\int dV_c \Sigma_f(r) \psi(r)} \\
\bar{\gamma}_X &= \frac{\int dV_c \gamma_X(r) \Sigma_f(r) \psi(r)}{\int dV_c \Sigma_f(r) \psi(r)} \\
\Upsilon &= \frac{\overline{\sigma_a^X \psi}}{\overline{X}} = \frac{\int dV_c \sigma_a^X(r) \psi(r) X(r, t)}{\int dV_c X(r, t)} \\
\epsilon_f &= \frac{\int dV_c \epsilon_f(r) \Sigma_f(r) \psi(r)}{\int dV_c \Sigma_f(r) \psi(r)}
\end{aligned} \tag{A.5}$$

and remember from section 3.4.1 that the shape function was normalised as:

$$\int dV_c \epsilon_f(r) \Sigma_f(r) \psi(r) = 1, \tag{A.6}$$

then follows

$$\begin{aligned}
\frac{\partial I(t)}{\partial t} &\equiv \frac{\bar{\gamma}_I}{\epsilon_f V_c} P_p(t) - \lambda_I I(t) \\
\frac{\partial X(t)}{\partial t} &\equiv \frac{\bar{\gamma}_X}{\epsilon_f V_c} P_p(t) + \lambda_I I(t) - \lambda_X X(t) - \Upsilon P_p(t) X(t)
\end{aligned} \tag{A.7}$$

The parameter  $P_p(t)$  denotes the total prompt power. The parameter  $\Upsilon$  is weighted with the time dependent xenon concentration  $X(r, t)$  and therefore is in fact time-dependent,  $\Upsilon(t)$ . However, in the present model  $\Upsilon(t)$  has been determined once at steady-state conditions and remains fixed.

If the core volume  $V_c$  has been divided in several layers, the only change to equations (A.7) is that the normalisation of equation (A.6) is no longer equal to one, but to the fraction given by the power produced in that layer divided by the total power. The volume  $V_c$  then of course denotes the volume of the layer.  $P_p(t)$  remains the total prompt power produced in the total core.



# Appendix B

---

## Recuperator Efficiency and Correction

---

The efficiency  $\eta_r$  for the recuperator can be defined as:

$$\eta_r = \frac{C_{\text{hot}}(T_{\text{hot,in}} - T_{\text{hot,out}})}{C_{\text{min}}(T_{\text{hot,in}} - T_{\text{cold,in}})} = \frac{C_{\text{cold}}(T_{\text{cold,out}} - T_{\text{cold,in}})}{C_{\text{min}}(T_{\text{hot,in}} - T_{\text{cold,in}})}, \quad (\text{B.1})$$

with the  $C_{\text{hot,cold}}$  denoting the mass flow heat capacity of the hot or cold recuperator side in  $\text{J K}^{-1} \text{s}^{-1}$  ( $C = \dot{m}C_p$ ).  $C_{\text{min}}$  denotes the lowest of the two, and  $T$  the temperature in K. The efficiency  $\eta_r$  is the ratio of actual transferred heat and the possible transferred heat in case of an infinitely large heat exchanging area. It is therefore very dependent on the geometry of the heat exchanger and has to be evaluated for each different design. Now that the current design is known, one can substitute the values for the temperature and mass flow from table 4.3 in equation (B.1) and conclude that  $\eta_r = 0.899$ . For a counterflow heat exchanger the relation is [101]:

$$\eta_r = \frac{1 - \exp(-\text{NTU}(1 - C_r))}{1 - C_r \exp(-\text{NTU}(1 - C_r))} \stackrel{C_r \rightarrow 1}{=} \frac{\text{NTU}}{1 + \text{NTU}}, \quad (\text{B.2})$$

$$\text{with} \quad \text{NTU} = \frac{\alpha A}{C_{\text{min}}} \quad (\text{B.3})$$

$$\text{and} \quad C_r = \frac{C_{\text{min}}}{C_{\text{max}}} \quad (\text{B.4})$$

with NTU the number of transfer units. The effective value for the heat transfer coefficient  $\alpha$  times the area for heat transfer  $A$  in  $\text{W K}^{-1}$  follows from summation over heat resistances (neglecting conductance through the thin steel wall):

$$\frac{1}{\alpha A} = \frac{1}{\alpha A} \Big|_{\text{hot}} + \frac{1}{\alpha A} \Big|_{\text{cold}} \quad (\text{B.5})$$

The number of transfer units, NTU, is related to the design of the entire recuperator. The NTU for a node is inversely proportional to the number of nodes that represent the recuperator. The Relap5 recuperator model uses 10 nodes, therefore  $A_{\text{cold}}$  or  $A_{\text{hot}}$ ,

are  $1/10$  of the total heat transfer area at the cold or hot side. This discretisation is inherent to the way of modelling in Relap5, with each node being ideally mixed in terms of temperature. As a result of the mixing the heat transfer will be lower because of the smaller driving force in temperature; the temperature difference between both recuperator sides becomes smaller. This can be remedied by choosing the number of nodes large ( $> 100$ ), but that will slow down the Relap5 calculations. Roughly speaking the calculation time is linear with the number of nodes. Therefore a correction factor  $G$  can be calculated for the nodes according to [48]:

$$G = \frac{\eta_r}{NTU(1 - C_r\eta_r - \eta_r)} \quad (B.6)$$

The heat transfer coefficient is multiplied by this factor  $G$ . It follows directly that for  $C_r = 1$  the recuperator cannot be modelled if  $\eta_r \geq 0.5$ . The correction factor for the 10-node recuperator is 5.16, knowing that:

- the heat transferring areas both on cold and hot side are  $4154 \text{ m}^2$ , so  $A_{\text{hot}} = S_{\text{cold}} = 415.4 \text{ m}^2$
- the heat transfer coefficient is for both sides about equal,  $\alpha \approx 520 \text{ W m}^{-2} \text{ K}^{-1}$ , so  $\alpha S$  from equation (B.5) becomes  $108.0 \cdot 10^3 \text{ W K}^{-1}$
- with  $C_{\min} = \dot{m}C_p = 25.18 \cdot 5195 = 1.308 \cdot 10^5 \text{ W K}^{-1}$ , NTU becomes 0.826. The mass flow on the cold side of the recuperator is  $25.18 \text{ kg/s}$ , on the hot side  $25.38 \text{ kg/s}$ . The difference is caused by the small leak flow from compressor outlet directly to turbine inlet, effectively bypassing cold recuperator side and reactor. It represents a leakage over the shaft connecting turbine and compressor, and a cooling of shaft and bearings. As a result  $C_r = 0.992$ , from equation (B.2) follows that  $\eta_r = 0.449$ .
- Inserting the value for  $\eta_r$  and  $C_r$  in equation (B.6) gives  $G = 5.16$ .

# Appendix C

---

## Energy Balance for Filling of Tank

---

The first law of thermodynamics for an open system is [43]:

$$\frac{\partial Q_{c.v.}}{\partial t} + \frac{\partial m_i}{\partial t} \left( h_i + \frac{v_i^2}{2} + gZ_i \right) = \frac{\partial m_e}{\partial t} \left( h_e + \frac{v_e^2}{2} + gZ_e \right) + \frac{\partial E_{c.v.}}{\partial t} + \frac{\partial W_{c.v.}}{\partial t} \quad (\text{C.1})$$

$$\text{with} \quad E_{c.v.} = m \left( u + \frac{v^2}{2} + gZ \right) \quad (\text{C.2})$$

$Q_{c.v.}$  = heat transferred into or out of the control volume during the process

$W_{c.v.}$  = work performed during the process

$E_{c.v.}$  = energy of fluid inside the control volume

$m_i$  = mass of fluid flowing into the control volume

$m_e$  = mass of fluid leaving the control volume

$h_i$  = specific enthalpy of fluid flowing into the control volume

$h_e$  = specific enthalpy of fluid leaving the control volume

$v_i$  = velocity of fluid entering the control volume

$v_e$  = velocity of fluid leaving the control volume

$Z_i$  = elevation of fluid entering the control volume

$Z_e$  = elevation of fluid leaving the control volume

$u$  = specific internal energy of fluid inside the control volume

$v$  = velocity of fluid inside the control volume

$Z$  = elevation of control volume

$g$  = gravitational constant

Consider a system that does not move as a whole, i.e.  $v = 0$ , and with zero elevation changes, i.e.  $Z_i = Z_e = Z = 0$ . In the case of the filling of a tank (control volume) from a reservoir at constant temperature  $T_s$  further simplifications are:

$Q_{c.v.} = 0$ , the process is assumed adiabatic

$W_{c.v.} = 0$ , no work is performed

$m_e = 0$ , no gas is leaving the tank

$v_i = 0$ , the kinetic energy is negligible compared to its enthalpy,  $h_i$

$h_i$  = constant, because of the constant temperature in the reservoir

This reduces equation (C.1) to:

$$\frac{\partial}{\partial t}(m \cdot u) = h_i \cdot \frac{\partial}{\partial t}m_i \quad (\text{C.3})$$

Integration over time from initial state (1) to final state (2) then yields for the tank:

$$m_2 \cdot u_2 - m_1 \cdot u_1 = h_i \cdot (m_2 - m_1). \quad (\text{C.4})$$

Note that if the tank were initially evacuated,  $u_2 = h_i$ , that is, all internal energy is supplied by the inflowing gas. The internal energy and enthalpy can be expressed as functions of gas temperature  $T_g$  and the specific heat capacity at constant pressure  $C_p$  and at constant volume  $C_v$ :

$$h = h_o + C_p T_g \quad (\text{C.5})$$

$$u = h - RT_g = h_o + C_p T_g - RT_g = h_o + C_v T_g \quad (\text{C.6})$$

so the arbitrary reference constant  $h_o$  cancels on both sides of equation (C.4) after insertion of equations (C.5) and (C.6):

$$C_v T_2 m_2 - C_v T_1 m_1 = C_p T_s (m_2 - m_1) \quad (\text{C.7})$$

Equation (C.7) can be written in terms of pressures  $p_{1,2}$ , tank volume  $V_t$  and reservoir temperature  $T_s$  using  $pV = mRT$  and  $C_p - C_v = R$ :

$$\Delta m = \frac{1}{(\kappa - 1)} \cdot \frac{V_t}{C_p T_s} (p_2 - p_1) \quad (\text{C.8})$$

---

# Nomenclature

---

## List of Symbols

$\alpha$	heat transfer coefficient	$\text{W m}^{-2} \text{K}^{-1}$
$\alpha_T$	temperature coefficient of reactivity	$\text{pcm K}^{-1}$
$\beta$	$= \sum_j \beta_j$ , total delayed-neutron fraction	-
$\bar{\beta}$	$= \sum_j \bar{\beta}_j$ , effective total delayed-neutron fraction	-
$\beta_j$	delayed neutron fraction for time group $j$	-
$\bar{\beta}_j$	effective delayed-neutron fraction for time group $j$	-
$\beta^q$	delayed neutron fraction for nuclide $q$	-
$\beta_j^q$	delayed neutron fraction, time group $j$ , nuclide $q$	-
$\beta_{j,g}$	delayed neutron fraction for nuclide mix, time group $j$ , energy group $g$	-
$\gamma$	reactivity ramp rate	$\text{pcm s}^{-1}$
$\gamma_n$	decay heat yield for group $n$	$\text{s}^{-1}$
$\gamma_I$	iodine fission yield	-
$\gamma_X$	xenon fission yield	-
$\bar{\gamma}_I$	space averaged iodine fission yield	-
$\bar{\gamma}_X$	space averaged xenon fission yield	-
$\epsilon_f$	average prompt energy release per fission	eV
$\varepsilon$	packing fraction (= percentage void) of pebble-bed	-
$\eta$	dynamic viscosity	$\text{Pa}\cdot\text{s}$
$\eta_c$	compressor stage design efficiency	-
$\eta_r$	recuperator efficiency	-
$\eta_t$	isentropic turbine efficiency	-
$\eta_t^o$	maximum turbine isentropic efficiency	-
$\eta_t'$	polytropic turbine efficiency	-
$\eta_c'$	polytropic compressor efficiency	-
$\kappa$	specific heat ratio	-
$\lambda$	work input coefficient for compressor map	-
$\lambda_{\text{design}}$	design work input coefficient for compressor map	-
$\bar{\lambda}$	average decay constant for delayed neutrons	$\text{s}^{-1}$
$\lambda_j$	decay constant for delayed neutron, time group $j$	$\text{s}^{-1}$
$\lambda_n$	decay constant for decay heat, time group $n$	$\text{s}^{-1}$
$\lambda_I$	decay constant for iodine	$\text{s}^{-1}$
$\lambda_X$	decay constant for xenon	$\text{s}^{-1}$
$\lambda_{\text{tr}}$	transport mean free path	m
$\lambda_f$	fluid thermal conductivity	$\text{W m}^{-1} \text{K}^{-1}$

$\lambda_g$	conductivity of graphite	$\text{W m}^{-1} \text{K}^{-1}$
$\lambda_s$	effective conductivity of solid part of mesh volume	$\text{W m}^{-1} \text{K}^{-1}$
$\lambda_{irr}$	conductivity of irradiated graphite	$\text{W m}^{-1} \text{K}^{-1}$
$\lambda_{unirr}$	conductivity of unirradiated graphite	$\text{W m}^{-1} \text{K}^{-1}$
$\Lambda$	mean neutron generation time	s
$\nu$	number of neutrons emitted per fission	-
$\nu_g^q$	number of neutrons emitted per fission by nuclide $q$ in energy group $g$	-
$\xi$	$^{135}\text{Xe}$ coefficient of reactivity	$\text{pcm} \cdot \text{m}^3$
$\pi$	pressure ratio (inlet/outlet)	-
$\rho$	reactivity	pcm
$\rho_X^0$	nominal xenon reactivity worth	pcm
$\Delta\rho_T$	temperature induced reactivity	pcm
$\Delta\rho_X$	xenon induced reactivity	pcm
$\Delta\rho_s$	control system induced reactivity	pcm
$\rho_s$	density of solid part of mesh volume	$\text{kg m}^{-3}$
$\rho_{He}$	helium density	$\text{kg m}^{-3}$
$\sigma_a^X$	microscopic absorption cross section for xenon	$\text{m}^2$
$\sigma_f^U$	microscopic fission cross section for uranium	$\text{m}^2$
$\Sigma_a$	macroscopic absorption cross section	$\text{m}^{-1}$
$\Sigma_{f,g}$	macroscopic fission cross section, energy group $g$	$\text{m}^{-1}$
$\Sigma_{r,g}$	macroscopic removal (absorption + outscattering) cross section, energy group $g$	$\text{m}^{-1}$
$\Sigma_{s,g'g}$	macroscopic scattering cross section from energy group $g'$ to $g$	$\text{m}^{-1}$
$\tau_c$	torque on shaft exerted by control system	$\text{N} \cdot \text{m}$
$\tau_i$	torque on shaft exerted by component $i$	$\text{N} \cdot \text{m}$
$\Upsilon$	space averaged product of $\sigma_a^X$ with shape function	$\text{m}^2$
$\phi$	flow coefficient	-
$\phi_{\text{design}}$	flow coefficient by design	-
$\varphi$	heat flow	$\text{J s}^{-1}$
$\Phi$	neutron flux	$\text{m}^{-2} \text{s}^{-1} \text{eV}^{-1} \text{sr}^{-1}$
$\Phi_g$	neutron flux, energy group $g$	$\text{m}^{-2} \text{s}^{-1} \text{eV}^{-1} \text{sr}^{-1}$
$\Phi^\dagger$	adjoint function	-
$\Phi_0^\dagger$	adjoint function for reference state	-
$\chi$	total neutron fission spectrum	-
$\chi_j$	delayed neutron fission spectrum, energy group $j$	-
$\tilde{\chi}_j$	delayed neutron fission spectrum, energy group $j$ , per unit solid angle	$\text{sr}^{-1}$
$\chi_p$	prompt neutron fission spectrum	-
$\tilde{\chi}_p$	prompt neutron fission spectrum per unit solid angle	$\text{sr}^{-1}$
$\chi_{p,g}$	prompt neutron fission spectrum, energy group $g$	-
$\psi$	shape function	$\text{m}^{-2} \text{s}^{-1} \text{eV}^{-1} \text{sr}^{-1}$
$\omega$	rotational speed	$\text{rad s}^{-1}$
$\omega_o$	design rotational speed	$\text{rad s}^{-1}$
$\omega_{\text{scaled}}$	rotational speed scaled on the design rotational speed	-
$\Omega$	neutron direction (unit vector)	sr
$A$	heat transfer area	$\text{m}^2$
$A_c$	core cross sectional area	$\text{m}^2$
$A_f$	flow cross sectional area	$\text{m}^2$

$a_i$	friction factor of component $i$ connected to shaft	$\text{N} \cdot \text{m} \cdot \text{s}$
$b$	a function of turbine reaction fraction	-
$C$	heat capacity of the reactor	$\text{J K}^{-1}$
$C_s$	heat capacity of solid part of mesh volume	$\text{J kg}^{-1} \text{K}^{-1}$
$C_{eff}$	effective heat capacity of reactor core	$\text{J K}^{-1}$
$C_{cold}$	heat capacity of mass flow rate of the cold recuperator side	$\text{J K}^{-1} \text{s}^{-1}$
$C_{hot}$	heat capacity of mass flow rate of the hot recuperator side	$\text{J K}^{-1} \text{s}^{-1}$
$C_{min}$	lowest in value of $C_{cold}$ , $C_{hot}$	$\text{J K}^{-1} \text{s}^{-1}$
$C_{max}$	highest in value of $C_{cold}$ , $C_{hot}$	$\text{J K}^{-1} \text{s}^{-1}$
$C_r$	ratio $C_{min}/C_{max}$	-
$C_p$	heat capacity at constant pressure for helium	$\text{J kg}^{-1} \text{K}^{-1}$
$C_v$	heat capacity at constant volume for helium	$\text{J kg}^{-1} \text{K}^{-1}$
$C_j$	precursor concentration in delayed group $j$	$\text{m}^{-3}$
$c_j$	adjoint weighted precursor concentration in delayed group $j$	- or $\text{J s}^{-1}$
$D$	neutron diffusion coefficient	$\text{m}$
$D_h$	heated equivalent diameter	$\text{m}$
$d$	factor of tank pressure in/decreases when filling/emptying the tank	-
$d_k$	pebble diameter	$\text{m}$
$E$	energy of neutron	$\text{eV, J}$
$F$	normalisation factor for point kinetic parameters	$\text{s}^{-1}$
$f$	factor of pressure change in ECS due to helium inventory change	-
$f_i$	fraction of the prompt power deposited in layer $i$	-
$G$	correction factor for heat transfer in recuperator	-
$g$	gravitational constant	$\text{m s}^{-2}$
$g$	ratio tank to system pressure at which inflow from system to tank stops	-
$g'$	ratio system to tank pressure at which outflow from tank to system stops	-
$h_{design}$	dimensionless polytropic compressor head, design value	-
$h_{ndim}$	dimensionless polytropic compressor head	-
$h_{ndim,scaled}$	$h_{ndim}$ scaled to the design value $h_{design}$	-
$h_{isent}$	specific isentropic enthalpy change	$\text{J kg}^{-1}$
$I$	iodine-135 concentration	$\text{m}^{-3}$
$I_i$	inertia of component $i$ connected to shaft	$\text{kg} \cdot \text{m}^2$
$K$	pressure ratio over compressor	-
$k$	effective neutron multiplication factor	-
$L$	neutron diffusion length	$\text{m}$
$\ell$	prompt fission chain length	$\text{m}$
$M$	neutron migration length	$\text{m}$
$m$	mass	$\text{kg}$
$\dot{m}$	helium mass flow rate	$\text{kg s}^{-1}$
$Nu$	Nusselt number	-
$NTU$	Number of Transfer Units	-
$P_d$	decay power	$\text{J s}^{-1}$
$P_{d,n}$	decay power of time group $n$	$\text{J s}^{-1}$
$P_p$	prompt fission power	$\text{J s}^{-1}$
$P_t$	total thermal reactor power	$\text{J s}^{-1}$
$P_{he}$	thermal power transferred to helium coolant	$\text{J s}^{-1}$
$P_{peb}$	power homogeneously generated in the fuel zone of a pebble	$\text{J s}^{-1}$
$P_{crit}$	prompt power at recriticality	$\text{J s}^{-1}$
$P_{max}$	maximum power during first power surge	$\text{J s}^{-1}$

$P_0$	equilibrium power of passively cooled condition	$\text{J s}^{-1}$
$Pr$	Prandtl number	-
$p_i$	helium pressure at inlet of component	Pa
$p_o$	helium pressure at outlet of component	Pa
$\Delta p$	pressure drop over pebble-bed	Pa
$p_{\max}$	pressure in ECS with nominal helium inventory	Pa
$p_{\max}^{\text{HP}}$	high pressure point in ECS with nominal helium inventory	Pa
$p_{\min}$	pressure in ECS with partial helium inventory	Pa
$p^{\text{HP}}$	high pressure point in ECS	Pa
$p^{\text{LP}}$	low pressure point in system	Pa
$p_1$	empty tank pressure, temperature in equilibrium with surroundings	Pa
$p_2$	full tank pressure, immediately after ending the mass transfer	Pa
$p_3$	full tank pressure, temperature in equilibrium with surroundings	Pa
$p_4$	empty tank pressure, immediately after ending the mass transfer	Pa
$Q$	neutron source	- or $\text{J s}^{-1}$
$q_c$	convective heat source	$\text{J s}^{-1}$
$q_n$	nuclear heat source	$\text{J s}^{-1}$
$Re$	Reynolds number	-
$R$	gas constant for helium, $R = 2077 \text{ J kg}^{-1} \text{ K}^{-1}$	$\text{J kg}^{-1} \text{ K}^{-1}$
$R_i$	radius of fuel zone in pebble	m
$R_o$	outer radius of pebble	m
$\mathcal{R}$	diffusion operator	-
$r$	reaction fraction of turbine stage	-
$T$	temperature, (uniform) fuel temperature in pebble-bed	K
$T_i$	(uniform) temperature in axial pebble-bed layer $i$	K
$T_0$	(uniform) nominal temperature in pebble-bed	K
$T_{Peb}^{ave}$	average temperature of a pebble	K
$T_{surf}$	surface temperature of pebble(-bed)	K
$T_{FZ}$	average temperature in pebble fuel zone	K
$T_{Sh}$	average temperature in pebble shell	K
$T_{env}$	ambient temperature	K
$T_g$	gas temperature	K
$T_{g,i}$	helium temperature at inlet of component	K
$T_{g,o}$	helium temperature at outlet of component	K
$T_{\text{cold,in}}$	helium inlet temperature at cold recuperator side	K
$T_{\text{cold,out}}$	helium outlet temperature at cold recuperator side	K
$T_{\text{hot,in}}$	helium inlet temperature at hot recuperator side	K
$T_{\text{hot,out}}$	helium outlet temperature at hot recuperator side	K
$T_{max}$	highest temperature in Brayton cycle for heat transfer	K
$T_{min}$	lowest temperature in Brayton cycle for heat transfer	K
$T_s$	temperature in energy conversion system at high pressure point	K
$T_1$	empty tank temperature when in thermal equilibrium with surroundings	K
$T_2$	full tank temperature, immediately after ending the mass transfer	K
$T_3$	full tank temperature when in thermal equilibrium with surroundings	K
$T_4$	empty tank temperature, immediately after ending the mass transfer	K
$T_{osc}$	oscillation period of power surges	s
$t$	time	s
$t_{crit}$	time of recriticality	s
$u$	specific internal energy change	$\text{J kg}^{-1}$



$V_c$	pebble-bed core volume	$\text{m}^3$
$V_s^{\text{HP}}$	effective ECS volume when all mass is thought to be at $p_{\text{max}}^{\text{HP}}, T_s$	$\text{m}^3$
$V_t$	storage tank volume	$\text{m}^3$
$v$	helium velocity	$\text{m s}^{-1}$
$v_t$	tangential velocity of rotating blade tips	$\text{m s}^{-1}$
$W_c$	compressor power	$\text{J s}^{-1}$
$W_t$	turbine power	$\text{J s}^{-1}$
$X$	xenon-135 concentration	$\text{m}^{-3}$
$Z$	elevation of storage tank	$\text{m}$

## Abbreviations and Acronyms

ACM	Aspen Custom Modeller
ACACIA	AdvanCed Atomic Cogenerator for Industrial Applications
AVR	Arbeitsgemeinschaft Versuchsreaktor
Brayton Cycle	Type of thermodynamic cycle
ECS	Energy Conversion System
ESKOM	Electricity Supply COMmission
GT-MHR	Gas Turbine Modular High-temperature helium Reactor
HTR	High Temperature (gas-cooled) Reactor
HTR-10	10 MW High Temperature Reactor
HTTR	High Temperature engineering Test Reactor
INCOGEN	INherently safe nuclear COGENeration (predecessor of ACACIA)
LOCI	Loss Of Coolant Incident
LOFI	Loss Of Flow Incident
MHTGR	Modular High Temperature Gas-cooled Reactor
MPa	MegaPascal ( $10^6 \text{ Pa}$ )
MW	MegaWatt ( $10^6 \text{ W}$ )
$\text{MW}_{th}$	MegaWatt thermal
$\text{MW}_e$	MegaWatt electric
NRG	Nuclear Research & Consultancy Group
OTTO	Once-Through-Then-Out
Panther	Pwr and Agr Neutron and Thermal Hydraulic Evaluation Route; software for core calculations
PAP	Peu-à-Peu
PBMR	Pebble-Bed Modular Reactor
pcm	per cent mille, i.e. $10^{-5}$ , measure for reactivity
Relap5	Software for thermodynamic cycle calculations
Talink	Software for linking thermodynamic cycle to neutronics calculations
Thermix-Direkt	Software for thermal hydraulics core calculations for pebble-bed geometry
THTR	Thorium High Temperature Reactor
TRISO	Four layer coated particle
UKNDL	United Kingdom Nuclear Data Library
Wims	Winfrith Improved Multigroup Scheme, ANSWERS Software Package for cross-sectional database generation



---

# Summary

---

Due to their high energy efficiency, combined heat and power plants have become increasingly popular in the Netherlands. Usually a gas, coal, or oil fired station supplies the heat, which is partly converted to electricity, partly to high caloric heat such as industrial steam. Low-caloric waste heat can be used for district heating. The Dutch ACACIA-project (AdvanCed Atomic Cogenerator for Industrial Applications) proposes two innovations:

- The first innovative proposal is the substitution of the conventional heat source by a small nuclear reactor. A High Temperature Reactor (HTR) seems a suitable candidate because of its inherent safety capabilities. The HTR potential to fulfill the requirement for inherent safety lies primarily in the combination of a low power density, a high heat capacity, a minimal excess reactivity, and a very high temperature of 1600°C up to which the coated particles can retain the fission products. The ACACIA design envisages a reactor simple in design and operation, therefore a pebble-bed type reactor has been chosen. Complexity in fuel management is avoided, and reduced even further with a peu-à-peu filling scheme: new fuel balls are dropped in the core cavity at a rate equal to fuel consumption. When the core is full after 5 to 10 years, it is discharged and the cycle starts again.
- The second innovation in the ACACIA design makes the heat exchanger redundant that separates the nuclear coolant circulation and the secondary, conventional steam cycle. The working fluid heated in the nuclear reactor is offered directly to the energy conversion system (ECS) that uses the direct, closed Brayton cycle as thermodynamic cycle. It resembles the Rankine cycle for steam cycles, but a single phase gaseous working fluid (helium) is used instead of a condensing fluid. The system consists of a single-shaft turbine-compressor with a directly coupled electricity generator. A precooler before the compressor and a recuperator further enhance the overall efficiency.

Due to the direct coupling, it is expected that the reactor and ECS have a larger and faster influence on each other than is the case in an indirect system.

In general, the fields of nuclear reactor physics and thermodynamics for the energy conversion system are strictly separated in calculational sense, and relate to each other in as much as posing the boundary conditions for the other system. Together with the historically limited computer power this led to modelling of each field separately. With faster computers, the coupling of detailed reactor and ECS models started in the

light water reactor industry in the early nineties. The present thesis deals with the coupling and modelling for a high temperature reactor system. With such a model the transient behaviour of the total system can be analysed. This study focuses on the HTR reactor, and assumes less detail for the ECS model; a second study on transient behaviour by Kikstra focuses on the ECS and assumes an uncomplicated reactor model.

The reactor has been modelled in various levels of detail; 3-dimensional or point kinetics for the neutronics part, 2- or 1-dimensional for the core thermal hydraulics. Less detail means a decrease in calculation time. Comparison of the models revealed that the neutronics calculation can greatly be reduced in complexity - without compromising accuracy - by using the point reactor kinetic model. In that model the assumption must be made that the power density distribution remains constant during the transients. This is a valid assumption as a result of the long fission chain range in a graphite reactor. For the ACACIA the range is twice as large as the physical dimensions of the core, and reactivity changes in one part of the core are certainly felt in all other parts. This means that the core is tightly coupled, acts as one entity from neutronic point of view, and can be modelled as a point. The necessary point kinetic parameters can be derived once from a detailed steady-state model, rendering a detailed transient code superfluous.

It turns out that for accuracy it is more important to provide for a detailed thermal hydraulic description of the pebble-bed. The temperature distribution is far from constant during transients, and in order to describe heat transfer by forced convection, radiation, conduction or free convection, a 2-dimensional model is a requirement.

The modelling of the energy conversion system has been performed with the Relap5 code that has been developed and validated for steam-cycle applications. A new subroutine has been added that replaces the water pump with a gas compressor. The available steam turbine model has been utilised for the gas turbine model, but it is advised to replace it in the future by a better model; it is suitable for conceptual studies, but a licensing authority will probably advise against it. All components of the ECS have been compared to the detailed model of Kikstra; the (small) differences can be explained and were considered to be acceptable for a conceptual study.

The control system for the ECS has been kept very straightforward, and focuses on keeping the shaft rotational speeds within bounds. Furthermore, the control system optimises the efficiency of the power production by matching the helium inventory in the cycle to the power demand. If less power is needed, helium is extracted from the cycle and temporarily stored in tanks. An analytic model has been derived for this helium storage tank system in order to determine the optimum in number of tanks and their sizes.

The transient calculations with the coupled system of reactor and energy conversion system show good agreement when compared to the total ACACIA model of Kikstra. The agreement tends to become less for far off-design conditions, when the Relap5 gas turbine model becomes less accurate.

Stand-alone reactor calculations have been performed, in order to consider the inherent safety aspect of the ACACIA reactor in more detail, i.e. which transients will cause the temperature in the coated particles to exceed  $1600^{\circ}\text{C}$ ? It has been shown in this thesis that previous ACACIA safety analyses are in error due to an erroneous assessment of the fuel temperature in the pebble. It turned out that for the present design the fuel temperatures can exceed  $1600^{\circ}\text{C}$  by more than  $200^{\circ}\text{C}$  at low helium coolant mass flow rates for prolonged periods of time. This is caused by the reduction in the xenon neutron poison concentration when the reactor operates at partial load for some time. This means, that - if no control rods are used - this reduction in negative reactivity has to be compensated by rising fuel temperatures, as by design the power production decreases with increasing temperature. In order to prevent fuel temperatures above  $1600^{\circ}\text{C}$  a number of adaptations in the reactor design have been suggested.

Furthermore, the reactor outlet gas temperature can reach such high temperatures that the gas turbine lifetime shortens dramatically. In order to prevent high outlet gas temperature and protect the gas turbine, the use of control rods is advised during operation. However, the reactor should be designed such that the control rods are never necessary to ensure a fuel temperature below  $1600^{\circ}\text{C}$ .

Most strikingly probably is the conclusion that the highest fuel temperatures are not experienced during a total loss of active coolant flow, but for transients with a small (1%) sustained mass flow rate of the coolant. In that case the produced heat is still collected and transported towards the bottom of the core, which results in a high pebble surface temperature. In contrast, during total loss of flow, there is no accumulation of heat at a certain point due to forced convection, and heat leaks away into the reflectors evenly distributed.



---

# Samenvatting

---

Warmte-kracht installaties zijn vanwege hun hoge rendement steeds meer in trek gekomen in Nederland. Normaal gesproken levert een gas-, kolen- of oliegestookte centrale de proceswarmte, die vervolgens deels wordt omgezet in electriciteit, deels in hoogwaardige warmte zoals industriële stoom. Restwarmte kan bijvoorbeeld gebruikt worden voor districtsverwarming. Het Nederlandse ACACIA project (geAvanCeerde Atomaire Cogenerator voor Industriële Applicaties) innoveert op twee punten het gangbare ontwerp:

- De eerste innovatie is de vervanging van de conventionele warmtebron door een kleine nucleaire reactor. De Hoge Temperatuur Reactor (HTR) lijkt een geschikte kandidaat vanwege de inherent veilige eigenschappen. De mogelijkheid van de HTR om aan de eis van inherente veiligheid te voldoen, ligt voornamelijk aan de combinatie van een lage vermogensdichtheid, een hoge warmtecapaciteit, een minimale overreactiviteit en een zeer hoge temperatuur tot 1600°C waarbij de splijtingsproducten niet vrijkomen uit de brandstof. Het ACACIA concept stelt dat de reactor eenvoudig van ontwerp en gebruik moet zijn, zodat gekozen is voor het kogelbedreactor type. Hiermee vervalt de vaak ingewikkelde beladingsstrategie van een reactor, in dit geval nog verder versimpeld door het peu-à-peu principe: nieuwe brandstofballen worden toegevoegd in een tempo dat gelijke tred houdt met het verbruik van brandstof. Als na 5 tot 10 jaar de kern vol is, wordt die in één keer gelegeerd en start de cyclus opnieuw.
- Als tweede innovatie in het ACACIA ontwerp wordt een directe cyclus voor het energieconversiesysteem (ECS) toegepast in plaats van een secundaire stoomcyclus. Als thermodynamische cyclus ontstaat zo de directe, gesloten Brayton cyclus. Deze lijkt op de Rankine cyclus die bij stoomcycli gebruikt wordt, maar nu wordt een niet condensierend fluïdum (helium) gebruikt als werkstof. Het systeem bestaat uit een enkele as met daaraan een turbocompressor en een direct gekoppelde elektriciteitsgenerator. Een voorkoeler voor de compressor en een recuperator worden aangewend ter verhoging van het rendement.

Vanwege de directe koppeling wordt verwacht dat de reactor en het ECS een grotere en snellere invloed op elkaar hebben dan in het geval van een indirect systeem.

In het algemeen bestaat er een strikte scheiding tussen de vakgebieden van de nucleaire reactorfysica en de thermodynamica van het energieconversiesysteem voor wat betreft berekeningen. Ze zijn in zoverre met elkaar verbonden dat ze elkaars randvoorwaarden

bepalen. De genoemde scheiding is een voortvloeisel uit de beperkte rekenkracht in vroeger tijden en heeft geleid tot modellering van elk gebied afzonderlijk. Door de beschikbaarheid van snellere computers begon in het begin van de jaren '90 de koppeling van gedetailleerde reactor en ECS-modellen in de lichtwaterreactor industrie.

Dit proefschrift behandelt de koppeling en modellering voor een HTR systeem. Met een dergelijk model kan het transient gedrag van het totale systeem onder de loep genomen worden. Deze studie richt zich vooral op de HTR reactor en gaat in detail minder in op het ECS model; een tweede studie naar het transient gedrag door Kikstra gaat juist wel dieper in op het ECS, maar gebruikt een eenvoudig reactor model.

De reactor is op meerdere manieren gemodelleerd, variërend in detail: 3-dimensionaal of puntkinetisch voor het neutronica gedeelte, 2- of 1-dimensionaal voor de thermohydraulica van de reactorkern. Minder detail betekent een vermindering in rekentijd. Vergelijking van de modellen onthulde dat de neutronicaberekening enorm vereenvoudigd kan worden door het punt kinetisch model te gebruiken - zonder noemenswaardige vermindering van de nauwkeurigheid. In dat model moet de aanname gemaakt worden dat de vermogensdichtheidsverdeling constant blijft gedurende de transiënten. Dit is een juiste aanname als gevolg van de grote lengte waarover een splijtingskettingreactie zich uitstrekt in een grafiet reactor. Voor de ACACIA is het bereik twee keer zo groot als de maximale fysische dimensies van de kern, waardoor een reactiviteitsverandering in het ene gedeelte van de kern zeker gevoeld wordt in alle andere gedeelten. Hierdoor is de kern sterk gekoppeld, kan uit neutronisch oogpunt gezien worden als één geheel, en kan gemodelleerd worden als een puntkern. De benodigde puntkinetische parameters kunnen hiervoor van een gedetailleerd stationair model afgeleid worden, waardoor een gedetailleerde transientcode overbodig wordt.

Het blijkt dat het voor de nauwkeurigheid belangrijker is om een gedetailleerde thermohydraulische beschrijving voor de kogelbedreactor te geven. De temperatuurverdeling is verre van constant gedurende de transiënten, waardoor een 2-dimensionaal model voor vrije en geforceerde convectie, straling en geleiding een vereiste is.

De modellering van het energieconversiesysteem is gedaan met de Relap5 code die is ontwikkeld en gevalideerd voor stoomcycli. Er is een nieuwe subroutine aan toegevoegd die de waterpomp vervangt door een gascompressor. Het beschikbare stoomturbinemodel is gebruikt voor het gasturbinemodel, maar geadviseerd wordt om het in de toekomst te vervangen door een beter model. Het is geschikt voor conceptuele studies, maar een vergunningverlenende instantie zal er waarschijnlijk problemen mee hebben. Alle componenten van het ECS zijn vergeleken met het gedetailleerde model van Kikstra; de (kleine) verschillen kunnen verklaard worden en worden aanvaardbaar geacht voor een conceptuele studie.

Het regelsysteem voor het ECS is erg eenvoudig gehouden en concentreert zich op het begrensd houden van de omloopsnelheid van de turbocompressor. Verder optimaliseert het regelsysteem het rendement van de vermogensproductie door de heliuminventaris in de cyclus aan te passen aan de vermogensvraag. Als minder vermogen nodig is, wordt helium aan de cyclus onttrokken en tijdelijk opgeslagen in vaten. Er is



een analytisch model opgesteld voor dit heliumopslagsysteem om het optimale aantal opslagvaten en hun volume te bepalen.

De transient berekeningen van het gekoppelde reactor- en energieconversiesysteem laten een goede overeenkomst zien met de berekeningen van het totale ACACIA model van Kikstra. De overeenkomst wordt wat minder voor condities die ver van de normale operationele werkelijkheid afliggen doordat het Relap5 gas turbine model daar minder accuraat is.

Er zijn ook berekeningen verricht aan alleen het reactor systeem om het aspect van 'inherent veilig' nader onder de loep te nemen voor de ACACIA. De vraag hierbij is: welke transients kunnen een temperatuur in de brandstof veroorzaken die boven de 1600°C komt?

In dit proefschrift is aangetoond dat voorgaande ACACIA veiligheidsstudies foutief zijn omdat voorbij gegaan wordt aan de temperatuurverdeling binnenin een brandstofkogel. Het bleek dat voor het huidig ontwerp langdurig temperaturen kunnen optreden die meer dan 200°C boven de 1600°C liggen bij situaties met lage massastroom van het helium koelmiddel. De oorzaak hiervoor ligt in de vermindering van de xenon neutronengifconcentratie wanneer de reactor gedurende langere periode op lager vermogen draait. Dit betekent dat - wanneer geen regelstaven worden gebruikt - die reductie in negatieve reactiviteit gecompenseerd moet worden door een stijging van de brandstoftemperatuur. Eén van de eigenschappen van het reactorontwerp is namelijk dat de vermogensproductie bij hogere temperatuur afneemt. Om brandstoftemperaturen boven 1600°C te voorkomen zijn een aantal aanpassingen in het reactor ontwerp gesuggereerd.

Verder blijkt dat de reactoruitlaattemperatuur zulke hoge waarden kan bereiken dat de levensduur van de gasturbine hierdoor dramatisch verkort wordt. Om de hoge uitlaatgastemperatuur te voorkomen en de gasturbine te beschermen, wordt het gebruik van regelstaven aanbevolen tijdens bedrijfsvoering. De reactor moet echter altijd zo ontworpen worden dat de regelstaven nooit nodig zijn om de brandstoftemperatuur beneden 1600°C te houden.

Waarschijnlijk is de meest verrassende conclusie dat de hoogste brandstoftemperaturen niet optreden tijdens een totaal verlies van actieve koeling, maar bij transients met een kleine (1%) massastroom van de koeling. In dat geval wordt de geproduceerde warmte nog steeds verzameld en getransporteerd naar de bodem van de kern, zodat de brandstofballen aldaar een hoge oppervlaktetemperatuur opgedrongen krijgen. Dit in tegenstelling tot de situatie bij totaal verlies aan actieve koeling, waarbij geen warmte accumulatie plaatsvindt op een bepaald punt als gevolg van geforceerde convectie. De warmte lekt in dat geval in alle richtingen gelijkmatig weg in de reflector.



---

# Acknowledgement

---

I would like to express my gratitude to everybody who helped me to complete the study presented in this thesis:

In the first place I would like to thank Prof. Dr Ir H. van Dam for his constant support, his valuable remarks and advice, and the pleasant cooperation. The same thanks go to Prof. Dr Ir A.H.M. Verkooijen, who always expressed great interest in this study.

I greatly appreciate the enthusiasm with which Prof. Dr Ir T.H.J.J. van der Hagen and Dr Ir J.E. Hoogenboom conducted the reactor physics courses in Delft.

I want to thank Dr Ir J.C. Kuijper for his day to day involvement in my research.

It has been my privilege to work together with the South-African PBMR-project team. Apart from the excitement of witnessing 'how to design a reactor', I am very grateful for the good care they took of me during those six months.

My colleagues at NRG all contributed in various degrees to my research, for which I am grateful. In this respect special thanks go to Ir Jan Foeke Kikstra and Dr Evert Bende with whom I had many interesting discussions, work related or not. With them, and among others Dr Marieke Duijvestijn, Dr Arjan Koning, Drs Rob van der Stad, Jorn Verwey MSc., Ir Wilko Verbakel and of course Ir Patricia Damen, a good working atmosphere was created.



---

# Curriculum Vitae

---

Ewout Verkerk was born on the 13<sup>th</sup> of February, 1970. After attending grammar school, the Berlingh College in Beverwijk, he took up applied physics study at the Delft University of Technology in 1988. In parallel he took up Italian Language and Literature studies at the University of Amsterdam in 1990 which he concluded in 1993 with the propaedeutic exam. The graduate research for the study physics was performed at the Interfacultair Reactor Instituut in Delft in the department of Radiation Physics. This research was concluded with the Master's thesis 'Microscopic Dynamics of Liquid  $^7\text{Li}$  at 843 K'. In 1994 he obtained the degree of Natuurkundig Ingenieur. He worked one year for RIVM (RijksInstituut voor Volksgezondheid en Milieu), after which he started with his Ph.D.-research in 1995 at ECN Petten (nowadays NRG, Nuclear Research and consultancy Group). The study comprised the dynamics of the pebble-bed type high temperature nuclear reactor when coupled directly to the energy conversion system, and resulted in this thesis.

In November 2000 he starts as a patent examiner at the European Patent Office in Rijswijk.